DESIGN AND FABRICATION OF WIDEBAND MULTIPLE INPUT MULTIPLE OUTPUT ANTENNA FOR 5G MOBILE APPLICATIONS

Thesis Submitted for the Award of the Degree of

DOCTOR OF PHILOSOPHY

in

(Electronics & Communication Engineering)

By

Nitasha Bisht

Registration Number: 41800762

Supervised By

Dr. Praveen Kumar Malik (23314)

Professor

School of Electronics & Electrical Engineering

Lovely Professional University, Punjab, India

Co-Supervised By

Dr. Sudipta Das

Associate Professor

Department of ECE

IMPS College of Engineering & Technology, West Bengal, India

LOVELY PROFESSIONAL UNIVERSITY, PUNJAB

2024

DECLARATION

I, hereby declared that the presented work in the thesis entitled "Design and Fabrication of Wideband Multiple Input Multiple Output Antenna for 5G Mobile Applications" in fulfillment of degree of **Doctor of Philosophy (Ph.D.)** is outcome of research work carried out by me under the supervision of Dr. Praveen Kumar Malik, working as Professor, in the School of Electronics and Electrical Engineering of Lovely Professional University, Punjab, India and co-supervision of Dr. Sudipta Das, working as Associate Professor, in the Department of Electronics and Communication Engineering of IMPS College of Engineering & Technology, Nityanandapur, Chandipur, Malda, West Bengal, India. In keeping with general practice of reporting scientific observations, due acknowledgements have been made whenever work described here has been based on findings of other investigator. This work has not been submitted in part or full to any other University or Institute for the award of any degree.

(Signature of Scholar)

Nitasha Bisht

Registration No.: 41800762

School of Electronics and Electrical Engineering

Lovely Professional University

Punjab, India

CERTIFICATE

This is to certify that the work reported in the Ph.D. thesis entitled "Design and Fabrication of Wideband Multiple Input Multiple Output Antenna for 5G Mobile Applications" submitted in fulfillment of the requirement for the reward of degree of **Doctor of Philosophy (Ph.D.)** in the School of Electronics and Electrical Engineering, is a research work carried out by Nitasha Bisht, 41800762, is bonafide record of her original work carried out under my/our supervision and that no part of thesis has been submitted for any other degree, diploma or equivalent course.

Dr. Praveen Kumar Malik
Professor
School of Electronics and Electrical Engineering
Lovely Professional University, Punjab, India

Dr. Sudipta Das
Associate Professor
Department of ECE
IMPS College of Engineering and Technology,
Nityanandapur, Chandipur,
Malda, West Bengal, India

ABSTRACT

Each new generation of wireless technology improves connectivity and speed, which has resulted in a revolution in the way in which we communicate with one another and gain access to information. The rapid development of wireless technology has been an essential factor in the rise of modern society. This has made it possible to communicate and interact with people all over the world in a seamless manner. The fifth generation of wireless networks, often known as 5G, stands out from the other iterations of wireless networks as a disruptive force that holds the possibility of reshaping our digital landscape. It introduces higher data transfer rates, lower latency, and superior reliability, all while supporting a vastly increased number of connected devices. 5G, functions within various frequency bands, each with distinct attributes and practical uses. The sub-6 GHz spectrum and the millimeter-wave (mm Wave) spectrum are widely recognized as the primary frequency bands employed in 5G networks. The band below 6 GHz, sometimes referred to as the sub-6 GHz spectrum, offers a favorable combination between coverage and capacity. Conversely, the millimeter-wave spectrum, spanning from 24 GHz to 100 GHz, offers exceptional data transmission rates and little latency. However, its coverage is constrained, and signal attenuation can occur in the presence of impediments such as buildings and trees. The optimization of 5G's capabilities is heavily reliant on the utilization of Multiple-Input Multiple-Output (MIMO) technology. Multiple-Input Multiple-Output (MIMO) is a communication method that employs multiple antennas at both the transmitting and receiving terminals of a system. The use of spatial diversity, multipath propagation, and beamforming techniques is employed to enhance signal quality, mitigate interference, and augment data rates. In the context of 5G networks, Multiple-Input Multiple-Output (MIMO) technology is commonly utilized, wherein a multitude of antennas are employed to cater to the needs of multiple users concurrently. This technological advancement improves the total capacity and dependability of networks, hence guaranteeing the fulfillment of high-speed, low-latency connectivity as promised by 5G networks. But the use of a greater number of antennas

resulted in an increase in the total size of the antenna construction. Therefore, the microstrip patch antenna emerges as the most viable option for use with the MIMO technology in order to circumvent this issue. Microstrip patch antennas play a crucial role in enabling effective and adaptable wireless communication within the framework of 5G and MIMO systems. The small and simple design of these antennas, together with their simplicity of integration into a wide range of devices, is well recognized. The adaptability of microstrip patch antennas enables engineers to create antennas that are specifically designed to meet the demands of particular frequency bands, bandwidths, and polarization needs. This level of customization is of utmost importance in the multifaceted realm of 5G communication. Due to their small dimensions, these devices are deemed appropriate for integration within smart phones, tablets, and other interconnected gadgets. Moreover, the capacity to function across many frequency ranges is in accordance with the multi-band specifications of 5G networks. In the field of literature, scholars employ various methodologies such as fractal geometry, insertion slots, slits, notches structures, diverse feeding approaches, and faulty ground structures etc to enhance the bandwidth, gain, and efficiency of microstrip patch antennas, while also achieving compactness and multiband features.

The primary goal of this thesis is to build two antennas prototypes optimized for mobile 5G networks, one operating in the mid-band and the other in the millimeter range. The first antenna is a modified circular disk-shaped microstrip patch antenna with multiband and wideband resonance characteristics has been developed for use in 5G mid band mobile applications. The proposed antenna incorporates a number of circular slots, the radii of which are optimized through a variety of iterative processes in order to realize the resonant frequency bands that are sought while maintaining a satisfactory impedance match. The proposed antenna receives its feeding via a recessed microstrip line that has a basic plane ground configuration. The HFSS electromagnetic simulation software was used to carry out the antenna modeling and corresponding simulation studies. In terms of differences in the thickness of the substrates, feeding techniques, substrate material and the number of design iteration stages, a comprehensive parametric analysis has been

carried out. The suggested antenna is innovative due to its multiband characteristics and increased wide operational bandwidth in a compact size without a monopole or any ground plane deflection. The prototype of the intended antenna was constructed on a 33.56 × 33.56 mm^2 physical foot print of FR-4 substrate and measured using vector network analyzer to corroborate the simulated findings. This was done so that the designed antenna construction could be validated. The suggested antenna has a resonant frequency of 3.35 GHz, 8.84 GHz, 12.62 GHz, and 15.68 GHz, with a reflection coefficient of -17.01 dB, -21.93 dB, -14.68 dB, -35.49 dB, and -20.63 dB, and an impedance bandwidth (IBW) of 100, 630, 540, 990, and 6390 MHz, respectively. In addition to this, the developed antenna exhibits characteristics of a steady radiation pattern as well as an attractive gain over the frequency band in which it operates. The recorded measured results are in good agreement with the results of the simulation. Because of its miniaturized size, good radiation parameters, and capability to handle numerous operating bands while maintaining good impedance matching and improved bandwidth, the antenna that has been suggested is appropriate for use in 5G applications.

The second antenna provides a comprehensive description of a MIMO antenna designed for 5G mm-wave mobile applications, utilizing fractal-based principles and micro-strip feeding. The proposed configuration consists of a fractal-based spherical structure that comprises spherical slots of varying iterations on the patch, along with rectangular slots on the ground plane. The purpose of these additions is to mitigate the phenomenon of patch isolation. The MIMO antenna under consideration consists of two closely spaced antenna elements that exhibit resonance at numerous frequencies within the range of 8 to 28 GHz. Specifically, these frequencies are 9.5 GHz, 11.1 GHz, 13.4 GHz, 15.8 GHz, 21.1 GHz, and 26.6 GHz. The operational frequency range of the antenna extends from 17.7 GHz to 28 GHz, with a bandwidth of 10300 MHz. Therefore, it is highly suitable for implementation in the millimetre wave (mm wave) domain, particularly for the 5G new radio frequency band n258. Additionally, it provides partial coverage for other frequency bands, namely X (8.9 - 9.9 GHz, 10.4 - 11.4 GHz) and Ku (13.1 - 13.7 GHz, 15.4 - 16.2 GHz). The isolation levels of all the resonating bands fall below the permitted

threshold of ($|S_{12}|$>-16 dB). The antenna under consideration employs a FR4 material with dimensions of 28.22 mm × 44 mm. A study is undertaken to assess the efficacy of several factors of the antenna, encompassing radiation pattern, surface current distributions, and S parameters. Moreover, a comprehensive analysis and assessment are carried out to evaluate the effectiveness of the diversity system inside the Multiple-Input Multiple-Output (MIMO) framework. This assessment involves the examination of important performance measures, including the envelope correlation coefficient (ECC), diversity gain (DG), and mean effective gain (MEG). The antenna characteristics have been assessed and found to fall within an appropriate range for the proposed MIMO configuration. The antenna design was subjected to experimental validation, and the simulated results were subsequently confirmed.

ACKNOWLEDGEMENT

I would like to express my deep gratitude and appreciation to all those who have contributed to the completion of this Ph.D. thesis. This journey has been challenging and rewarding, and I could not have achieved this milestone without the support and assistance of many individuals and organizations.

First and foremost, I am profoundly thankful to my supervisor, Dr. Praveen Kumar Malik, for their unwavering guidance, patience, and mentorship throughout the entire research process. Their insights and expertise have been invaluable, and I am truly fortunate to have the opportunity to work under their supervision. I would also like to thanks my Co-Supervisor's Dr. Sudipta Das, their role as my co-supervisor has been instrumental in enriching the scope of my research and providing me with an alternative perspective. The strength of this thesis was greatly enhanced by their generosity with their time, knowledge, and attitude of cooperation.

I would like to express my gratitude for the infrastructure and facilities offered by the School of Electrical and Electronics Engineering at Lovely Professional University, as well as the research department for their assistance in guiding me in a timely manner with regards to norms and rules.

I express profound gratitude to my parent institution, Jawaharlal Nehru Government Engineering College, Sundernagar (H.P), for the consistent support, encouragement, and provision of software and hardware resources during my Ph.D. journey. Along with this, many thanks to Antenna Fidelity Solutions, Bangalore, India for providing the testing facility for the fabricated antennas.

I am extremely grateful to my parents, sister, brother-in-law and in-laws for their support throughout the duration of my research. Mridul, my husband, who has always stood by my side during the most difficult moments of my life and encouraged me to complete my research, and Bhaavya & Divisha, my beloved daughters, who are one of my most cherished sources of inspiration and happiness.

TABLE OF CONTENT

LIST OF FIGURES

LIST OF TABLES

LIST OF ABBREVIATIONS

5G - Fifth Generation

NR - New Radio

FR - Frequency Range

ITU - International Telecom Unit

SISO - Single Input Single Output

MIMO - Multiple Input Multiple Output

MM - Millimeter

ECC - Envelope Correlation Coefficient

DG - Diversity Gain

MEG - Mean effective Gain

TARC - Total Active Reflection Coefficient

CCL - Channel Capacity Loss

MPA - Microstrip Patch Antenna

VSWR - Voltage Standing Wave Ration

BW = Bandwidth

DGS - Defective Ground Structure

DSR - Dual Square Ring

UWB - Ultra Wideband

CMA - Character Mode Analysis

MRC - Maximum Ratio Combining

SCSRR - Slotted Complementary Split-Ring Resonator

TCM - Theory of Characteristic Mode

HFSS - High Frequency Structure Simulator

VNA - Vector Network Analyzer

IBW - Impedance Bandwidth

CHAPTER 1

INTRODUCTION

The wireless technology essentially relies on the transmission and reception of information through the use of radio waves rather than cables and wires. Using a variety of electronic devices such as computers, tablets, mobile phones, pagers, and the like, billions of people are able to communicate with one another and share information, thanks to the development of wireless technology [1]. At this point, every organization is either sharing information or accessing it through a digital network. The market for wireless technology has had rapid expansion over the course of the most recent few years, and projections indicate that this method will continue to expand at a rate of twenty-five percent over the next ten to fifteen years. The wireless technology that is available now has the capability of reaching almost anywhere on this planet. It is anticipated that the volume of mobile information traffic would increase by 45 percent over the next few years, which will translate to a tenfold increase between 2016 and 2023 [2]. This swift progress is being made with the goal to make phone and data services available at any time and in any location. Despite the fact that wireless technologies have been in use since the 1970s, the growing demand for wireless networking technology has prompted researchers to focus their efforts on developing faster wireless communication systems. These systems will not only boost the capacity of the system but also give a higher data transfer rate. The best choice for a high-speed wireless communication system is 5G technology.

1.1 Fifth Generation Mobile Technology

The utilization of 5G technology enables the instantaneous transmission and reception of signals. This technology will enable the rapid downloading of documents. The advent of instant communication technologies has revolutionized the way individuals and organizations interact with their colleagues, friends, and clients. This advancement has eliminated the challenges associated with dropped calls and poor connections [3]. The fifth generation (5G) of wireless networks effectively addresses the current requirements of seamless coverage, improved bandwidth, minimal latency, large data rates, and dependable communication. The utilization of 5G technology

enables the interconnection of numerous devices at a rapid pace. The frequency bands allocated for 5G New Radio (5G NR) band are categorized into two distinct frequency ranges [4]:

- The initial frequency range, known as Frequency Range 1 (FR1), includes all frequencies below 6GHz.
- Another frequency range, known as Frequency Range 2 (FR2), encompasses frequency bands ranging from 24.25 GHz to 71.0 GHz.

Table 1.1 Frequency range 1 (FR1) bands [5]

Frequency (MHz)	**Band**
470 - 698	n71
698 - 960	n5, n8, n12, n15, n20, n25, n28, n29, n81 - n83, n89, n91 - n94
1427 - 1518	n50, n51, n74 - n76, n91 - n94
1710 - 2025	n1 - n3, n 34, n39, n65, n66, n70, n84, n86, n95
2110 - 2200	n65, n66
2300 - 2400	n30, n40
2500 - 2690	n7, n38, n41, n90
3300 - 3400	n77, n78
3400 - 3600	n48, n77, n78
3600 - 3700	n48, n77, n78
3700 - 4200	n77
4400 - 4990	n80

As per the telecommunications regulatory body, predominant attention has been directed towards the 3.5 GHz frequency range (specifically 3.3 - 3.8 GHz) in order to facilitate the early deployment of 5G networks. Subsequently, there has been a subsequent allocation of mm wave spectrum in the 26 GHz and 28 GHz bands [6].

Table 1.2 Frequency range 2 (FR2) bands [7] [8]

Frequency (GHz)	Band
28	n257
26	n258
41	n259
39	n260
28	n261
47	n262
60	n263

The antenna is a crucial element in a 5G device, necessitating operation at increased gain, wider bandwidth, and reduced radiation losses. The design of an antenna assumes significant importance in order to attain the aforementioned characteristics. According to the reference provided [4], the design of 5G antennas can be broadly categorized into two classifications i.e. Input output ports and antenna type as shown in Figure 1.1.

1.2 Input Output Port

The system is partitioned into a port with a single input and single output (SISO) and a port with multiple inputs and multiple outputs (MIMO) for the antenna.

1.2.1 Single Input Single Output (SISO) System

A single antenna is employed for transmission and another for reception, rendering the design and implementation process straightforward in SISO system. Furthermore, it can be seamlessly included into 5G communication equipment. However, while operating in frequency bands above 6 GHz, the signal experiences significant propagation losses and a decline in signal quality [4]. This is because the free-space path loss is proportional to the square of the frequency. Higher frequencies thus experience greater losses over the same distance compared to lower frequencies. Along with this, higher frequency signals are more susceptible to absorption by

atmospheric gases and water vapor. For instance, frequencies above 6 GHz, particularly those in the millimeter-wave bands (30 GHz to 300 GHz), experience significant absorption by rain, humidity, and other atmospheric conditions. This effect is more pronounced at higher frequencies. Even, at higher frequencies, the signal wavelength is shorter, which makes it more likely to be scattered by obstacles and irregularities in the environment. This scattering can cause additional losses and degrade signal quality.

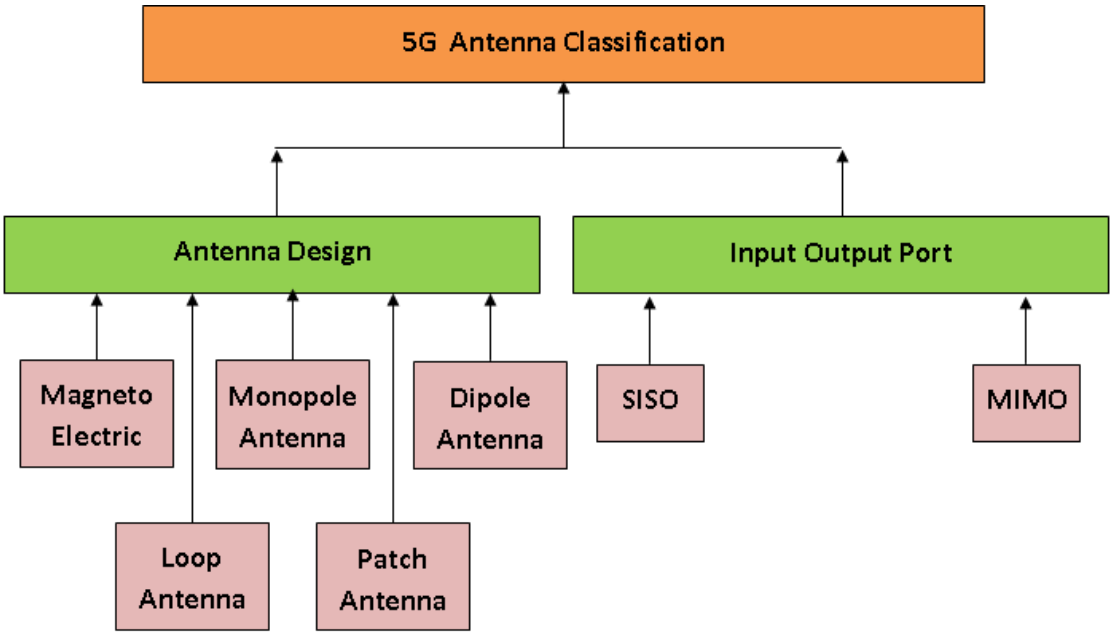

Figure 1.1 Classification of 5G antenna

In order to attain consistent and optimal performance, it is necessary to substitute a singular antenna element with multiple antenna elements.

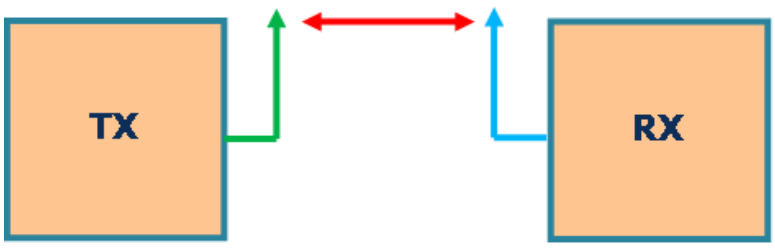

Figure 1.2 SISO Port

1.2.2 Multiple Input Multiple Output System

Wireless communication is susceptible to various challenges like interference,

multipath fading, and radiation losses. Moreover, the challenges become more critical as the frequencies increase. In order to address these challenges, the incorporation of MIMO antennas assumes significant importance as it effectively extends the broadcast coverage without necessitating an increase in signal power. Basically, MIMO, is a wireless communication method that employs multiple transmitters and receivers to facilitate the concurrent transmission of a greater amount of information [9]. The process involves the division of a singular data stream into numerous distinct streams, which are then sent using multiple antennas. This technique greatly improves the performance of a specific channel due to the use of multiple antennas. In this technological context, the inclusion of each pair of antennas leads to an automatic rise in the output of the channel.

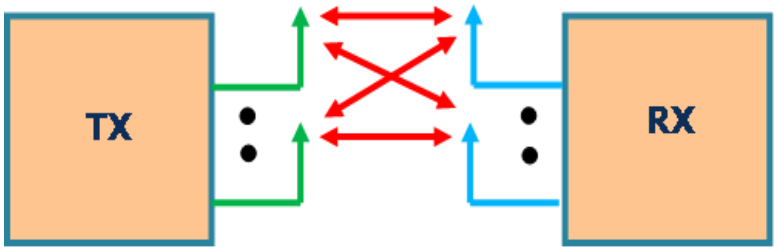

Figure 1.3 Multiple input multiple output port

MIMO technology has emerged as a highly significant wireless approach in recent years. The utilization of MIMO systems enhances the reliability of the communication link, resulting in a reduction in the occurrence of fading phenomena [10]. Therefore, the utilization of MIMO design in the context of 5G can facilitate the attainment of reduced latency, enhanced throughput, and improved efficiency.

Wideband Multiple Input Multiple Output Antenna System

Wideband MIMO, is a wireless communication method that makes use of numerous antennas in order to send and receive signals across a wide frequency range. This strategy improves data speed and reliability by enabling the simultaneous transmission of numerous data streams. It does this by utilizing both spatial diversity and frequency diversity. Wideband MIMO antennas are designed to operate across a wide frequency range while supporting several communication standards. It provides additional bandwidth, allowing for faster data rates and more adaptable applications across several systems. The development of wireless communication technology is

significantly aided by the utilization of both wideband MIMO and standard MIMO antennas. While MIMO antennas improve data capacity and signal reliability, wideband MIMO antennas provide flexibility across different frequency bands Together, they make it possible for wireless communication to be as effective and reliable as possible across a wide range of applications, like 5G, mobile devices and many more.

By amalgamating the attributes of both MIMO and wideband functionalities into a singular design, adaptable antennas may be developed that proficiently satisfy the requirements of modern wireless communication systems.

1.2.2.1 MIMO Diversity Technique

The frequency diversity, time diversity, and antenna diversity are commonly employed techniques to mitigate the spatial correlation between antennas and to create signal replicas for the aim of enhancing diversity. This section exclusively focuses on antenna diversity approaches, such as pattern, polarization and spatial, as they pertain to the subject matter of this thesis. All multi-element antennas use these diversity strategies in order to attain great performance when employed in MIMO systems.

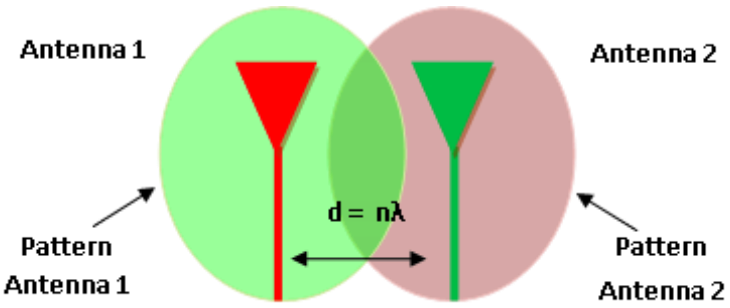

Figure 1.4 Spatial diversity

- **Spatial Diversity**

Spatial diversity is the most elementary and prevalent representation of diversity in wireless communications, as illustrated in Figure 1.4. The introduction of antennas at distinct spatial locations enables the utilization of phase delay to achieve uncorrelated fading signals between the second antenna and the first antenna. To attain satisfactory

decorrelation, it is necessary for the antennas to be spaced adequately, taking into consideration environmental factors, such as multipath angle of arrival width. Previous research has demonstrated that in metropolitan areas, a distance of at least 10λ is necessary to achieve complete decorrelation. Conversely, in indoor environments characterized by rich scattering, a minimum spacing of 0.5λ suffices, as indicated by [11].

- **Polarization Diversity**

Polarization diversity is a method employed in MIMO wireless communication systems with the objective of enhancing the dependability and efficiency of wireless connections. This technique offers notable enhancements in terms of data throughput and resilience against fading and interference. Polarization diversity enhances the aforementioned concept by leveraging the polarization properties of electromagnetic waves [12]. Electromagnetic waves possess both amplitude and polarization properties. Typical polarizations encompass horizontal (H) and vertical (V), however alternative polarizations such as circular or diagonal may also be employed.

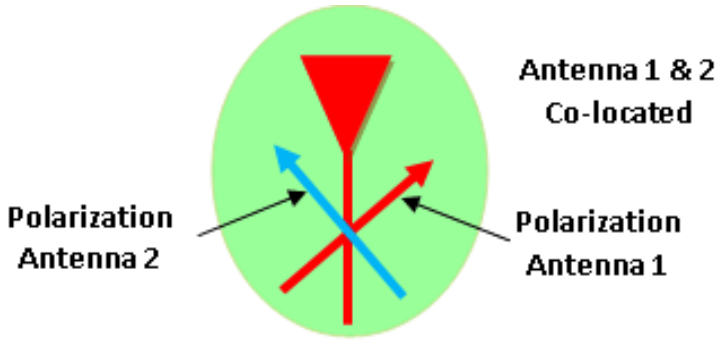

Figure 1.5 Polarization diversity

Polarization diversity involves the utilization of antennas that are equipped with distinct polarizations as shown in Figure 1.5. The transmitter simultaneously transmits data using various polarization antennas. Similar to this, the receiver gathers and combines the incoming signals using antennas with various polarizations. The receiver can enhance signal quality and raise the likelihood of correctly decoding the transmitted data by doing this. The process of combining can be executed using a range of strategies, including maximal ratio combining (MRC) and selection combining [13]. It is noteworthy to mention that the utilization of polarization

diversity is frequently employed in conjunction with spatial diversity within multiple-input multiple-output (MIMO) systems, hence enhancing overall performance.

- **Pattern Diversity**

The potential for significant diversity gain arises when many antennas exhibit distinct radiation patterns. Having multiple antennas in close proximity to one another that radiate in different directions is what is meant by "pattern diversity" in an antenna system. Antenna patterns encompass the characteristics of directionality and gain shown by the antenna over various spatial angles. Several typical antenna patterns that are commonly encountered in the field include omni-directional, directional, and sectorized patterns. In pattern diversity, the transmission of data is facilitated by the utilization of antennas with distinct radiation patterns in a concurrent manner [14]. At the receiver, antennas with distinct patterns are utilized to gather incoming signals originating from diverse spatial orientations. Each antenna is designed with a distinct pattern that is optimized for capturing signals from particular directions. The selection of these patterns aims to maximize diversity in order to enhance signal reception.

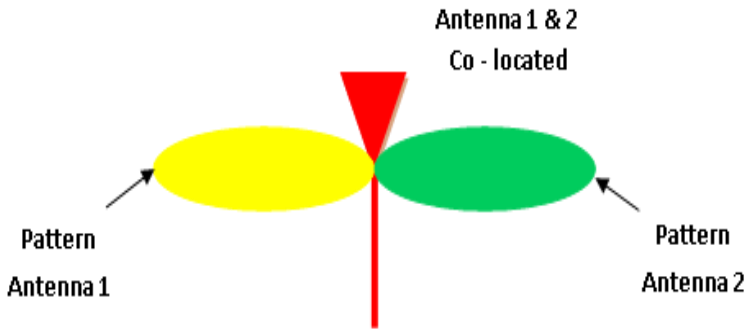

Figure 1.6 Pattern diversity

At the recipient end, the signals obtained from antennas exhibiting distinct radiation patterns are integrated. This can be achieved through the utilization of several strategies, including but not limited to maximal ratio combining (MRC), selection combining, or other diversity combining methods. The amalgamation of signals originating from diverse patterns contributes to the enhancement of signal quality and augments the probability of effectively deciphering the transmitted data.

1.2.2.2 MIMO Key Parameters

The adoption of MIMO technology has caused a dramatic shift in the focus of research towards the creation of several antennas at both the transmitter and the reception portion. The implementation of many antennas in compact sizes presents new design challenges, and furthermore, introduces additional performance criteria compared to a standard single antenna system. In order to fully characterize MIMO antennas, it is necessary to include many metrics. These metrics include overall radiation efficiency, radiation patterns, reflection coefficient, and operating bandwidth, which are commonly used for single antenna analysis. However, additional metrics like as ECC, DG and MEG have been introduced to account for the unique characteristics of MIMO antennas.

- **Envelope Correlation Coefficient (ECC)**

ECC assessment is important to assessing antenna system component isolation. ECC can be calculated by two methods depending on antenna configurations. The main method uses antenna component far field emission patterns and in second method, S parameters are used which is a simpler strategy that uses fewer processing resources. The second way is often, making the s-parameter approach the best. The value less than 0.05 is recommended criterion for ECC [15]. The equation presented employs s-parameter techniques for MIMO systems comprising two elements.

$$ECC = \frac{|S_{11}^{*}\, S_{12} + S_{21}^{*}\, S_{22}|^2}{(1-|S_{11}|^2-|S_{21}|^2)(1-|S_{12}|^2-|S_{22}|^2)} \quad (1.1)$$

- **Diversity Gain (DG)**

The evaluation of the effectiveness of diversity can be measured using a quantitative metric called diversity gain, as defined by equation (1.2). For optimal practical implementation, the value more than 9.95 dB is recommended criterion for DG [16].

$$DG = 10\sqrt{1 - ECC^2} \quad (1.2)$$

- **Mean Effective Gain (MEG)**

Mean Effective Gain (MEG) compares diversity antenna power to isotropic antenna output under fading conditions. [17]. The computation is performed using equation (1.3),

$$MEG_i = 0.5\,\{1 - \sum_{j=1}^{k} |S_{ij}|^2\} \quad (1.3)$$

In this context, the variable "i" is used to denote a specific antenna being discussed, whereas the variable "k" represents the total count of antennas.

$$MEG_1 = 0.5\,\{1 - |S_{11}|^2 - |S_{12}|^2\} \quad (1.4)$$

$$MEG_2 = 0.5\,\{1 - |S_{21}|^2 - |S_{22}|^2\} \quad (1.5)$$

As shown by the citation [18], For best diversity performance, the suggested two-port element antenna's MEG1/MEG2 ratio should not exceed 3 dB.

1.2.2.3 Benefits of MIMO System

1. Improve data rate.
2. Improve coverage area.
3. Excited by the same radio energy as that of single antenna.
4. Improve the reliability of connections that are less fading.
5. Redundancy of system gets improved.

1.2.2.4 Concerns in MIMO System

MIMO systems improve communication, reliability and capacity; however they raise several issues, such as;

1. Real-world capacities are lower due to antenna correlation, inaccurate channel estimate, and potential synchronization issues.
2. Equipment size and processing capacity are the key limitations.
3. The price of equipment grows with number of antenna used.

Another significant approach to classification might be founded on the many types of antennas, as illustrated in Figure 1.1.

1.3 Antenna Types

According to reference [4], various types of antennas have been identified as being suitable for 5G applications. These include:

Monopole Antenna

A quarter-wavelength microstrip line is employed in the structure. According to the existing literature, several modifications have been suggested to alter the fundamental

structure into different forms such as conical, spiral, and others based on specific uses and needs. It is easy to design and build but requires more ground surface and performs poorly in bad weather [19], [20].

Dipole Antenna

The structure is comprised of two microstrip lines that are straight and have a length of λ/4. The feeding mechanism is positioned between these two microstrip lines. The overall length of a dipole antenna is equal to half of the wavelength (λ/2). Design and fabrication are easy, but long-range communication is not suggested [21], [22].

Magneto Electric Antenna

A planar magnetic dipole and planar electric dipole make up this structure. The magnetic dipole is fed from the underside of the substrate. It has a wider bandwidth but is complicated and expensive to make [23], [24].

Loop Antenna

The structure is comprised of a ring shape, which might be circular, rectangular, square, or any other geometric form Loop antennas have a smaller radius than wavelengths. It is simple to design but cannot meet 5G specifications as a single loop [3].

The development of a MIMO antenna for 5G devices, such as contemporary wireless devices including laptops, phones, and tablets, necessitates the utilization of compact antenna designs due to the limited space available within these devices. Microstrip patch antennas have gained significant appeal in the design of MIMO antennas due to its advantageous characteristics such as lightweight construction, low profile, cost-effectiveness, ease of mass production, and simplified installation. This section of the thesis exclusively focuses on microstrip patch antenna as it pertains to the subject matter at hand, among all the other 5G antenna types.

1.3.1 Microstrip Patch Antenna

In today's world, there exists a substantial demand for an antenna that possesses compact dimensions, lightweight composition, superior operational capabilities, effortless installation, and streamlined design. The microstrip antenna is considered

the most suitable choice that satisfies all essential criteria [25]. The structure has 3 No's layers: the bottom plane (last layer), dielectric substrate (middle layer), & radiating patch (top layer) (Figure 1.7). A copper patch is usually the top layer, sandwiched between a dielectric substrate layer and a conductive ground plane. [26]. The radiating patch can assume several geometric shapes, such as rectangular, triangular, circular, elliptical, or ring-shaped configurations. Microstrip patch antennas emit due to fringing fields between the patch edge and the ground plane. [27].

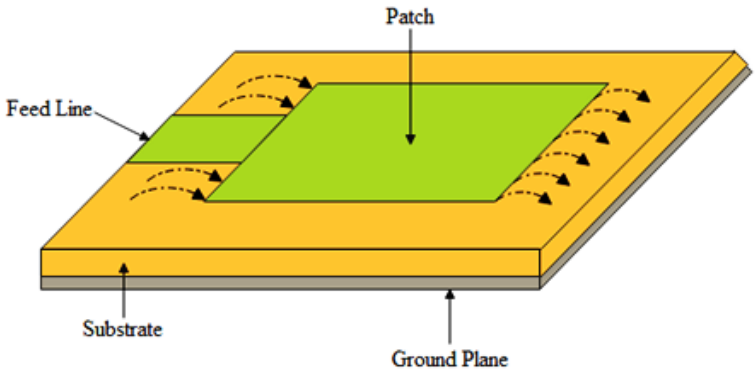

Figure 1.7 Microstrip Patch Antenna

1.3.2 Feeding Techniques

Contacting and Non-contacting are the main feeding methods for MPA. A microstrip wire sends RF power to the radiating patch in the first way. Power is transferred between the microstrip line and radiating patch using electromagnetic field coupling in latter method. [11]. The microstrip line, coaxial probe, aperture coupling, and proximity coupling are widely employed feed techniques in many applications. These techniques encompass both contacting schemes, such as microstrip line and coaxial probe, as well as non-contacting systems, such as aperture coupling and proximity coupling.

1.3.2.1 Microstrip Line Feed

Figure 1.7 shows a conducting strip attached directly to the Micro-strip patch edge in this feed. Etching the feed on a comparable substrate creates a planar structure, making this feed configuration advantageous. [27]. Compared to the patch, the

conducting strip is narrower. The junction inset cut in the patch matches the feed line and patch input impedances without a matching device.

1.3.2.2 Coaxial Probe Feed

In coaxial probe feed, the inner conductor of the cable crosses the dielectric material and solders to the radiating metal patch. As seen in figure 1.8, the ground plane connects to the cable's outer conductor. [28]. One of the main advantages of this feeding method is its ability to set the feed at any location on the patch, hence allowing for the matching of cable impedance with the antenna input impedance. This particular feeding method yields a minimal quantity of extraneous radiation [29]. However, a notable limitation of this approach is its limited bandwidth and the challenges associated with its modeling. This is due to the requirement of drilling a hole in the substrate, which allows the connector to extend beyond the ground plane. Moreover, when dealing with substrates of greater thickness, an elongation of the probe length leads to a higher degree of inductance in the input impedance, hence resulting in impedance matching challenges.

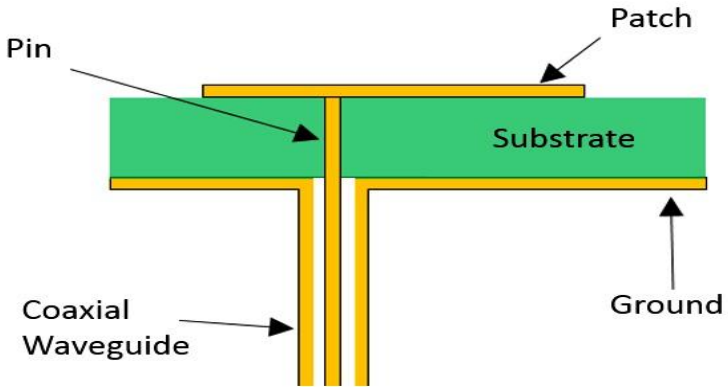

Figure 1.8 Coaxial Probe feed

1.3.2.3 Aperture Coupled Feed

A slot or aperture in the ground plane joins the radiating patch and microstrip feed line in Figure 1.9. Due to configuration symmetry and decreased cross-polarization, the coupling aperture often appears under the patch. Feed line-patch coupling varies on aperture position, shape, and size. The ground plane between the patch and feed line reduces spurious radiation. Bottom substrates have strong dielectric and top substrates are thick and low dielectric constant to maximize patch radiation. Multiple

layers increase antenna thickness and are difficult to make. This feeding method has restricted bandwidth [30].

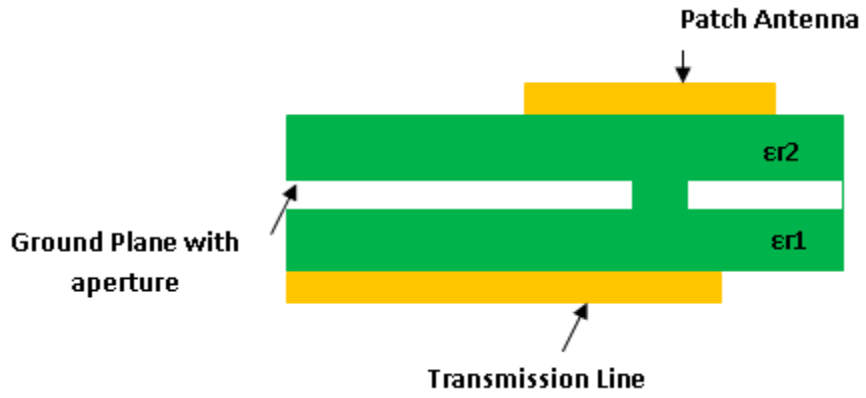

Figure 1.9 Aperture Coupled feed

1.3.2.4 Proximity Coupled Feed

This feed method is called electromagnetic coupling. Figure 1.10 shows two dielectric substrates with the feed line between them and the radiating patch on top. This feed method eliminates spurious radiation and provides high bandwidth. (as high as 13%) [31], due to microstrip patch antenna thickness enhancement. Fixing feed line length and patch width-to-line ratio matches. This feed method is difficult to build because two dielectric layers must be aligned. Also, antenna thickness rises.

1.3.3 Microstrip Patch Antenna Key Parameters

Parameters must be defined to describe antenna performance. Bandwidth, radiation pattern, gain, input impedance, efficiency, polarization, VSWR and others are often utilized antenna properties.

Bandwidth

The operational effectiveness of an antenna is determined by its bandwidth, which refers to the range of frequencies within which it can function optimally. The typical characterization of a device is based on the frequency range in which its performance parameters, such as gain and impedance, satisfy the specified criteria.

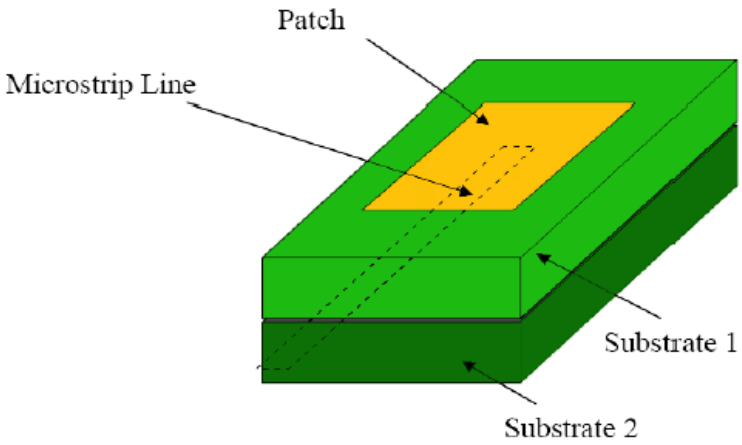

Figure 1.10 Proximity Coupled feed

Radiation Pattern

The characterization of an antenna's electromagnetic radiation in terms of its directionality is referred to as its radiation pattern [32]. This shows how the antenna radiates energy horizontally and vertically.

Directivity

The concept of directivity pertains to the degree of radiation concentration in a certain direction relative to that of an isotropic radiator. The term is frequently employed in a manner that is interchangeable with the concept of gain.

Gain

The concept of antenna gain pertains to the capacity of an antenna to concentrate or steer its emitted power in a specific direction [33]. Typically, it is denoted in decibels (dBi or dBd).

Input Impedance

Antennas possess an input impedance that necessitates alignment with the impedance of the transmission line and accompanying equipment, often set at 50 ohms or 75 ohms in numerous instances [34]. Ensuring a correct impedance match is essential for achieving optimal power transfer.

Efficiency

Antenna efficiency is its ability to convert electrical power into electromagnetic waves. Increased efficiency results in reduced power loss inside the antenna structure.

Polarization

Antennas have linear, circular, or elliptical polarization. [35]. Ensuring the alignment of the polarization between the transmitting and receiving antennas is crucial in facilitating optimal signal transmission.

Voltage standing wave ratio (VSWR)

VSWR measures the impedance matching of an antenna, transmission line, and transmitter or receiver. A decreased Voltage Standing Wave Ratio (VSWR) signifies an improved impedance match and reduced signal reflection.

1.3.4 Benefits of Patch System

1. Operations in several frequency bands are possible.
2. Light weight and very thin antenna.
3. Easily made using low-cost materials like FR4.
4. Ease of manufacturing process.

1.3.5 Concerns in MIMO System

1. Limited bandwidth.
2. Inadequate Efficiency.
3. Minimal Gain.

Microstrip antennas have some significant limitations, including a restricted bandwidth, poor efficiency, and low gain. Various techniques are employed to address these limits, including the application of fractal geometry (iterations), it is mostly employed to characterize composite forms within a family that exhibit self-similarity in their geometric structure [35], the incorporation of slot insertion [36], the implementation of shorting pins [37], and defective ground structure [38].

1.4 Motivation

With the accelerated development of wireless technology, every organization now

shares or accesses digital network information. Over the course of the last few years, the market for wireless technology has expanded at a rapid rate. The greatest way to meet the need for the fastest wireless technology is with networks of the 5G (Fifth Generation) generation. It is an emerging mobile technology that has the potential to completely transform economies, societies, and the way people live their hectic lives. For the design and operation of 5G networks, antennas assume a pivotal role. The role they play is of utmost importance in facilitating the essential features and capabilities of 5G technology. Antennas connect the physical world to the wireless network. They are accountable for transmitting network signals to user devices and receiving network signals from user devices. In 5G, antennas must effectively transmit and receive signals across a broad spectrum of frequencies. The 5G New Radio (5G NR) bands are divided into two separate frequency ranges: FR 1, which covers the sub 6 GHz band (Mid Band), and FR 2, which includes frequency bands spanning from 24.25 GHz to 71.0 GHz, commonly referred to as the millimeter band (MM band). The design of antennas necessitates their effective operation throughout diverse frequency bands and the ability to accommodate fluctuating frequency demands. Prior to the implementation of a 5G network, it is important to ascertain the technological aspects and the specific type of antenna employed for the network. In the context of the sub 6 GHz band, it is recommended to employ SISO technology for the construction of 5G antennas. This choice is motivated by several factors, including its lower complexity, reduced hardware cost, enhanced spectrum efficiency, less interference, and compatibility with pre-existing infrastructure. In the context of the millimetre (mm) frequency range, the utilization of MIMO technology has heightened significance. The propagation properties of millimeter-wave signals change significantly due to their shorter wavelengths and increased vulnerability to route loss. Consequently, the utilization of spatial diversity and beam forming techniques offered by MIMO systems becomes crucial in order to ensure the preservation of signal quality and coverage. Along with these technologies, type of antenna is also important factor for 5G network. There exists a variety of antennas that are deemed ideal for 5G applications. However, microstrip patch antennas have been the ideal choice for such applications because to their notable advantages, including cost-effectiveness and compactness. Microstrip antennas exhibit certain limitations, including restricted

bandwidth, suboptimal efficiency, and diminished gain. However, according to the findings of the literature review, various techniques have been employed to mitigate these drawbacks. Some of these techniques encompass the utilization of fractal geometry (iteration), which is primarily employed to describe composite forms that demonstrate self-similarity in their geometric structure. Additionally, the incorporation of slot insertion, the utilization of shorting pins, and the implementation of defective ground structure are among the strategies employed to address these limitations. Further, in order to enable the early implementation of 5G networks, the international telecommunication union (ITU) advised that attention be focused primarily on the 3.5 GHz frequency band (more specifically, 3.3 - 3.8 GHz). A subsequent allocation of millimeter wave spectrum in the 26 GHz and 28 GHz bands has taken place. All of these factors motivate me to build antennas for 5G mid and millimeter band applications employing microstrip patch antennas using fractal geometry (iteration technique) in conjunction with SISO and MIMO technology, which provide superior bandwidth, isolation, gain, and other diversity performance factors.

This thesis presents the design, fabrication, and testing of two antennas specifically developed for 5G mobile applications.

The initial antenna has been developed, manufactured, and evaluated for its suitability in 5G mid band mobile applications. This antenna utilizes a single element microstrip patch design using fractal geometry (iteration technique), resulting in improved bandwidth, gain, and efficiency. A second antenna has been developed, manufactured, and evaluated for utilization in the millimeter range (n258 band) of 5G mobile applications. This antenna employs a 2-element MIMO, MPA configuration with a faulty base structure and fractal geometry (iteration technique). It also offers improved bandwidth, gain, and diversity performance factors.

1.5 Research Objective

Research embodied in the present thesis investigates iteration strategies for designing patches of microstrip and MIMO antennas. In order to obtain the appropriate performance characteristics, some parametric studies are carried out in both the

antennas. Additionally, a suitable defective ground structure is adopted and installed at the MIMO antenna in a suitable location to achieve a suitable band for 5G applications. The thesis's objectives are described in this context as follows:

1. To design wideband microstrip antenna for emerging technology Multiple Input and Multiple Output (MIMO).
2. Designing and fabrication of an antenna by optimizing dielectric constant of the substrate, thickness of the substrate and insertion of slots/slits to enhance the bandwidth and efficiency.
3. The antenna will be optimized for the desired performance parameter like gain and return loss.
4. The main prominence will be on the development of compact antenna with better isolation between the multiple antennas.

In order to accomplish these objectives, a quantitative research approach is employed in this study.

1.6 Research Methodology

For achieving objective 1, 2 and 3 following steps were considered:

- **Step 1: Designing** - Microstrip antenna patch is designed using iteration techniques.
- **Step 2: Parametric Analysis** - The parametric effect of various parameters like dielectric constant, thickness of substrate, insertion of slots, feeding techniques of the said antenna is analyzed to achieve desired performance. The proposed antenna is designed and simulated using HFSS 15.0. Once the desired results are achieved as per the literature surveys, then we proceed with fabrication process.
- **Step 3: Fabrication** - Final single element microstrip patch antenna is fabricated using EP-42 Auto PCB prototype machine.
- **Step 4: Testing and Validation** - S_{11} and VSWR are measured using SMA connector connected manufactured antenna to VNA (Rohde and Schwarz ZNB - 40 VNA 100 KHZ to 40 GHz)). In anechoic chamber with broadband reference horn antenna transmitter, antenna radiation

patterns and gain are measured.

For achieving objective 4 following steps were considered:

- **Step 1: Design -** Two port MIMO antenna patch is designed using iteration techniques.
- **Step 2: Analysis and DGS -** Distance optimization, orientation analysis and DGS is introduced to achieve desired performance. The proposed antenna is designed and simulated using HFSS 15.0. Once the desired results are achieved as per the literature surveys, then we proceed with fabrication process.
- **Step 3: Fabrication** - Final two port MIMO antenna is fabricated using EP-42 Auto PCB prototype machine.
- **Step 4: Testing and Validation** - The SMA connector connected the antenna to a VNA (Rohde and Schwarz ZNB - 40 VNA 100 KHZ to 40 GHz) for S parameters measurements. In anechoic chamber with broadband reference horn antenna transmitter, antenna radiation patterns are measured.

1.7 Thesis Organization

The work carried out in this thesis is structured into six chapters as follows:

Chapter 1: This chapter presents an introductory overview of wireless technologies and the 5G system. Additionally, it furnishes information regarding the diverse technologies and sorts of antennas employed in 5G applications. The text offers a succinct summary of MIMO technology and microstrip patch antenna, elucidating the underlying reasons for the research endeavor, and presenting the structure of the thesis.

Chapter 2: This chapter provides an overview of the current state of research in the field of the present work. This literature review focuses on microstrip antennas and their associated approaches for enhancing antenna efficiency, as well as MIMO

antennas and their strategies for improving performance parameters in the context of 5G applications. Additionally, the review addresses the existing research gap in this area.

Chapter 3: This chapter outlines the objectives of the thesis and provides a concise discussion of the strategies employed to accomplish these objectives, including the inclusion of a flow chart.

Chapter 4: This chapter presents a modified circular shaped microstrip antenna designed for fifth generation midband mobile applications. The initial phase involves providing a concise explanation of each step in the antenna design process. This study delves into the parametric analysis of many antenna characteristics, including the impact of substrate height, iterations, substrate type, and feeding procedures on the antenna. Finally, the antenna is manufactured and subjected to testing. The evaluation of the planned antenna's characteristics encompasses the analysis of return loss, gain, efficiency, and radiation patterns. This evaluation is substantiated through the utilization of simulations and measurements for validation purposes.

The created antenna is small, wide-bandwidth, and simple compared to earlier antennas.

Chapter 5: This chapter introduces a modified MIMO antenna for the n258 (5G New Radio (NR) band), which operates at 24.25–27.25 GHz. Firstly, a single patch antenna is constructed and simulated using iterative approaches. After that, a two-element MIMO antenna is developed using optimization analysis, which includes evaluating the spacing between the antennas, the orientation of the antennas, and creating a defect on the ground plane. The antenna design has been successfully implemented and afterwards subjected to fabrication and testing processes. The antenna design exhibits a small physical footprint and demonstrates satisfactory performance, as confirmed through both simulation and experimental analysis. Port isolation, radiation pattern, efficiency, peak gain, ECC, MEG, and diversity gain are evaluated for the MIMO/diversity antenna. The performance of the antenna is evaluated in comparison to other research projects.

The final chapter summarizes this thesis's study and outlines potential avenues for further research.

CHAPTER 2

LITERATURE REVIEW

This chapter presents a comprehensive examination of several studies pertaining to microstrip antenna and MIMO antenna for 5G mid and millimeter band applications. The aforementioned investigations are divided into two distinct sections, namely section 1 and section 2. A variety of methods for designing and achieving the appropriate performance parameters of a microstrip antenna have been covered in section 1 of this chapter. This is followed by Section 2, which explores numerous investigations pertaining to MIMO antennas.

2.1 Microstrip Patch Antenna Design and Techniques

This section covers microstrip patch antenna research. Numerous researchers have used various methods to improve antenna parameters.

Kaur and Malik [39], introduced a novel design of a microstrip antenna with a defective ground plane, featuring an elliptical form patch fractal. The defective ground plane structure is comprised of a rectangular shape with a triangular component positioned above it, along with capacitive steps that have been carved into the structure. Figure 2.1(a) depicts the visual representation of the antenna's configuration. The antenna is 50 mm × 50 mm × 0.8 mm in size. The fractal architecture of the elliptical shape enables the potential for miniaturization. Moreover, the utilization of defective ground structures offers a significant advantage in terms of providing a broad impedance bandwidth of 410 MHz, 1070 MHz and 4840 MHz and increased gain of 5.42, 6.52. 7.67 dBi. Devesh et al. [40], presents a novel design for a microstrip antenna that incorporates a hexagonal gasket fractal structure as a loading element. The design of the antenna involved the implementation of 240 triangles of varying sizes, resulting in four iterations of fractal geometry. Subsequently, the manufactured antenna was used to verify the findings. The application of fractal approach results in a reduction of 68.4% in the area of the patch. The dimensions of the antenna are 50 mm × 50 mm × 1.6 mm. The antenna exhibits resonance at six distinct frequencies, each with a corresponding bandwidth of 75, 151, 192, 358, 137, and 206 MHz. The gain values for these frequencies are 6, 8.37, 9.65, 9, 7.84, 9.34

dB, respectively. The antenna is observed in Figure 2.1 (b). Siddiqui et al. [32], developed an A-shaped triangular microstrip antenna inspired on Koch's snowflake design. The triangle is divided into four line segments on each of its sides. The antenna underwent analysis using the cavity model methodology. The dimensions of the antenna include 80 mm in length, 90 mm in width, and 1.6 mm in thickness. The antenna in discussion exhibits resonance at five distinct frequencies, specifically 11.44, 13.78, 15.48, 19.90, and 23.52 GHz. These resonant frequencies are accompanied by corresponding return loss values of -19, -27.37, -20.16, -20.74, and -35.52 dB, respectively. Figure 2.1 (c) illustrates the geometric arrangement of the antenna.

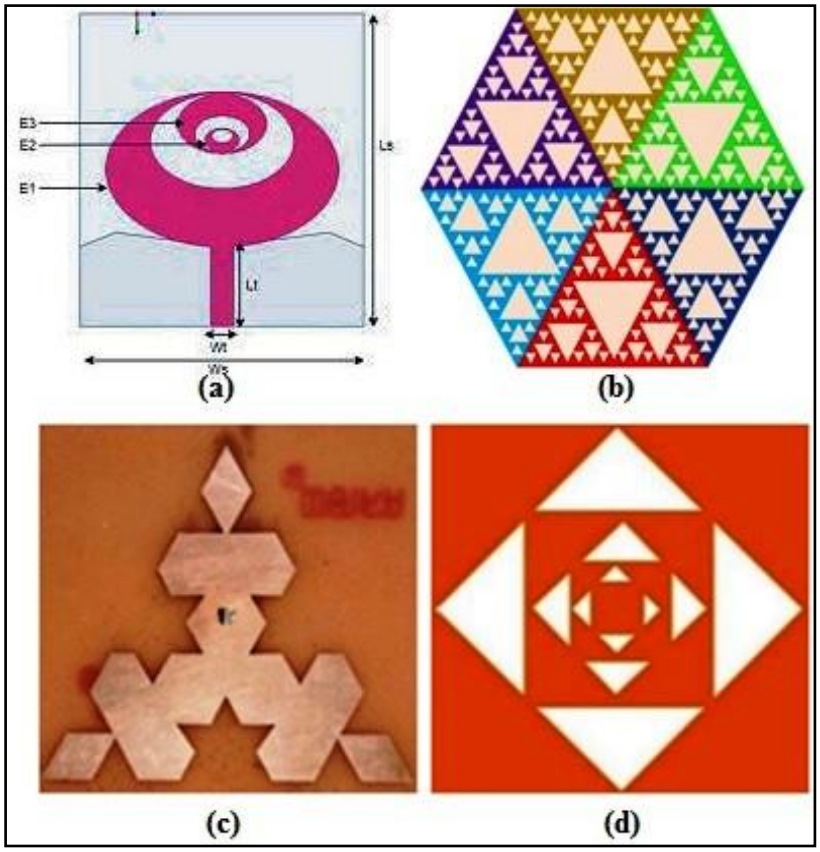

Figure 2.1 (a) Elliptical fractal geometry, (b) Hexagonal gasket fractal geometry [License Number: 5877490199175], (c) Kosh snowflake geometry, (d) Sierpinski triangular fractal geometry [License Number: 5877561357264]

Devesh et al. [41], developed a microstrip antenna using a square Sierpinski triangle fractal design. Triangular slots are loaded within a square patch throughout each

iteration, specifically up to the third iteration. The antenna under consideration comprises of a total of twelve triangular slots, with four slots per stage and three stages in total. The antenna exhibits resonance at frequencies of 15.91, 20.04, 23.07, and 27.77 GHz, accompanied by corresponding S_{11} values of -20, -25, -22, and -28 dB, respectively. The suggested antenna exhibits gain values of 6.81 dB, 7.91 dB, 7.32 dB, and 8.89 dB at the specified resonating frequencies. The geometric configuration of the antenna being considered is depicted in Figure 2.1 (d). El-Khamy et al. [42], designed a multiband fractal antenna for Ultra-Wideband (UWB) and 5G applications. Initial patch design considers first-order structure. This structure has a fundamental circular patch of radius R1. The basic patch is reproduced with a scaling factor of 0.5 to create a second-order structure with three circles with a radius of R2. Finally, scaling the basic circular patch by 0.52 yields nine circles with a radius of R3 for the third order structure. These circles are connected using sub feed lines to improve impedance matching. The suggested antenna is 90 mm × 110 mm × 1.6 mm and has a 9-dB gain with 5300, 2000, 1500, and 3700 MHz bandwidth. Figure 2.2(a) shows antenna setup.

A fractal microstrip patch antenna in the shape of a wheel was created by Gupta et al. [43]. The initial stage of antenna design involves the commencement of the 0th iteration. In this iteration, a circular patch with a radius of 8mm is selected as the foundational element for constructing the fractal antenna. Subsequently, square patches are affixed to the circumference of a circle at an angle of 45 degrees. Additionally, a smaller circle with a radius of 6mm is excised from the aforementioned circle. In the first iteration, a circle with a radius of 4mm, accompanied by a square patch, is appended, while a circle with a radius of 2mm is removed. The antenna increased bandwidth to 6.06 GHz. Figure 2.2 (b) shows antenna setup. Singh et al. [44], propose a circular MPA with a DGS and rectangular slot. The ground is cut semi circularly to improve radiation. The first iteration of the geometric process involves removing a 21-mm slit from the circular patch. In the second generation, two 7-mm slots are cut. Finally, the third generation cuts four 2.33 mm slots. At four frequencies, the antenna resonates with bandwidth of 120, 200, 330,

and 690 MHz with gain of 9.19, 3.04, 5.19, and 5.39 dBi. The antenna is 55 mm × 46 mm × 1.58 mm. Figure 2.2(c) shows antenna configuration.

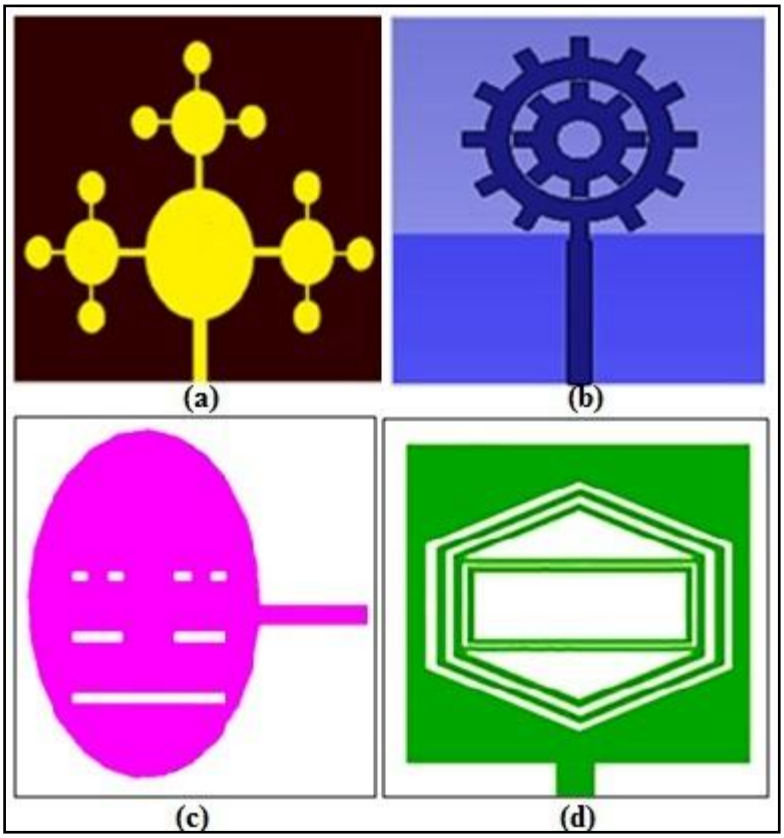

Figure 2.2 (a) Circular fractal geometry [License Number: 5877621446773], (b) Wheel shape fractal geometry [License Number: 5877570129237], (c) Circular fractal geometry with rectangular slot [License Number: 5877630173028], (d) Hexagonal fractal geometry

Anand and Chawla [45], suggest a hexagonal slotted patch antenna design. The improvement in impedance matching and bandwidth is observed as the hexagonal fractals rise in geometric complexity. Furthermore, within the innermost hexagonal slot, a rectangular slot of a self-similar nature is introduced. Moreover, in order to augment the behavior, the rectangular slot is equipped with eight self-similar square-shaped coils. The antenna under consideration exhibits an impedance bandwidth of 530 and 1070 MHz, accompanied by reflection coefficients of -29.38 and -28.19 dB. The proposed antenna arrangement is depicted in Figure 2.2(d). Sharma and Sharma [46], developed two types of antennas: one utilizing the Koch Koch hybrid slot

geometry, and the other employing the Koch Minkowski hybrid slot antenna. The two antennas exhibit resonance at frequencies of 2.77 GHz and 2.46 GHz, respectively. The utilization of an MPA with Koch Koch hybrid slot geometry results in a gain of 5.73 dB and 6.15 dB for the first case antenna, while the second case antenna achieves a gain of 1.57 dB and 5.62 dB. The dimensions of the antenna are 45 mm in length, 38.92 mm in width, and 1.6 mm in thickness. Figure 2.3 (a) depicts the visual representations of the aforementioned antenna.

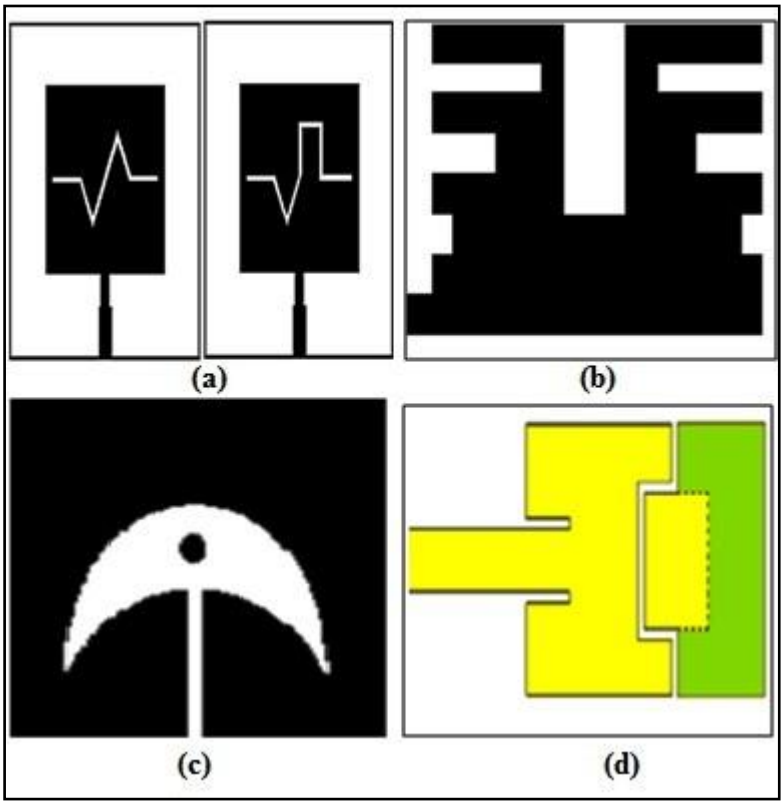

Figure 2.3 (a) Koch Koch & Koch Minkowski hybrid slot geometry, (b) Rectangular slot geometry [License Number: 5877630473877], (c) Circular arc geometry [License Number: 5877630678059], (d) Square shape slot geometry

Verma and Srivastva [47], proposed a design for a triple band rectangular patch micro-strip antenna, which can be utilized in a range of wireless technology applications. The antenna patch under consideration has been constructed by sequentially incorporating rectangular patches of varying dimensions (length and width) above the ground plane in a progressive manner. The antenna initially resonates at a frequency of 1.422 GHz. However, by loading a rectangular slot, the

antenna exhibits resonance at two more frequencies, specifically 1.79 GHz and 2.46 GHz. The antenna's arrangement is depicted in Figure 2.3 (b). Singh et. al [48], proposed design entails a new hexa band circular shape patch antenna that has four inverted L-shape notches. The resonant frequencies that were measured are observed to be 11.6, 13.92, 17.11, 19.47, 21.11, and 23.05 GHz. The measured simulated gains for the antenna at different frequencies are as follows: 7.39 dBi at 11 GHz, 2.25 dBi at 13.3 GHz, 6.65 dBi at 16.6 GHz, 5.83 dBi at 19 GHz, 6.02 dBi at 20.6 GHz, and 7.31 dBi at 22.2 GHz. Meloui and Essaaidi [49], introduced a rectangular patch antenna that incorporates a rectangular slot on its top side, measuring 20 mm × 5 mm. Additionally, two parallel triangular slots are included on the right and left sides of the antenna. The purpose of incorporating these slots is to enhance the performance of the antenna in its dual-band operation. The antenna exhibits resonance at two distinct frequencies, each with unique impedance bandwidths of 500 MHz. The first resonance occurs at 7 GHz, while the second resonance occurs at 10.7 GHz. Furthermore, the antenna maintains stable emission patterns throughout these frequencies. Ang and Chung [50], proposed the concept of a wideband patch antenna in the shape of the letter E. The patch design includes the integration of two parallel slots, which serve the purpose of perturbing the route of the surface current. This perturbation leads to an enhanced bandwidth of 830 MHz, spanning from 5.05 GHz to 5.88 GHz.

Panda and Mishra [51], developed a bi-circular patch antenna. The conventional circular patch is modified to incorporate a distinct geometry characterized by the placement of two circular arcs at a specific distance from one another. In order to increase the available bandwidth, a strategically designed circular slot was constructed at the central location of the arc. The antenna is depicted in Figure 2.3 (c). Sharaf et al. [52] developed an electromagnetically coupled configuration consisting of two rectangular patch antennas, specifically built for the purpose of 5G mobile applications. The dimensions of the first and second patch are designed to enable the first patch to function at a frequency of 38 GHz and the second patch to operate at a frequency of 60 GHz. During the simulation of the antenna, it was observed that the capacitive load of the antenna had grown. In order to mitigate this load, an extension was made to the side of the initial patch. Additionally, cuts are implemented on the

side of the first patch in order to enhance the concentration of surface current on the second patch. Furthermore, a square-shaped gap at the centre and two slots at the corners are incorporated to decrease the area of the second patch.

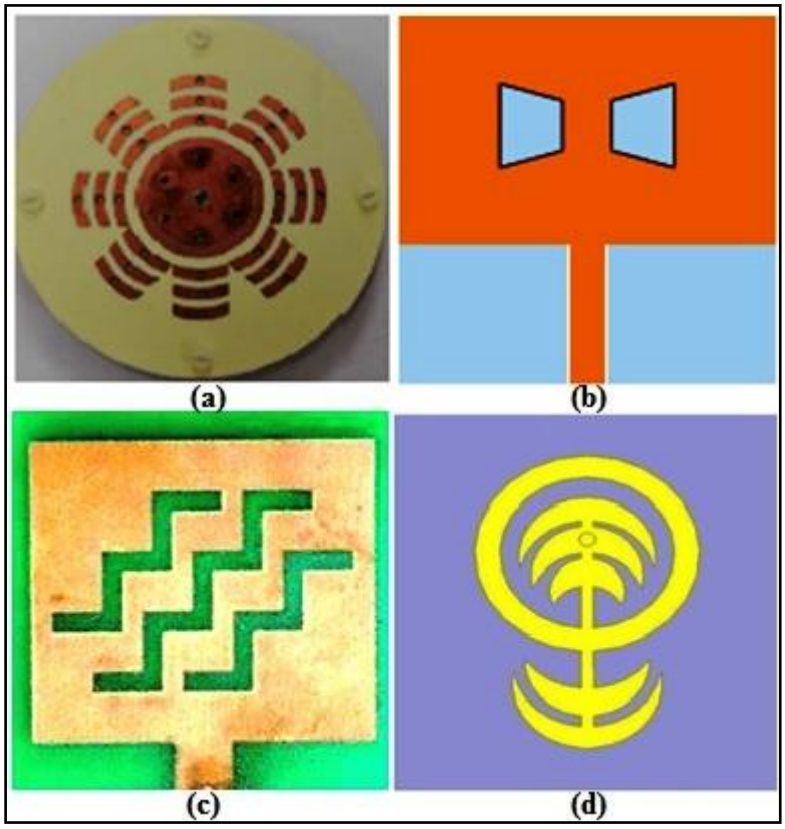

Figure 2.4 (a) Circular slot geometry, (b) Trapezoidal slot geometry, (c) Stepped slot geometry, (d) Crescent moon shape geometry [License Number: 5877570630130]

The geometric configuration of the antenna is depicted in Figure 2.3 (d). Liu et al. [53], proposed a methodology for the design and fabrication of a broadband circular patch shape antenna. The authors incorporated artificial structures into the antenna to effectively boost its gain. In this study, a comparative analysis is conducted between an antenna featuring a single ring and a circular-shaped patch (CPAIR) and an antenna with a single ring, circular-shaped patch, and loaded by three layers of I-shaped structure (CPAIR3I). The utilization of proximity feeding technology, in conjunction with the incorporation of six shorting pins, slots, and rings, enhances the matching quality of the antenna. The depicted configuration can be observed in Figure 2.4(a). The antenna is capable of achieving a bandwidth ranging from 1070 to 1270 MHz, while exhibiting a gain of 1.8 dB. Raviteja [54], introduced a rectangular

microstrip patch antenna (MPA) that incorporates two trapezoidal slots, specifically designed for wireless applications. The study commenced with the simulation of a conventional rectangular antenna, followed by the simulation of the proposed antenna. Subsequently, a comparison was made between the results obtained from the proposed antenna and the conventional rectangular antenna. The antenna in discussion achieves a gain of 9.67 dB. The proposed antenna has dimensions of 25.4 mm × 19.4 mm × 1.6 mm. The geometric configuration of the antenna is depicted in Figure 2.4(b). Babu and Sivakumar [55], developed a suspended stepped slot microstrip patch antenna measuring 50 × 50 mm, specifically designed for potential use in 5G applications. To enhance impedance matching, a coaxial power feed is strategically connected to a predetermined spot on the microstrip feed. The simulation analysis is conducted on two distinct types of ground surfaces. The first ground plane is a basic copper structure, whereas the second ground plane is specifically designed for solar cell applications. The first antenna exhibits resonance at three distinct frequencies, while the second antenna resonates at two frequencies, demonstrating superior bandwidth characteristics. The design of the suggested antenna is illustrated in Figure 2.4(c).

Tumah et al. [56], developed a unique configuration for a microstrip antenna, specifically an annular ring patch, with the Shape of Crescents Moon (SCMs) as a basis. The antenna's performance was assessed through both simulation and measurement, demonstrating its suitability for multiband applications. The design has five separate shape of crescents moon (SCMs) that vary in size. Three of the shape of crescents moon (SCMs) is positioned within the annular ring patch, while the remaining two are situated outside. The antenna that has been fabricated is exhibiting resonance at three distinct frequencies, namely 11.30, 18.07, and 20.72 GHz. The measured bandwidths are 474 MHz, 620 MHz, and 810 MHz, respectively. The antenna is presented in Figure 2.4 (d). Gangwar et al. [57], provide a modified circular ring-shaped slot antenna with dimensions of 48 × 48 × 1.6 mm. This antenna is designed specifically for dual-band wireless applications. The proposed system utilizes two frequency bands: 1.69 to 1.94 GHz and 3.64 to 3.88 GHz. These bands exhibit impedance bandwidths of 14.1% and 6.4% respectively. Figure 2.5 (a) shows the proposed antenna geometry. Kumar et al. [58], introduce a rectangular patch

antenna that is excited by an I-shaped slot and incorporates two shorted metallic vias, as depicted in Figure 2.5 (b). The aforementioned configuration leads to an increase in the available bandwidth. The antenna exhibits resonance at three distinct frequencies, namely 5.27, 5.49, and 5.93 gigahertz (GHz), accompanied by corresponding peak gains of 7.2, 7.1, and 7.0 decibels isotropic (dBi), respectively.

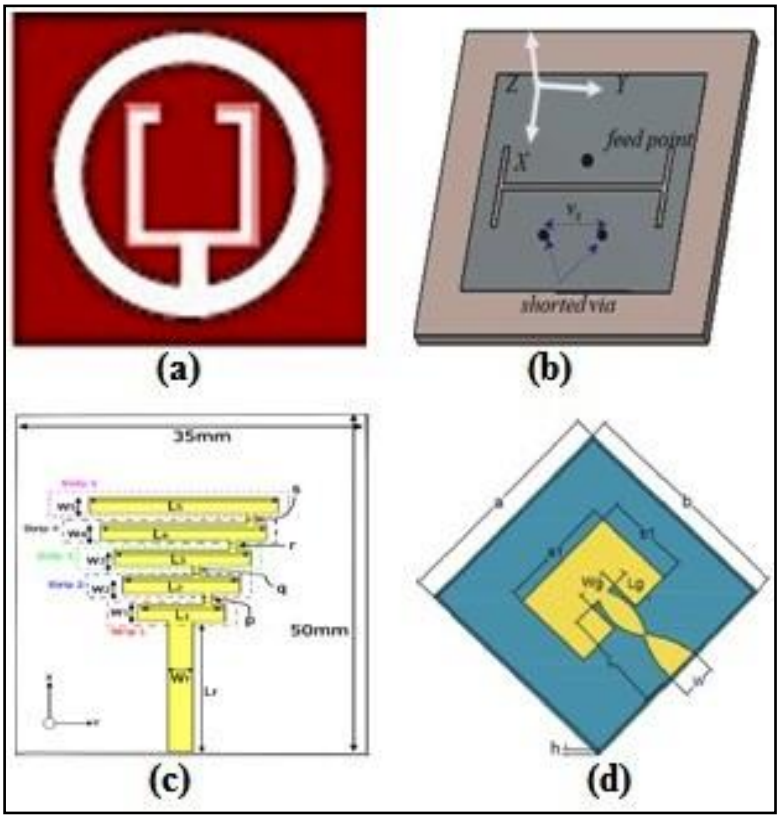

Figure 2.5 (a) Circular and U slot geometry [License Number: 5877640122087], (b) I shaped slot geometry, (c) Rectangular strips geometry, (d) Non uniform transmission line feed antenna

Bag et al. [59], introduce a low profile monopole antenna. The uppermost layer of the substrate is composed of radiating strips arranged in a parallel strip and T-shaped microstrip feed line configuration. The lower surface of the substrate undergoes partial etching, while the remaining portion is preserved as a ground plane. Furthermore, the impedance characteristic is enhanced by the inclusion of two rectangular stubs on the ground plane. The antenna's overall dimensions were 50 × 35 × 1.6 mm. The antenna exhibits resonance at frequencies of 1.61, 2.83, 3.75, 5.24, and 5.56 GHz, with corresponding bandwidth enhancements of 690, 130, 350, 180, and

670 MHz. The gain values for these frequencies are 0.8, 0.75, 0.6, 1.45, and 2.3 dB, respectively. Figure 2.5 (c) shows the antenna geometry.

Farahani and Nezhad [60], introduces a unique wideband microstrip patch antenna that incorporates a non uniform transmission line feed as shown in figure 2.5 (d). Nonlinear model predictive control (NMPC) is employed to attain a non uniform transmission line that aligns with the MPA. The design of the transmission line ensures that the impedance of the input port is matched to the impedance of the microstrip antenna at the resonance frequency and its neighboring frequencies. The antenna resonates at 5.25, 5.5 and 5.75 GHz with 6.5 dBi peak gain. Garcia et al. [61], developed a wideband antenna utilizing a tapered Coplanar Waveguide (CPW) feeding mechanism. An excellent impedance matching was achieved when two trapezoidal ground planes were introduced between the U-shaped monopole structure and the tapering CPW supplied antenna in the design. The antenna under consideration operates within two broad frequency ranges, with central frequencies of 3.3 and 5 GHz. The initial band demonstrated a bandwidth of 0.6 gigahertz, whereas the second band had a bandwidth of 0.75 gigahertz. The designed antenna is present in figure 2.6 (a)

Maurya et al.[62], developed an innovative microstrip patch antenna with a hexagonal ring structure that exhibits circular polarization shown in figure 2.6 (b). The antenna design incorporates an asymmetrical feed mechanism. The ground plane incorporates a semi-arc-shaped slot, while the hexagonal ring is inclined at a 25-degree angle relative to the asymmetric microstrip-line feed. This configuration generates a circularly polarized ultra-wideband signal. The adoption of the asymmetrical feed has resulted in a significant increase in the impedance bandwidth, measuring 134% (equivalent to a bandwidth of 9.55 GHz). This expanded bandwidth ranges from 2.34 to 11.89 GHz, with the centre frequency being 7.12 GHz. The axial ratio bandwidth (B.W) at a 3-dB level is 2.8% (7.1-7.3 GHz) and 21.8% (9.8-12.2 GHz) inside the ultra-wideband (UWB) frequency range. The suggested antenna has an average gain of 4.15 dBi. Chen et al. [63], developed a compact fish-shaped patch antenna that incorporates a tilt-folded patch feed, stepped arms, a U-shaped slot, and a shorting wall, as depicted in Figure 2.6 (c). The impedance bandwidth of 132% is achieved by

employing a U-shaped slot and stepped arms on the upper patch, together with a tilt-folded patch feed. This configuration generates four resonances, allowing for a frequency range of 4.28 to 21 GHz.

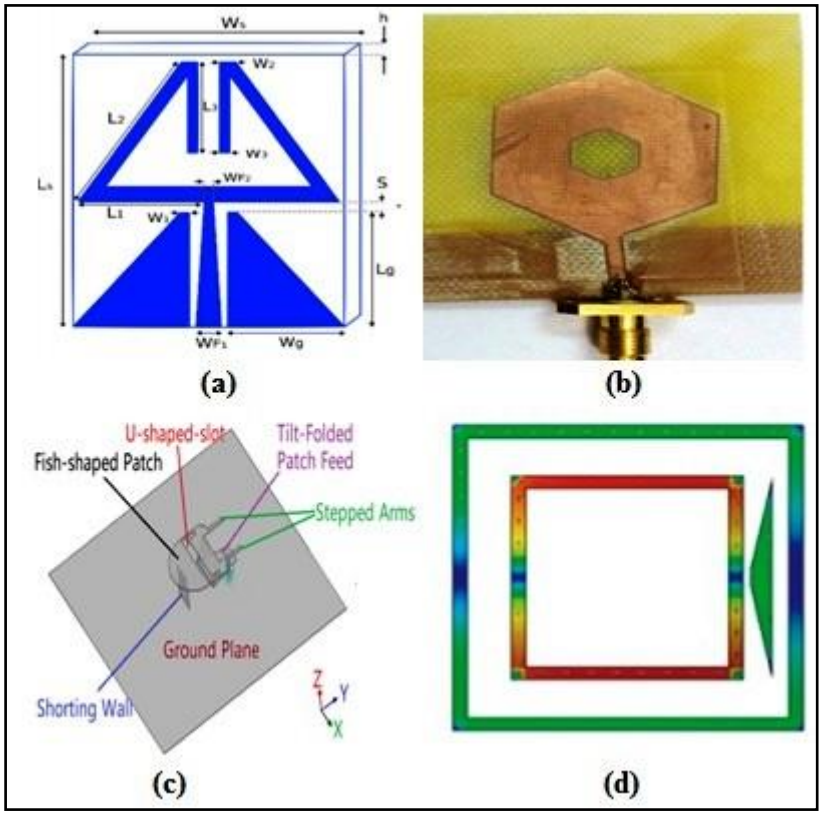

Figure 2.6 (a) Tapered coplanar feed antenna [License Number: 5877580742930], (b) asymmetric feed antenna [License Number: 5877640495345], (c) tilt folded feed antenna, (d) quadratic feed antenna

Swain and Sharma [64], proposed the design of a compact planar dual-square ring (DSR) microstrip patch antenna for Wi-Fi/WLAN and 5G-NR wireless applications as shown in figure 2.6 (d). The utilization of DSR geometry on a single layer dielectric is implemented in this study. The geometry is stimulated through electromagnetic coupling by employing a quadrilateral feed patch. The planar DSR structure resonates at 2.4 GHz and 3.7 GHz with bandwidths above 100 MHz and 200 MHz. Additionally, it demonstrates a maximum gain response of 4.3 dBi, accompanied by a VSWR of 2. Bendahmane et al [65], designed an antenna which composed of a rectangular star-shaped slotted microstrip patch antenna (MPA) with patch dimensions measuring 28.5 × 37.56 mm^2. This MPA is printed on a FR-4

substrate with a permittivity of εr = 4.3 and a thickness of h = 1.5 mm. The utilization of the high permittivity substrate technology, in conjunction with slot and defected ground structure (DGS) techniques, enables a significant reduction in the total size of the star-shaped slotted dualband microstrip patch antenna (MPA). This reduction exceeds 74% and is achieved while maintaining operation at frequencies of 2.4 and 5 GHz. The antenna achieves gains of 2.45 dBi and 4.27 dBi, with efficiencies of 83% and 68% respectively. Kishore et al. [66], introduced a novel multiband antenna design including a faulty ground construction. On the ground plane, it has rectangular slots in various sizes and a modified T-shaped patch. The coupling between the slots and patch, in conjunction with the feed line, results in the generation of six resonant frequencies. These frequencies are observed at 1.57 GHz, 2.45 GHz, 3.9 GHz, 5 GHz, 5.9 GHz, and 7.95 GHz. The corresponding bandwidths for these frequencies are 300 MHz, 1.2 GHz, 300 MHz, 200 MHz, 1 GHz, and 1.3 GHz, respectively. Prasad & Prasad [67], developed a rectangular slit patch antenna featuring a faulty ground structure measuring 32 × 32 × 1.6 mm in dimensions. The antenna exhibits operational frequencies of 3.271 GHz, 4.92 GHz, 6.35 GHz, and 11.04 GHz, accompanied by corresponding gains of 3.25 dB, 2.45 dB, 5.65 dB, and 4.47 dB, respectively, which are increased in nature.

2.2 MIMO Antenna Design and Techniques

This section critically examines numerous investigations aimed at improving isolation, gain, and other performance characteristics related to diversity, such as ECC, MEG and DG.

Gurjar et al. [68], introduced a modified rectangular fractal ultra wideband MIMO antenna consisting of 2 elements. The antenna's ground plane has a square funnel-like stub for wideband, isolation and miniaturization. The dimensions of the object are 24 × 30 × 0.8 mm. The antenna under consideration offers a bandwidth of 9.6 GHz, an isolation level of less than -16.3 dB, a diversity gain of 9.95 dB, and ECC value that is below 0.05. Figure 2.7(a) illustrates the geometry of the MIMO antenna, which consists of a rectangular patch with a fractal pattern. Ullah et al. [69], developed a super wideband MIMO antenna featuring a semi-circular form and a tapered microstrip feeding mechanism. The dimensions of the antenna were measured to be

40 × 47 × 1.5mm. T-shaped parasitic elements in the ground plane improve isolation. The antenna under consideration exhibits an Isolation value of less than -20 dB, a Diversity Gain of 10 dB, and less than 0.02 an ECC value. The arrangement of the antenna is depicted in Figure 2.7(b).

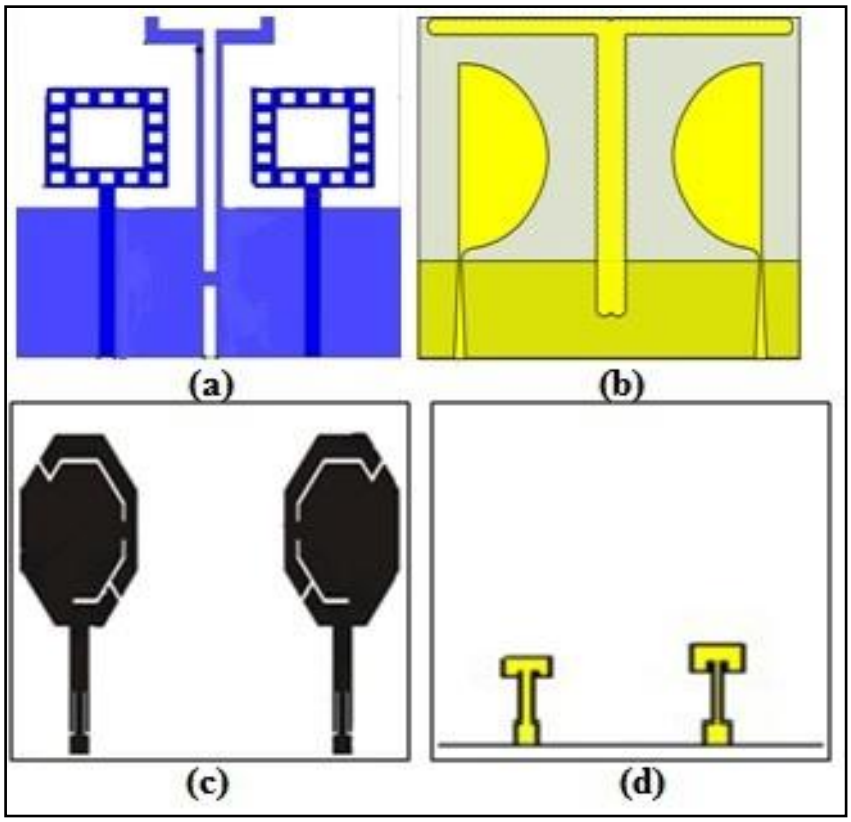

Figure 2.7 (a) Rectangular shape antenna [License Number: 5877580544375], (b) Semi circular shape antenna, (c) Hexagonal shape antenna [License Number: 5877580352573], (d) I shape antenna

Kumar et al. [70], conducted a study on an UWB-MIMO antenna that exhibits dual band notched characteristics. A two-element MIMO antenna's patch and ground plane have different stubs and slots to increase bandwidth and isolation. The antenna under consideration achieves a bandwidth of 7.5 GHz, an isolation level of less than -18 dB, a diversity gain of 9.7 dB, and less than 0.13 ECC value. The dimensions of the antenna are 19 × 30 × 0.8 mm. The geometric configuration of the MIMO antenna, which is in the shape of an octagonal patch, is seen in Figure 2.7(c). Marzouk et al. [71], introduced a dual band MIMO antenna system. The antenna design incorporates a 4-element MIMO antenna configuration. It features an inverted I-shaped slot on the

patch and another slot on the ground plane, which together constitute a faulty ground structure. Figure 2.7(d) illustrates the geometry of the MIMO antenna. The suggested antenna achieves a bandwidth of 1.0683/1.4306 GHz, an isolation of -28.32 dB/-26.27 dB, a diversity gain of 7.95/8.27 dB, and an error correction coefficient (ECC) value of less than 0.0005.The dimensions of the antenna are 55 mm × 110 mm × 0.5 mm.

Kumar and Khanna [72], developed a two-port MIMO antenna. Characteristics Mode Analysis (CMA) may enhance bandwidth. [73] has been suggested as a method to improve bandwidth. The antenna functions at frequencies of 3.5 GHz, 4.3 GHz, 28 GHz, and 35 GHz. The antenna exhibits a bandwidth exceeding 400 MHz throughout multiple frequency ranges, including 3.5 GHz and 4.3 GHz, and greater than 12 GHz, at 28 GHz and 35 GHz, which shows wideband behavior of antenna. The meta material unit cell produces a minimum isolation of 21 dB for frequencies of 3.5 GHz and 4.3 GHz, while a minimum isolation of 24 dB at frequencies of 28 GHz and 35 GHz. The ECC value is less than 0.05. Figure 2.8(a) illustrates the geometry of the MIMO antenna. Hussain et al. [74], proposed the design of a wideband MIMO antenna that integrates a rectangular slot, 2 vertical slots on the ground plane, and a square slot on the patch. Furthermore, to improve the bandwidth to a value of 6400, a microstrip feed line featuring a tapered profile is employed. Additionally, the isolation level is measured to be less than -35.8 dB. The dimensions of the MIMO antenna system are 15 mm in length, 30 mm in width, and 0.254 mm in thickness. The antenna under consideration exhibits a diversity gain of 9.99 and an error correction coefficient (ECC) value of less than 0.005. Figure 2.8(b) illustrates the geometry of the MIMO antenna. Khan et al. [75], presented a UWB MIMO antenna with patch elliptical slots and bottom plane Tee-shaped stubs. This design modification was found to yield a substantial bandwidth enhancement of 7900 MHz and improved isolation. The antenna being discussed in this study were fabricated on a FR4 substrate, with dimensions measuring 34 × 18 × 1.6 mm^3. The level of isolation exhibits a decrease of less than -15 dB within the frequency range of 3.1 to 5 GHz, and a decrease of less than -18 dB within the frequency range of 5 GHz to 11 GHz. The Envelope Correlation Coefficient (ECC) is found to be less than 0.01, indicating a weak correlation between the envelopes of two signals. On the other hand, the Diversity Gain (DG) is measured to be greater than 9.96 dB, suggesting a significant

improvement in signal quality due to diversity techniques. Figure 2.8 (c) presents the said antenna pictorial representation.

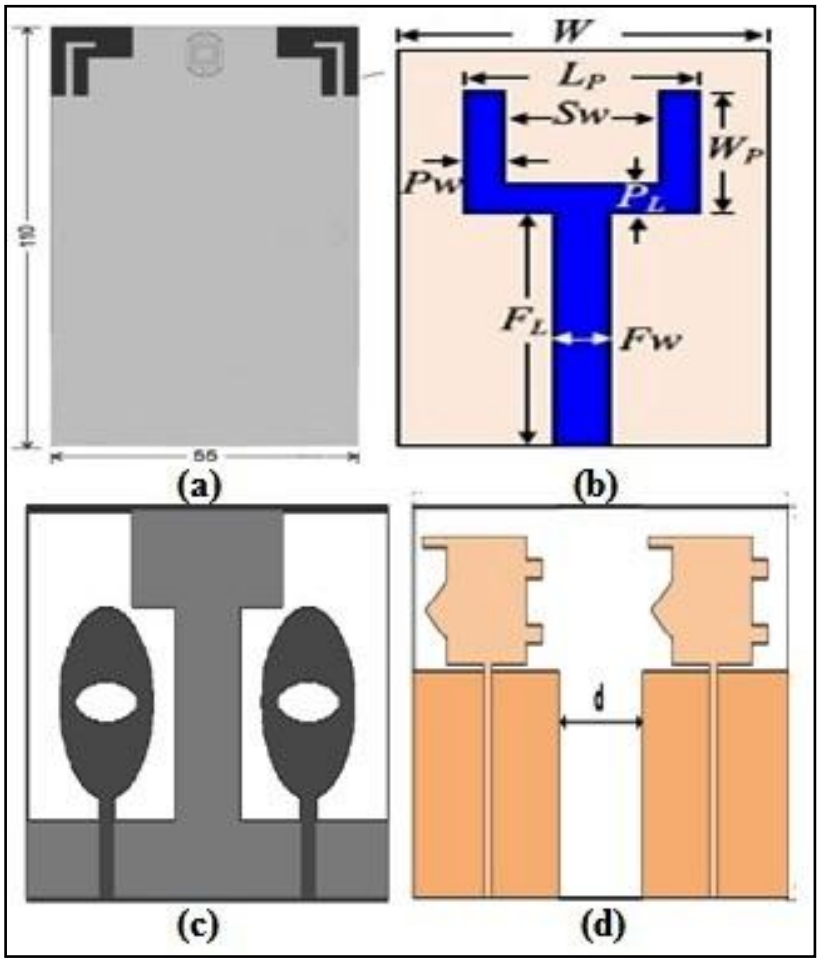

Figure 2.8 (a) Planar inverted F shape antenna [License Number: 5877641212547], (b) Rectangular shape with slot antenna [License Number: 5877580025608], (c) Elliptical shape antenna, (d) Rectangle with triangular stubs shape antenna

Sabek et. al [76] developed an antenna that incorporates rectangular and triangular stubs, as well as a partial ground plane, to enable dual band functionality. The proposed antenna design incorporates two elements that are strategically positioned at right angles to each other in order to achieve the desired high isolation characteristics of the MIMO configuration operating at frequencies of 28/38 GHz, specifically with isolation levels exceeding -34 dB and -22 dB. The MIMO setup possesses dimensions of 27.65 × 12 × 0.273 mm^3. The S_{21} value exhibits a decrease below -20 dB over the two operational frequency bands, which have respective bandwidths of 1900 and

5500. The antenna is depicted in Figure 2.8 (d). In order to enhance the bandwidth by 8700 MHz and achieve isolation of less than -30 dB, Sehrai et al. [77], built a wideband MIMO antenna with a flawed ground structure and dielectric layer to improve bandwidth and isolation. The antenna system has a maximum gain of around 5.48 dB. However, when a dielectric layer is introduced, the gain value is enhanced to 8.47 dB. The antenna is depicted in Figure 2.9(a). Hassan et. al [78], design an antenna that consists of primary and secondary patches that are capacitively connected. This configuration is intended to provide impedance matching and generate suitable radiation patterns across the four frequency bands. The acquired bandwidths at frequencies of approximately 28, 45, 51, and 56 GHz are measured to be around 0.6, 2.0, 1.8, and 1.3 GHz, respectively. Figure 2.9(b) presents the said antenna pictorial representation.

Sharawi et al. [79], developed a MIMO antenna system utilizing millimeter-wave dielectric resonators (DR). The system was created with two linear arrays. A MIMO antenna is comprised of an array consisting of four cylindrical DR antenna (cDRA) elements. These elements operate at a frequency of 30 GHz and possess a minimum bandwidth of 1 GHz. The ECC values, which were found to be below 0.002, were measured across the whole band of operation. Additionally, the peak gains were seen to be greater than 7 dBi. The antenna is depicted in Figure 2.9(c). Sharma et. al [80], presents a proposal for a 5G application, which involves a multiband modified 'W' shaped, wideband MIMO antenna as shown in figure 2.9(d). The suggested antenna incorporates a metamaterial inspired isolator to enhance isolation. This antenna setup covers 5G's sub-6 GHz (3.42-4.25 GHz) and mm Wave (24.8-26.5 GHz) bands. The antenna system has a sub-6 GHz bandwidth of 821 MHz and a millimeter Wave bandwidth of 1630 MHz. It exhibits excellent isolation characteristics across all frequency bands, with a minimum $|S_{12}|$ value exceeding -16 dB. Additionally, the antenna achieves a peak gain of 7.8 dBi, a low ECC below 0.05, and demonstrates strong diversity gain of 9.98 dB as well as an approximate efficiency of 91.38%. In order to increase isolation. Bawri et al. [81], used compact planar-patterned metamaterial (MTM) structures in their proposed design as shown in figure 2.10(a). The 52 mm × 23 mm antenna has DG > 9:99, low ECC, low CCL, low TARC, and total efficiencies of over 98%. A 5G-shaped strip, as proposed by Ali et al. [82], with

a modified G shape on the patch and a DGS as presented in figure 2.10(b) to improve antenna bandwidth, ECC, and isolation, has been presented.

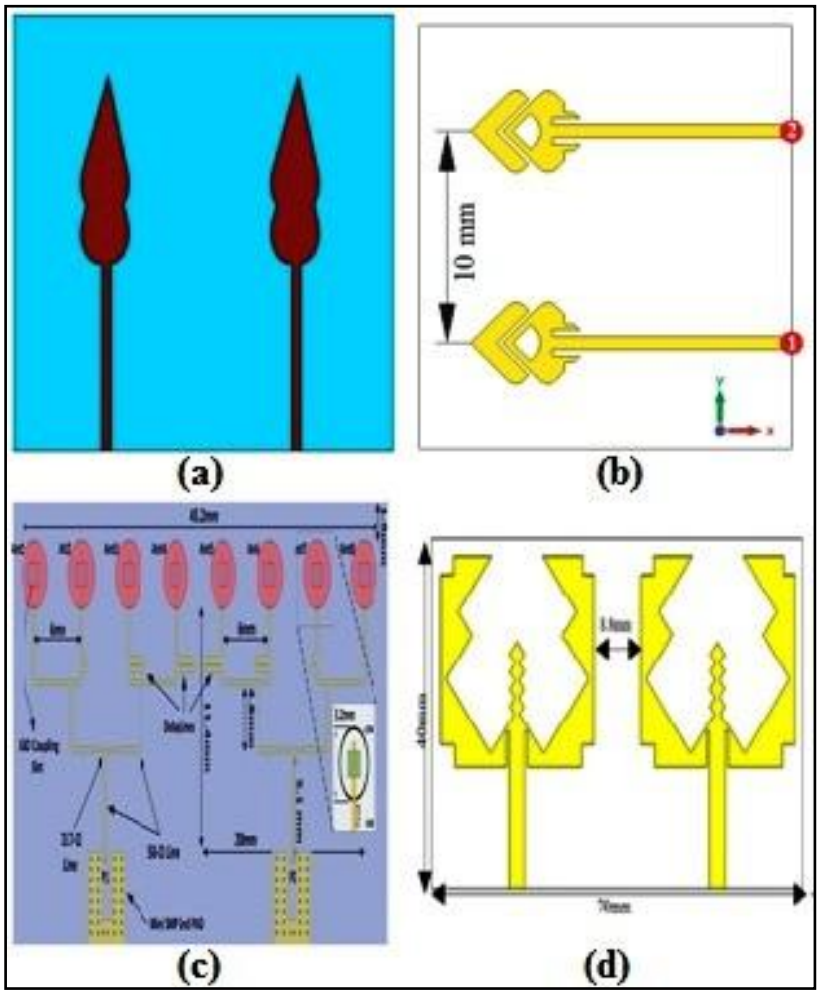

Figure 2.9 (a) Sharp leaf shape antenna, (b) Rhombic shape antenna, (c) Cylindrical shape antenna, (d) Modified W shaped antenna [License Number: 5877641046296]

In order to increase isolation and bandwidth, Ghadeer et al. [83], showed Sierpinski triangle fractal geometry with a composite right/left back structure. The antenna is presented in figure 2.10(c). Adding rectangular slits and slots to the patch surface and bottom plane, as well as employing orthogonal polarization, significantly reduces mutual coupling, as proposed by Dkiouak et al [84]. The measured findings demonstrate that the suggested antenna has a strong isolation of roughly 19 dB at both the 5.09-5.29 GHz and 7.38-7.87 GHz frequency bands. ECC is less than 0.13, and a small antenna of 27 by 21 mm^2 has been demonstrated in figure 2.10(d). Abdelaziz et al. [85], introduce a concise 5G MIMO microstrip antenna in their study. The antenna

design incorporates a SCSRR to promote isolation, and the TCMs is employed. Figure 2.11(a) illustrates the antenna configuration. The meta material unit is comprised of three complementary split ring resonators (CSRR) that are interconnected by additional slots. These extra slots considerably increase the bandwidth. The MIMO antenna element under consideration exhibited an isolation of -54 dB at a frequency of 28 GHz, while the envelope correlation was measured to be 0.005. A modified two element MIMO antenna was suggested by Ghannad et al. [86], in order to enhance isolation, a low profile feeding structure is employed, comprising a narrow slot on the ground plane, along with two narrow T-shaped stubs integrated into the feed line, and a narrow rectangular stub positioned between them. A comparative analysis was conducted to assess the performance of the suggested antenna in relation to other existing antennas. The results indicate that the proposed antenna exhibits a significantly superior reduction in mutual coupling, with a value of -46.5 dB. The value of ECC is determined to be 0.15, while the diversity gain is measured at 9.5 dB. The antenna geometry under consideration is seen in Figure 2.11(b). The construction possesses dimensions of 33 × 22 × 1 mm. Babu and Anuradha [87], developed a MIMO antenna with excellent performance, utilizing the Minkowski shape. The design of the patch for the suggested antenna involves the implementation of rectangular slots of varying lengths on the square patch. This approach facilitates the reduction of mutual coupling and enables miniaturization. The performance of the aforementioned antenna is compared to that of other antennas, and it is determined that the proposed antenna exhibits superior performance in comparison to the others. The geometric characteristics of the antenna are visually depicted in Figure 2.11(c). The obtained measurements for isolation are -54/-50/-40/-44 dB, accompanied by corresponding measurements for ECC of 0.03/0.00473/0.0075/0.0495 and bandwidth of 430/450/630/610 MHz. Abdullah et al. [88], introduced a novel methodology aimed at improving the isolation between MIMO antennas. In this study, the author implemented a technique wherein six metallic pins were strategically placed along the outer edges of the two square radiating patches, with the purpose of minimizing the mutual coupling. These metallic pins were connected to the ground plane. This approach additionally offers orthogonal polarization between the antenna by effectively attenuating the transmission of surface waves. The achieved isolation is -

20 dB, with a diversity gain value of 5.80 dB and an ECC value of less than 0.01. The geometric configuration of the MIMO antenna, depicted in Figure 2.11(d), is a square patch with dimensions of 30 × 55 × 1.524.

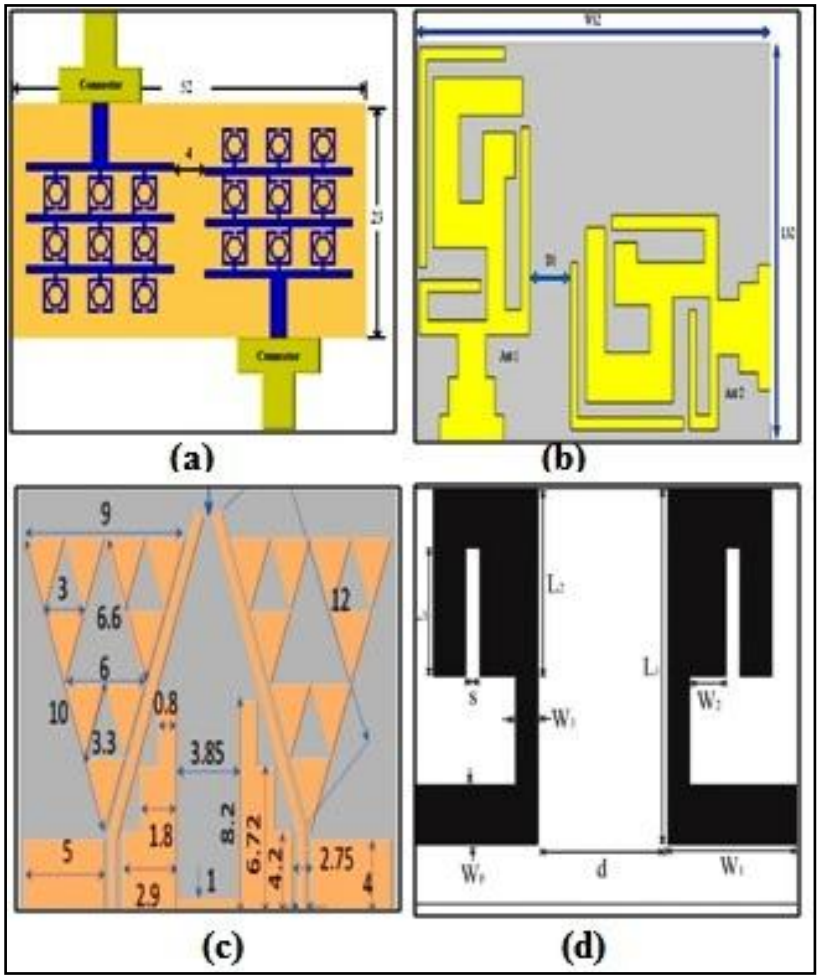

Figure 2.10 (a) Hexagonal shape antenna, (b) Modified G shape with strips antenna, (c) Sierpinski fractal shape antenna, (d) Modified nine shaped antenna

Jilani et al. [89], introduced a mm wave MIMO antenna with a rectangular patch in the shape of a T. The geometry of the antenna consists of a single T-shaped rectangular patch antenna accompanied by five split ring slots incorporated into the ground plane. The initial iteration involves the addition of a slot in the central area of the ground, which is directly connected to the top layer of the patch. Two more spaces were positioned on either side of the initial slot. In order to enhance the resonant response of the antenna, a second iteration was implemented, involving the placement of two additional slots in the ground plane at a suitable distance. Following the

completion of the design process for a single element antenna, a four element MIMO antenna configuration was established. The geometry of the MIMO antenna, which is a rectangular patch in the shape of a T, is depicted in Figure 2.12(a). The obtained values for isolation are -22 dB, accompanied by equivalent values for ECC of 0.1 and bandwidth of 12.4 GHz.

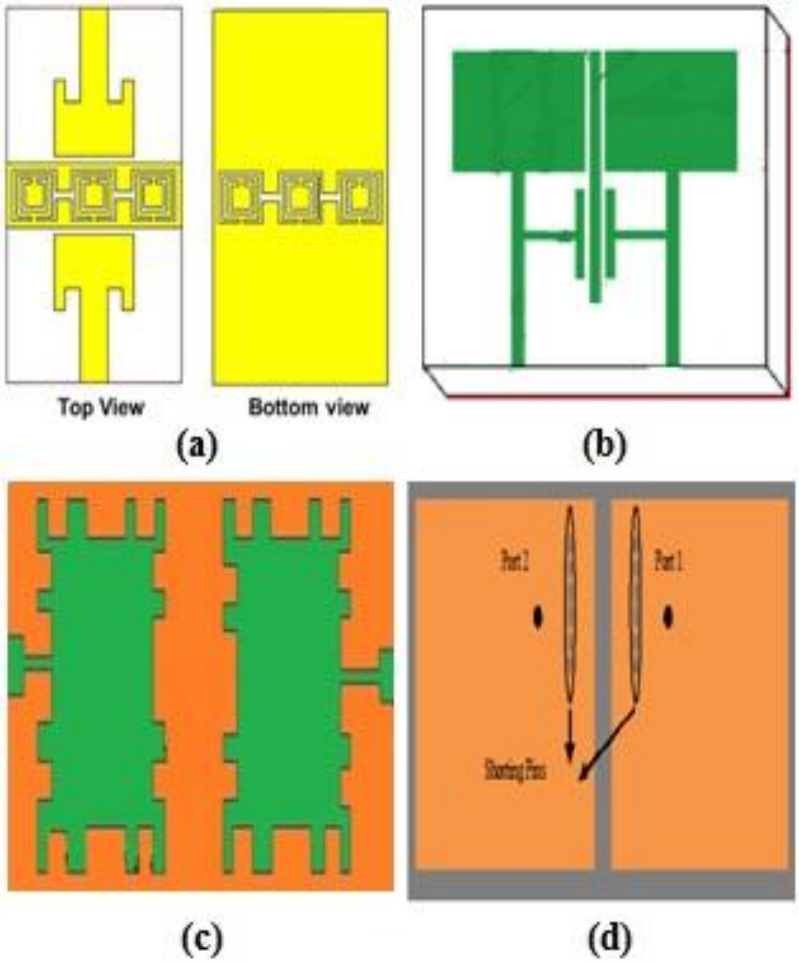

Figure 2.11 (a) Rectangular shape with split ring resonator antenna, (b) Modified rectangular shape antenna, (c) Minkowski shape antenna, (d) Square shaped antenna with shorting pins

The new concept of designing and fabricating a novel UWB 2×2 MIMO antenna was introduced by Saif et al. [90]. The antenna is constructed utilizing two 'F' shaped structures that are asymmetrical to one another and incorporate a flawed ground. In order to mitigate the level of coupling between two radiating elements, a strategic approach is taken by placing them at a separation distance of 13.9 mm. The geometric

characteristics of the antenna are depicted in Figure 2.12 (b). The dimensions of the antenna are 13 × 25 × 0.254 mm. The antenna exhibits a bandwidth (BW) of 10 GHz, a diversity gain of 9.8 dB, an ECC value of 0.009, and an isolation level of -20 dB.

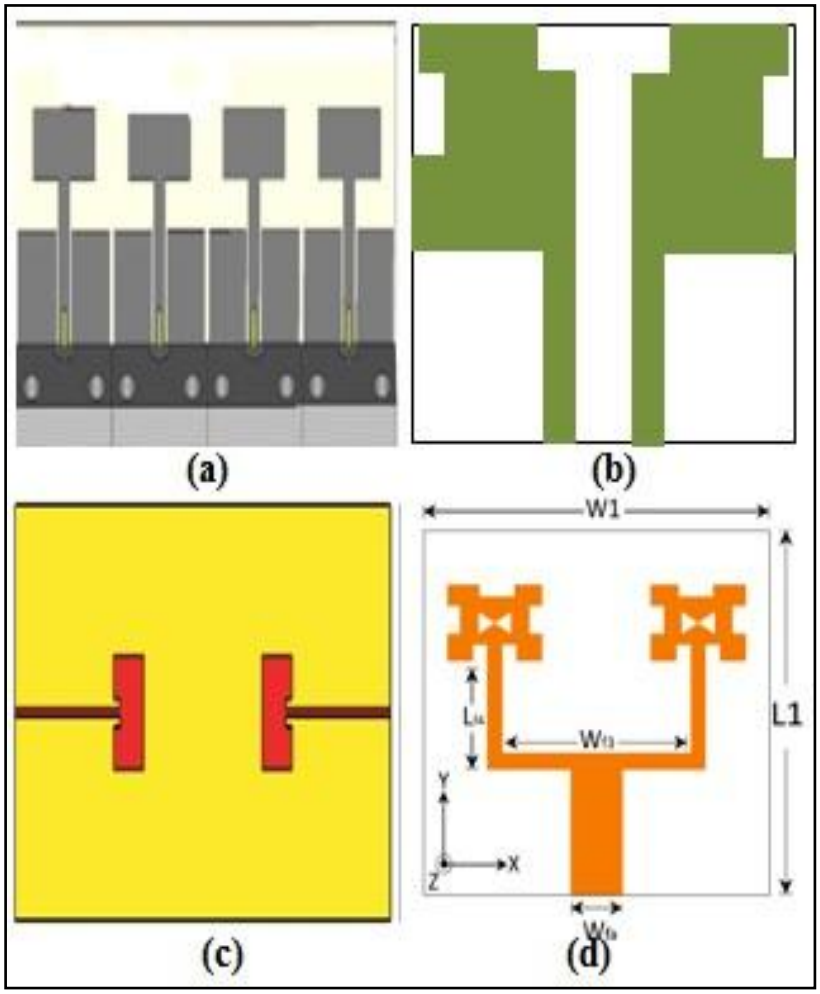

Figure 2.12 (a) T shape rectangular patch antenna, (b) Modified rectangular F shape antenna, (c) Minkowski fractal DGS shape antenna, (d) Rectangular shaped antenna with bow tie shape slot

For 5G mm-wave applications, Fatah et al. [91], designed a wideband MIMO antenna based on Minkowski fractal (MF)-DGS. The initial step is the design and analysis of a fundamental patch antenna including slotted MF-DGS. The utilization of MF-DGS in the design of a basic patch antenna results in the generation of numerous adjacent resonance frequencies, hence leading to an expansion of the antenna's bandwidth and better isolation. The 2-port MIMO antenna design under consideration operates within the frequency range of 24.8 to 27.6 GHz. Furthermore, the DG exhibits a significant

value of 9.9, while the computed ECC and CCL are both less than 0.001. DGS provide enhanced bandwidth and isolation [92]. This suggests that the MIMO system is suitable for 5G mm-wave frequencies. The geometric characteristics of the antenna are depicted in Figure 2.12 (c).

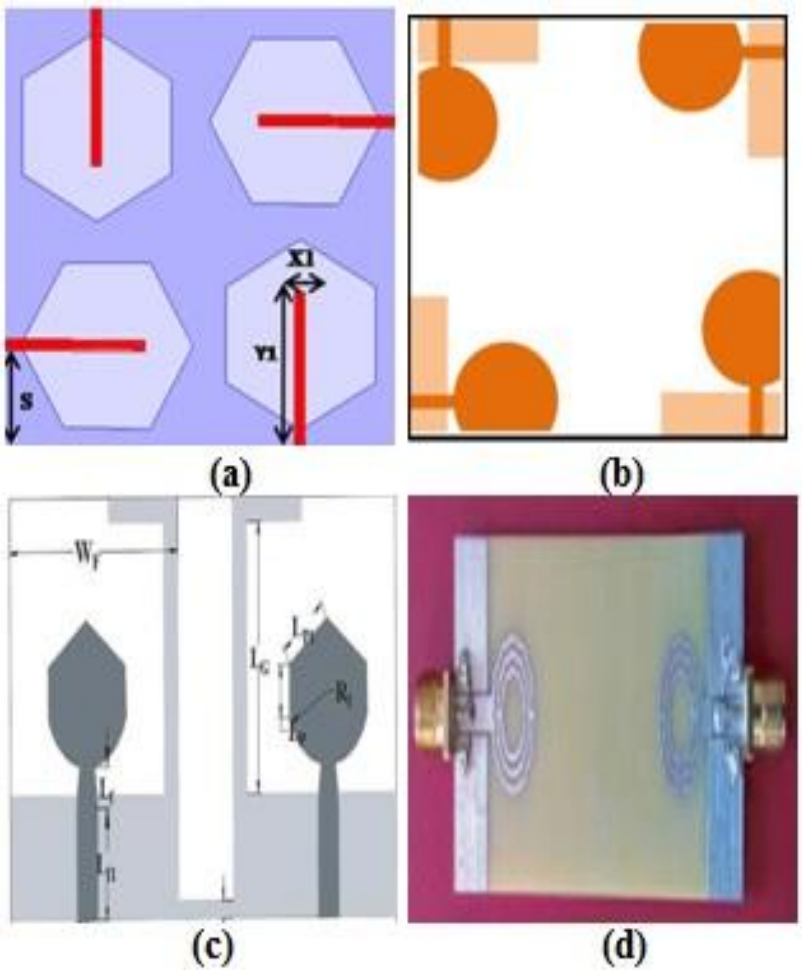

Figure 2.13 (a) Hexagonal shape DGS antenna, (b) Circular shape antenna, (c) Square slot with inverted L DGS shape antenna, (d) Decagon shaped antenna with rings

Bilai et al. [93], introduced a MIMO antenna design consisting of a rectangular patch with bow-tie-shaped slots positioned at the centre, as well as rectangular slits located at the top and sides of the patch as shown in figure 2.12 (d). The dimensions of the substrate for a single antenna are 15.5 × 15.5 mm. Impedance matching is achieved in the antenna's feedline by the utilization of a matching network based on a quarter-wave transformer. In order to optimize the radiation properties of the antenna and promote isolation, the implementation of a decoupling structure and a Defected

Ground Structure (DGS) is proposed. The decoupler is composed of a horizontally etched zig-zag pattern on the top layer, while the bottom layer utilizes the Defected Ground Structure (DGS) with four rectangular slots arranged both vertically and horizontally. Singh et al. [94], proposed a UWB MIMO antenna layout including 4 similar hexagonal-shaped slotted ground planes and 4 microstrip line feeds as shown in figure 2.13 (a). The MIMO antenna consists of four components that are organized in an orthogonal manner, so ensuring a significant degree of inter-element isolation. The antenna prototype is made on a substrate with dimensions of 12.5×12.5×0.8 mm^3. The MIMO antenna under consideration exhibits an impedance bandwidth of 30.47% across the frequency spectrum spanning from 26.7 GHz to 36.3 GHz. This characteristic renders it well-suited for utilization in the 5G NR frequency bands n257/n258/n261, which are associated with Millimeter-Wave Communication. Firmansyah et al. [95], developed a 2×2 MIMO circular patch microstrip antenna featuring a beleved half-cut structure This study examines the outcomes of three different antenna configurations: the ordinary circular patch shape antenna (CCSA) referred to as M1, the circular patch shape beleved antenna (CSBA) referred to as M2, and the MIMO circular patch shaped beleved structure (MIMO CSBA) referred to as M3. The term "beleved" refers to the act of removing one side of the antenna patch. The reduction in antenna size can be achieved by this approach. The findings of this study demonstrate that the M3 antenna exhibited favorable levels of mutual coupling. The dimensions of the substrate for a single antenna are 180 × 180 mm. The antenna exhibits a bandwidth (BW) of 2.322 GHz, and an isolation level of -26.18 dB. The shape of the MIMO antenna is seen in Figure 2.13(b).

A unique UWB antenna design by Thakur et al. [96], features a square slot and an inverse L-shaped ground plane strip. This design increased antenna element isolation. The proposed antenna demonstrates a mutual coupling value of less than -17 dB and an Envelope Correlation Coefficient of 0.15. The dimensions of the planned antenna are 27 × 17 × 1.6 mm^3. The frequency range of the planned antenna spans from 1 to 30 gigahertz (GHz). Figure 2.13 (c) depicts the antenna. Dileepan et al. [97], proposed an antenna that comprises three focused decagon-shaped rings that are responsible for acquiring the three resonance frequencies. The dimensions of the antenna element under consideration measure 23.5 mm × 26.5 mm. It exhibits an impedance

bandwidth of -10 dB throughout three frequency ranges: 2.4-2.52 GHz, 3.66-4 GHz, and 4.62-5.54 GHz. The direction of the antenna element results in significant levels of isolation, with values of -30.5 dB and 18.5 dB. The error correction coefficient (ECC) values exhibit a level below 0.001, while a diversity gain (DG) of 10 dB is attained across the operating frequencies. The shape of the MIMO antenna is seen in Figure 2.13(d).

2.3 Research Gap

This chapter presents a literature overview on microstrip antennas and MIMO antennas for 5G applications. The chapter began with an overview of the research conducted on microstrip antenna designs. Additionally, the study included pertinent studies on MIMO antennas. The historical overview mentioned above reveals that there have been many articles published on the subject of microstrip and mimo antenna design. The existing body of research indicates that the bandwidth and gain of the proposed designs are constrained, rendering them unsuitable for efficient utilization of antennas in actual applications. Only a small number of researchers have prioritized the isolation aspect at the expense of other performance parameters. Therefore, it is imperative to fill this research gap. The objective of this suggested study is to develop antennas for 5G mid and millimeter band applications employing microstrip patch antennas using fractal geometry (iteration technique) in conjunction with SISO and MIMO technology, which provide superior bandwidth, isolation, gain, and other diversity performance factors.

This thesis presents the design, fabrication, and testing of two antennas specifically developed for 5G mobile applications.

- The initial antenna has been developed, manufactured, and evaluated for its suitability in 5G mid band mobile applications. This antenna utilizes a single element microstrip patch design using fractal geometry (iteration technique), resulting in improved bandwidth, gain, and efficiency.
- A second antenna has been developed, manufactured, and evaluated for utilization in the millimeter range (n258 band) of 5G mobile

applications. This antenna employs a 2-element MIMO MPA configuration with a rectangular slot on ground plane and fractal geometry (iteration technique). It also offers improved bandwidth, gain, and diversity performance factors.

CHAPTER 3

METHODOLOGY

3.1 Research Objective

Research embodied in the present thesis investigates iteration strategies for designing patches of microstrip and MIMO antennas. In order to obtain the appropriate performance characteristics, some parametric studies are carried out in both the antennas. Additionally, a suitable defective ground structure is adopted and installed at the MIMO antenna in a suitable location to achieve a suitable band for 5G applications. The thesis's objectives are described in this context as follows:

1. To design wideband microstrip antenna for emerging technology Multiple Input and Multiple Output (MIMO).
2. Designing and fabrication of an antenna by optimizing dielectric constant of the substrate, thickness of the substrate and insertion of slots/slits to enhance the bandwidth and efficiency.
3. The antenna will be optimized for the desired performance parameter like gain and return loss.
4. The main prominence will be on the development of compact antenna with better isolation between the multiple antennas.

In order to accomplish these objectives, a quantitative research approach is employed in this study. The flowchart depicted in Figure 3.1 illustrates the methodology employed to accomplish these objectives.

3.2 Research Methodology

For achieving objective 1, 2 and 3 following steps were considered:

- **Step 1: Designing** - Microstrip antenna patch is designed using iteration techniques.
- **Step 2: Parametric Analysis** - The parametric effect of various parameters like dielectric constant, thickness of substrate, insertion of slots, feeding techniques of the said antenna is analyzed to achieve

desired performance. The proposed antenna is designed and simulated using HFSS 15.0. Once the desired results are achieved as per the literature surveys, then we proceed with fabrication process.

- **Step 3: Fabrication** - Final single element microstrip patch antenna is fabricated using EP-42 Auto PCB prototype machine.
- **Step 4: Testing and Validation** - S_{11} and VSWR are measured using SMA connector connected manufactured antenna to VNA (Rohde and Schwarz ZNB - 40 VNA 100 KHZ to 40 GHz). In anechoic chamber with broadband reference horn antenna transmitter, antenna radiation patterns and gain are measured.

For achieving objective 4 following steps were considered:

- **Step 1: Design** - Two port MIMO antenna patch is designed using iteration techniques.
- **Step 2: Analysis and DGS** - Distance optimization, orientation analysis and DGS is introduced to achieve desired performance. The proposed antenna is designed and simulated using HFSS 15.0. Once the desired results are achieved as per the literature surveys, then we proceed with fabrication process.
- **Step 3: Fabrication** - Final two port MIMO antenna is fabricated using EP-42 Auto PCB prototype machine.
- **Step 4: Testing and Validation** - The SMA connector connected the antenna to a VNA (Rohde and Schwarz ZNB - 40 VNA 100 KHZ to 40 GHz) for S parameters measurements. In anechoic chamber with broadband reference horn antenna transmitter, antenna radiation patterns are measured.

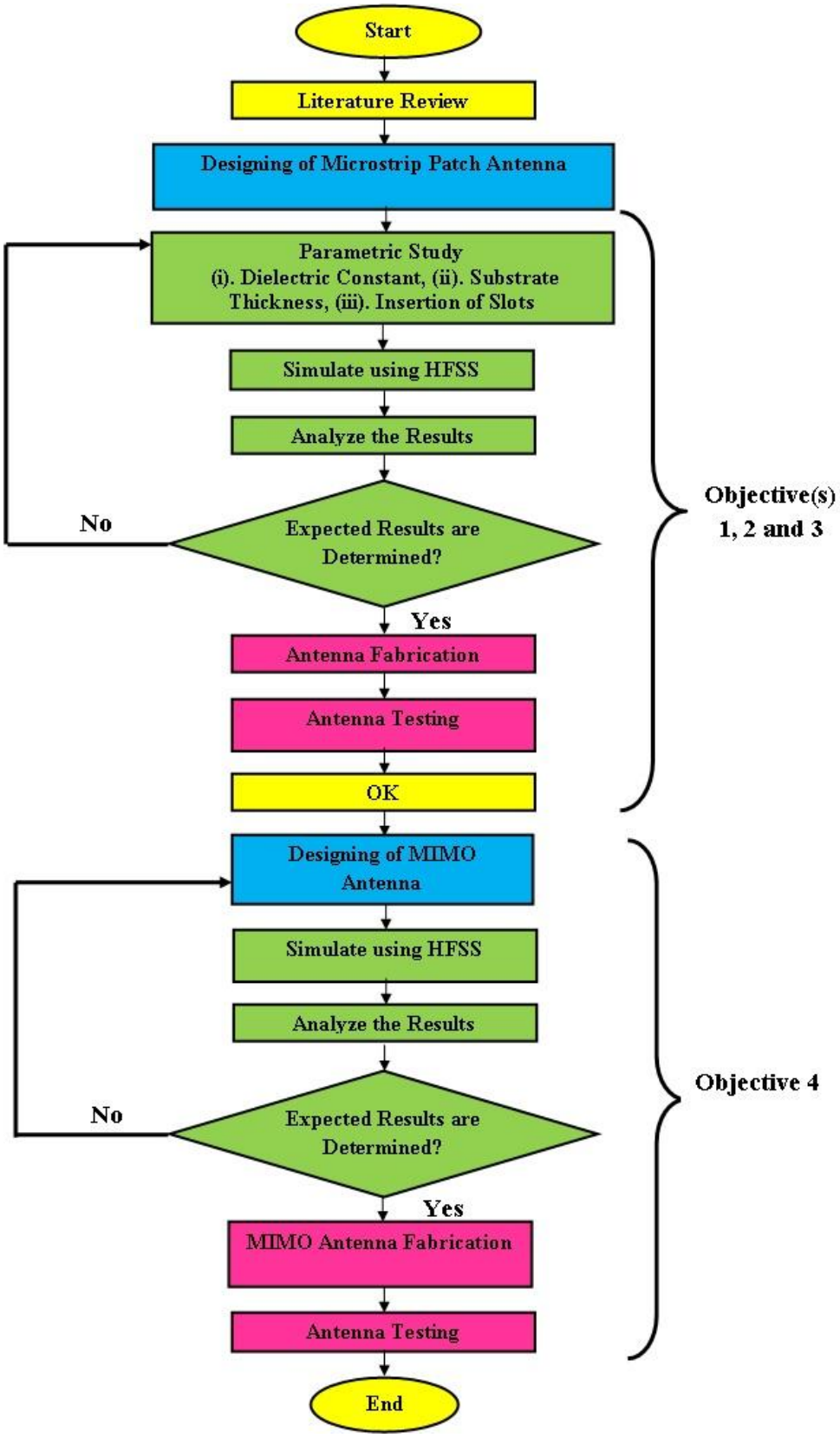

Figure 3.1 Flow chart for research methodology

CHAPTER 4

DESIGN AND DEVELOPMENT OF CIRCULAR SHAPED ANTENNA FOR 5G MID BAND MOBILE APPLICATION WITH ENHANCED BANDWIDTH

This chapter presents a redesigned circular MPA with multiband and wideband resonance for 5G midband mobile applications. To achieve suitable resonant frequency ranges and good impedance matching, the suggested antenna design uses an iterative approach to estimate the radii of many circular slots. The suggested antenna uses a recessed microstrip line and a simple plane ground construction. A comprehensive parametric analysis has been conducted to examine the effects of changes in substrate thickness and design iteration phases. The antenna modeling and simulation were done using HFSS 15.0. A 33.56 × 33.56 mm^2 FR-4 substrate was used to build a physical prototype of the proposed antenna structure to test its effectiveness. The prototype was then subjected to measurements using a vector network analyzer and an anechoic chamber to evaluate the accuracy of the simulated results. The proposed antenna exhibits favorable characteristics for 5G applications, including its compact dimensions, favorable radiation properties, and capacity to accommodate numerous operating frequencies while maintaining good impedance matching and expanded bandwidth.

Multiband features and enhanced operational bandwidth in a compact size without a monopole arrangement or DGS make the proposed work innovative. The proposed antenna meets compactness, multiband resonance, and operational bandwidth requirements. The antenna under consideration exhibits resonance at frequencies of 15.68, 12.62, 8.84, 6.68, and 3.35 GHz, accompanied with an IBW of -10 dB, spanning 6390, 990, 540, 630, and 100 MHz, respectively. In addition, the antenna that has been designed exhibits consistent radiation pattern characteristics and desirable gain throughout the whole frequency range in which it operates.

The suggested work covers these objectives in this chapter:

1. Design of a circular shaped patch antenna for 5G mobile application using HFSS software.
2. Analyze feeding techniques, slot insertion, substrate material and thickness, for optimal results in gain, return loss and bandwidth.
3. The optimized antenna is built and tested experimentally.

4.1 Circular Patch Antenna Designing using HFSS software

The substrate selection is the most crucial antenna design step. Substrate height and dielectric constant affected antenna bandwidth and impedance matching. As the bandwidth of an antenna is proportional to its resonance frequency and quality factor (Q factor). A greater dielectric constant can result in a broader bandwidth by lowering the antenna's resonance frequency and allowing for more relaxed impedance matching conditions. This is because the dielectric constant influences the effective wavelength within the material, which can change the antenna's impedance and thus bandwidth.

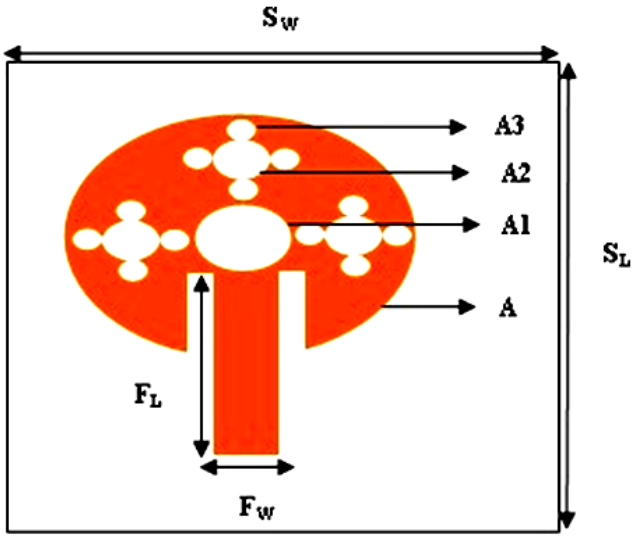

Figure 4.1 Proposed modified circular patch antenna

So, FR4 (εr = 4.4) substrate material of 1.6 mm thickness is used in the suggested antenna. Basically, FR4 is a standard designation for a specific type of composite material used in electronic applications that is flame-retardant and ideal for PCB manufacture. Where, F: indicates that the material is flame retardant. This means that it possesses qualities that make it less likely to catch fire or burn. R stands for "resin," which refers to the epoxy resin utilized in the laminate.

And 4: indicates the exact grade or kind of the material in the FR series. In this scenario, FR4 is a popular grade that offers an excellent blend of electrical insulating qualities, mechanical strength, and flame resistance. FR4 substrate is chosen for its low cost and market availability.

Patch antenna with circular shape and resonating frequency of 3.5 GHz (Mid band of 5G Applications) was chosen for the designing of the proposed antenna. Figure 4.1 represents the proposed microstrip patch antenna. The optimized parameters of proposed antenna are depicted in Table 4.1. The proposed antenna is designed and simulated using HFSS software.

Table 4.1 Parameters of proposed antenna

Sr. No.	**Parameter**	**Formula**	**Size (mm)**
1.	Radius (A)	$A_e = \frac{1.8412 \text{ x Vo}}{2 \times 3.14 \times \text{fr} \times \sqrt{\text{Er}}}$	11.98
2.	Length of substrate	$S_L = L + 6H$	33.56
3.	Width of substrate	$S_W = W + 6H$	33.56
4.	Substrate with thickness	----------	FR4/1.6
5.	Length of feed	----------	12.78
6.	Width of feed	$F_w = \frac{7.48H}{e^{\left(Z_0 \times \frac{\sqrt{(\varepsilon_r + 1.41}}{87}\right)}} - 1.25t$	2.99
7.	Radius of circle after 1st iteration process (A1)	N1 = No. of circle = 5^1 L1 = Scaling factor for radius of circle = $\left(\frac{1}{3}\right)$ ^1 = 0.333 So, (0.333 × 11.98 = 3.99)	3.99
8.	Radius of circle after 2nd iteration process (A2)	N2 = No. of circle = 5^2 L2 = Scaling factor for radius of circle = $\left(\frac{1}{3}\right)$ ^2 = 0.111	1.33

		So, (0.111 × 11.98 = 1.32)	
9.	Radius of circle after 3rd iteration process (A3)	N3 = No. of circle = 5^3 L3 = Scaling factor for radius of circle = $\left(\frac{1}{3}\right)$ ^3 = 0.037 So, (0.037 × 11.98 = 0.44)	0.44

Initialization of HFSS Software

To initiate the HFSS software, the user should locate and click on the HFSS icon. This action will prompt the HFSS screen to appear. Subsequently, the user should proceed to right-click on the project and proceed with renaming it. Next, select the "Project" option from the toolbar and proceed to click on "Insert HFSS Design". After that, we moved on to the design of an antenna. The initial task involves the design of the substrate and ground plane.

4.1.1 Designing Process

For substrate: To initiate the process, the user should locate and select the "draw box (3D)" option from the toolbar. Following this, the user should proceed to click on any desired location on the screen to create a box. Subsequently, the user should double-click on the box inside the project management interface to access its properties. Inside this menu, the user can modify the name of the box (Rectangular Substrate) and select the appropriate substrate, namely the FR4 option. Finally, the user should confirm their selections by pressing the "ok" button. Subsequently, go to right-click on the "create box" option and modify the dimensions in accordance with the specified requirements.

Position = -16.78, -16.78, 0

X = 33.56 mm

Y= 33.56 mm

Z = 1.6 mm

For ground: Rotate the substrate to the back position, then click at an edge of the substrate, drag the arrow to another edge of the substrate, and finally release the arrow. Then rename the box to ground.

After the design of the substrate and ground has been completed, the next task involves the design of the patch.

For patch: Figure 4.2 showcases the circular patch, wherein each circle is assigned a unique number to facilitate comprehension of its respective position and radius.

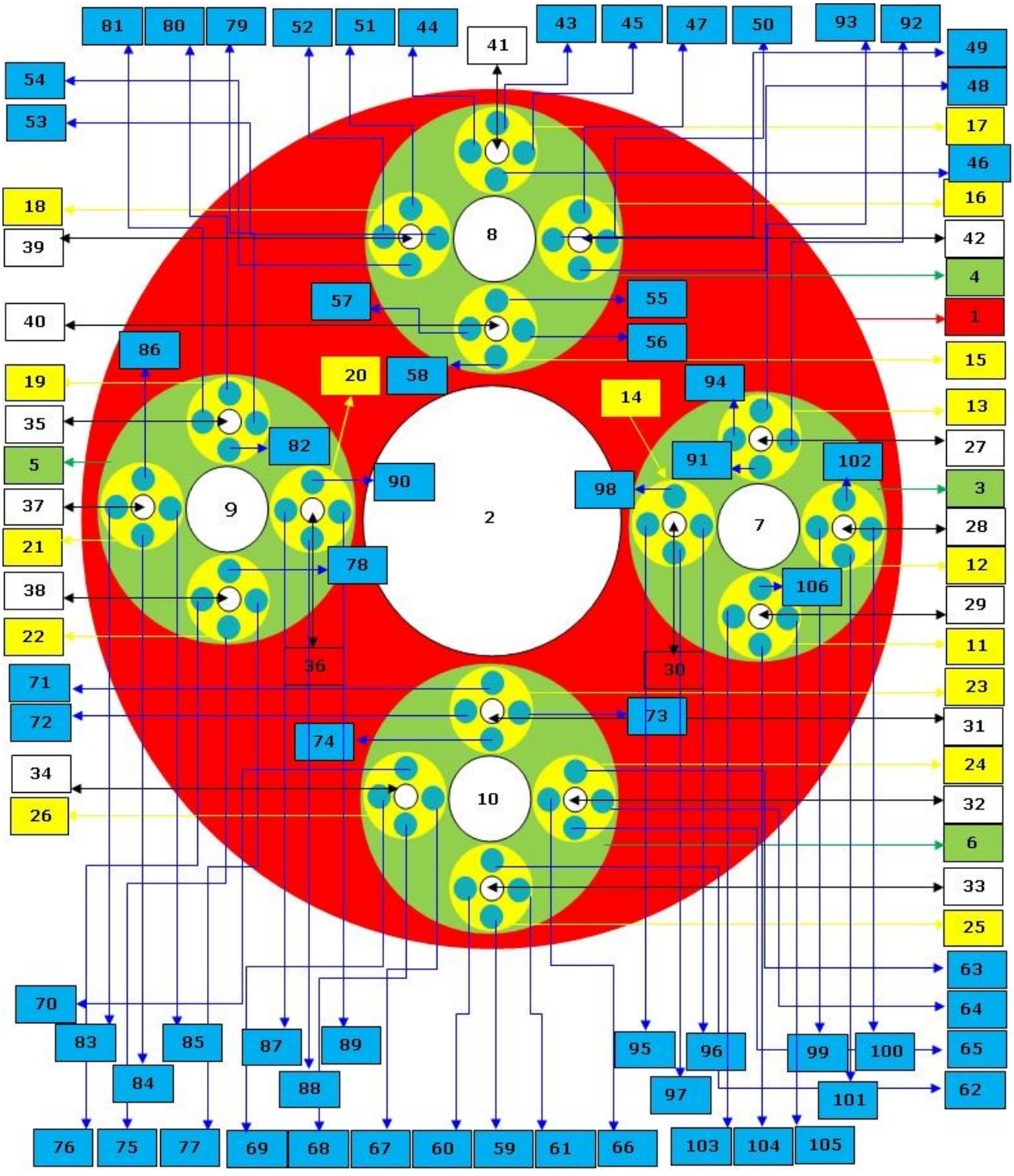

Figure 4.2 Modified circular shaped antenna patch

The illustration presented in Figure 4.3 depicts a fractal configuration that has been employed in the development of an antenna patch design.

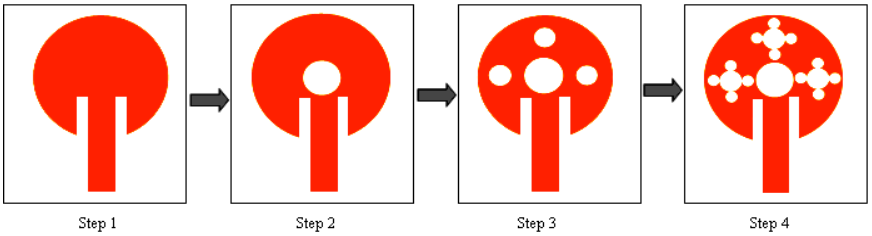

Figure 4.3 Evaluation steps of modified circular disk shaped antenna

For Step 1 (Zeroth iteration)

Process:

- A circular patch of a radius A (11.98 mm) is utilized as the basis structure **(1)**.

Designing Process:

- To initiate the patch design process, it is recommended to first locate the circular icon located within the toolbar. Subsequently, proceed to double-click on circle within the project window. Following this action, modify the name of the selected circle to "circle 1." Next, proceed to right-click on the "create circle" option and make adjustments to the proportions.

Circle 1:

Position = 0, 0, 1.6

R = 11.98 mm

For Step 2 (First iteration)

Process:

- The base construction (1) is scaled by one-third, resulting in 5 little circles (**2, 3, 4, 5, and 6**) with radius A1 (3.99 mm). One central circle (**2**) is removed from the five little circles, leaving four (**3, 4, 5, and 6**).

Designing Process:

- Choose a circle from the toolbar, rename it as "circle 2", and afterwards, perform a right-click on the "create circle" option to adjust the placements according to the specified instructions.

Circle 2:

Position = 0, 0, 1.6

R = 3.99 mm

For Circle 3, 4, 5 and 6;

First, select circle 2 by clicking on it. Next, locate the "edit" option and click on it. Once the editing menu is open, select the "copy" function. Afterward, find an appropriate location and choose the "paste" option. By completing these steps, circle 3 will be successfully formed. Please replicate this procedure for circles **4, 5, and 6.** Now, from the tool bar, select move and move the circles 3, 4, 5, and 6 to the positions indicated below.

Circle 3:

Move = 0, 8, 0

Circle 4:

Move = 0, -8, 0

Circle 5:

Move = -8, 0, 0

Circle 6:

Move = 8, 0, 0

Then, using the tool bar's subtract option, subtract circle 2 from circle 1. Simply choose circle 1, then circle 2, and then press the subtract option.

For Step 3 (Second iteration)

Process:

- To achieve this, repeat the previous steps on the remaining 4 circles (**3, 4, 5, and 6**). This involves dividing the 4 circles into 5 small circles (**7, 8, 9, 10, 11, 12, 13, 14, 15, 16, 17, 18, 19, 20, 21,22, 23, 24, 25, and 26**) of radius (A2) (1.33 mm), removing one centre circle from each, and leaving 16 total circles (**7, 8, 9 and 10**) , and leaving 16 circles (**11, 12, 13, 14, 15, 16, 17, 18, 19, 20, 21 ,22, 23, 24, 25, and 26**).

Designing Process:

- Choose a circle from the toolbar, rename it as "circle **7**", and afterwards, perform a right-click on the "create circle" option to adjust the placements according to the specified instructions.

Circle 7:

Position = 0, 8, 1.6

R = 1.33 mm

For Circle 11, 12, 13 and 14;

First, select circle 7 by clicking on it. Next, locate the "edit" option and click on it. Once the editing menu is open, select the "copy" function. Afterward, find an appropriate location and choose the "paste" option. By completing these steps, circle **11** will be successfully formed. Please replicate this procedure for circles **12, 13, and 14.** Now, from the tool bar, select move and move the circles 11, 12, 13, and 14 to the positions indicated below.

Circle 11:

Move = 0, 2.66, 0

Circle 12:

Move = 0, -2.66, 0

Circle 13:

Move = -2.66, 0, 0

Circle 14:

Move = 2.66, 0, 0

Then, using the tool bar's subtract option, subtract circle 7 from circle 3. Simply choose circle 3, then circle 7, and then press the subtract option.

Then same process is repeated for remaining circles 8, 9 and 10.

- Choose a circle from the toolbar, rename it as "**circle 9**", and afterwards, perform a right-click on the "create circle" option to adjust the placements according to the specified instructions.

Circle 9:

Position = 0, -8, 1.6

R = 1.33 mm

For Circle 19, 20, 21 and 22;

First, select circle 9 by clicking on it. Next, locate the "edit" option and click on it. Once the editing menu is open, select the "copy" function. Afterward, find an appropriate location and choose the "paste" option. By completing these steps, circle **19** will be successfully formed. Please replicate this procedure for circles **20, 21 and 22.** Now, from the tool bar, select move and move the circles 19, 20, 21, and 22 to the positions indicated below.

Circle 19:

Move = 0, 2.66, 0

Circle 20:

Move = 0, -2.66, 0

Circle 21:

Move = -2.66, 0, 0

Circle 22:

Move = 2.66, 0, 0

Then, using the tool bar's subtract option, subtract circle 9 from circle 5. Simply choose circle 5, then circle 9, and then press the subtract option.

- Choose a circle from the toolbar, rename it as "**circle 8**", and afterwards, perform a right-click on the "create circle" option to adjust the placements according to the specified instructions.

Circle 8:

Position = -8, 0, 1.6

R = 1.33 mm

For Circle 15, 16, 17 and 18;

First, select circle 8 by clicking on it. Next, locate the "edit" option and click on it. Once the editing menu is open, select the "copy" function. Afterward, find an appropriate location and choose the "paste" option. By completing these steps, circle **15** will be successfully formed. Please replicate this procedure for circles **16, 17 and 18.** Now, from the tool bar, select move and move the circles 15, 16, 17, and 18 to the positions indicated below.

Circle 15:

Move = 0, 2.66, 0

Circle 16:

Move = 0, -2.66, 0

Circle 17:

Move = -2.66, 0, 0

Circle 18:

Move = 2.66, 0, 0

Then, using the tool bar's subtract option, subtract circle 8 from circle 4. Simply choose circle 4, then circle 8, and then press the subtract option.

- Choose a circle from the toolbar, rename it as "**circle 10**", and afterwards, perform a right-click on the "create circle" option to adjust the placements according to the specified instructions.

Circle 10:

Position = 8, 0, 1.6

R = 1.33 mm

For Circle 23, 24, 25 and 26;

First, select circle 10 by clicking on it. Next, locate the "edit" option and click on it. Once the editing menu is open, select the "copy" function. Afterward, find an appropriate location and choose the "paste" option. By completing these steps, circle **23** will be successfully formed. Please replicate this procedure for circles **24, 25 and 26.** Now, from the tool bar, select move and move the circles 23, 24, 25, and 26 to the positions indicated below.

Circle 23:

Move = 0, 2.66, 0

Circle 24:

Move = 0, -2.66, 0

Circle 25:

Move = -2.66, 0, 0

Circle 26:

Move = 2.66, 0, 0

Then, using the tool bar's subtract option, subtract circle 10 from circle 6. Simply choose circle 6, then circle 10, and then press the subtract option.

For Step 4 (Third iteration)

Process:

- In this step the remaining 16 circles (**11, 12, 13, 14, 15, 16, 17, 18, 19, 20, 21 ,22, 23, 24, 25, and 26**) are then further divided into 5 smaller circles(**27, 28, 29, 30, 31, 32, 33, 34, 35, 36, 37, 38, 39, 40, 41, 42, 43, 44, 45, 46, 47, 48, 49, 50, 51, 52, 53, 54, 55, 56, 57, 58, 59, 60, 61, 62, 63, 64, 65, 66, 67, 68, 69, 70, 71, 72, 73, 74, 75, 76, 77, 78, 79, 80, 81, 82, 83, 84, 85, 86, 87, 88, 89, 90, 91, 92, 93, 94, 95, 96, 97, 98, 99, 100, 101, 102, 103, 104, 105, 106**) of radius (A3)(.44 mm), and once again the one centre circle is eliminated from each of the five smaller circles (**27, 28, 29, 30, 31, 32, 33, 34, 35, 36, 37, 38, 39, 40, 41, 42**) leaving a total of 64 circles (**43, 44, 45, 46, 47, 48, 49, 50, 51, 52, 53, 54, 55, 56, 57, 58, 59, 60, 61, 62, 63, 64, 65, 66, 67, 68, 69, 70, 71, 72, 73, 74, 75, 76, 77, 78, 79, 80, 81, 82, 83, 84, 85, 86, 87, 88, 89, 90, 91, 92, 93, 94, 95, 96, 97, 98, 99, 100, 101, 102, 103, 104, 105, 106**).

Designing Process:

"**Consider Circle 3**"

- Choose a circle from the toolbar, rename it as "**circle 28**", and afterwards, perform a right-click on the "create circle" option to adjust the placements according to the specified instructions.

Circle 28:

Position = 0, 10.66, 1.6

R = .44 mm

For Circle 99, 100, 101 and 102;

First, select circle 28 by clicking on it. Next, locate the "edit" option and click on it. Once the editing menu is open, select the "copy" function. Afterward, find an appropriate location and choose the "paste" option. By completing these steps, circle **100** will be successfully formed. Please replicate this procedure for circles **99, 101, and 102.** Now, from the tool bar, select move and move the circles 99, 100, 101 and 102 to the positions indicated below.

Circle 100:

Move = 0, 0.88, 0

Circle 99:

Move = 0, -0.88, 0

Circle 101:

Move = 0.88, 0, 0

Circle 102:

Move = -0.88, 0, 0

Then, using the tool bar's subtract option, subtract circle 28 from circle 12. Simply choose circle 12, then circle 28, and then press the subtract option.

- Choose a circle from the toolbar, rename it as "**circle 30**", and afterwards, perform a right-click on the "create circle" option to adjust the placements according to the specified instructions.

Circle 30:

Position = 0, 5.33, 1.6

R = .44 mm

For Circle 95, 96, 97 and 98;

First, select circle 30 by clicking on it. Next, locate the "edit" option and click on it. Once the editing menu is open, select the "copy" function. Afterward, find an appropriate location and choose the "paste" option. By completing these steps, circle **95** will be successfully formed. Please replicate this procedure for circles **96, 97, and 98.** Now, from the tool bar, select move and move the circles 95, 96, 97 and 98 to the positions indicated below.

Circle 95:

Move = 0, 0.88, 0

Circle 96:

Move = 0, -0.88, 0

Circle 98:

Move = 0.88, 0, 0

Circle 97:

Move = -0.88, 0, 0

Then, using the tool bar's subtract option, subtract circle 30 from circle 14. Simply choose circle 14, then circle 30, and then press the subtract option.

- Choose a circle from the toolbar, rename it as "**circle 27**", and afterwards, perform a right-click on the "create circle" option to adjust the placements according to the specified instructions.

Circle 27:

Position = 0, 8, 1.6

R = .44 mm

Move = -2.66, 0, 0

For Circle 91, 92, 93 and 94;

First, select circle 27 by clicking on it. Next, locate the "edit" option and click on it. Once the editing menu is open, select the "copy" function. Afterward, find an appropriate location and choose the "paste" option. By completing these steps, circle **91** will be successfully formed. Please replicate this procedure for circles **92, 93, and 94.** Now, from the tool bar, select move and move the circles 91, 92, 93 and 94 to the positions indicated below.

Circle 92:

Move = -2.66, 0.88, 0

Circle 94:

Move = -2.66, -0.88, 0

Circle 93:

Move = -3.54, 0, 0

Circle 91:

Move = -1.77, 0, 0

Then, using the tool bar's subtract option, subtract circle 27 from circle 13. Simply choose circle 13, then circle 27, and then press the subtract option.

- Choose a circle from the toolbar, rename it as "**circle 29**", and afterwards, perform a right-click on the "create circle" option to adjust the placements according to the specified instructions.

Circle 29:

Position = 0, 8, 1.6

R = .44 mm

Move = 2.66, 0, 0

For Circle 103, 104, 105 and 106;

First, select circle 29 by clicking on it. Next, locate the "edit" option and click on it. Once the editing menu is open, select the "copy" function. Afterward, find an appropriate location and choose the "paste" option. By completing these steps, circle

103 will be successfully formed. Please replicate this procedure for circles **104, 105, and 106.** Now, from the tool bar, select move and move the circles 103, 104, 105 and 106 to the positions indicated below.

Circle 105:

Move = 2.66, 0.88, 0

Circle 103:

Move = 2.66, -0.88, 0

Circle 104:

Move = 3.54, 0, 0

Circle 106:

Move = 1.77, 0, 0

Then, using the tool bar's subtract option, subtract circle 29 from circle 11. Simply choose circle 11, then circle 29, and then press the subtract option.

"**Consider Circle 5**"

- Choose a circle from the toolbar, rename it as "**circle 37**", and afterwards, perform a right-click on the "create circle" option to adjust the placements according to the specified instructions.

Circle 37:

Position = 0, -10.66, 1.6

R = .44 mm

For Circle 83, 84, 85 and 86;

First, select circle 37 by clicking on it. Next, locate the "edit" option and click on it. Once the editing menu is open, select the "copy" function. Afterward, find an appropriate location and choose the "paste" option. By completing these steps, circle **83** will be successfully formed. Please replicate this procedure for circles **84, 85 and 86.** Now, from the tool bar, select move and move the circles 83, 84, 85 and 86 to the positions indicated below.

Circle 85:

Move = 0, 0.88, 0

Circle 83:

Move = 0, -0.88, 0

Circle 84:

Move = 0.88, 0, 0

Circle 86:

Move = -0.88, 0, 0

Then, using the tool bar's subtract option, subtract circle 37 from circle 21. Simply choose circle 21, then circle 37, and then press the subtract option.

- Choose a circle from the toolbar, rename it as "**circle 36**", and afterwards, perform a right-click on the "create circle" option to adjust the placements according to the specified instructions.

Circle 36:

Position = 0, -5.33, 1.6

R = .44 mm

For Circle 87, 88, 89 and 90;

First, select circle 36 by clicking on it. Next, locate the "edit" option and click on it. Once the editing menu is open, select the "copy" function. Afterward, find an appropriate location and choose the "paste" option. By completing these steps, circle **87** will be successfully formed. Please replicate this procedure for circles **88, 89, and 90.** Now, from the tool bar, select move and move the circles 87, 88, 89 and 90 to the positions indicated below.

Circle 89:

Move = 0, 0.88, 0

Circle 87:

Move = 0, -0.88, 0

Circle 88:

Move = 0.88, 0, 0

Circle 90:

Move = -0.88, 0, 0

Then, using the tool bar's subtract option, subtract circle 36 from circle 20. Simply choose circle 20, then circle 36, and then press the subtract option.

- Choose a circle from the toolbar, rename it as "**circle 35**", and afterwards, perform a right-click on the "create circle" option to adjust the placements according to the specified instructions.

Circle 35:

Position = 0, -8, 1.6

R = .44 mm

Move = -2.66, 0, 0

For Circle 79, 80, 81 and 82;

First, select circle 35 by clicking on it. Next, locate the "edit" option and click on it. Once the editing menu is open, select the "copy" function. Afterward, find an appropriate location and choose the "paste" option. By completing these steps, circle **79** will be successfully formed. Please replicate this procedure for circles **80, 81 and 82.** Now, from the tool bar, select move and move the circles 79, 80, 81 and 82 to the positions indicated below.

Circle 79:

Move = -2.66, 0.88, 0

Circle 81:

Move = -2.66, -0.88, 0

Circle 80:

Move = -3.54, 0, 0

Circle 82:

Move = -1.77, 0, 0

Then, using the tool bar's subtract option, subtract circle 35 from circle 19. Simply choose circle 19, then circle 35, and then press the subtract option.

- Choose a circle from the toolbar, rename it as "**circle 38**", and afterwards, perform a right-click on the "create circle" option to adjust the placements according to the specified instructions.

Circle 38:

Position = 0, -8, 1.6

R = 0.44 mm

Move = 2.66, 0, 0

For Circle 75, 76, 77 and 78;

First, select circle 38 by clicking on it. Next, locate the "edit" option and click on it. Once the editing menu is open, select the "copy" function. Afterward, find an appropriate location and choose the "paste" option. By completing these steps, circle

75 will be successfully formed. Please replicate this procedure for circles **76, 77, and 78.** Now, from the tool bar, select move and move the circles 75, 76, 77 and 78 to the positions indicated below.

Circle 77:

Move = 2.66, 0.88, 0

Circle 76:

Move = 2.66, -0.88, 0

Circle 75:

Move = 3.54, 0, 0

Circle 78:

Move = 1.77, 0, 0

Then, using the tool bar's subtract option, subtract circle 38 from circle 22. Simply choose circle 22, then circle 38, and then press the subtract option.

"**Consider Circle 6**"

- Choose a circle from the toolbar, rename it as "circle **33**", and afterwards, perform a right-click on the "create circle" option to adjust the placements according to the specified instructions.

Circle 33:

Position = 10.66, 0, 1.6

R = .44 mm

For Circle 59, 60, 61 and 62;

First, select circle 33 by clicking on it. Next, locate the "edit" option and click on it. Once the editing menu is open, select the "copy" function. Afterward, find an appropriate location and choose the "paste" option. By completing these steps, circle **59** will be successfully formed. Please replicate this procedure for circles **60, 61 and 62.** Now, from the tool bar, select move and move the circles 59, 60, 61 and 62 to the positions indicated below.

Circle 61:

Move = 0, 0.88, 0

Circle 60:

Move = 0, -0.88, 0

Circle 59:

Move = 0.88, 0, 0

Circle 62:

Move = -0.88, 0, 0

Then, using the tool bar's subtract option, subtract circle 33 from circle 25. Simply choose circle 25, then circle 33, and then press the subtract option.

- Choose a circle from the toolbar, rename it as "circle **31**", and afterwards, perform a right-click on the "create circle" option to adjust the placements according to the specified instructions.

Circle 31:

Position = 5.33, 0, 1.6

R = .44 mm

For Circle 71, 72, 73 and 74;

First, select circle 31 by clicking on it. Next, locate the "edit" option and click on it. Once the editing menu is open, select the "copy" function. Afterward, find an appropriate location and choose the "paste" option. By completing these steps, circle **71** will be successfully formed. Please replicate this procedure for circles **72, 73 and 74.** Now, from the tool bar, select move and move the circles 71, 72, 73 and 74 to the positions indicated below.

Circle 73:

Move = 0, 0.88, 0

Circle 72:

Move = 0, -0.88, 0

Circle 74:

Move = 0.88, 0, 0

Circle 71:

Move = -0.88, 0, 0

Then, using the tool bar's subtract option, subtract circle 31 from circle 23. Simply choose circle 23, then circle 31, and then press the subtract option.

- Choose a circle from the toolbar, rename it as "**circle 32**", and afterwards, perform a right-click on the "create circle" option to adjust the placements according to the specified instructions.

Circle 32:

Position = 8, 0, 1.6

R = .44 mm

Move = 0, 2.66, 0

For Circle 63, 64, 65 and 66;

First, select circle 32 by clicking on it. Next, locate the "edit" option and click on it. Once the editing menu is open, select the "copy" function. Afterward, find an appropriate location and choose the "paste" option. By completing these steps, circle **63** will be successfully formed. Please replicate this procedure for circles **64, 65 and 66.** Now, from the tool bar, select move and move the circles 63, 64, 65 and 66 to the positions indicated below.

Circle 64:

Move = 0.88, 2.66, 0

Circle 66:

Move = -0.88, 2.66, 0

Circle 65:

Move = 0, 3.54, 0

Circle 63:

Move = 0, 1.77, 0

Then, using the tool bar's subtract option, subtract circle 32 from circle 24. Simply choose circle 24, then circle 32, and then press the subtract option.

- Choose a circle from the toolbar, rename it as "**circle 34**", and afterwards, perform a right-click on the "create circle" option to adjust the placements according to the specified instructions.

Circle 34:

Position = 8, 0, 1.6

R = 0.44 mm

Move = 0, -2.66, 0

For Circle 67, 68, 69 and 70;

First, select circle 34 by clicking on it. Next, locate the "edit" option and click on it. Once the editing menu is open, select the "copy" function. Afterward, find an appropriate location and choose the "paste" option. By completing these steps, circle

67 will be successfully formed. Please replicate this procedure for circles **68, 69 and 70.** Now, from the tool bar, select move and move the circles 67, 68, 69 and 70 to the positions indicated below.

Circle 67:

Move = 0.88, -2.66, 0

Circle 69:

Move = -0.88, -2.66, 0

Circle 68:

Move = 0, -3.54, 0

Circle 70:

Move = 0, - 1.77, 0

Then, using the tool bar's subtract option, subtract circle 34 from circle 26. Simply choose circle 26, then circle 34, and then press the subtract option.

"**Consider Circle 4**"

- Choose a circle from the toolbar, rename it as "**circle 41**", and afterwards, perform a right-click on the "create circle" option to adjust the placements according to the specified instructions.

Circle 41:

Position = -10.66, 0, 1.6

R = 0.44 mm

For Circle 43, 44, 45 and 46;

First, select circle 41 by clicking on it. Next, locate the "edit" option and click on it. Once the editing menu is open, select the "copy" function. Afterward, find an appropriate location and choose the "paste" option. By completing these steps, circle **43** will be successfully formed. Please replicate this procedure for circles **44, 45 and 46.** Now, from the tool bar, select move and move the circles 43, 44, 45 and 46 to the positions indicated below.

Circle 45:

Move = 0, 0.88, 0

Circle 44:

Move = 0, -0.88, 0

Circle 46:

Move = 0.88, 0, 0

Circle 43:

Move = -0.88, 0, 0

Then, using the tool bar's subtract option, subtract circle 41 from circle 17. Simply choose circle 17, then circle 41, and then press the subtract option.

- Choose a circle from the toolbar, rename it as "**circle 40**", and afterwards, perform a right-click on the "create circle" option to adjust the placements according to the specified instructions.

Circle 40:

Position = -5.33, 0, 1.6

R = 0.44 mm

For Circle 55, 56, 57 and 58;

First, select circle 40 by clicking on it. Next, locate the "edit" option and click on it. Once the editing menu is open, select the "copy" function. Afterward, find an appropriate location and choose the "paste" option. By completing these steps, circle **55** will be successfully formed. Please replicate this procedure for circles **56, 57 and 58.** Now, from the tool bar, select move and move the circles 55, 56, 57 and 58 to the positions indicated below.

Circle 56:

Move = 0, 0.88, 0

Circle 57:

Move = 0, -0.88, 0

Circle 55:

Move = 0.88, 0, 0

Circle 58:

Move = -0.88, 0, 0

Then, using the tool bar's subtract option, subtract circle 40 from circle 15. Simply choose circle 15, then circle 40, and then press the subtract option.

- Choose a circle from the toolbar, rename it as "**circle 42**", and afterwards, perform a right-click on the "create circle" option to adjust the placements according to the specified instructions.

Circle 42:

Position = -8, 0, 1.6

R = 0.44 mm

Move = 0, -2.66, 0

For Circle 47, 48, 49 and 50;

First, select circle 42 by clicking on it. Next, locate the "edit" option and click on it. Once the editing menu is open, select the "copy" function. Afterward, find an appropriate location and choose the "paste" option. By completing these steps, circle **47** will be successfully formed. Please replicate this procedure for circles **48, 49 and 50.** Now, from the tool bar, select move and move the circles 47, 48, 49 and 50 to the positions indicated below.

Circle 49:

Move = 0.88, 2.66, 0

Circle 50:

Move = -0.88, 2.66, 0

Circle 47:

Move = 0, -3.54, 0

Circle 48:

Move = 0, -1.77, 0

Then, using the tool bar's subtract option, subtract circle 42 from circle 16. Simply choose circle 16, then circle 42, and then press the subtract option.

- Choose a circle from the toolbar, rename it as "**circle 39**", and afterwards, perform a right-click on the "create circle" option to adjust the placements according to the specified instructions.

Circle 39:

Position = -8, 0, 1.6

R = 0.44 mm

Move = 0, 2.66, 0

For Circle 51, 52, 53 and 54;

First, select circle 39 by clicking on it. Next, locate the "edit" option and click on it. Once the editing menu is open, select the "copy" function. Afterward, find an appropriate location and choose the "paste" option. By completing these steps, circle

51 will be successfully formed. Please replicate this procedure for circles **52, 53 and 54.** Now, from the tool bar, select move and move the circles 51, 52, 53 and 54 to the positions indicated below.

Circle 53:

Move = 0.88, 2.66, 0

Circle 52:

Move = -0.88, 2.66, 0

Circle 51:

Move = 0, 3.54, 0

Circle 54:

Move = 0, 1.77, 0

Then, using the tool bar's subtract option, subtract circle 39 from circle 18. Simply choose circle 18, then circle 39, and then press the subtract option.

For microstrip inset feedline: To start the process, the user should go to the toolbar and choose the "draw rectangle" choice. The user should then click anywhere on the screen to make a rectangle. Then, the user should double-click on the rectangle inside the project management window to get to its properties. The user can change the name of the rectangle (feed line) in this menu. Lastly, the user should press the "OK" button to confirm their choices. Then, right-click on "create box" and change the positions to meet the standards.

Position = 33.56/2, 2.99/2, 1.6

X = -16.78 + 4 = -12.78 mm

Y= -2.99 mm

Next, make cuts along both sides of the feedline. For cut 1, first choose the rectangle, then move the cursor from the feedline's top right edge to the patch's bottom right edge. Next, right-click the newly created rectangle and modify the y-axis's settings to Y = 1.2 mm. Then, for cut 2, choose the duplicate along line option from the toolbar and move the cursor from the top of the cut1 on the right to the top of the feedline on the left. The next stage is to combine feedline and patch. To do this, click on (patch + control + feedline), then select the unite option from the toolbar. When you click on

patch + Control + cut1 + control + cut2 and then select the option to subtract from the toolbar, cut1 and cut2 are subtracted from the patch.

For assigning boundaries to ground and patch: right-click the patch, select assign boundaries, and then click Perfect E. Same process is repeated for ground.

For lump port: Change the axis to "yz" first. Then choose a rectangle and give it the new name lump port. Then, right-click on "Create Rectangle" and modify its attributes as follows:
Position: 16.78, -1.495, 1.6
y = 2.99 mm
z = -1.6
For lump port excitation, right-click on the lump port rectangle in the project window, select Assign Excitation, select Lump Port (50 Ohm), select Next, select Integration (double click), select New Line, drag a triangle-shaped cursor from the lower edge to the upper edge, select Next, and then select Finish.

For radiation box: To initiate the process, the user should locate and select the "draw box (3D)" option from the toolbar. Following this, the user should proceed to click on any desired location on the screen to create a box. Subsequently, the user should double-click on the box inside the project management interface to access its properties. Inside this menu, the user can modify the name of the box (radiation box) and select the vaccum option. Finally, the user should confirm their selections by pressing the "ok" button. Subsequently, go to right-click on the "create box" option and modify the dimensions in accordance with the specified requirements.
Position: -16.78, -16.78, 0
X = 33.56 mm
Y = 33.56 mm
Z = 21.42 mm
Next, proceed to choose the five facets of the radiation boxes and thereafter utilize the right-click function to allocate boundaries. Finally, click on the radiation option.

Then, check validation.

For analysis:

To initiate the analysis on the project management window, the user should perform a right-click action. Following this, they should select the option labeled "Add solution set up." Within this setup, the user will be prompted to specify the solution frequency in gigahertz (GHz), with a recommended value of 3.5 GHz for the proposed antenna. The maximum number of passes is set at 20. Subsequently, proceed to perform a right-click action on the setup option, followed by selecting the sweep function. Proceed to input the desired start value (2 GHz) and end value (20 GHz), and subsequently specify the step size (0.1 GHz). Subsequently, save the field configuration and confirm the changes by selecting the "OK" option.

After the completion of validation and analysis, the subsequent step involves assessing the results of our suggested antenna with regards to several performance metrics.

For calculating "S_{11}" of the proposed antenna, following steps are followed:

- In the project management box, right-click on the result option.
- Next, click Create modal solution setup data report.
- Then select Rectangular plot • S parameter • New report

For calculating "VSWR" of the proposed antenna, following steps are followed:

- In the project management box, right-click on the result option.
- Next, click Create modal solution setup data report.
- Then select Rectangular plot • VSWR • New report

For calculating "Gain" of the proposed antenna, following steps are followed:

- In the project management box, right-click on the radiation option, then choose far field, then infinite sphere
- Then, with a step size of 90, alter phi from 0 to 90 degrees, and with a step size of 10, change theta from 0 to 360 degrees.

- Then, on the tool bar, click on the analyzing all option, then go to the result, click on far field report, then click radiation report, then select correct infinite sphere and other settings like Gain in dB, then click OK.
- For peak Gain calculation, select antenna parameter in radiation report and then click on peak gain.

For calculating "Surface Current Distribution" of the proposed antenna, following steps are followed:

- Select patch, right-click to "Add plot fields," select "Mag_ Jsurf," "all object," "concern resonant frequency," "ok," and "start analyze all"
- For calculation of current distribution at other frequencies, click "analysis" in the project manager window, "click" on "solution setup," "change frequency," "ok," and "start analyze all".

For calculating "Surface Current Density Distribution" of the proposed antenna, following steps are followed:

- Select patch, right-click to "Add plot fields," select "Mag_ Jvol," "all object," "concern resonant frequency," "ok," and "start analyze all"

For calculating "Radiation Pattern" of the proposed antenna, following steps are followed:

- In the project management box, right-click on the radiation option, then choose far field, then infinite sphere
- Then, with a step size of 90, alter phi from 0 to 90 degrees, and with a step size of 10, change theta from -180 to 180 degrees.
- Then, on the tool bar, click on the analyzing all option, then go to the result, click on far field report, then click radiation report, then select gain phi and gain theta.
- Then in families, select all for phi and select the frequency, then click OK.

- For calculation of radiation pattern at other frequencies, click "analysis" in the project manager window, "click" on "solution setup," "change frequency," "ok," and "start analyze all".
- For Co polarization (H Plain); gain phi for phi = 90 degree
- For Co polarization (E Plain); gain theta for phi = 0 degree
- For Cross polarization (H Plain); gain phi for phi = 0 degree
- For Cross polarization (E Plain); gain theta for phi = 90 degree

4.2 Parametric Analysis of Proposed Antenna

To investigate the efficacy of the antenna, a number of the most influential design parameters have been analyzed. It has been observed that the frequency response of an antenna is determined by the feeding techniques, shape of the patch and the dimension of the substrate. Feeding mechanisms, slot insertion on circular patch substrate thickness and material have been researched utilizing iteration to improve antenna performance.

4.2.1 Effect of Feeding Technique

There are multiple methods available for the delivery or transmission of electromagnetic energy to a microstrip patch antenna. In order to improve the antenna's ability to match input impedance, feeding is essential for achieving peak antenna performance. These two feeding approaches are widely observed and commonly practiced:

A. Coaxial Probe Feed
B. Micro-strip Line Feed

4.2.1.1 Coaxial Probe Feed

The feeding techniques often employed for microstrip patch antennas include coaxial cable and probe feeding methods. This phenomenon can be attributed to its widespread adoption. As depicted in Figure 4.4, the inner conductor of the cable crosses the dielectric material and solders to the radiating metal patch. As seen in figure 4.4, the ground plane connects to the cable's outer conductor. The obtained parameter values for feeding are presented in Table 4.2. One of the main advantages

of this feeding method is its ability to set the feed at any location on the patch, hence allowing for the matching of cable impedance with the antenna input impedance. This particular feeding method yields a minimal quantity of extraneous radiation. However, a notable limitation of this approach is its limited bandwidth and the challenges associated with its modeling. This is due to the requirement of drilling a hole in the substrate, which allows the connector to extend beyond the ground plane. Moreover, when dealing with substrates of greater thickness, an elongation of the probe length leads to a higher degree of inductance in the input impedance, hence resulting in impedance matching challenges.

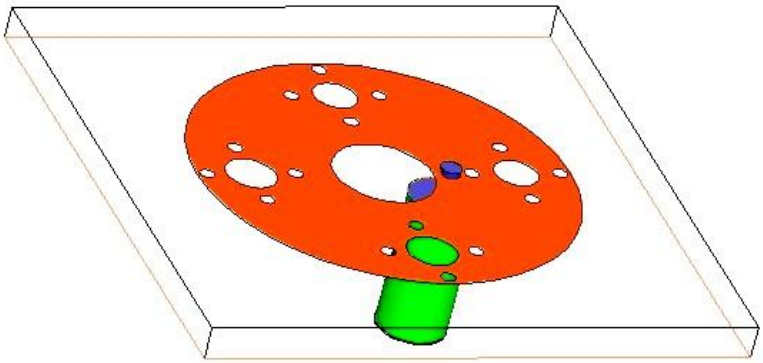

Figure 4.4 Coaxial probe feeding technique

Table 4.2 Coaxial probe feed parameters

Name	Value (mm)	Description
R_I	0.63	Radius of inner conductor of coaxial feed
ε_r	2.1	Dielectric constant of feed
R_O	2.61	Radius of outer conductor of coaxial feed

4.2.1.2 Micro-strip Line Feed

A conducting strip is instantly linked to the Micro-strip patch edge, as shown in Figure 4.5. The advantage of employing this particular feed arrangement is in the ability to etch the feed on the similar substrate, resulting in a planar structure. Compared to the patch, the conducting strip is narrower. The junction inset cut in the patch matches the feed line and patch input impedances without a matching device. The estimated parameters for micro-strip line feeding are presented in Table 4.3. The

desired outcome can be achieved by modifying the placement and measurements of the inset incision. Hence, the aforementioned feeding system can be considered straightforward in its design, since it is characterized by its uncomplicated construction, straightforward modeling, and effective impedance matching. Nevertheless, when the dielectric substrate thickness increases, the occurrence of surface waves and unwanted feed radiations also increases, resulting in a decrease in the antenna's bandwidth. The production of cross-polarized radiation is also observed as a result of the feed radiation.

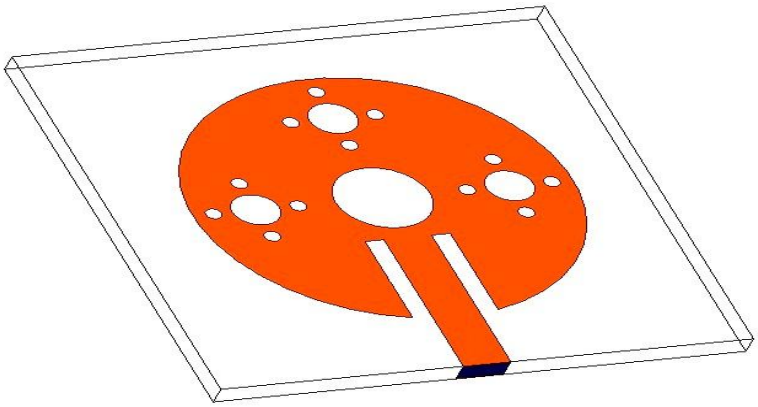

Figure 4.5 Circular patch antenna with inset microstrip feeding

Table 4.3 Microstrip line feed parameters

Name	**Value (mm)**	**Description**
F_L	12.79	Length of feedline
F_W	2.99	Width of feedline
G_{PF}	1.2	Gap between the feedline and patch

The proposed antenna's parameters VSWR, BW, S_{11} and and resonant frequency were compared using Coaxial Probe and Micro-strip Line feeding methods. Figure 4.6 illustrates the fluctuation of the reflection coefficient (S_{11}). S_{11} represents the reflection coefficient of a device. It measures how much of the input signal is reflected back to the input port of the device under test (DUT). In other words, it quantifies how much of the signal sent into port 1 is reflected back from that port due to impedance mismatches. With a coaxial probe, the suggested antenna has a bandwidth of 360, 720 and 1800 MHz at 12.5 and 7.5 GHz. A micro-strip feedline gives the antenna bandwidths of 2250, 1170, 90, 450, and 180 MHz at 17.5, 15, 12.8,

7 and 3.5 GHz respectively. Both feedline techniques will attain a VSWR that is deemed satisfactory, with a value below 2. Micro-strip feedlines have better bandwidth than coaxial probe feedlines. The micro-strip feedline antenna has five frequency bands, while the coaxial probe feed antenna has three. The study examines the impact of various feeding approaches, and the findings are consolidated and shown in Table 4.4.

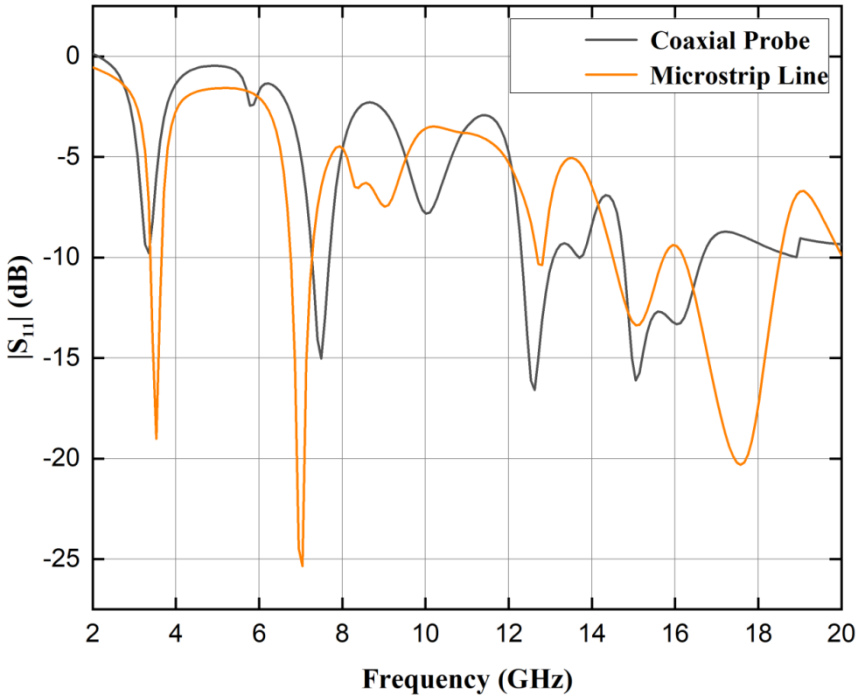

Figure 4.6 Simulated S_{11} curves for various feeding techniques

4.2.2 Substrate Material Effect

Studying the antenna's reflection coefficient (S_{11}), voltage standing wave ratio (VSWR), operating bandwidth (BW), and resonant frequencies (fr) on FR4 and Rogers 5880 substrates assessed its performance. The analysis of the variations in S_{11} is carried out and the findings are depicted in Figure 4.7. The summary of the differences in other distinctive parameters can be found in Table 4.4.

4.2.3 Substrate Thickness Effect

In order to examine, how substrate material thickness affects antenna resonance and impedance matching, the substrate material thickness was purposefully varied. Figure 4.8 illustrates the fluctuations in the S_{11} parameter according to different substrate

thicknesses. Table 4.4 displays the range of variations in VSWR. It is worth mentioning that the optimal outcomes are attained when the substrate thickness (h) is equal to 1.6 mm.

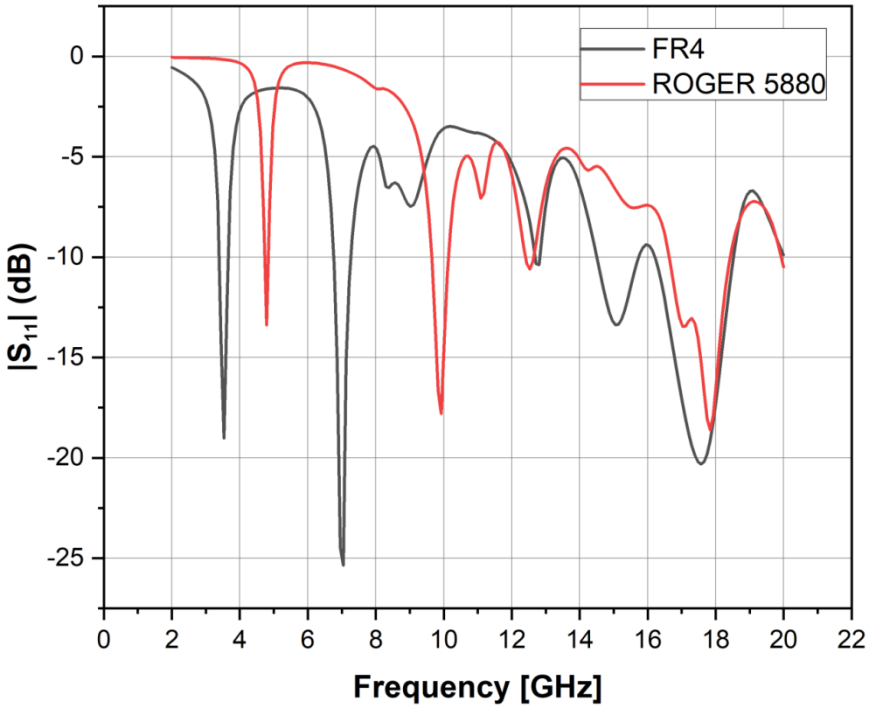

Figure 4.7 Simulated S_{11} curves for various substrates

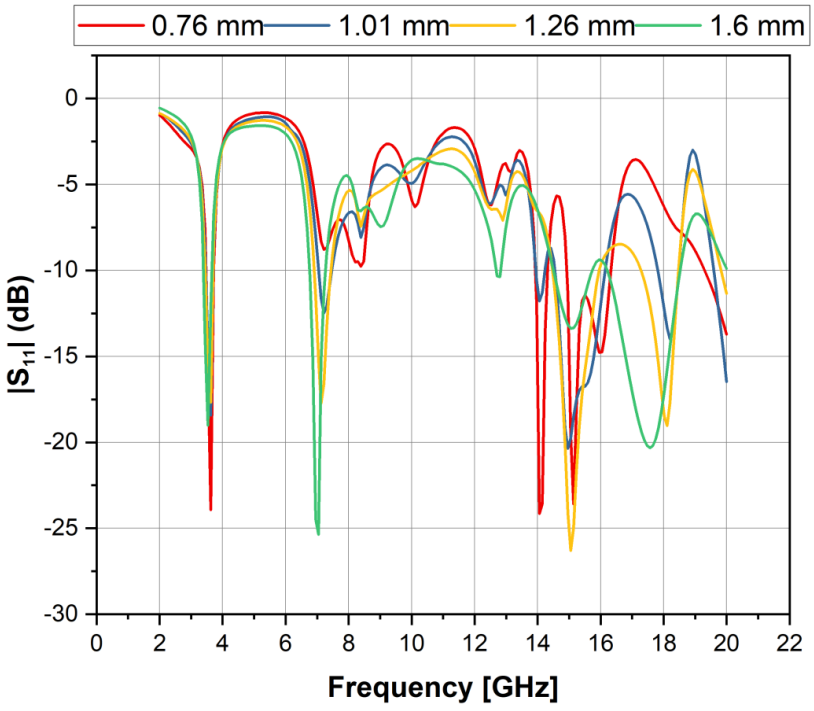

Figure 4.8 Simulated S_{11} curves for variations in substrate thickness

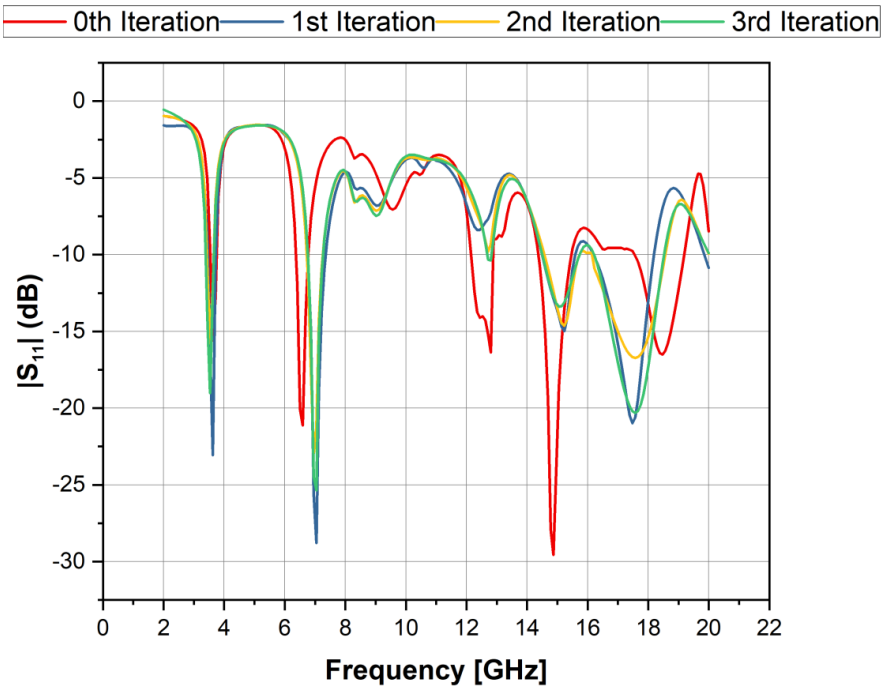

Figure 4.9 S_{11} curves for different iteration (Simulated)

4.2.4 Effect of Iteration

The study examines the impact of various iterations and presents the findings in Table 4.4.

Table 4.4 Analysis of parameters performance

Parameter Variation		**BW (MHz)**	**VSWR**	**S_{11} (dB)**	**f_r (GHz)**
Feeding Effect	Coaxial Probe	1800, 720, 360	1.5, 1.3, 1.3	-12.9, -16.11, -16.12	7.5, 12.5, 15
	Inset Microstrip Line	**180, 450, 90, 1170, 2250**	**1.2, 1.1, 1.8, 1.5, 1.2**	**-19, -25.3, -10.3, -13.3, -20.2**	**3.5, 7, 12.8, 15, 17.5**
Substrate Material	Roger (5880)	60, 540, 540, 1189	1.4, 1.3, 1.8, 1.2	-13, -18, -10, -25	4.8, 9.9, 12.5, 17.8
	FR4	**180, 450, 90, 1170, 2250**	**1.2, 1.1, 1.8, 1.5, 1.2**	**-19, -25.3, -10.3, -13.3, -20.2**	**3.5, 7, 12.8, 15, 17.5**

Substrate thickness (mm)	0.75	90, 270, 1350, 540	1.2, 1.2, 1.1, 1.5	-27, -31, -26, -13.71	3.6, 14.1, 15.1, 20
	1.01	90, 270, 180, 1530, 630, 360	1.3, 1.6, 1.7, 1.2, 1.4, 1.3	-20, -12, -12, -20, -13, -16	3.6, 7.2, 14.1, 15, 18.2, 20
	1.26	90, 450, 1350, 1080, 90	1.4, 1.3, 1.1, 1.2, 1.7	-19, -17, -26, -19, -11	3.6, 7.1, 15.1, 18.1, 20
	1.6	**180, 450, 90, 1170, 2250**	**1.2, 1.1, 1.8, 1.5, 1.2**	**-19, -25.3, -10.3, -13.3, -20.2**	**3.5, 7, 12.8, 15, 17.5**
Iteration	0th Iteration	90, 270,90, 990, 1530	1.4, 1.1, 1.3, 1.06, 1.3	-16, -21, -16, -29, -16	3.6, 6.6, 12.8, 14.8, 18.5
	1st Iteration	180, 540, 990, 1890	1.2, 1.1, 1.4, 1.2	-26, -34, -15, -21	3.6, 7, 15.2, 17.5
	2nd Iteration	180, 450, 1080, 2250	1.3, 1.2, 1.4, 1.3	-16, -25, -14, -16	3.5, 7, 15.2, 17.6
	3rd iteration	**180, 450, 90, 1170, 2250**	**1.2, 1.1, 1.8, 1.5, 1.2**	**-19, -25.3, -10.3, -13.3, -20.2**	**3.5, 7, 12.8, 15, 17.5**

Figure 4.9 displays the S_{11} vs. frequency plot, illustrating the relationship between processed iterations and antenna performance. It is clear that bandwidth increases with iterations. The antenna resonates at five frequencies during the 0th iteration, but with a low BW. Resonance occurs at four frequencies below the -10 dB S_{11} level in the first and second iteration. In the third iteration, quintuple resonance frequencies and increased bandwidths are reached. Thus, the 3rd antenna design balances resonating frequencies and impedance bandwidth. The third iteration stage is considered as final stage for antenna designing as the desired results have been obtained. Further execution of iteration has not been carried out due to fabrication constraints and it would make the structure more complex.

Based on the findings presented in Table 4.4, it is evident that the circular patch antenna, including an inset microstrip feed line, a FR4 substrate with a thickness of 1.6 mm, and up to the third iteration, yields the most favorable outcomes. Therefore, these parameters are deemed to be the definitive parameters for subsequent simulations.

4.3 Surface Current Distribution and Surface Current Density Distribution

The suggested antenna surface current distributions at various resonant frequencies are illustrates in Figure 4.10. This visual representation offers a valuable perspective on the functionality of the proposed antenna.

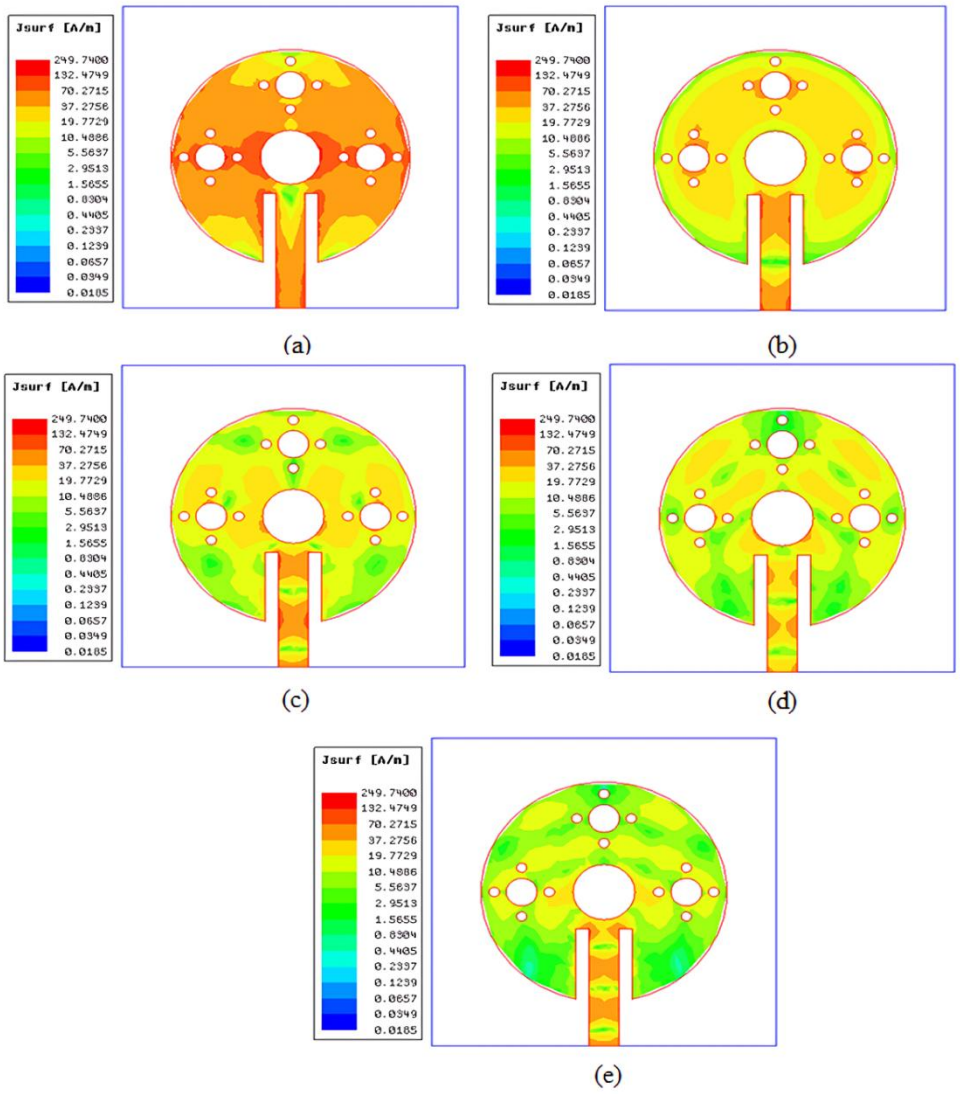

Figure 4.10 (a) 3.5 GHz; (b) 7 GHz; (c) 12.8 GHz; (d) 15 GHz; (e) 17.5 GHz; Surface current distribution

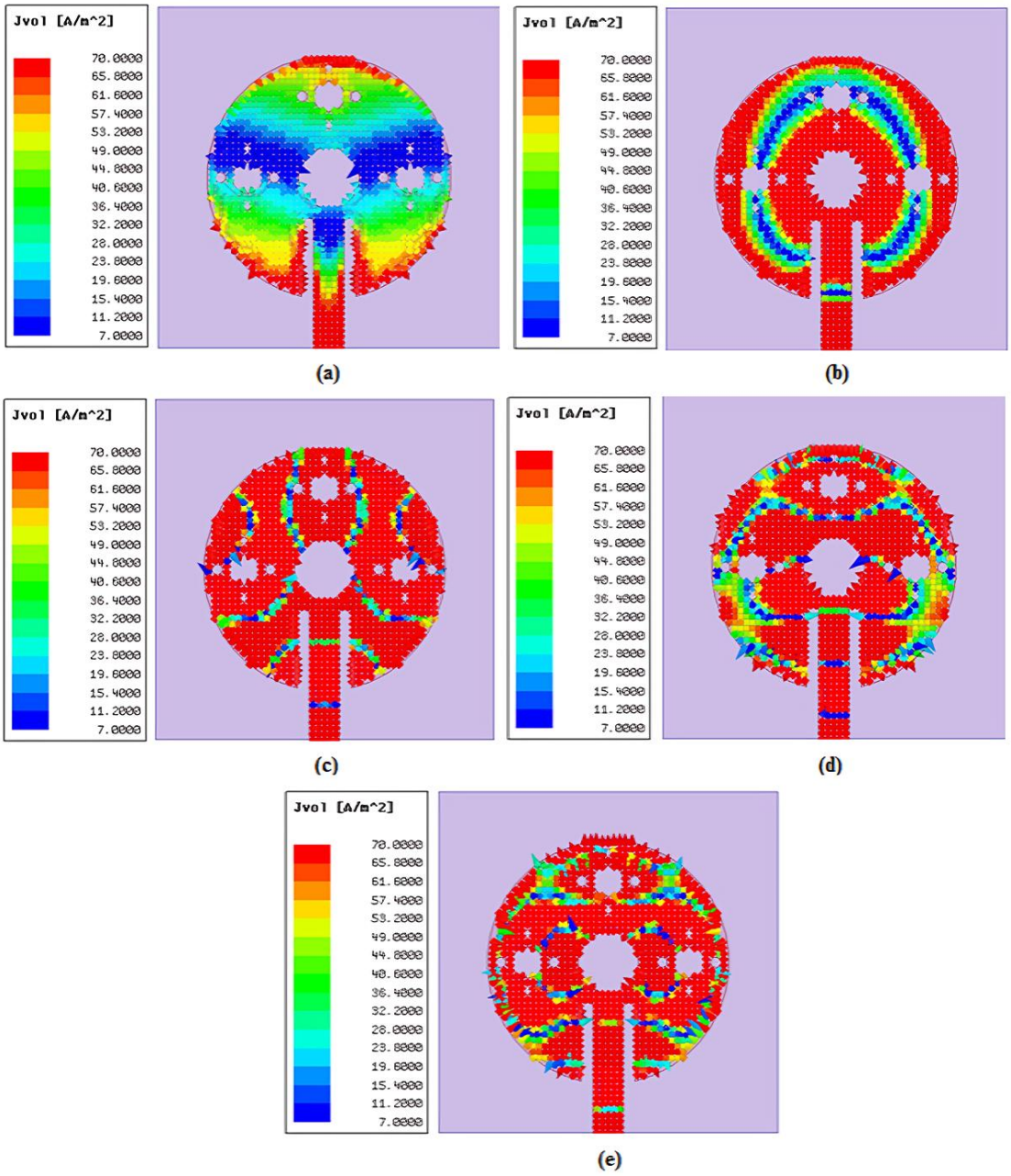

Figure 4.11 (a) 3.5 GHz; (b) 7 GHz; (c) 12.8 GHz; (d) 15 GHz; (e) 17.5 GHz; Surface current density distribution

Figure 4.10 (a) shows that the feed line spreads surface current inside the radiating patch during 3.5 GHz operation. Moreover, the intensity of the surface current is particularly pronounced along the circular slots of the radiating patch. In the case of frequencies at 7 GHz & 12.8 GHz, the dispersed currents primarily exhibit confinement within the circular slots and microstrip feed line. A concentrated surface current is observed at frequencies of 15 GHz and 17.5 GHz in close proximity to the

edges of the feed line. Additionally, a portion of this current circulates through the integrated slots of the radiating patch. This finding supports the idea that adding slots to the radiating patch will improve the antenna's current density at its resonant frequencies. Figure 4.11 illustrates the surface current density distribution (A/m^2) over the circular patch for 5 resonating frequencies to better understand the antenna structure's radiating properties. Based on the observations made in Figure 4.11 (a), it is evident that the distribution of high current density is predominantly concentrated along the feedline and in close proximity to the borders of the circular patch. This particular distribution pattern is accountable for the resonant frequency seen at 3.5 GHz. The current flowing into the patch intensifies as the frequency rises, resulting in heightened excitement of the patch. This heightened excitement is accountable for the resonant frequencies seen at 7 GHz and 12.8 GHz, as depicted in Figure 4.11 (b-c). Based on the observations made from Figure 4.11(d-e), it can be deduced that as the frequency increases, the current distribution becomes more uniform over the patch and in close proximity to the slots. Consequently, the antenna construction exhibits resonance at frequencies of 15 GHz and 17.5 GHz.

4.4 Discussion on Antenna Fabrication and Measurements Results

For experimental validation, the antenna is fabricated on 1.6-millimeter FR4. Figure 4.12 shows the proposed multiband antenna model. The suggested antenna was made on the EP-42 Auto PCB prototype machine. An HFSS file that ended in dxf was imported into the Proteus programme in order to generate a Gerber file, which was the first stage in the process of fabricating the suggested antenna. The further steps are outlined below. After that, the gerber file was imported into the PCAM simulation software that was included with the PCB prototype machine. After that, the prototype machine will swiftly perform operations for the manufacture of the final planned antenna such as engraving, routing, milling, and drilling. Connecting the manufactured antenna to the vector network analyzer (Rohde and Schwarz ZNB - 40 VNA 100 KHZ to 40 GHz) in order to measure the reflection coefficient (S_{11}) and voltage standing wave ratio (VSWR) required the usage of a SMA connector. In an anechoic room, gain & radiation pattern of the antenna are evaluated using a broadband reference horn antenna as the instrumentation for the transmitter. Both the

constructed antenna and the reference horn antenna are positioned directly opposite one another in an anechoic chamber. The appropriate distance between them is determined by applying the far field formula. Figure 4.13 depicts the measurement setup that will be used for the proposed antenna.

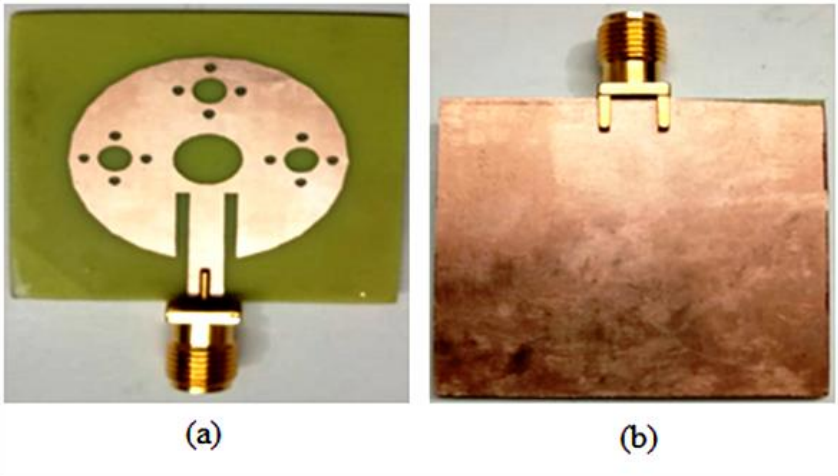

Figure 4.12 Fabricated circular patch microstrip antenna (a) front side (b) back side

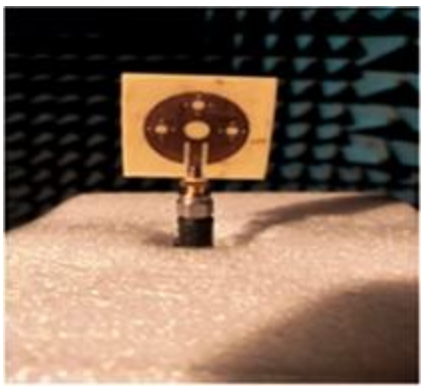

Figure 4.13 Measurement setup for experimental analysis

Figures 4.14, 4.15, 4.16, and 4.17, respectively, exhibit the measured and simulated values for S_{11}, VSWR, realized Gain, and radiation pattern, respectively. According to the results of the simulation, the suggested antenna is capable of resonating at five different frequencies: 17.5, 15, 12.8, 7 and 3.5 GHz with a -10 dB impedance bandwidth of 2250, 1170, 90, 450, and 180 MHz, respectively, for each of these frequencies. Figure 4.14 shows that measurements produced five frequency bands with resonant frequencies of 15.68, 12.62, 8.84, 6.68 and 3.35 GHz and impedance

bandwidths of 6390, 990, 540, 630 and 100 MHz, respectively. These frequencies correspond to the bands' respective resonant frequencies.

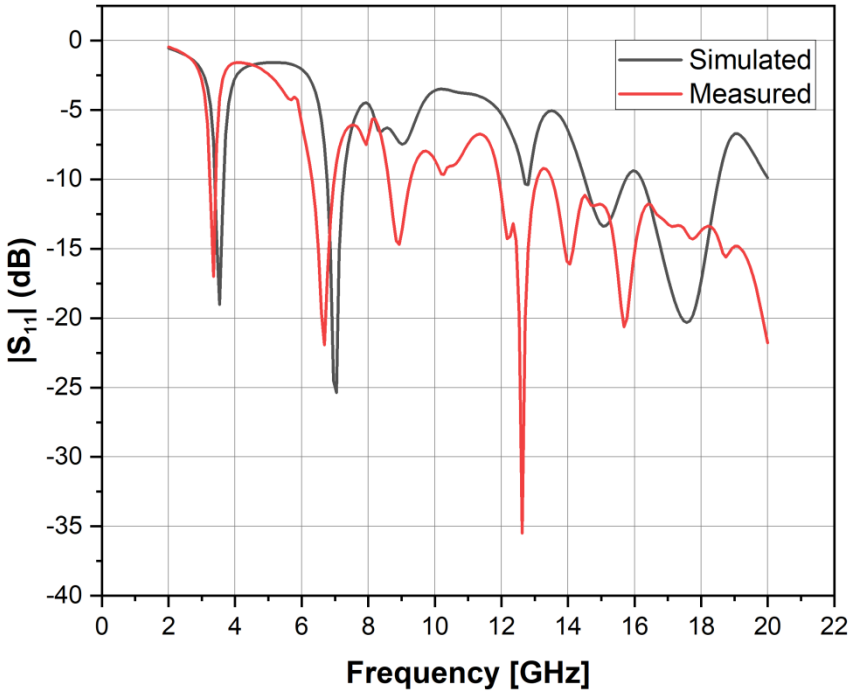

Figure 4.14 Graph of S_{11} (Simulated and measured)

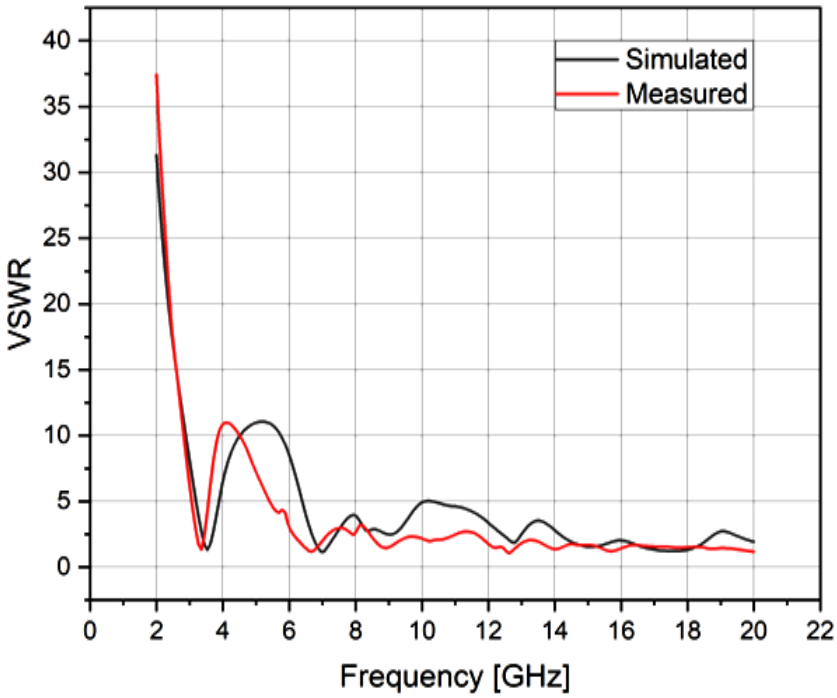

Figure 4.15 Graph of VSWR (Simulated and measured)

The VSWR plot shows that the antenna resonates at 15.68, 12.62, 8.84, 6.68 and 3.35 GHz with VSWR values of 1.20, 1.03, 1.46, 1.17 and 1.32 respectively [see Figure 4.15]; these frequencies have measured VSWR values between 1.03 and 1.20. [see Figure 4.15]. The simulated VSWR and the observed VSWR are both within 2, which indicate that the impedance matching is accurate. Comparing simulated and measured S_{11} values shows a shift in resonant frequencies. Possible variations in the measurements results could occur due to fabrication tolerances, soldering effects of the connectors, losses caused by the feed connector, and measuring cables. However, the fundamental purpose of this research, which was to improve bandwidth overall and keep multiband resonance characteristics, was successfully accomplished. Figure 4.16 presents a graphical representation of the comparative study of the simulated and measured realized gains. Simulation results show that the antenna achieves 6.60 dBi peak gain at 17.5 GHz. However, the largest peak gain achieved was 5.90 dBi according to measured results. Due to multi-reflection in the measurement environment, the reported measured gain result and the simulated gain result vary and are inconsistent.

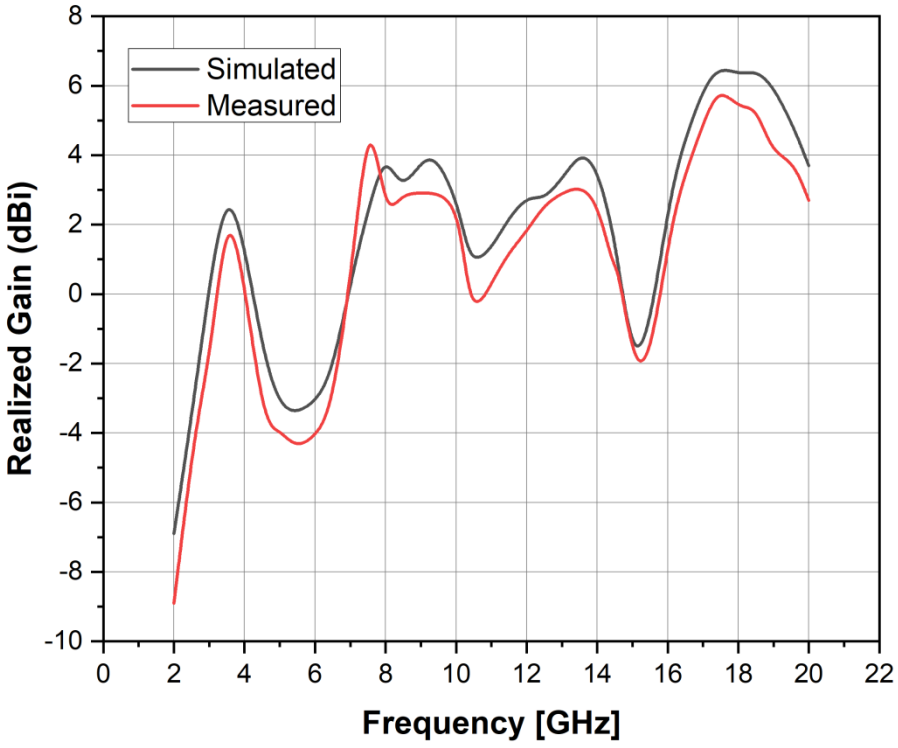

Figure 4.16 Graph of Realized Gain (Simulated and measured)

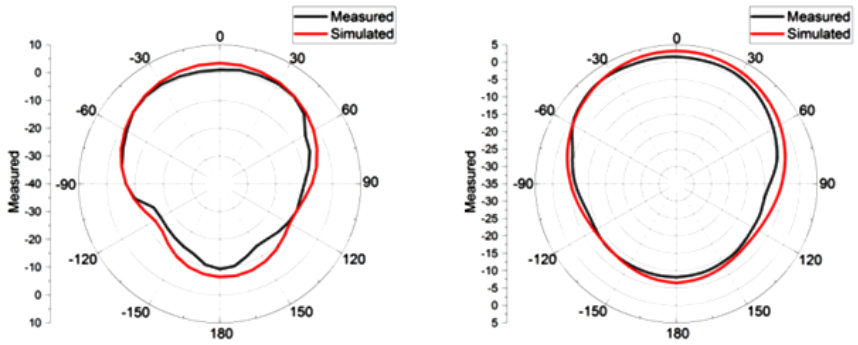
Measured
Simulated
Measured
E Plane
H Plane

(a)

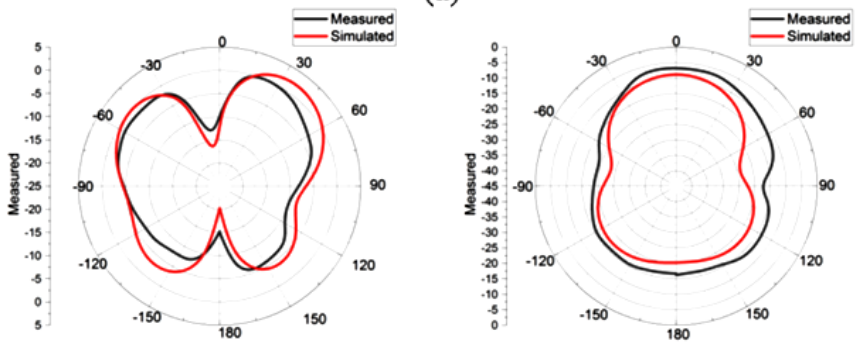
Measured
Simulated
Measured
E Plane
H Plane

(b)

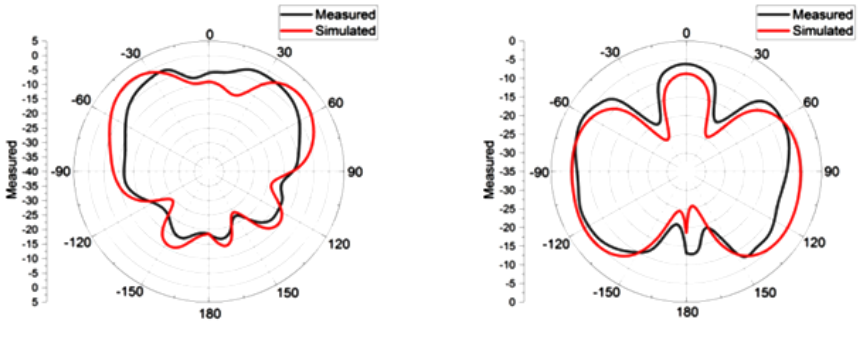
Measured
Simulated
Measured
E Plane
H Plane

(c)

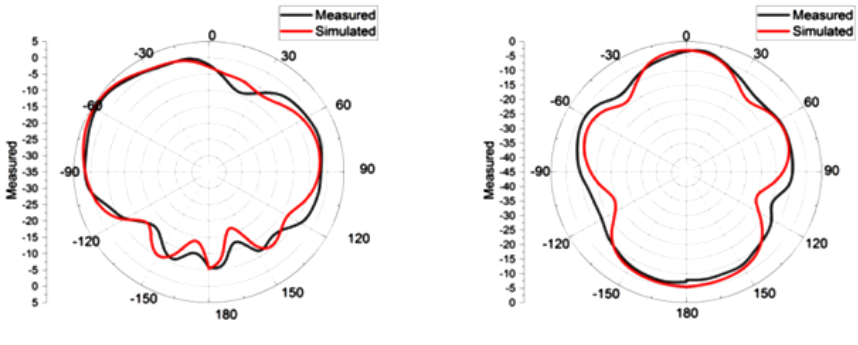
Measured
Simulated
Measured
E Plane
H Plane

(d)

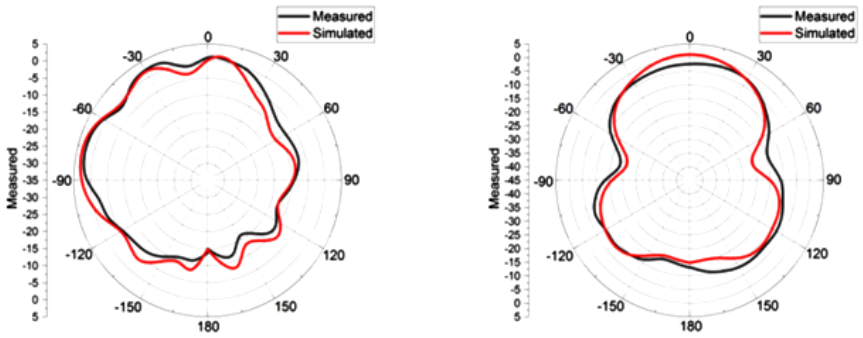

(e)

Figure 4.17 (a) 3.5 GHz, (b) 7 GHz, (c) 12.8 GHz, (d) 15 GHz, and (e) 17.5 GHz, radiation pattern (measured and simulated)

Figure 4.17 depicts the measured and simulated radiation pattern in the E plane (XZ, phi = 0°) and H plane (YZ, phi = 90°) at 3.5, 7, 12.8, 15, and 17.5 GHz, respectively. At 17.5, 15, and 3.5 GHz, the radiation pattern of the suggested antenna is practically omni-directional and steady. At 12.8 and 7 GHz, the pattern is of a dipole nature, which is adequate for the intended applications. The results obtained through simulation and those obtained through experimentation are consistent with one another.

4.5 Performance Comparison of Proposed Antenna with Other Reported Antenna

The efficiency of the proposed penta band antenna is evaluated next to that of several different multiband microstrip antennas that are currently in use. A comparison of the analyzed performance is presented in Table 4.5 and the percentage enhancement and losses of various parameters of the proposed antenna are shown in Figure 4.18 (a, b, c, d). Circular slots on the radiating patch of the proposed antenna make it smaller and increase current density. As shown in the performance comparison table, this antenna operates up to penta band with a broader bandwidth than previous known antenna configurations. Moreover, the proposed antenna is suitable for different wireless communication standards such as mid band 5G Mobile Applications, X, and Ku bands with an attractive miniaturized size.

Table 4.5 Reported MPA studies comparison

Reference	**Size (mm^2)**	**Resonant Frequency (GHz)**	**Bandwidth (MHz)**	**Maximum Peak Gain (dBi)**	**Frequency Bands**	**Application**
[25]	39 × 45	2.34, 3.5, 5.2, 5.5, 5.8	100, 370, 200, 460	4.2	Quad	WiBro, WiMAX and WLAN Application
[31]	32 × 40	2.4, 3.1, 4.5, 6	180, 520, 2090	3.8	Quad	GSM 1800, 2.4/5.2/5.5 WLAN, WiMAX
[34]	80 × 40	2.0, 3.0, 4.0	2650	2.91	Single	Wireless Communication Systems
[36]	56 × 44	1.575, 2.45, 3.5, 5.2	90, 145, 73, 206	5.02	Quad	GPS, WiMAX and WLAN Application
[39]	50 × 50	2.6, 6, 8.2	410, 1070, 4840	5.8	Triple	Wi-Fi, WLAN, Wireless Body Area Network, X and S Band
[45]	40 × 40	5.98, 7.62, 8.20	630, 1350	7.023	Dual	C and X Band Application
[46]	45 × 38.92	2.68, 8.38	180, 3237	5.62	Dual	Bluetooth, X-Band Application

[55]	50 × 50	5.5, 7.2, 8.5	220,220,810	---	Triple	5G Future Mobile Communication
[57]	48 × 48	1.775, 3.725	250, 240	-	Dual	GSM and WiMAX Application
[58]	34.6 × 33.05	5.27, 5.49, 5.93	1010	7.2	Single	5G Wi-Fi Communication
[59]	50 × 35	1.61, 2.83, 3.75, 5.24, 5.56	690, 130, 350, 180, 670	2.3	Penta	GPS, WiMAX and WLAN Application
[60]	31 × 42	5.25, 5.5, 5.75	700	6.5	Single	----
Proposed (X)	**33.56 × 33.56**	**3.35, 6.68, 8.84, 12.62, 15.68**	**100, 630, 540, 990, 6390**	**5.90**	**Penta**	**Ku and Mid band 5G Mobile Application**

The proposed antenna is designed as modified circular disk-shaped patch with simple ground plane structure and microstrip feedline, by adopting parametric analysis on substrate material, substrate thickness and iteration technique to achieve optimum results in terms of compact size, wider bandwidth, better gain and bands. Figure 4.18 (a) clearly shows that the dimensions of the proposed antenna are minimal when compared to prior research. It is only 35% of the maximum dimension reference antenna [34]. Figure 4.18 (b) shows that the suggested antenna bandwidth is used as a baseline for calculating bandwidth increase in percentages, and when the base value is

compared to other references, it appears that other antenna studies yield less bandwidth. For example, reference no. 25 is just 7% of the base value, indicating that the proposed antenna generates 93% more bandwidth.

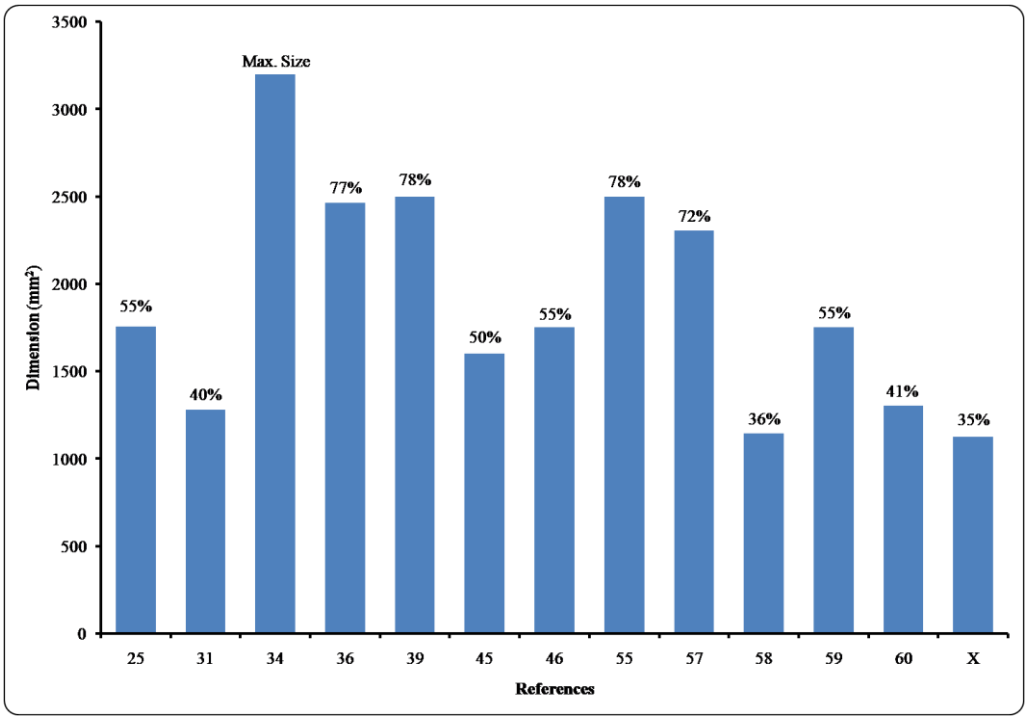

(a)

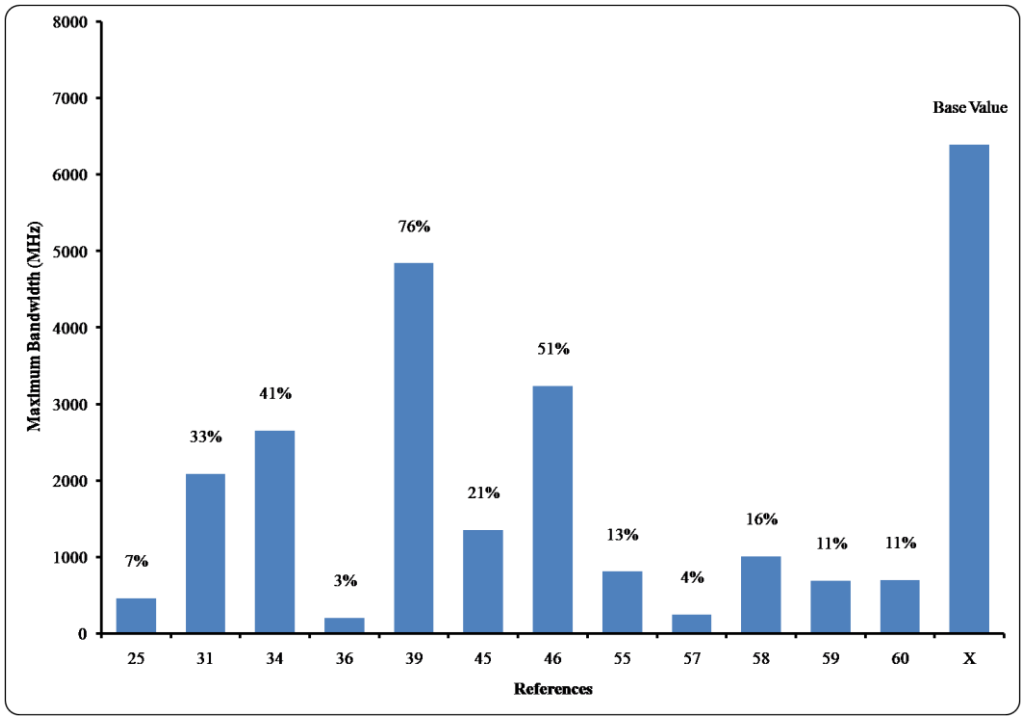

(b)

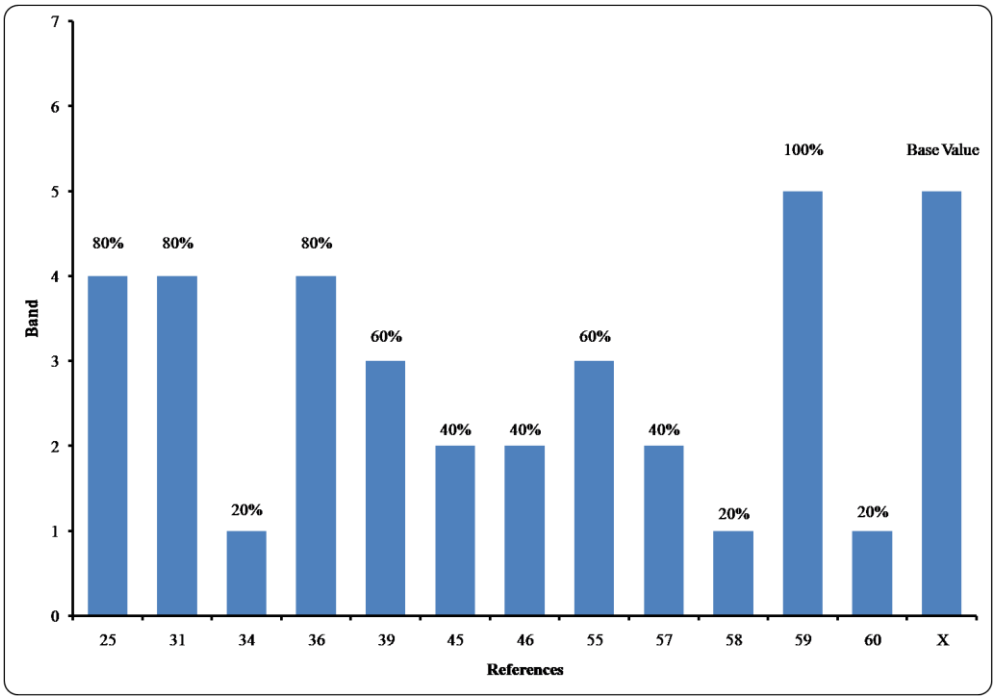

(c)

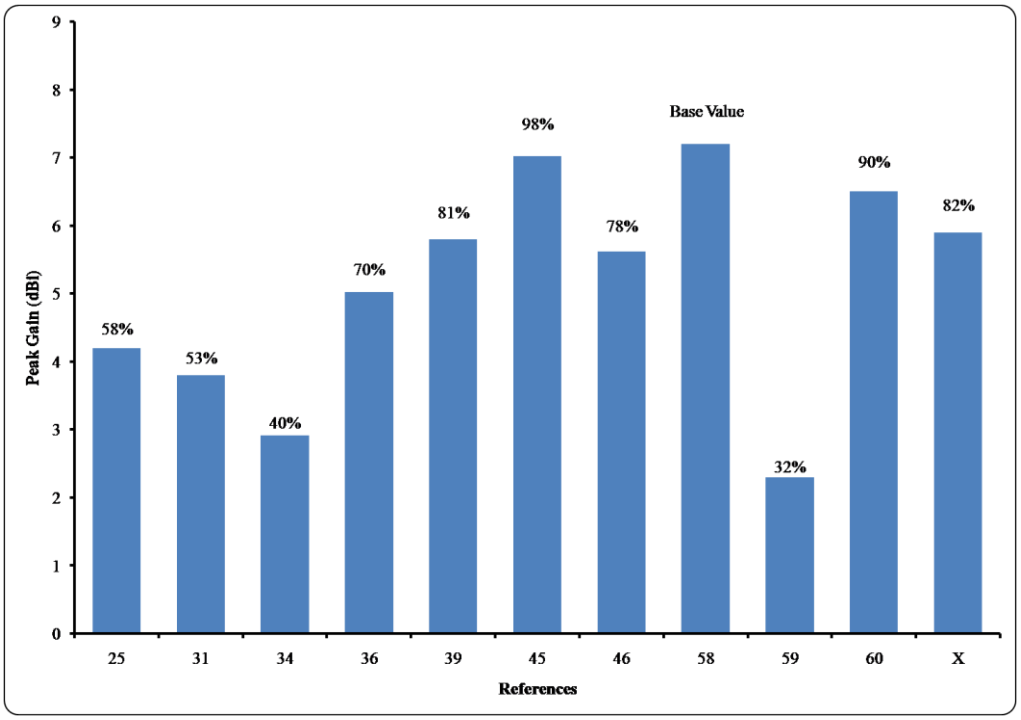

(d)

Figure 4.18 Performance comparison of proposed antenna with other studies in % enhancement and loss (a) Dimension, (b) Bandwidth, (c) Bands, (d) Peak Gain

Figure 4.18(c) depicts the antenna's multiband behaviour. The graph clearly shows that the proposed antenna produces penta band as compared to other studies. Figure 4.18 (d) illustrates the peak gain of the antennas. The value of reference paper 58 is used as a baseline (maximum) when computing peak gain enhancement and losses in percentage. The graph reveals that the proposed antenna is only 82% of its maximum value, indicating that its peak gain is smaller than that of reference papers 58, 45, and 60. However, when compared to these references, the suggested antenna has a wider bandwidth and a smaller size.

Summary

This research study presents a compact circular shaped multiband patch antenna with increased BW. The antenna was designed using circular discs. A comprehensive parametric analysis has been performed on the antenna. For antenna performance validation, experimental study was done and there is a good agreement between the measured values and the simulated values that have been obtained. It has reflection coefficients of -17.01,-21.93,-14.68,-35.49,-20.63 dB and resonates at 3.35, 6.68, 8.84, 12.62, and 15.68 GHz. It covers frequency bands ranging from 3.26 to 3.36 GHz, 6.32 to 6.95 GHz, 8.66 to 9.20 GHz, 11.99 to 12.98 GHz, &13.61 to 20 GHz. Five frequency bands have -10 dB operational BW: 100, 630, 540, 990, & 6390 MHz. The proposed antenna is straightforward in terms of both its design and its implementation. The results show that our proposed antenna outperforms other multiband antennas. The unique antenna structure maintains stable radiation patterns and appropriate gains across all operating frequency bands while working in quintuple bands with enlarged bandwidths in a compact attractive size. This aspect also contributes to the originality of the proposed antenna structure. The suggested antenna is well suited for use in 5G mobile applications operating in the X, Ku, and Mid bands.

CHAPTER 5

DEVELOPMENT OF MODIFIED MIMO ANTENNA FOR N258 (24.25-27.25 GHZ) 5G NEW RADIO (NR) BAND APPLICATIONS

This chapter examines a fractal based micro-strip-fed MIMO antenna for 5G mm-wave mobile applications. The proposed design consists of a circular structure that is based on fractal principles. This structure has rectangular ground plane slot and circular patch slots of various iterations. Patch isolation gets reduced by addition of these slots. The MIMO antenna has two close-together antenna elements. These antenna components exhibit resonance at numerous frequencies within the frequency range of 8 to 28 GHz. Specifically, the resonant frequencies of the antenna elements are seen at 26.6, 21.1, 15.8, 13.4, 11.1 and 9.5 GHz. The antenna's maximum operational frequency range, with a bandwidth of 10300 MHz, is from 17.7 GHz to 28 GHz. Thus, it is ideal for, (n258), 5G NR frequency band especially for the mm wave application and shows the wideband antenna behavior. By combining the features of both MIMO and wideband functions into a single design, adaptive antennas may be created that effectively meet the needs of modern wireless 5G communication systems. Additionally, it partially encompasses other frequency bands like as X and Ku. All of the bands that exhibit resonance demonstrate isolation levels that fall below the permissible threshold of ($|S_{12}|$>-16 dB). The antenna under consideration employs a substrate made of FR4 material, which has dimensions measuring 28.22 mm by 44 mm. A study is undertaken to assess the efficacy of various antenna characteristics, such as S parameters, surface current distributions and radiation pattern. Moreover, a comprehensive analysis and assessment are undertaken to evaluate the effectiveness of the diversity system inside the MIMO architecture. An ECC, DG, and MEG are examined in this study. Assessed antenna properties are suitable for the suggested MIMO configuration. The antenna design was validated through experiment, and the results of the simulation were then confirmed.

The suggested work covers these objectives in this chapter:

1. Circular shaped MIMO antenna design for fifth generation new radio band

(n258) applications using HFSS software.

2. Optimal outcomes are the goal of investigations. The analysis begins by optimizing antenna element spacing. Next, the antenna is checked in three orientations and for ground plane defects.
3. The optimized antenna is built and tested experimentally.

5.1 Design Procedure

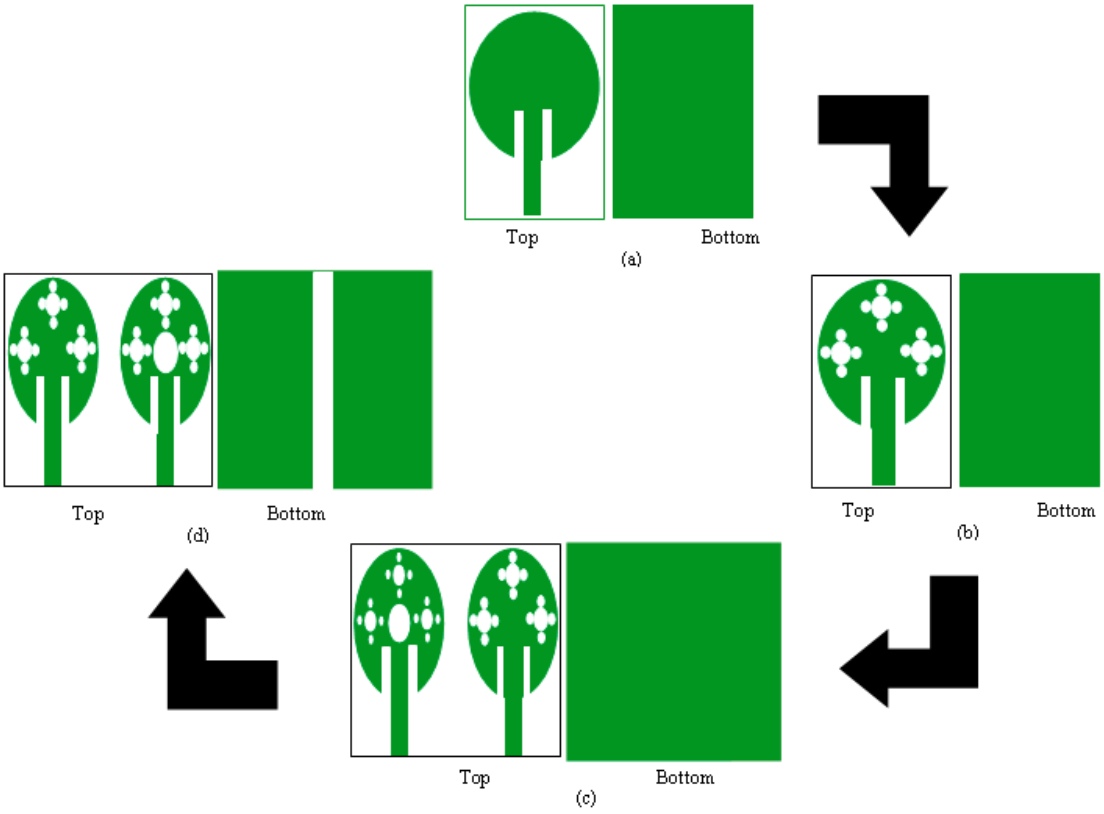

Figure 5.1 Design Method: (a) normal spherical MPA (b) spherical MPA (fractal) (c) MIMO spherical antenna (d) MIMO antenna with DGS

Figure 5.1 (a) shows a circular patch-shaped single-element antenna which is designed first. At this point, antenna design begins. The patch is then fractalized, as illustrated in Figure 5.1 (b), and Figure 5.1 (c) displays the design with a two-element MIMO structure. This study aims to create a MIMO antenna with a defective rectangular ground plane (Figure 5.1 (d)). This will enable 5G applications using millimeter wave frequencies, the paper's main goal. The step-by-step design approach, optimization, and results will follow.

Table 5.1 Parameters of single element circular patch microstrip antenna

Sr. No.	Parameter	Formula	Size (mm)
1.	Radius (A)	$A_e = \frac{1.8412 \text{ x Vo}}{2 \times 3.14 \times \text{fr} \times \sqrt{\text{Er}}}$	9.31
2.	Length of substrate	$S_L = L + 6H$	28.22
3.	Width of substrate	$S_W = W + 6H$	28.22
4.	Substrate with thickness	----------	FR4/1.6
5.	Length of feed	$\mathbf{F_w} = \frac{7.48H}{e^{\left(z_0 \times \frac{\sqrt{(\varepsilon_r + 1.41)}}{87}\right)}} - 1.25t$	11.007 mm
6.	Width of feed	F_W	2.99 mm

5.1.1 Evaluation of Single-Element Antenna Design

Figure 5.2 shows a fractal structure used to build a single antenna element. Selection of a circular patch antenna with a resonant frequency of 9.5 GHz was made for the purpose of designing the proposed antenna. The circular micro-strip patch antenna parameters can be calculated using Table 5.1 formulae. Figure 5.3 and Table 5.2 illustrates the several stages of iteration and the methodology employed for determining the radius of the inner circles.

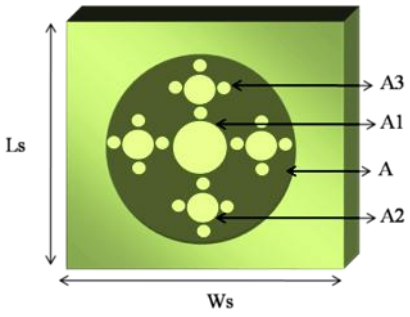

Figure 5.2 Single element circular patch microstrip antenna

5.1.2 Single Element Antenna Results and Discussion

The analysis of S-parameters is conducted in order to obtain a deeper understanding of the performance characteristics shown by the antenna. Figure 5.4 illustrates each stage of the single-antenna iteration process, together with the corresponding

scattering parameter values. Additionally, Table 5.3 presents the outcomes of several iteration studies, focusing on the impact of their findings. The graph shows that bandwidth and bands improve with iterations. In the first iteration (0th), the antenna design uses a circular patch (Figure 5.3). The circular antenna architecture enables multiple resonance modes for each frequency band. Table 5.3 shows that the antenna resonates at 26.4 GHz, 18.8 GHz, and 9 GHz.

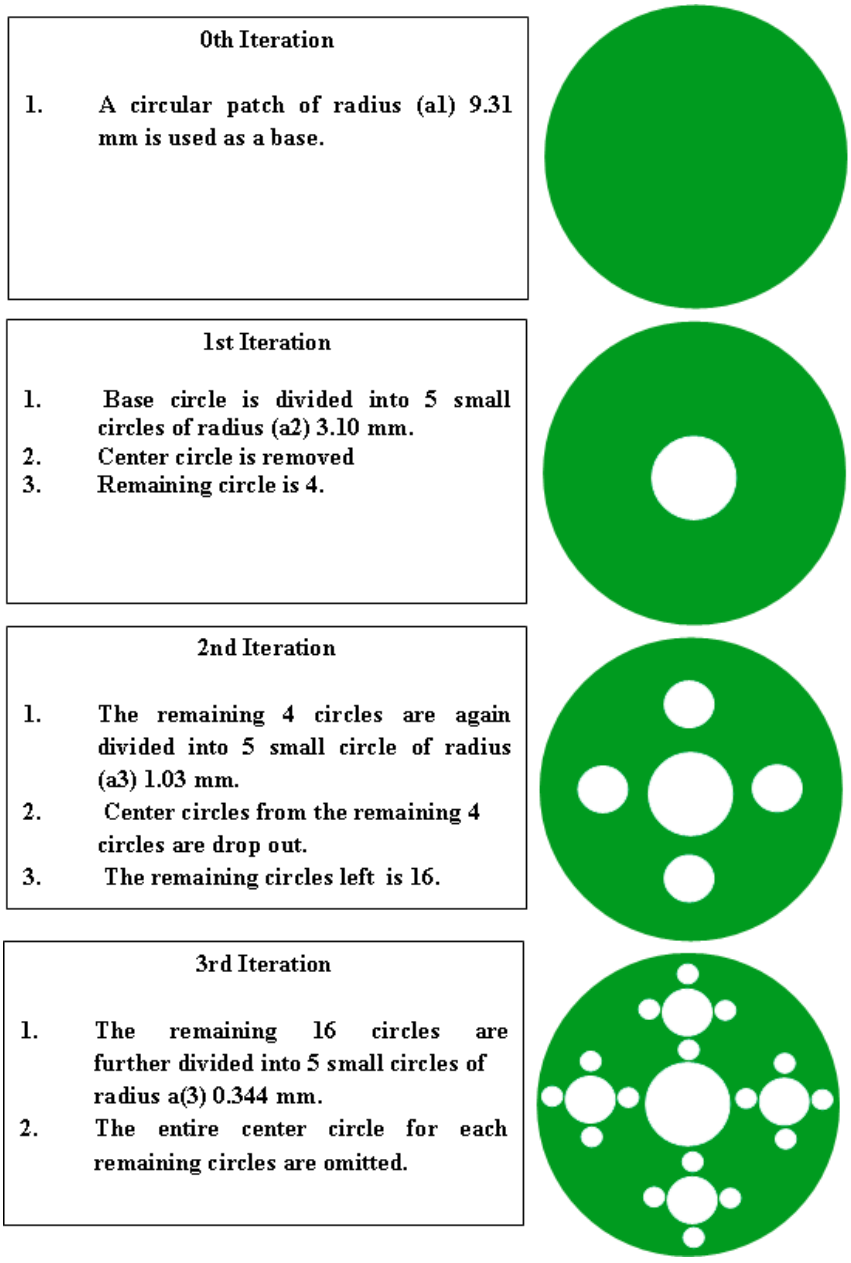

Figure 5.3 Proposed antenna development iterations stages

Table 5.2 Radius calculation process

A1	**A2**	**A3**
N1 : Circle No's $= 5^1$	N2 : Circle No's $= 5^2$	N3 : Circle No's $= 5^3$
S1 : Scaling factor $S1 = (1/3)^1 = 0.333$	S2 : Scaling factor $S2 = (1/3)^2 = 0.111$	S3 : Scaling factor $S3 = (1/3)^3 = 0.037$
A1 : 0.333×9.31 $= 3.10$ mm	A2 : 0.111×9.31 $= 1.03$ mm	A3 : 0.037×9.31 $= 0.344$ mm

The antenna resonates at 26.2 GHz, 21.7 GHz and 9.3 GHz with a single slot (1st iteration) on the patch, as shown in Figure 5.3. Slot loading on the radiating patch changes antenna resonance. This phenomenon can be attributed to the increased concentration of scattered surface currents in the vicinity of the edges of the embedded slots. Thus, the antenna's resonant properties change due to electric field & magnetic field distribution changes. The surface currents that are produced at the borders of the slots give rise to supplementary resonance, leading to a wider bandwidth when compared to the original iteration. During the second iteration, resonance is observed at four distinct frequencies, all of which have signal intensity below -10 dB S_{11}. Consequently, the iterative process has been executed for the subsequent iteration (iteration 3), yielding an antenna that exhibits resonance at five distinct frequencies, thereby augmenting its bandwidth. The aforementioned analysis suggests that the antenna arrangement employed in the third iteration yields equitable results regarding of BW and resonating frequencies.

The graphical representation in Figure 5.5 depicts the maximum peak gain achieved by a single antenna. The graphic shows that the proposed antenna has 8.46 dBi peak gain. The antenna's radiation efficiency is shown in Figure 5.6. The depicted graph indicates that the highest efficiency achieved by the proposed antenna is 78%. Figure 5.7 shows the simulated E and H plane radiation patterns of the single element patch antenna at different resonant frequencies. At 21.5 and 26.7 GHz, the antenna has many lobes and partially omni directional radiation.

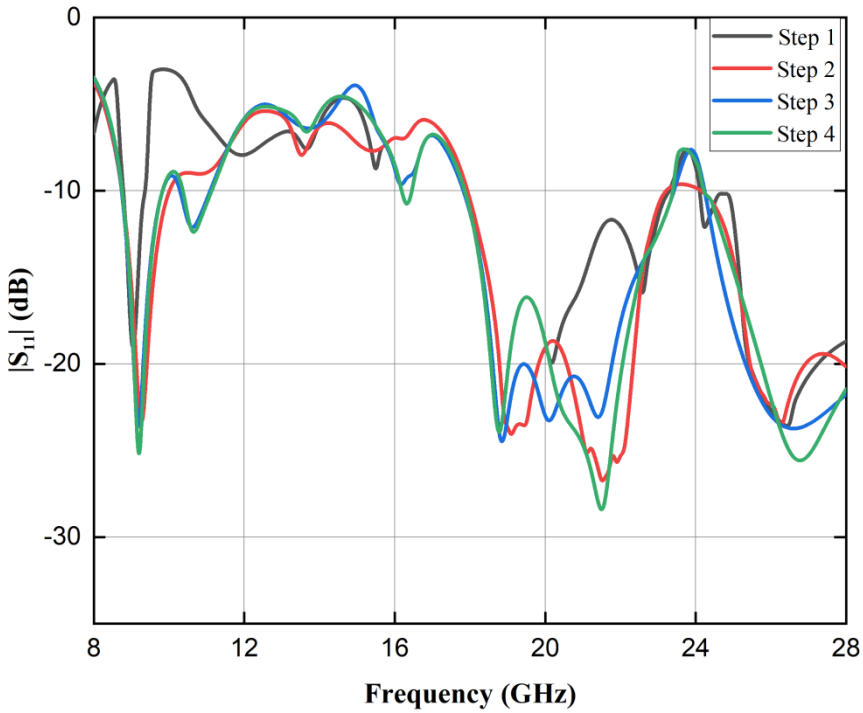

Figure 5.4 Single element scattering parameters

Table 5.3 Single element iteration effect

Parameters (Iteration)	**f_r (GHz)**	**BW (MHz)**	**S_{11} (dB)**
Zeroth	9, 18.8, 26.4	400, 5400, 3800	-19.6, -24.2, -23.5
First	9.3, 21.7, 26.2	1200, 5200, 3800	-23.8, -26.2, -23.4
Second	9.2, 10.6, 18.8, 26.6	1000,700,5500,3700	-24.7, -12.1, -24.5, -23.7
Third	9.2, 10.6,16.3, 21.5, 26.7	1000,700,200,5500,3800	-26.8, -12.4, -10.8, -28.6, -25.5

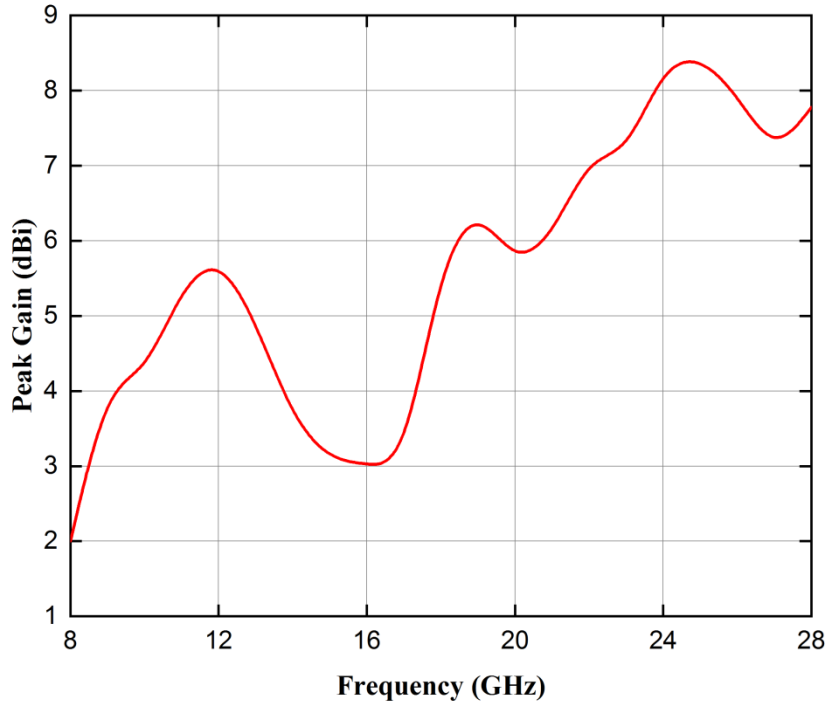

Figure 5.5 Single element antenna gain

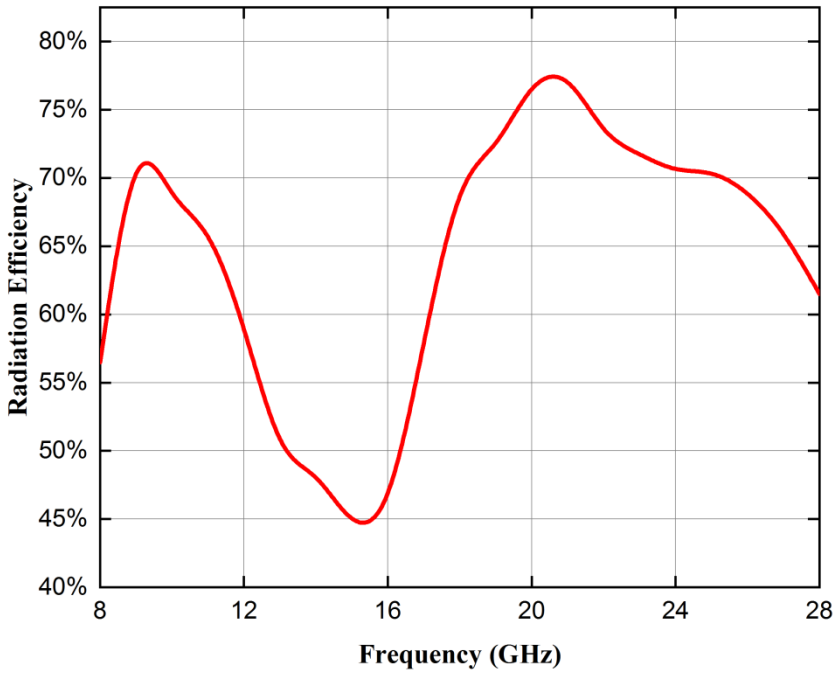

Figure 5.6 Single element antenna radiation efficiency

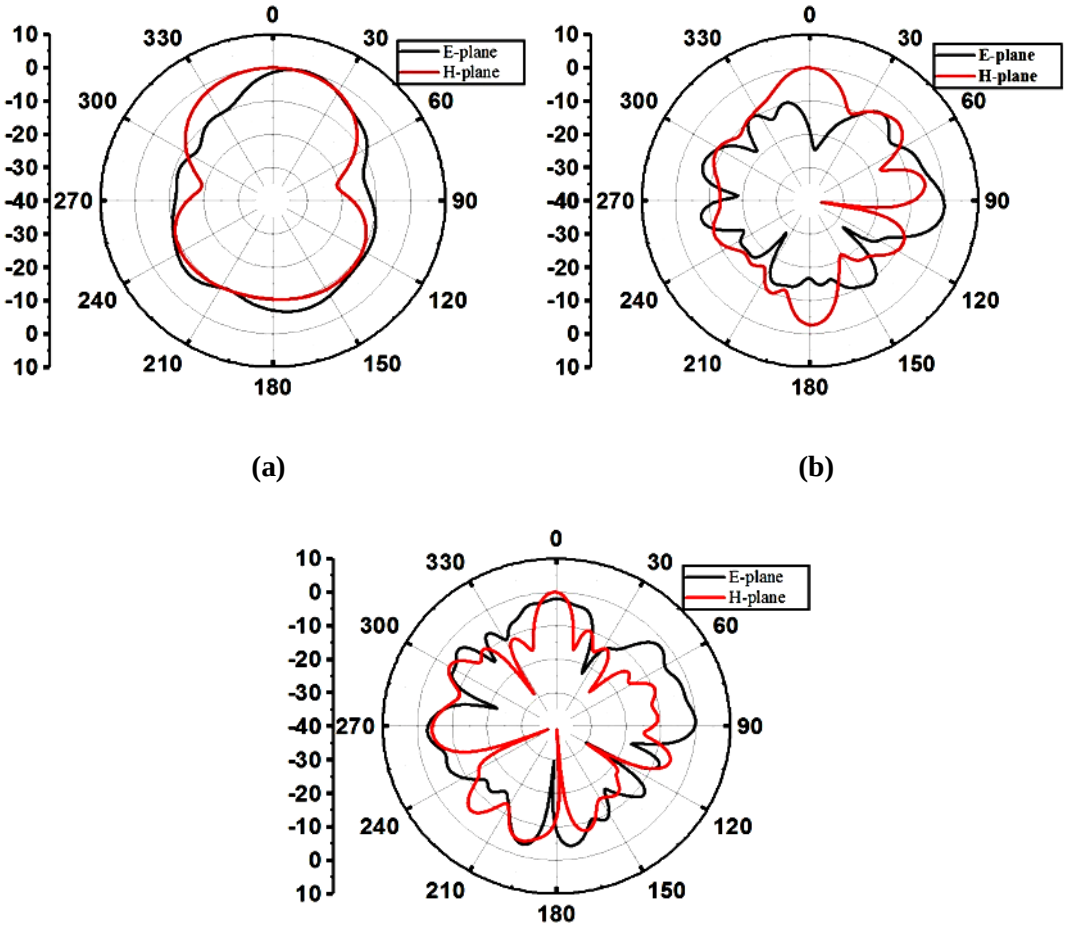

Figure 5.7 Co Polarization Radiation pattern simulation (a) 9.2 GHz (b) 21.5 GHz) (c) 26.7 GHz

5.2 MIMO (2 No's Element) Antenna Design Process using HFSS Software

The proposed antenna is a wideband antenna with two ports. The antenna under consideration is a fractal geometry MIMO system with a faulty ground structure. The multiband features and large bandwidth with good mutual coupling are novel qualities of our work. The proposed antenna resonates at 26.6, 21.1, 15.8, 13.4, 11.1 and 9.5 GHz. with bandwidth of 10300, 800, 600, 1000, and 1000 MHz. The antenna has 0.004 ECC and -48.37 dB isolation. Its physical dimensions measure 28.22 mm × 44 mm × 1.6 mm. Additionally, the antenna has excellent diversity gain across all frequencies. Figure 5.8 depicts the modified 2-element MIMO antenna.

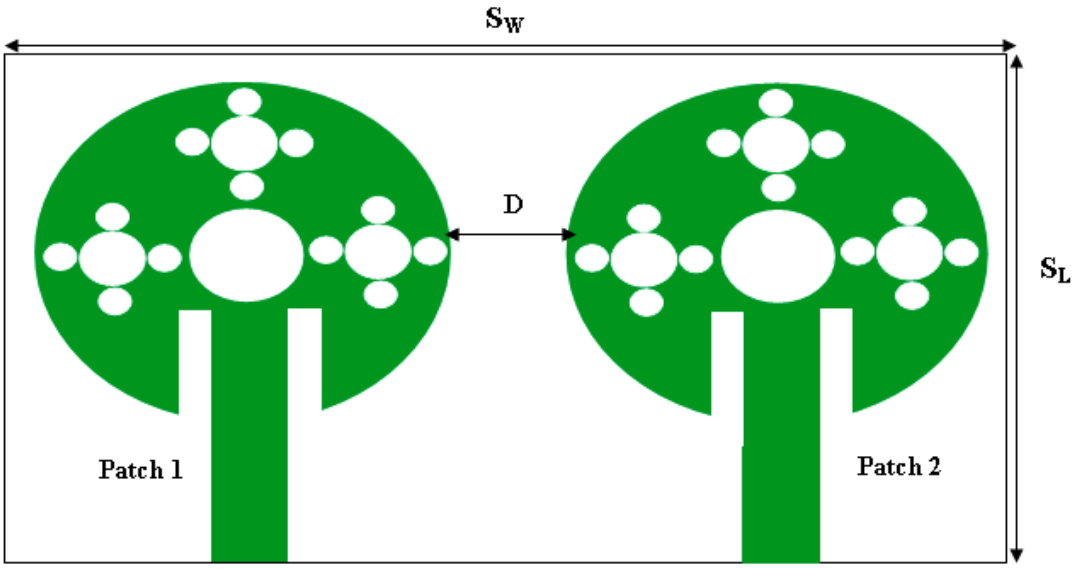

Figure 5.8 MIMO antenna with 2 elements

Initialization of HFSS Software

To initiate the HFSS software, the user should locate and click on the HFSS icon. This action will prompt the HFSS screen to appear. Subsequently, the user should proceed to right-click on the project and proceed with renaming it. Next, select the "Project" option from the toolbar and proceed to click on "Insert HFSS Design". After that, we moved on to the design of an antenna. The initial task involves the design of the substrate and ground plane.

5.2.1 Designing Process

For substrate: To initiate the process, the user should locate and select the "draw box (3D)" option from the toolbar. Following this, the user should proceed to click on any desired location on the screen to create a box. Subsequently, the user should double-click on the box inside the project management interface to access its properties. Inside this menu, the user can modify the name of the box (Rectangular Substrate) and select the appropriate substrate, namely the FR4 option. Finally, the user should confirm their selections by pressing the "ok" button. Subsequently, go to right-click on the "create box" option and modify the dimensions in accordance with the specified requirements.

Position = -14.11,-22, 0

X = 28.22 mm

Y= 44 mm

Z = 1.6 mm

For ground: Rotate the substrate to the back position, then click at an edge of the substrate, drag the arrow to another edge of the substrate, and finally release the arrow. Then rename the box to ground.

After the design of the substrate and ground has been completed, the next task involves the design of the patch.

For patch: Figure 5.9 illustrates the common design for both patches, namely patch 1 and patch 2. The design of both patches is identical. The sole distinction is in the positioning of the patch on the substrate, where each circle is designated a distinct number to enhance understanding of its specific position and radius.

For 0^{th} iteration

Process:

- A 9.31 mm radius of circular patch is the basis structure (1).

Designing Process:

- To initiate the patch design process, it is recommended to first locate the circular icon located within the toolbar. Subsequently, proceed to double-click on circle within the project window. Following this action, modify the name of the selected circle to "circle 1". Next, proceed to right-click on the "create circle" option and make adjustments to the proportions.

Circle 1:

Parameter	Patch 1	Patch 2
Position	0, 11.31, 1.6	0, -11.31, 1.6
Radius	9.31	9.31

For 1^{st} iteration

Process:

- The base construction (1) is scaled by one-third, resulting in 5 little circles (**2, 3, 4, 5, and 6**) with radius A1 (3.10 mm). One central circle (**2**) is removed from the five little circles, leaving four (**3, 4, 5, and 6**).

Designing Process:

- Choose a circle from the toolbar, rename it as "circle 2", and afterwards, perform a right-click on the "create circle" option to adjust the placements according to the specified instructions.

Circle 2:

Parameter	Patch 1	Patch 2
Position	0, 11.31, 1.6	0, -11.31, 1.6
Radius	3.10	3.10

For Circle 3, 4, 5 and 6;

First, select circle 2 by clicking on it. Next, locate the "edit" option and click on it. Once the editing menu is open, select the "copy" function. Afterward, find an appropriate location and choose the "paste" option. By completing these steps, circle 3 will be successfully formed. Please replicate this procedure for circles **4, 5, and 6.** Now, change the position of each circles 3, 4, 5, and 6 to the positions indicated below.

Circle	Parameter	Patch 1	Patch 2
Circle 3	Position	0, 5.11, 1.6	0, -5.11, 1.6
Circle 4	Position	0, 17.51, 1.6	0, -17.51, 1.6
Circle 5	Position	-6.20, 11.31, 1.6	-6.20, -11.31, 1.6
Circle 6	Position	6.20, 11.31, 1.6	6.20, -11.31, 1.6

Then, using the tool bar's subtract option, subtract circle 2 from circle 1. Simply choose circle 1, then circle 2, and then press the subtract option.

For 2nd iteration

Process:

- To achieve this, repeat the previous steps on the remaining 4 circles (**3, 4, 5, and 6**). This involves dividing the 4 circles into 5 small circles (**7, 8, 9, 10, 11, 12, 13, 14, 15, 16, 17, 18, 19, 20, 21, 22, 23, 24, 25, and 26**) of radius (A2) (1.03 mm), removing one centre circle from each 5 small circles (**7, 12, 17 and 22**), and leaving 16 total circles (**8, 9, 10, 11, 13, 14, 15, 16, 18, 19, 20, 21, 23, 24, 25, and 26**).

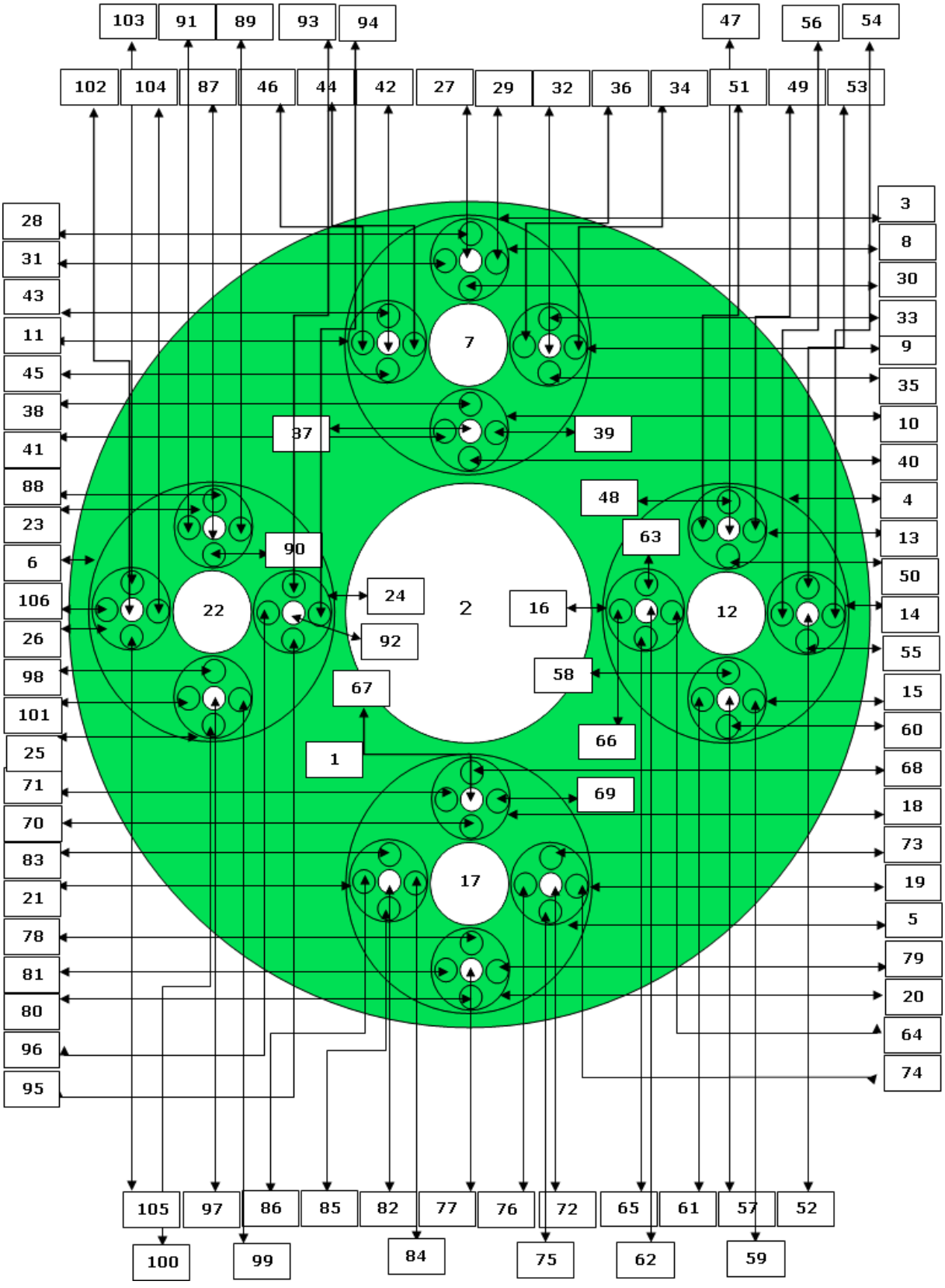

Figure 5.9 Modified circular shaped MIMO antenna patch

Designing Process:

- Choose a circle from the toolbar, rename it as "circle **7**", and afterwards, perform a right-click on the "create circle" option to adjust the placements according to the specified instructions.

Circle 7:

Parameter	**Patch 1**	**Patch 2**
Position	-6.20, 11.31, 1.6	-6.20, -11.31, 1.6
Radius	1.03	1.03

For Circle 8, 9, 10 and 11;

First, select circle 7 by clicking on it. Next, locate the "edit" option and click on it. Once the editing menu is open, select the "copy" function. Afterward, find an appropriate location and choose the "paste" option. By completing these steps, circle **8** will be successfully formed. Please replicate this procedure for circles **9, 10, and 11.** Now, change the position of each circles 8, 9, 10, and 11 to the positions indicated below.

Circle	**Parameter**	**Patch 1**	**Patch 2**
Circle 8	Position	8.26,11.31. 1.6	-8.26, -11.31, 1.6
Circle 9	Position	6.2, 11.31, 1.6	6.2, -11.31, 1.6
	Move	0, 2.06, 0	0, 2.06, 0
Circle 10	Position	6.2, 11.31, 1.6	6.2, -11.31, 1.6
	Move	0, -2.06, 0	0, -2.06, 0
Circle 11	Position	4.13, 11.31, 1.6	-4.13, -11.31, 1.6

Then, using the tool bar's subtract option, subtract circle 7 from circle 3. Simply choose circle 3, then circle 7, and then press the subtract option.

Then same process is repeated for remaining circles 12, 17 and 22.

- Choose a circle from the toolbar, rename it as "circle **12**", and afterwards, perform a right-click on the "create circle" option to adjust the placements according to the specified instructions.

Circle 12:

Parameter	Patch 1	Patch 2
Position	0, 17.51, 1.6	0, -17.51, 1.6
Radius	1.03	1.03

For Circle 13, 14, 15 and 16;

First, select circle 12 by clicking on it. Next, locate the "edit" option and click on it. Once the editing menu is open, select the "copy" function. Afterward, find an appropriate location and choose the "paste" option. By completing these steps, circle **13** will be successfully formed. Please replicate this procedure for circles **14, 15 and 16.** Now, change the position of each circles 13, 14, 15, and 16 to the positions indicated below.

Circle	Parameter	Patch 1	Patch 2
Circle 13	Position	0, 17.51, 1.6	0, -17.51, 1.6
	Move	-2.06, 0, 0	-2.06, 0, 0
Circle 14	Position	0, 19.57, 1.6	0, -19.57, 1.6
Circle 15	Position	0, 17.51, 1.6	0, -17.51, 1.6
	Move	2.06, 0, 0	2.06, 0, 0
Circle 16	Position	0, 15.44, 1.6	0, -15.44, 1.6

Then, using the tool bar's subtract option, subtract circle 12 from circle 4. Simply choose circle 4, then circle 12, and then press the subtract option.

- Choose a circle from the toolbar, rename it as "circle **17**", and afterwards, perform a right-click on the "create circle" option to adjust the placements according to the specified instructions.

Circle 17:

Parameter	Patch 1	Patch 2
Position	6.20, 11.31, 1.6	6.20, -11.31, 1.6
Radius	1.03	1.03

For Circle 18, 19, 20 and 21;

First, select circle 17 by clicking on it. Next, locate the "edit" option and click on it. Once the editing menu is open, select the "copy" function. Afterward, find an appropriate location and choose the "paste" option. By completing these steps, circle **18** will be successfully formed. Please replicate this procedure for circles **19, 20 and 21.** Now, change the position of each circles 18, 19, 20, and 21 to the positions indicated below.

Circle	Parameter	Patch 1	Patch 2
Circle 18	Position	8.26,11.31. 1.6	-8.26, -11.31, 1.6
Circle 19	Position	6.2, 11.31, 1.6	6.2, -11.31, 1.6
	Move	0, 2.06, 0	0, 2.06, 0
Circle 20	Position	6.2, 11.31, 1.6	6.2, -11.31, 1.6
	Move	0, -2.06, 0	0, -2.06, 0
Circle 21	Position	4.13, 11.31, 1.6	-4.13, -11.31, 1.6

Then, using the tool bar's subtract option, subtract circle 17 from circle 5. Simply choose circle 5, then circle 17, and then press the subtract option.

- Choose a circle from the toolbar, rename it as "circle **22**", and afterwards, perform a right-click on the "create circle" option to adjust the placements according to the specified instructions.

Circle 22:

Parameter	Patch 1	Patch 2
Position	0, 5.11, 1.6	0, -5.11, 1.6
Radius	1.03	1.03

For Circle 23, 24, 25 and 26;

First, select circle 22 by clicking on it. Next, locate the "edit" option and click on it. Once the editing menu is open, select the "copy" function. Afterward, find an appropriate location and choose the "paste" option. By completing these steps, circle **23** will be successfully formed. Please replicate this procedure for circles **24, 25 and 26.** Now, change the position of each circles 23, 24, 25 and 26 to the positions indicated below.

Circle	Parameter	Patch 1	Patch 2
Circle 23	Position	0, 5.11, 1.6	0, -5.11, 1.6
	Move	-2.06, 0, 0	-2.06, 0, 0
Circle 24	Position	0, 7.18, 1.6	0, -7.18, 1.6
Circle 25	Position	0, 5.11, 1.6	0, -5.11, 1.6
	Move	2.06, 0, 0	2.06, 0, 0
Circle 26	Position	0, 3.05, 1.6	0, 3.05, 1.6

.

Then, using the tool bar's subtract option, subtract circle 22 from circle 6. Simply choose circle 6, then circle 22, and then press the subtract option.

For Step 4 (3rd iteration)

Process:

- In this step the remaining 16 circles (**7, 8, 9, 10, 11, 12, 13, 14, 15, 16, 17, 18, 19, 20, 21 ,22, 23, 24, 25, and 26**) are then further divided into 5 smaller circles (**27, 28, 29, 30, 31, 32, 33, 34, 35, 36, 37, 38, 39, 40, 41, 42, 43, 44, 45, 46, 47, 48, 49, 50, 51, 52, 53, 54, 55, 56, 57, 58, 59, 60, 61, 62, 63, 64, 65, 66, 67, 68, 69, 70, 71, 72, 73, 74, 75, 76, 77, 78, 79, 80, 81, 82, 83, 84, 85, 86, 87, 88, 89, 90, 91, 92, 93, 94, 95, 96, 97, 98, 99, 100, 101, 102, 103, 104, 105, 106**) of radius (A3) (.344 mm), and once again the one centre circle is eliminated from each of the five smaller circles (**27, 32, 37, 42, 47, 52, 57, 62. 67, 72, 77, 82, 87, 92, 97, 102**) leaving a total of 64 circles (**28, 29, 30, 31, 33, 34, 35, 36, 38, 39, 40, 41, 43, 44, 45, 46, 48, 49, 50, 51, 53, 54, 55, 56, 58, 59, 60, 61, 63, 64, 65, 66, 68, 69, 70, 71, 73, 74, 75, 76, 78, 79, 80, 81, 83, 84, 85, 86, 88, 89, 90, 91, 93, 94, 95, 96, 98, 99, 100, 101, 103, 104, 105, 106**).

Designing Process:

"**Consider Circle 3**"

- Choose a circle from the toolbar, rename it as "circle **27**", and afterwards, perform a right-click on the "create circle" option to adjust the placements according to the specified instructions.

Circle 27:

Parameter	Patch 1	Patch 2
Position	-8.26, 11.31, 1.6	-8.26, -11.31, 1.6
Radius	.344	.344

For Circle 28, 29, 30 and 31;

First, select circle 27 by clicking on it. Next, locate the "edit" option and click on it. Once the editing menu is open, select the "copy" function. Afterward, find an appropriate location and choose the "paste" option. By completing these steps, circle **28** will be successfully formed. Please replicate this procedure for circles **29, 30, and 31.** Now, from the tool bar, select move and move the circles 28, 29, 30 and 31 to the positions indicated below.

Circle	Parameter	Patch 1	Patch 2
Circle 28	Move	0, 0.88, 0	0, 0.88, 0
Circle 29	Move	0, -0.88, 0	0, -0.88, 0
Circle 39	Move	0.88, 0, 0	0.88, 0, 0
Circle 31	Move	-0.88, 0, 0	-0.88, 0, 0

Then, using the tool bar's subtract option, subtract circle 27 from circle 8. Simply choose circle 8, then circle 27, and then press the subtract option.

- Choose a circle from the toolbar, rename it as "circle **32**", and afterwards, perform a right-click on the "create circle" option to adjust the placements according to the specified instructions.

Circle 32:

Parameter	Patch 1	Patch 2
Position	-6.2 ,11.31 ,1.6	-6.2 ,-11.31 ,1.6
Move	0 ,2.06 ,0	0 ,2.06 ,0
Radius	.344	.344

For Circle 33, 34, 35 and 36;

First, select circle 32 by clicking on it. Next, locate the "edit" option and click on it. Once the editing menu is open, select the "copy" function. Afterward, find an appropriate location and choose the "paste" option. By completing these steps, circle **33** will be successfully formed. Please replicate this procedure for circles **34, 35, and 36.** Now, from the tool bar, select move and move the circles 33, 34, 35 and 36 to the positions indicated below.

Circle	Parameter	Patch 1	Patch 2
Circle 33	Move	0, 0.88, 0	0, 0.88, 0
Circle 34	Move	0, -0.88, 0	0, -0.88, 0
Circle 35	Move	0.88, 0, 0	0.88, 0, 0
Circle 36	Move	-0.88, 0, 0	-0.88, 0, 0

Then, using the tool bar's subtract option, subtract circle 32 from circle 9. Simply choose circle 9, then circle 32, and then press the subtract option.

- Choose a circle from the toolbar, rename it as "circle **37**", and afterwards, perform a right-click on the "create circle" option to adjust the placements according to the specified instructions.

Circle 37:

Parameter	Patch 1	Patch 2
Position	-4.13 ,-11.31 ,1.6	-4.13 ,11.31 ,1.6
Radius	.344	.344

For Circle 38, 39, 40 and 41;

First, select circle 37 by clicking on it. Next, locate the "edit" option and click on it. Once the editing menu is open, select the "copy" function. Afterward, find an appropriate location and choose the "paste" option. By completing these steps, circle **38** will be successfully formed. Please replicate this procedure for circles **39, 40 and 41.** Now, from the tool bar, select move and move the circles 38, 39, 40 and 41 to the positions indicated below.

Circle	Parameter	Patch 1	Patch 2
Circle 38	Move	-2.66, 0.88, 0	-2.66, 0.88, 0

Circle 39	Move	-2.66, -0.88, 0	-2.66, -0.88, 0
Circle 40	Move	-3.54, 0, 0	-3.54, 0, 0
Circle 41	Move	-1.77, 0, 0	-1.77, 0, 0

Then, using the tool bar's subtract option, subtract circle 37 from circle 10. Simply choose circle 10, then circle 37, and then press the subtract option.

- Choose a circle from the toolbar, rename it as "circle **42**", and afterwards, perform a right-click on the "create circle" option to adjust the placements according to the specified instructions.

Circle 42:

Parameter	**Patch 1**	**Patch 2**
Position	-6.2 ,11.31 ,1.6	-6.2 ,-11.31 ,1.6
Move	0 ,-2.06 ,0	0 ,-2.06 ,0
Radius	.344	.344

For Circle 43, 44, 45 and 46;

First, select circle 42 by clicking on it. Next, locate the "edit" option and click on it. Once the editing menu is open, select the "copy" function. Afterward, find an appropriate location and choose the "paste" option. By completing these steps, circle **43** will be successfully formed. Please replicate this procedure for circles **44, 45, and 46.** Now, from the tool bar, select move and move the circles 43, 44, 45 and 46 to the positions indicated below.

Circle	**Parameter**	**Patch 1**	**Patch 2**
Circle 43	Move	2.66, 0.88, 0	2.66, 0.88, 0
Circle 44	Move	2.66, -0.88, 0	2.66, -0.88, 0
Circle 45	Move	3.54, 0, 0	3.54, 0, 0
Circle 46	Move	1.77, 0, 0	1.77, 0, 0

Then, using the tool bar's subtract option, subtract circle 42 from circle 11. Simply choose circle 11, then circle 42, and then press the subtract option.

"**Consider Circle 4**"

➢ Choose a circle from the toolbar, rename it as "circle **47**", and afterwards, perform a right-click on the "create circle" option to adjust the placements according to the specified instructions.

Circle 47:

Parameter	Patch 1	Patch 2
Position	0 ,-17.51 ,1.6	0 ,17.51 ,1.6
Move	-2.06 ,0 ,0	-2.06 ,0 ,0
Radius	.344	.344

For Circle 48, 49, 50 and 51;

First, select circle 47 by clicking on it. Next, locate the "edit" option and click on it. Once the editing menu is open, select the "copy" function. Afterward, find an appropriate location and choose the "paste" option. By completing these steps, circle **48** will be successfully formed. Please replicate this procedure for circles **49, 50 and 51.** Now, from the tool bar, select move and move the circles 48, 49, 50 and 51 to the positions indicated below.

Circle	Parameter	Patch 1	Patch 2
Circle 48	Move	0, 0.88, 0	0, 0.88, 0
Circle 49	Move	0, -0.88, 0	0, -0.88, 0
Circle 50	Move	0.88, 0, 0	0.88, 0, 0
Circle 51	Move	-0.88, 0, 0	-0.88, 0, 0

Then, using the tool bar's subtract option, subtract circle 47 from circle 13. Simply choose circle 13, then circle 47, and then press the subtract option.

➢ Choose a circle from the toolbar, rename it as "circle **52**", and afterwards, perform a right-click on the "create circle" option to adjust the placements according to the specified instructions.

Circle 52:

Parameter	Patch 1	Patch 2
Position	0 ,19.57 ,1.6	0 ,-19.57 ,1.6
Radius	.344	.344

For Circle 53, 54, 55 and 56;

First, select circle 52 by clicking on it. Next, locate the "edit" option and click on it. Once the editing menu is open, select the "copy" function. Afterward, find an appropriate location and choose the "paste" option. By completing these steps, circle **53** will be successfully formed. Please replicate this procedure for circles **54, 55 and 56.** Now, from the tool bar, select move and move the circles 53, 54, 55 and 56 to the positions indicated below.

Circle	Parameter	Patch 1	Patch 2
Circle 53	Move	0, 0.88, 0	0, 0.88, 0
Circle 54	Move	0, -0.88, 0	0, -0.88, 0
Circle 55	Move	0.88, 0, 0	0.88, 0, 0
Circle 56	Move	-0.88, 0, 0	-0.88, 0, 0

Then, using the tool bar's subtract option, subtract circle 52 from circle 14. Simply choose circle 14, then circle 52, and then press the subtract option.

- Choose a circle from the toolbar, rename it as "circle **57**", and afterwards, perform a right-click on the "create circle" option to adjust the placements according to the specified instructions.

Circle 57:

Parameter	Patch 1	Patch 2
Position	0 ,17.51 ,1.6	0 ,-17.51 ,1.6
Move	2.06 ,0 ,0	2.06 ,0 ,0
Radius	.344	.344

For Circle 58, 59, 60 and 61;

First, select circle 57 by clicking on it. Next, locate the "edit" option and click on it. Once the editing menu is open, select the "copy" function. Afterward, find an appropriate location and choose the "paste" option. By completing these steps, circle **58** will be successfully formed. Please replicate this procedure for circles **59, 60 and 61.** Now, from the tool bar, select move and move the circles 58, 59, 60 and 61 to the positions indicated below.

Circle	Parameter	Patch 1	Patch 2
Circle 58	Move	-2.66, 0.88, 0	-2.66, 0.88, 0
Circle 59	Move	-2.66, -0.88, 0	-2.66, -0.88, 0
Circle 60	Move	-3.54, 0, 0	-3.54, 0, 0
Circle 61	Move	-1.77, 0, 0	-1.77, 0, 0

Then, using the tool bar's subtract option, subtract circle 57 from circle 15. Simply choose circle 15, then circle 57, and then press the subtract option.

- Choose a circle from the toolbar, rename it as "circle **62**", and afterwards, perform a right-click on the "create circle" option to adjust the placements according to the specified instructions.

Circle 62:

Parameter	Patch 1	Patch 2
Position	0 ,15.44 ,1.6	0 ,-7.18 ,1.6
Radius	.344	.344

For Circle 63, 64, 65 and 66;

First, select circle 62 by clicking on it. Next, locate the "edit" option and click on it. Once the editing menu is open, select the "copy" function. Afterward, find an appropriate location and choose the "paste" option. By completing these steps, circle **63** will be successfully formed. Please replicate this procedure for circles **64, 65 and 66.** Now, from the tool bar, select move and move the circles 63, 64, 65 and 66 to the positions indicated below.

Circle	Parameter	Patch 1	Patch 2
Circle 63	Move	2.66, 0.88, 0	2.66, 0.88, 0
Circle 64	Move	2.66, -0.88, 0	2.66, -0.88, 0
Circle 65	Move	3.54, 0, 0	3.54, 0, 0
Circle 66	Move	1.77, 0, 0	1.77, 0, 0

Then, using the tool bar's subtract option, subtract circle 62 from circle 16. Simply choose circle 16, then circle 62, and then press the subtract option.

"**Consider Circle 5**"

➢ Choose a circle from the toolbar, rename it as "circle **67**", and afterwards, perform a right-click on the "create circle" option to adjust the placements according to the specified instructions.

Circle 67:

Parameter	**Patch 1**	**Patch 2**
Position	8.26, 11.31, 1.6	8.26, -11.31, 1.6
Radius	.344	.344

For Circle 68, 69, 70 and 71;

First, select circle 67 by clicking on it. Next, locate the "edit" option and click on it. Once the editing menu is open, select the "copy" function. Afterward, find an appropriate location and choose the "paste" option. By completing these steps, circle **68** will be successfully formed. Please replicate this procedure for circles **69, 70, and 71.** Now, from the tool bar, select move and move the circles 68, 69, 70 and 71 to the positions indicated below.

Circle	**Parameter**	**Patch 1**	**Patch 2**
Circle 68	Move	0, 0.88, 0	0, 0.88, 0
Circle 69	Move	0, -0.88, 0	0, -0.88, 0
Circle 70	Move	0.88, 0, 0	0.88, 0, 0
Circle 71	Move	-0.88, 0, 0	-0.88, 0, 0

Then, using the tool bar's subtract option, subtract circle 67 from circle 18. Simply choose circle 8, then circle 67, and then press the subtract option.

➢ Choose a circle from the toolbar, rename it as "circle **72**", and afterwards, perform a right-click on the "create circle" option to adjust the placements according to the specified instructions.

Circle 72:

Parameter	**Patch 1**	**Patch 2**
Position	6.2 ,11.31 ,1.6	6.2 ,-11.31 ,1.6
Move	0 ,2.06 ,0	0 ,2.06 ,0
Radius	.344	.344

For Circle 73, 74, 75 and 76;

First, select circle 72 by clicking on it. Next, locate the "edit" option and click on it. Once the editing menu is open, select the "copy" function. Afterward, find an appropriate location and choose the "paste" option. By completing these steps, circle **73** will be successfully formed. Please replicate this procedure for circles **74, 75, and 76.** Now, from the tool bar, select move and move the circles 73, 74, 75 and 76 to the positions indicated below.

Circle	Parameter	Patch 1	Patch 2
Circle 73	Move	0, 0.88, 0	0, 0.88, 0
Circle 74	Move	0, -0.88, 0	0, -0.88, 0
Circle 75	Move	0.88, 0, 0	0.88, 0, 0
Circle 76	Move	-0.88, 0, 0	-0.88, 0, 0

Then, using the tool bar's subtract option, subtract circle 72 from circle 19. Simply choose circle 19, then circle 72, and then press the subtract option.

- Choose a circle from the toolbar, rename it as "circle **77**", and afterwards, perform a right-click on the "create circle" option to adjust the placements according to the specified instructions.

Circle 77:

Parameter	Patch 1	Patch 2
Position	4.13 ,-11.31 ,1.6	4.13 ,11.31 ,1.6
Radius	.344	.344

For Circle 78, 79, 80 and 81;

First, select circle 77 by clicking on it. Next, locate the "edit" option and click on it. Once the editing menu is open, select the "copy" function. Afterward, find an appropriate location and choose the "paste" option. By completing these steps, circle **78** will be successfully formed. Please replicate this procedure for circles **79, 80 and 81.** Now, from the tool bar, select move and move the circles 78, 79, 80 and 81 to the positions indicated ahead.

Circle	Parameter	Patch 1	Patch 2
Circle 78	Move	-2.66, 0.88, 0	-2.66, 0.88, 0
Circle 79	Move	-2.66, -0.88, 0	-2.66, -0.88, 0
Circle 80	Move	-3.54, 0, 0	-3.54, 0, 0
Circle 81	Move	-1.77, 0, 0	-1.77, 0, 0

Then, using the tool bar's subtract option, subtract circle 77 from circle 20. Simply choose circle 20, then circle 17, and then press the subtract option.

- Choose a circle from the toolbar, rename it as "circle **82**", and afterwards, perform a right-click on the "create circle" option to adjust the placements according to the specified instructions.

Circle 82:

Parameter	Patch 1	Patch 2
Position	6.2 ,11.31 ,1.6	6.2 ,-11.31 ,1.6
Move	0 ,-2.06 ,0	0 ,-2.06 ,0
Radius	.344	.344

For Circle 83, 84, 85 and 86;

First, select circle 82 by clicking on it. Next, locate the "edit" option and click on it. Once the editing menu is open, select the "copy" function. Afterward, find an appropriate location and choose the "paste" option. By completing these steps, circle **83** will be successfully formed. Please replicate this procedure for circles **84, 85, and 86.** Now, from the tool bar, select move and move the circles 83, 84, 85 and 86 to the positions indicated below.

Circle	Parameter	Patch 1	Patch 2
Circle 83	Move	2.66, 0.88, 0	2.66, 0.88, 0
Circle 84	Move	2.66, -0.88, 0	2.66, -0.88, 0
Circle 85	Move	3.54, 0, 0	3.54, 0, 0
Circle 86	Move	1.77, 0, 0	1.77, 0, 0

Then, using the tool bar's subtract option, subtract circle 82 from circle 21. Simply choose circle 21, then circle 22, and then press the subtract option.

"**Consider Circle 6**"

- Choose a circle from the toolbar, rename it as "circle **87**", and afterwards, perform a right-click on the "create circle" option to adjust the placements according to the specified instructions.

Circle 87:

Parameter	Patch 1	Patch 2
Position	0 ,5.11 ,1.6	0 ,-17.51 ,1.6
Move	-2.06 ,0 ,0	-2.06 ,0 ,0
Radius	.344	.344

For Circle 88, 89, 90 and 91;

First, select circle 87 by clicking on it. Next, locate the "edit" option and click on it. Once the editing menu is open, select the "copy" function. Afterward, find an appropriate location and choose the "paste" option. By completing these steps, circle **88** will be successfully formed. Please replicate this procedure for circles **89, 90 and 91.** Now, from the tool bar, select move and move the circles 88, 89, 90 and 91 to the positions indicated below.

Circle	Parameter	Patch 1	Patch 2
Circle 88	Move	0, 0.88, 0	0, 0.88, 0
Circle 89	Move	0, -0.88, 0	0, -0.88, 0
Circle 90	Move	0.88, 0, 0	0.88, 0, 0
Circle 91	Move	-0.88, 0, 0	-0.88, 0, 0

Then, using the tool bar's subtract option, subtract circle 87 from circle 23. Simply choose circle 23, then circle 87, and then press the subtract option.

- Choose a circle from the toolbar, rename it as "circle **92**", and afterwards, perform a right-click on the "create circle" option to adjust the placements according to the specified instructions.

Circle 92:

Parameter	Patch 1	Patch 2
Position	0 ,-15.44 ,1.6	0 ,7.18 ,1.6
Radius	.344	.344

For Circle 93, 94, 95 and 96;

First, select circle 92 by clicking on it. Next, locate the "edit" option and click on it. Once the editing menu is open, select the "copy" function. Afterward, find an appropriate location and choose the "paste" option. By completing these steps, circle **93** will be successfully formed. Please replicate this procedure for circles **94, 95 and 96.** Now, from the tool bar, select move and move the circles 93, 94, 95 and 96 to the positions indicated below.

Circle	Parameter	Patch 1	Patch 2
Circle 93	Move	0, 0.88, 0	0, 0.88, 0
Circle 94	Move	0, -0.88, 0	0, -0.88, 0
Circle 95	Move	0.88, 0, 0	0.88, 0, 0
Circle 96	Move	-0.88, 0, 0	-0.88, 0, 0

Then, using the tool bar's subtract option, subtract circle 92 from circle 24. Simply choose circle 24, then circle 92, and then press the subtract option.

- Choose a circle from the toolbar, rename it as "circle **97**", and afterwards, perform a right-click on the "create circle" option to adjust the placements according to the specified instructions.

Circle 97:

Parameter	Patch 1	Patch 2
Position	0 ,5.11 ,1.6	0 ,-17.51 ,1.6
Move	2.06 ,0 ,0	2.06 ,0 ,0
Radius	.344	.344

For Circle 98, 99, 100 and 101;

First, select circle 97 by clicking on it. Next, locate the "edit" option and click on it. Once the editing menu is open, select the "copy" function. Afterward, find an appropriate location and choose the "paste" option. By completing these steps, circle **98** will be successfully formed. Please replicate this procedure for circles **99, 100 and 101.** Now, from the tool bar, select move and move the circles 98, 99, 100 and 101 to the positions indicated below.

Circle	Parameter	Patch 1	Patch 2
Circle 98	Move	0.88, 2.66, 0	0.88, 2.66, 0
Circle 99	Move	-0.88, 2.66, 0	-0.88, 2.66, 0
Circle 100	Move	0, -3.54, 0	0, -3.54, 0
Circle 101	Move	0, -1.77, 0	0, -1.77, 0

Then, using the tool bar's subtract option, subtract circle 97 from circle 25. Simply choose circle 25, then circle 97, and then press the subtract option.

- Choose a circle from the toolbar, rename it as "circle **102**", and afterwards, perform a right-click on the "create circle" option to adjust the placements according to the specified instructions.

Circle 102:

Parameter	Patch 1	Patch 2
Position	0 ,-19.57 ,1.6	0 ,3.05 ,1.6
Radius	.344	.344

For Circle 103, 104, 105 and 106;

First, select circle 102 by clicking on it. Next, locate the "edit" option and click on it. Once the editing menu is open, select the "copy" function. Afterward, find an appropriate location and choose the "paste" option. By completing these steps, circle **103** will be successfully formed. Please replicate this procedure for circles **104, 105 and 106.** Now, from the tool bar, select move and move the circles 103, 104, 105 and 106 to the positions indicated ahead.

Circle	Parameter	Patch 1	Patch 2
Circle 103	Move	0.88, 2.66, 0	0.88, 2.66, 0
Circle 104	Move	-0.88, 2.66, 0	-0.88, 2.66, 0
Circle 105	Move	0, 3.54, 0	0, 3.54, 0
Circle 106	Move	0, 1.77, 0	0, 1.77, 0

Then, using the tool bar's subtract option, subtract circle 102 from circle 26. Simply choose circle 26, then circle 102, and then press the subtract option.

For microstrip inset feedline: To start the process, the user should go to the toolbar and choose the "draw rectangle" choice. The user should then click anywhere on the screen to make a rectangle. Then, the user should double-click on the rectangle inside the project management window to get to its properties. The user can change the name of the rectangle (feed line) in this menu. Lastly, the user should press the "OK" button to confirm their choices. Then, right-click on "create box" and change the positions to meet the standards.

Parameter	Patch 1	Patch 2
Position	14.11, (11.31 + 1.495), 1.6	14.11, (-11.31 + 1.495), 1.6
X	-11.007	-11.007
Y	-2.99	-2.99

Next, make cuts along both sides of the feedline. For cut 1, first choose the rectangle, then move the cursor from the feedline's top right edge to the patch's bottom right edge. Next, right-click the newly created rectangle and modify the y-axis's settings to Y = 0.931 mm. Then, for cut 2, choose the duplicate along line option from the toolbar and move the cursor from the top of the cut1 on the right to the top of the feedline on the left. The next stage is to combine feedline and patch. To do this, click on (patch + control + feedline), then select the unite option from the toolbar. When you click on patch + Control + cut1 + control + cut2 and then select the option to subtract from the toolbar, cut1 and cut2 are subtracted from the patch.

For assigning boundaries to ground and patch: right-click the patch, select assign boundaries, and then click Perfect E. Same process is repeated for ground.

For lump port: Change the axis to "yz" first. Then choose a rectangle and give it the new name lump port. Then, right-click on "Create Rectangle" and modify its attributes as follows:

Parameter	Patch 1	Patch 2
Position	14.11 ,-12.805 ,1.6	14.11 ,9.815 ,1.6
Y	2.99	2.99
Z	-1.6	-1.6

For lump port excitation, right-click on the lump port rectangle in the project window, select Assign Excitation, select Lump Port (50 Ohm), select Next, select Integration (double click), select New Line, drag a triangle-shaped cursor from the lower edge to the upper edge, select Next, and then select Finish.

For radiation box: To initiate the process, the user should locate and select the "draw box (3D)" option from the toolbar. Following this, the user should proceed to click on any desired location on the screen to create a box. Subsequently, the user should double-click on the box inside the project management interface to access its properties. Inside this menu, the user can modify the name of the box (radiation box) and select the vaccum option. Finally, the user should confirm their selections by pressing the "ok" button. Subsequently, go to right-click on the "create box" option and modify the dimensions in accordance with the specified requirements.

Position: -22.44,-30.33,-16.66

X = 44.88 mm

Y = 60.66 mm

Z = 33.32 mm

Next, proceed to choose the five facets of the radiation boxes and thereafter utilize the right-click function to allocate boundaries. Finally, click on the radiation option.

Then, check validation.

For analysis:

To initiate the analysis on the project management window, the user should perform a right-click action. Following this, they should select the option labeled "Add solution

set up." Within this setup, the user will be prompted to specify the solution frequency in gigahertz (GHz), with a recommended value of 9.5 GHz for the proposed antenna. The maximum number of passes is set at 20. Subsequently, proceed to perform a right-click action on the setup option, followed by selecting the sweep function. Proceed to input the desired start value (8 GHz) and end value (28 GHz), and subsequently specify the step size (0.1 GHz). Subsequently, save the field configuration and confirm the changes by selecting the "OK" option.

After the completion of validation and analysis, the subsequent step involves assessing the results of our suggested antenna with regards to several performance metrics.

For calculating "Reflection coefficient and Transmission coefficient)" of the proposed antenna, following steps are followed:

- In the project management box, right-click on the result option.
- Next, click Create modal solution setup data report.
- Then select Rectangular plot • S parameter • S_{11}, S_{22}, S_{12}, S_{21}.
- New report

For calculating "Gain", following steps are followed:

- In the project management box, right-click on the radiation option, then choose far field, then infinite sphere
- Then, with a step size of 90, alter phi from 0 to 90 degrees, and with a step size of 10, change theta from 0 to 360 degrees.
- Then, on the tool bar, click on the analyzing all option, then go to the result, click on far field report, then click radiation report, then select correct infinite sphere and other settings like Gain in dB, then click OK.
- For peak Gain calculation, select antenna parameter in radiation report and then click on peak gain.

For calculating "Surface Current Distribution", following steps are followed:

- Select patch, right-click to "Add plot fields," select "Mag_ Jsurf," "all object," "concern resonant frequency," "ok," and "start analyze all"
- For calculation of current distribution at other frequencies, click "analysis" in the project manager window, "click" on "solution setup," "change frequency," "ok," and "start analyze all".

For calculating "Surface Current Density Distribution", following steps are followed:

- Select patch, right-click to "Add plot fields," select "Mag_ Jvol," "all object," "concern resonant frequency," "ok," and "start analyze all"

For calculating "Radiation Pattern", following steps are followed:

- In the project management box, right-click on the radiation option, then choose far field, then infinite sphere
- Then, with a step size of 90, alter phi from 0 to 90 degrees, and with a step size of 10, change theta from -180 to 180 degrees.
- Then, on the tool bar, click on the analyzing all option, then go to the result, click on far field report, then click radiation report, then select gain phi and gain theta.
- Then in families, select all for phi and select the frequency, then click OK.
- For calculation of radiation pattern at other frequencies, click "analysis" in the project manager window, "click" on "solution setup," "change frequency," "ok," and "start analyze all".
- For Co polarization (H Plane); gain phi for phi = 90 degree
- For Co polarization (E Plane); gain theta for phi = 0 degree
- For Cross polarization (H Plane); gain phi for phi = 0 degree
- For Cross polarization (E Plane); gain theta for phi = 90 degree

Two distinct researches are conducted in order to achieve ideal outcomes for the development of a dual-port MIMO antenna. First, distance optimization and secong orientation analysis.

5.2.2 Distance Optimization

Analysis of distance is an important component in the computation of isolation in MIMO antennas. Using distance analysis, we can determine the most suitable position for antennas to avoid interference. In the proposed work, two antennas are placed at D = 2, 4, and 6 mm. Figure 5.10 a, b, and c provide a visual representation of the variation in S_{11}, S_{22} and S_{12}, S_{21}. Meanwhile, Table 5.4 presents a concise summary of the obtained data. The antenna resonates at 9.7, 16.3, 18.8, and 21.4 GHz at 4 mm with greater bandwidths of 3100, 600, and 10100 MHz than at 2 mm and 6 mm. At 4 mm D, isolation is best at -40 dB. The maximal isolation levels are -38.9 and -38.6 dB for 2 and 6 mm diameters, respectively. This finding demonstrates that when the diameter (D) of the antenna is 4 millimeters, it yields superior outcomes. Moreover, obtaining almost constant isolation levels depends on a number of underlying factors, including signal propagation characteristics, path loss, reflection, and multipath, among others.

Table 5.4 Analysis of MIMO distance variation

Parameters	**BW**	**f_r**	**S_{12} (max. isolation)**
D = 2 mm	3100, 400, 10000	9.2, 16.3, 18.9, 21.3	-38.9
D = 4 mm	3100, 600, 10100	9.7, 16.3, 18.8, 21.4	-40
D = 6 mm	2800, 600, 9900	9.1, 16.5, 18.9, 21	-38.6

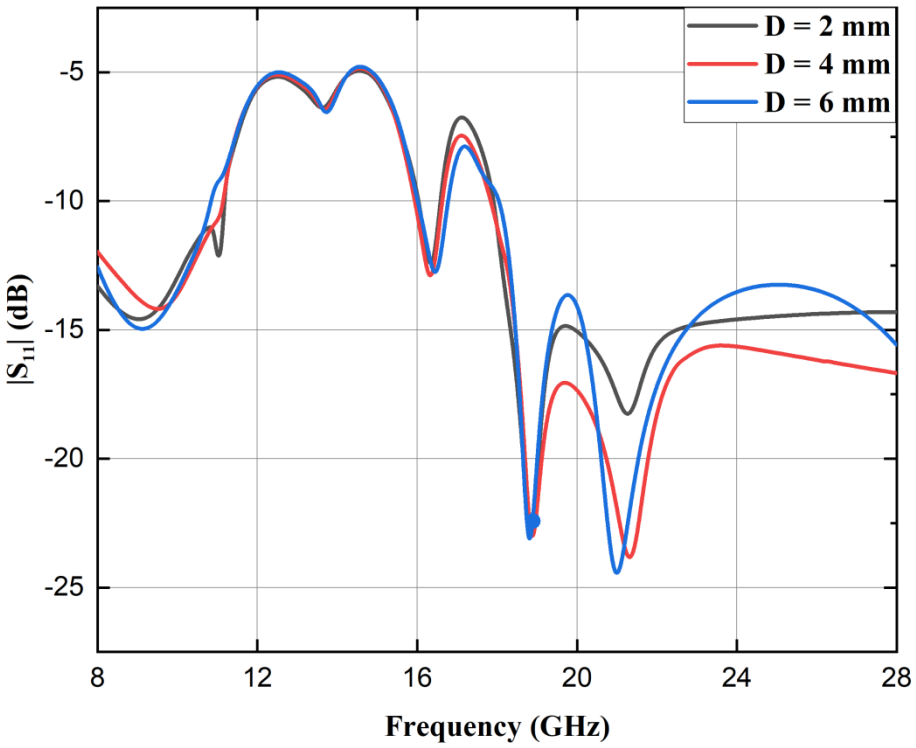
D = 2 mm
D = 4 mm
D = 6 mm
-5
-10
-15
-20
-25
|S11| (dB)
8
12
16
20
24
28
Frequency (GHz)

(a)

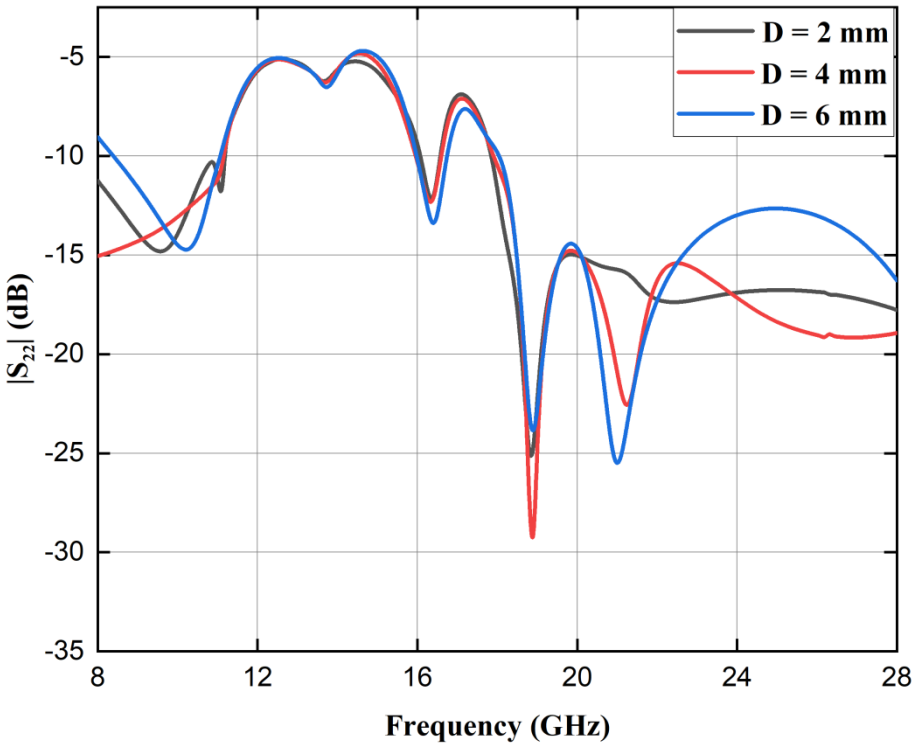
D = 2 mm
D = 4 mm
D = 6 mm
-5
-10
-15
-20
-25
-30
-35
|S22| (dB)
8
12
16
20
24
28
Frequency (GHz)

(b)

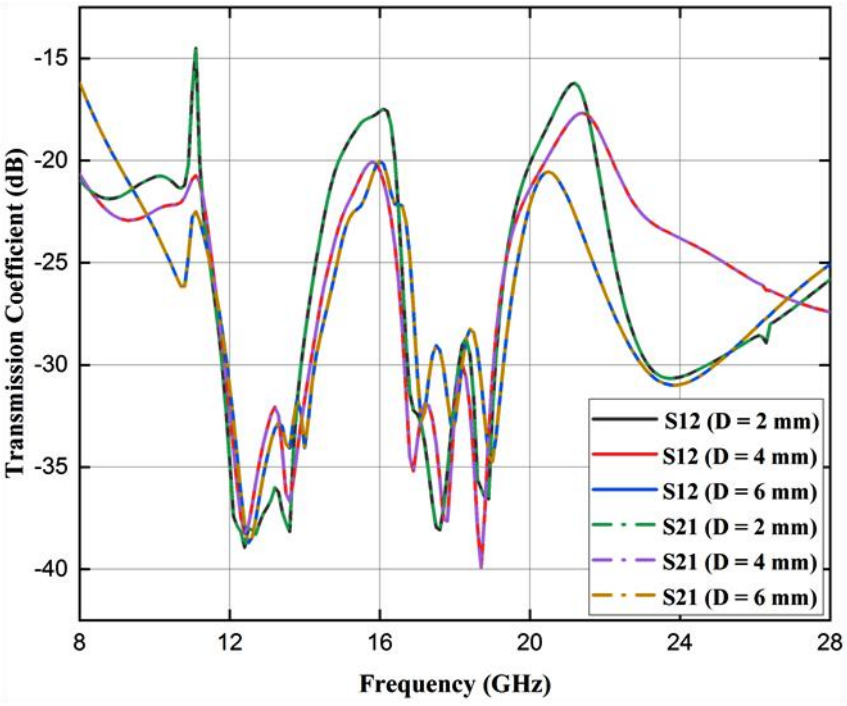

(c)

Figure 5.10 Scattering parameters (a), S_{11} (b) S_{22} and (c) Transmission Coefficient

5.2.3 Orientation Analysis

The isolation between antennas in a MIMO system can be considerably influenced by their direction. The extent of antenna signal interference determines isolation. Different orientations can isolate differently due to multiple decoupling mechanisms. Spatial diversity decoupling is used in said antenna. It is achieved by the utilization of physically separated antennas. By varying the orientation of these antennas, they are able to capture signals from distinct spatial routes, hence decreasing the probability of both antennas being affected by fading or interference simultaneously. Figure 5.11a shows the antenna's two components precisely 4 mm apart in orientation 1. The antenna's bandwidth and isolation improve during configuration. Figure 5.12 a, b, and c show that the antenna resonates at 9.7, 16.3, 18.8, and 21.4 GHz. The antenna covers three frequency bands: 8–11.1 GHz, 16–16.5 GHz, and 17.9–28 GHz.. Figure 5.11 b shows how Orientation II inverts antenna II while keeping antenna I unaltered. Using figures 5.12 a, b, and c, the antenna's fr and BW in this orientation can be calculated. The antenna has resonance frequencies of 10.3, 16.4, 18.8, & 21.5 GHz and bandwidths of 3000, 600, & 9900 MHz. Figure 5.11 c shows orientation III with

both antennas rotated 90 degrees. The antenna has resonance at 8.2 and 19.2 GHz and a maximum isolation of -37.21 dB. Orientation I outperforms the other two in bandwidth and isolation. Table 5.5 summarizes all three orientations' results. Orientation I is considered the best MIMO antenna system design.

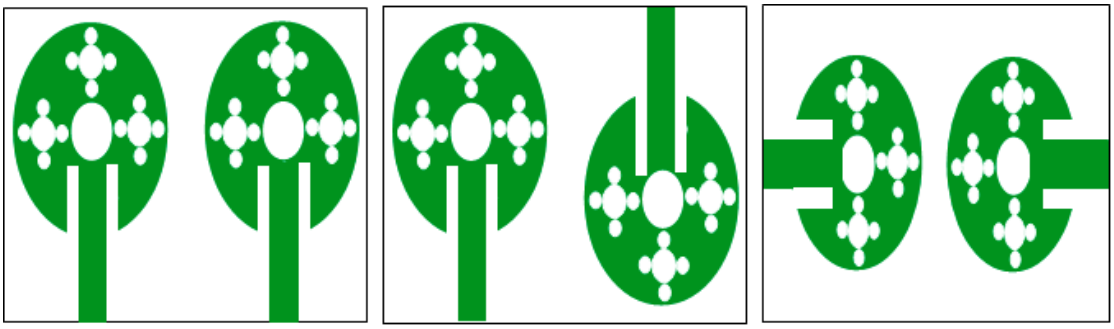

Figure 5.11 Differently oriented antenna

Table 5.5 Analysis of MIMO orientation variation

Parameters (Orientation)	**BW**	**f_r**	**S_{12} (max. isolation)**
I	3100, 600, 10100	9.7, 16.3, 18.8, 21.4	-40
II	3000, 600,9900	10.3, 16.4, 18.8, 21.5	-38.74
III	2700, 9800	8.2, 19.2	-37.21

5.2.4 MIMO Antenna with Rectangular slot DGS

To improve antenna isolation, imperfect ground construction is used. For the proposed antenna, a single vertical rectangular slot with a width of 1 mm is added in the ground plane (Figure 5.13 b). The transmission coefficient curves in Figure 5.14 b show that slots reduce near-field coupling between MIMO antennas. Maximum isolation inside antenna components has increased from -40 dB to -52.72 dB. Thus, deploying the ground plane slot improved isolation by 12 dB. The summarized outcomes of MIMO and MIMO with DGS are shown in Table 5.6. MIMO with DGS antenna radiation efficiency is shown in Figure 5.15. Peak radiation efficiency is 72% in the 8.2–10.4 GHz frequency spectrum. Radiation efficiency peaks at 55% in the second band at 16.1–16.5 GHz. In conclusion, the third band (18.1–28 GHz) has a maximum radiation efficiency of 73%. Figure 5.16 shows the highest peak gain of a

DGS-equipped MIMO. The graphic shows that the proposed antenna has 8.5 dBi peak gain.

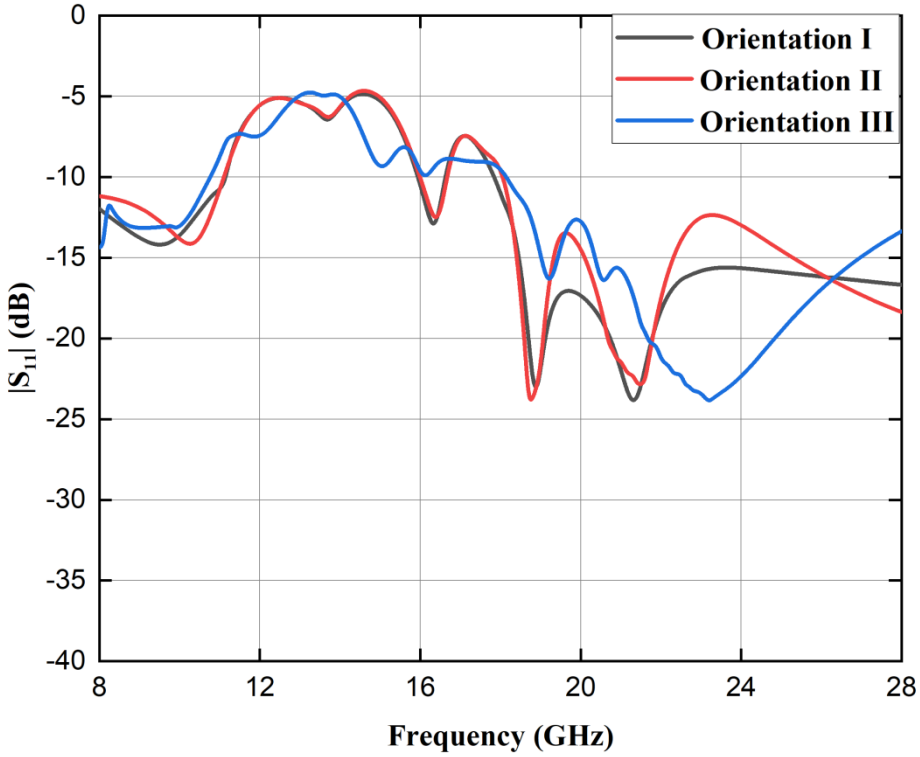

(a)

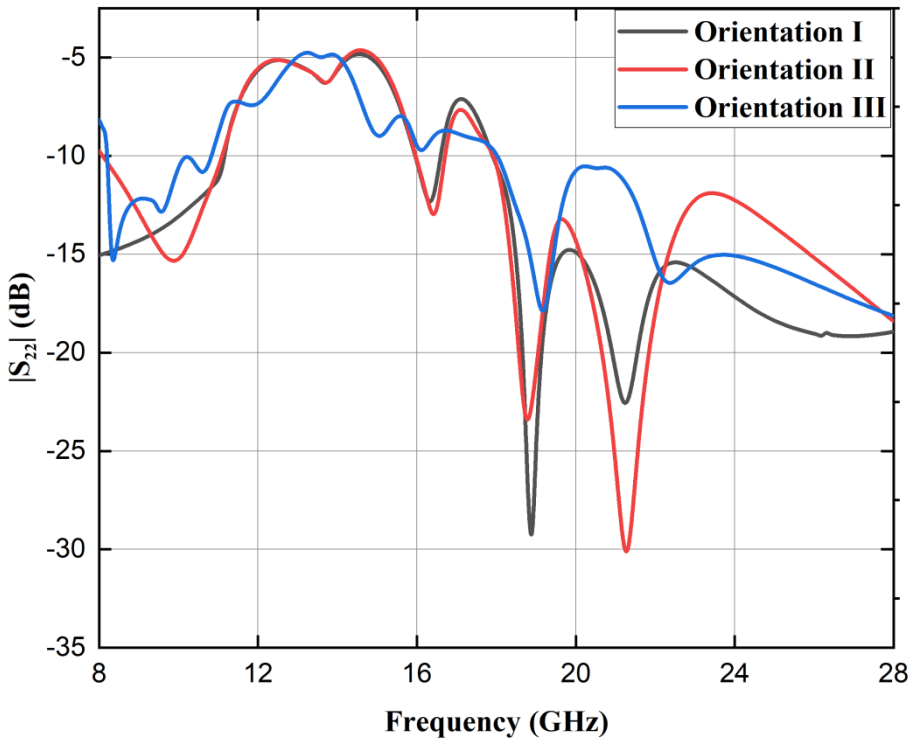

(b)

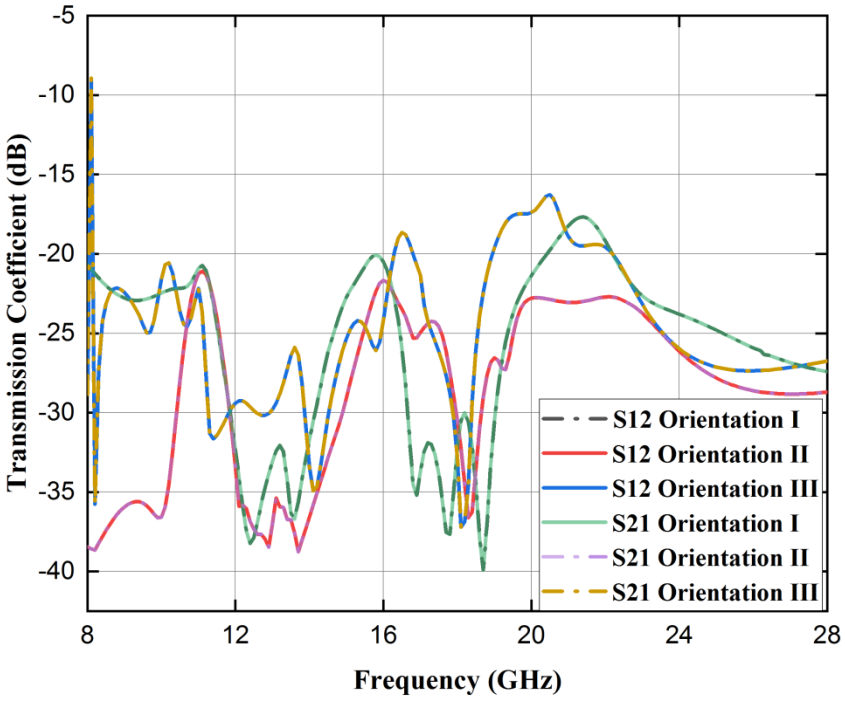

(c)

Figure 5.12 Scattering parameters (a) S_{11}, (b) S_{22} and (c) S_{12} & S_{21}, Orientation analysis

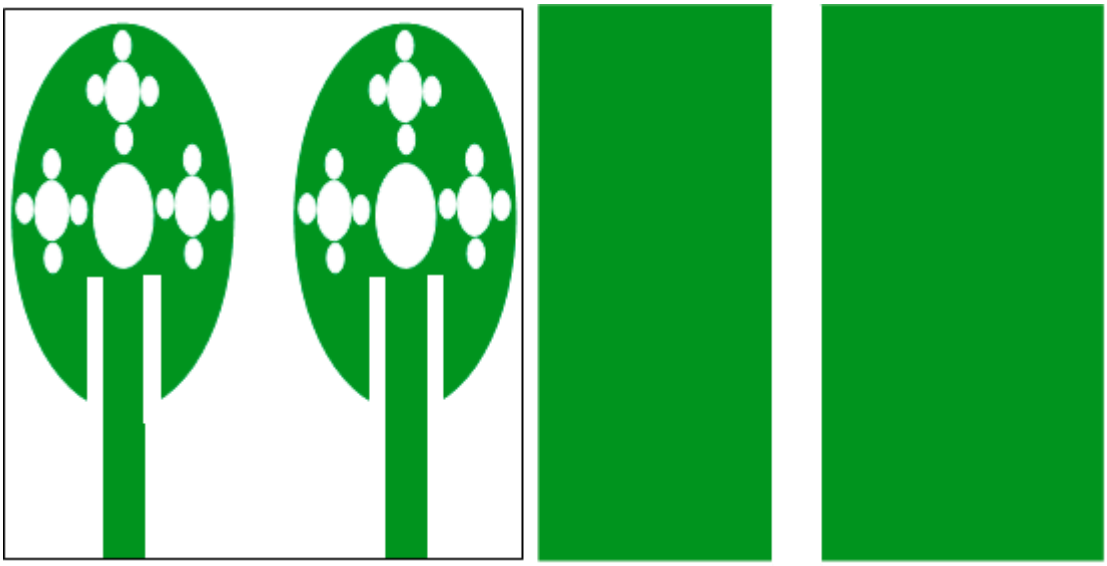

(a) **(b)**

Figure 5.13 Ground structural flaw in MIMO antenna (a) Top and (b) Bottom view

Table 5.6 MIMO and MIMO DGS analysis

Parameters	**BW (MHz)**	**f_r(GHz)**	**S_{12} (dB) (max. isolation)**
MIMO	3100, 600, 10100	9.7, 16.3, 18.8, 21.4	-40
MIMO DGS	2200, 400, 9900	9.7, 16.3, 18.8, 21.4	-52.72

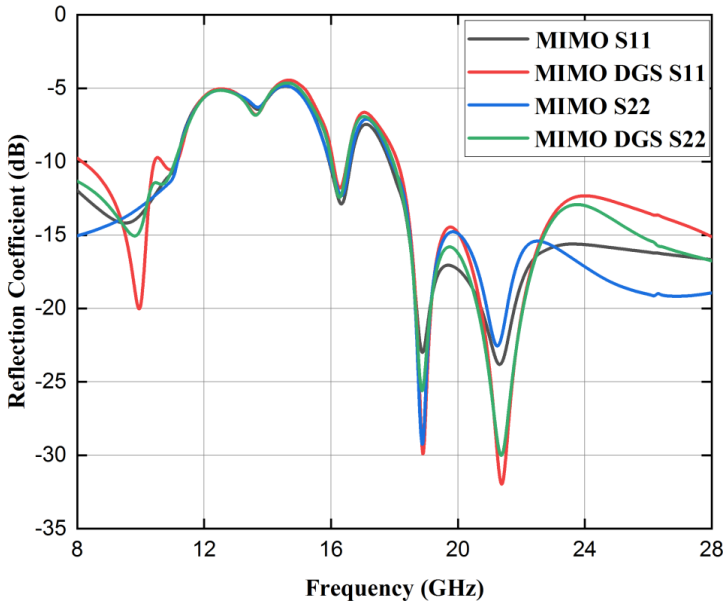

(a)

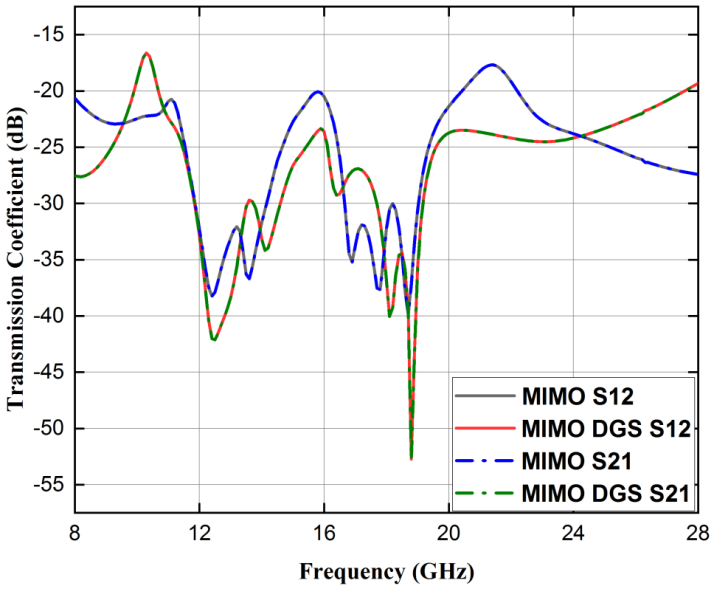

(b)

Figure 5.14 Scattering parameters (a) S_{11} (dB) & S_{22} (dB), and (b) S_{12} (dB) & S_{21} (dB), DGS MIMO

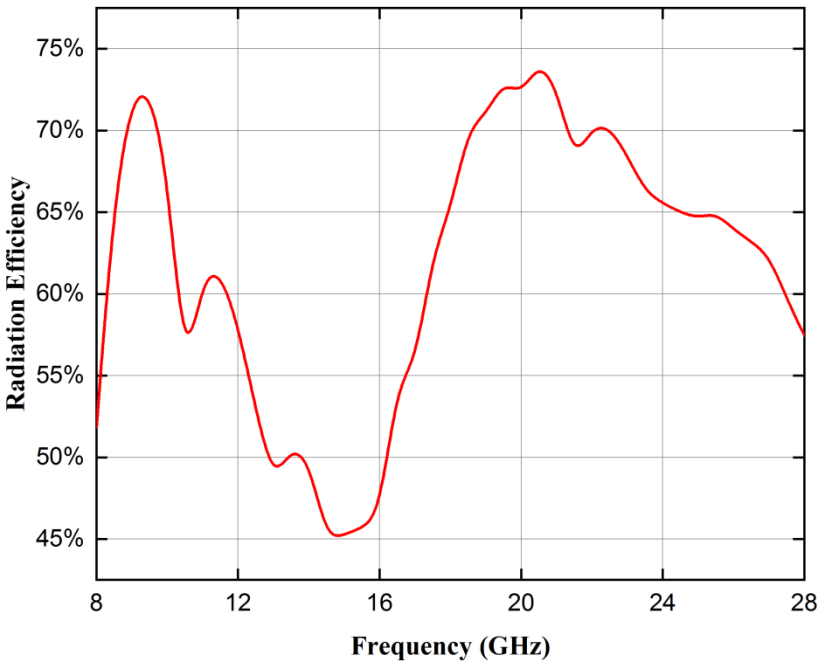

Figure 5.15 MIMO DGS antenna radiation efficiency

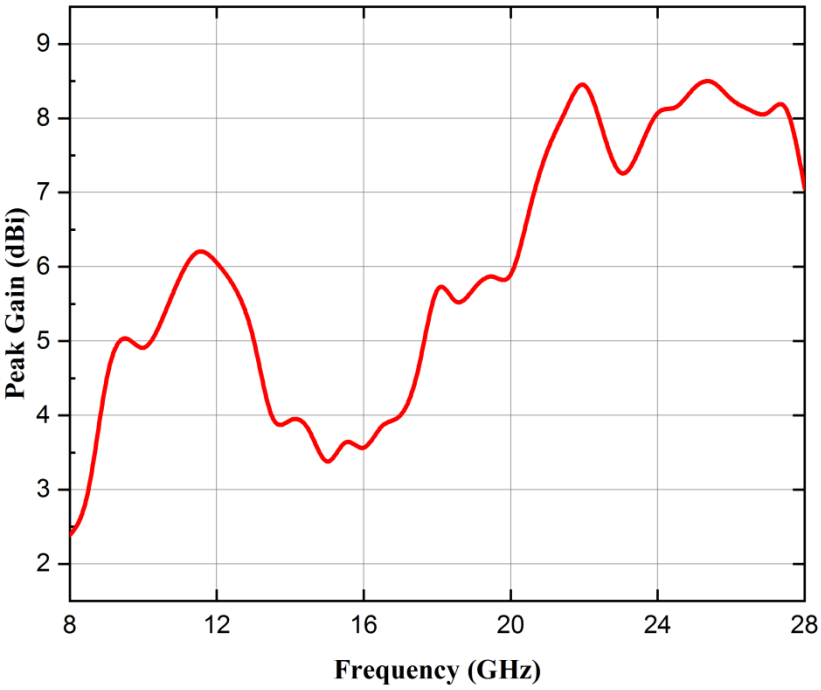

Figure 5.16 MIMO DGS antenna peak gain

Figure 5.17 shows current distribution effects at 9.7, 18.8, and 21.4 GHz. To analyze surface current distribution (A/m), stimulate one MIMO antenna port and terminate the other. Therefore, port one is activated and port two of the intended antenna is terminated. Figure 5.17 shows a high current concentration in port 1's major radiating

patch. Surface current at port 2 decreases. The observed effect clearly reduces antenna mutual coupling.

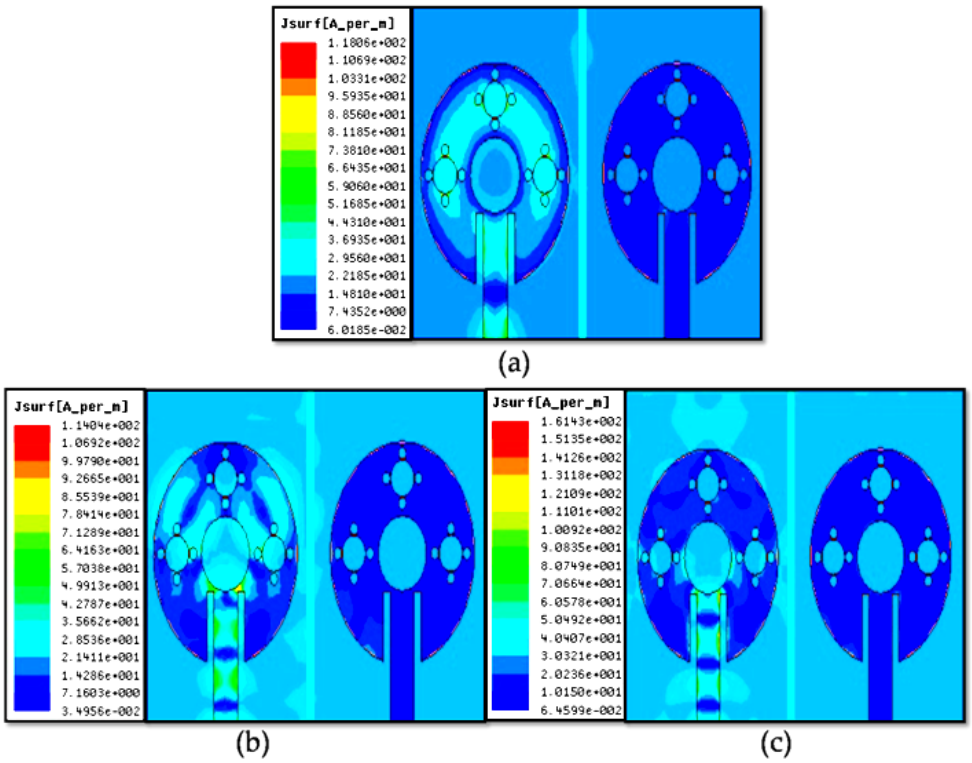

Figure 5.17 Surface current distribution at (a) 9.7 GHz, (b) 18.8 GHz, and (c) 21.4 GHz, after exciting port 1 and discontinuing port 2

5.3 MIMO Antenna with DGS Fabrication and Discussion on Measurements Results

An antenna is built on a FR4 substrate to verify results. Figures 5.18 (a) and 5.18 (b) illustrate the antenna's frontal and lateral views. On the EP-42 Auto PCB prototype machine, fabrication occurs. Connectors are employed for the purpose of affixing the proposed antenna to the ZNB-40 Vector Network Analyzer (VNA) with the intention of evaluating its transmission and reflection coefficients. The measured data captured from the VNA are depicted in Figure 5.19 (a). Figure 5.19 (b) shows the suggested antenna's radiation pattern in an anechoic environment with a reference horn antenna transmitting.

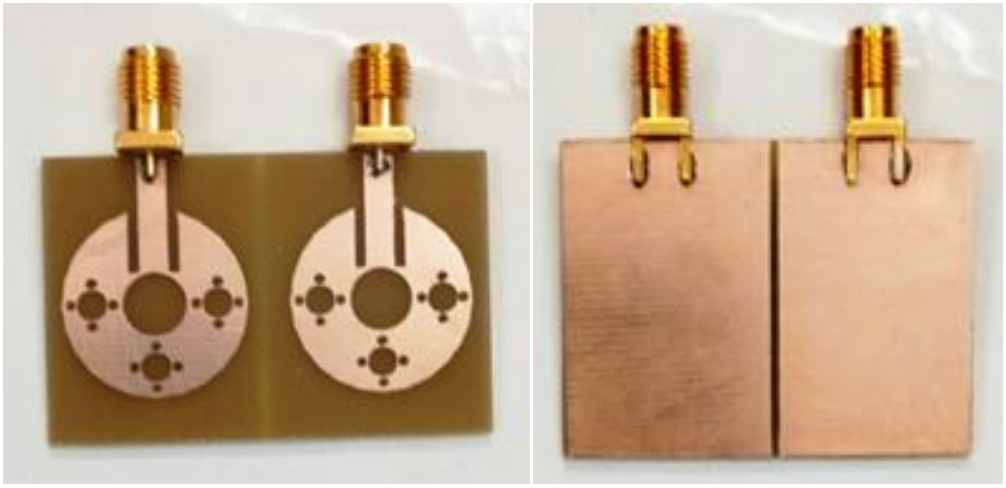

(a) **(b)**

Figure 5.18 Fabricated DGS MIMO antenna (a) Top and, (b) Lateral view

Figure 5.20 (a) and (b) show measured and simulated reflection and transmission coefficients. The antenna has resonances at 9.5 GHz, 11.1 GHz, 13.4 GHz, 15.8 GHz, 21.1 GHz, and 26.6 GHz, with S11 (dB) values of -32.15, -11.95, -13.3, -17.0, -33.2, and -26.14. Resonances extend from 8.9 to 9.9 GHz, 10.4 to 11.4 GHz, 13.1 to 13.7 GHz, 15.4 to 16.2 GHz, and 17.7 to 28 GHz. In addition, the antenna has higher impedance bandwidths of 1000 MHz, 1000 MHz, 600 MHz, 800 MHz, and 10300 MHz over various frequency ranges. Maximum isolation between the antennas is -48.37 dB. Simulated results show antenna resonance at 9.7, 16.3, 18.8, and 21.4 GHz.

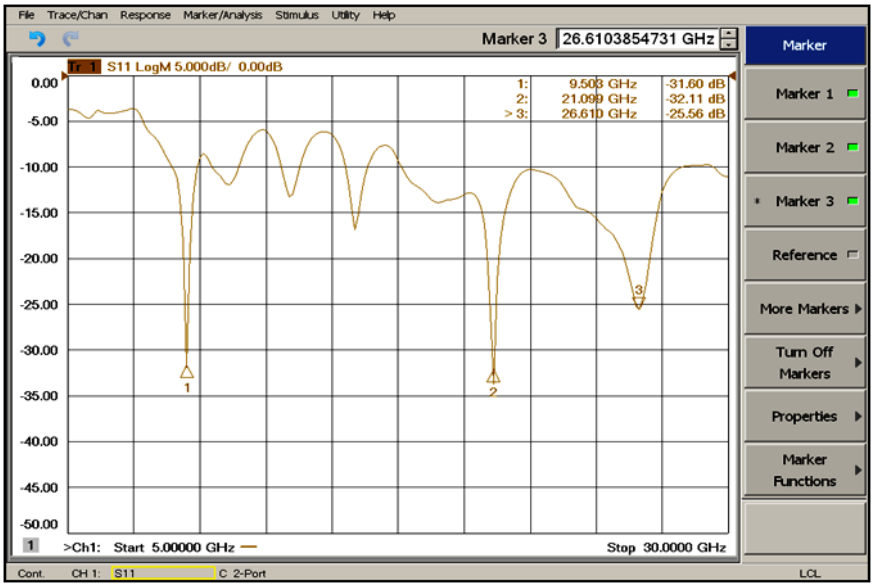

(a)

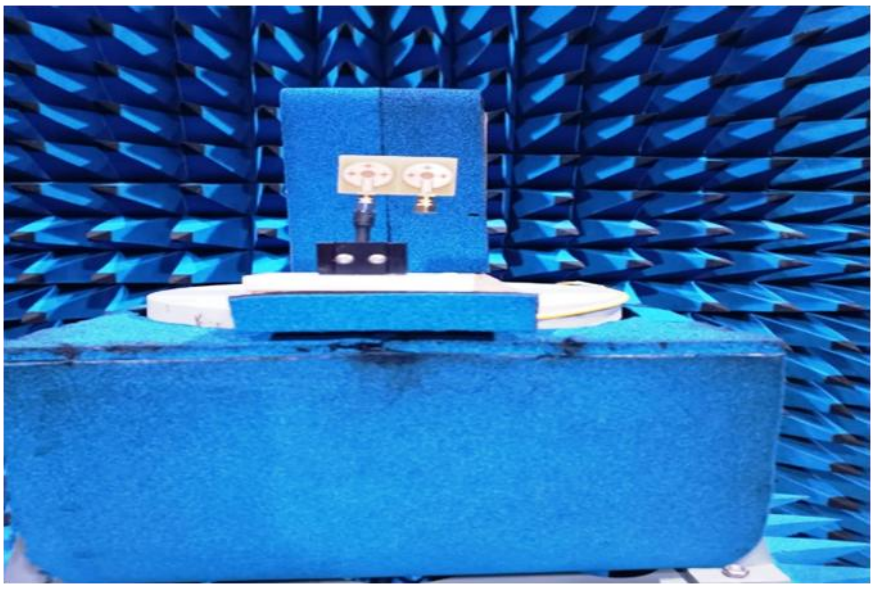

(b)

Figure 5.19 Experimental setup (a) S_{11} dB reflection coefficient (b) radiation pattern

These resonances have reflection coefficients of -20.04, -12, -31.9, and -32.3 dB. The simulation covers three coverage bands: 8.2–10.4 GHz, 16.1–16.5 GHz, and 18.1–28 GHz. The impedance bandwidths for these bands are 2200, 400, and 9900 MHz. The experimental results show a peak isolation level of -52.72 dB. Measurements and simulations show resonance frequency discrepancies that may be due to manufacturing faults, SMA connectors, and substrate-model mismatches.

Figure 5.21 shows simulated and measured radiation patterns in the vertical (E) and horizontal (H) fields planes at 9.5, 21.1, and 26.6 GHz At 9.5 GHz, the antenna being assessed radiates practically omnidirectionally. At 21.1 GHz and 26.6 GHz resonant frequencies nulls are observed in both planes. Many reflections in the measurement environment can cause disparities between measured and simulated findings. Proposed antenna radiation is generally steady.

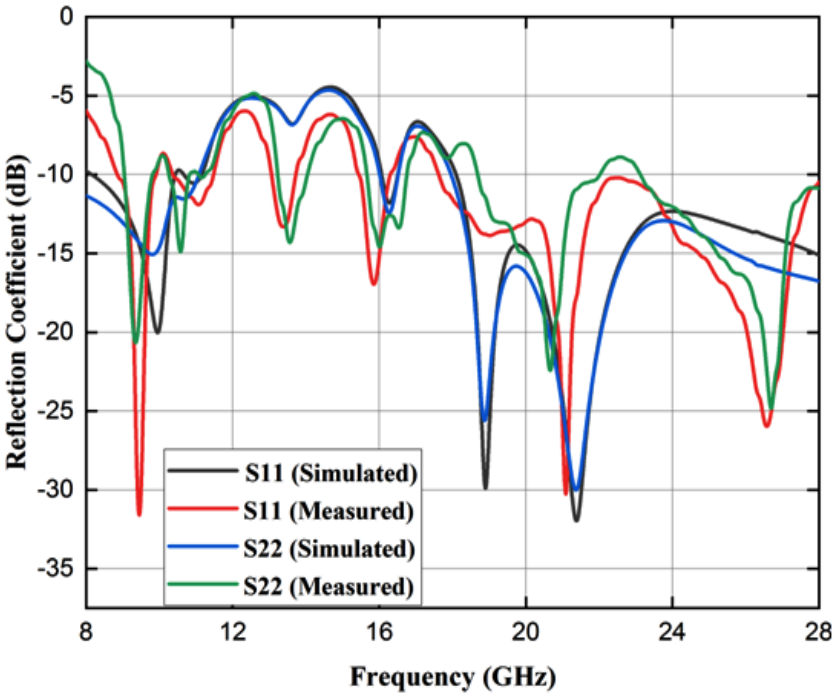

(a)

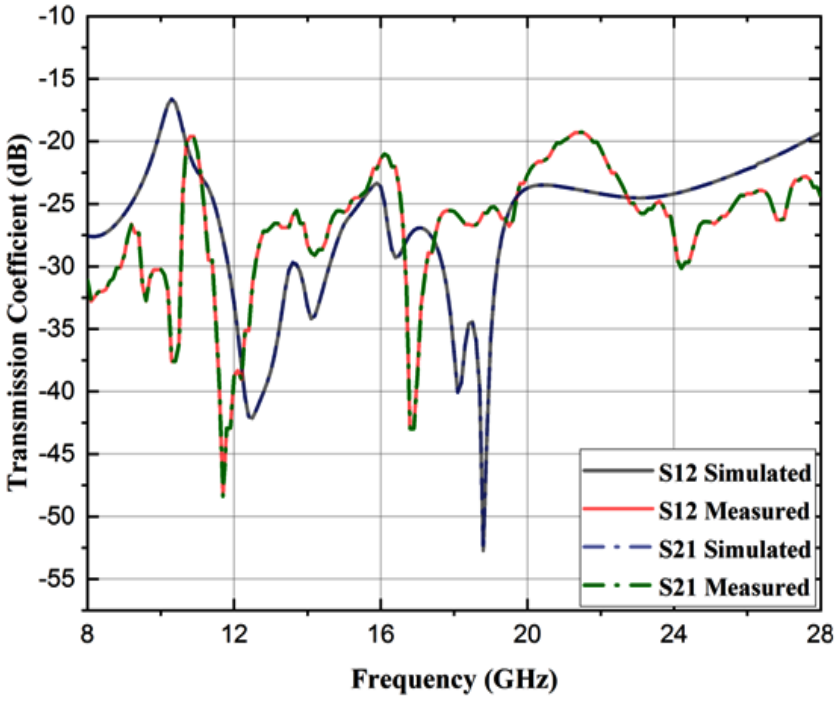

(b)

Figure 5.20 Scattering Parameters of MIMO with DGS (a) Reflection Coefficient, and (b) Transmission Coefficient

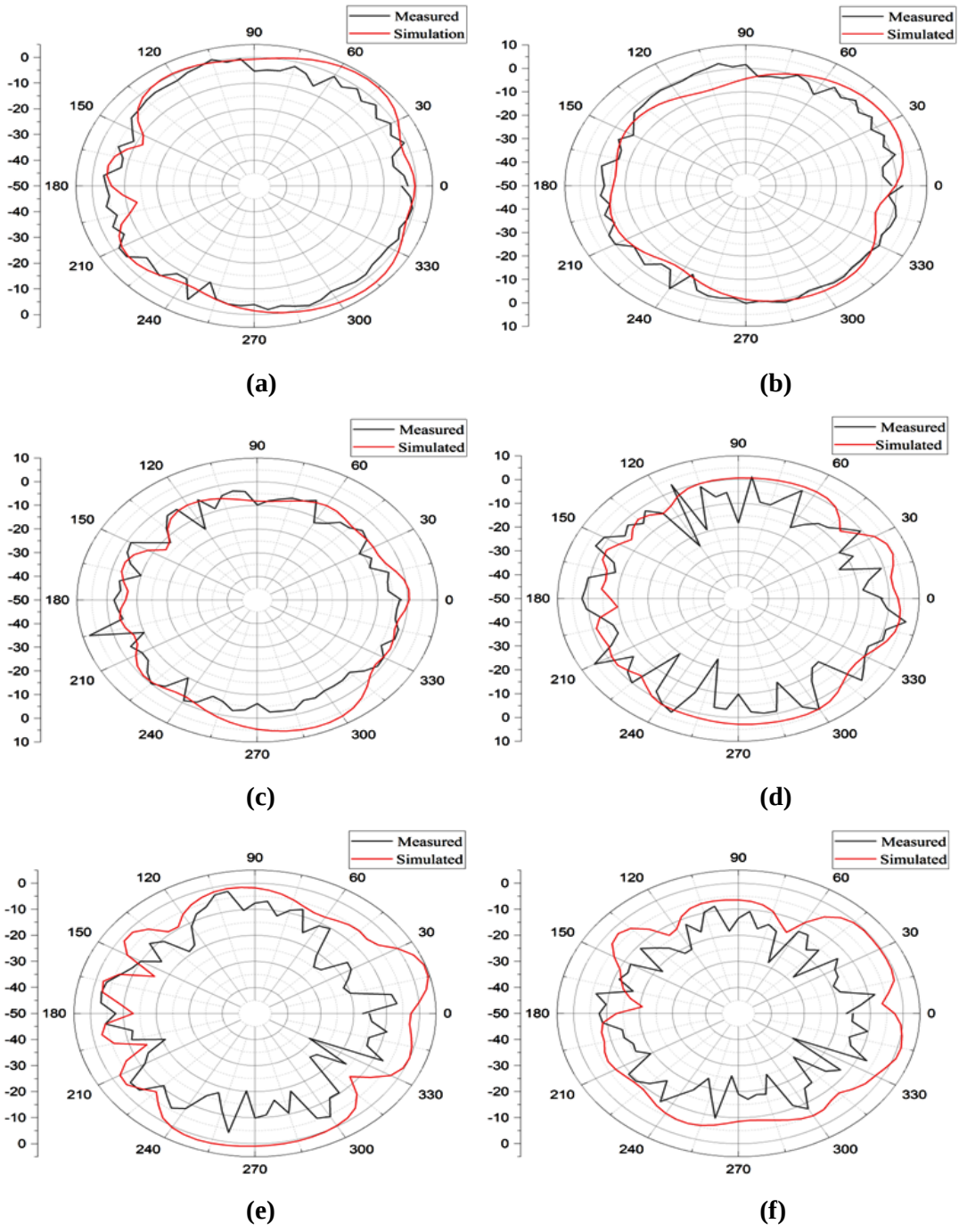

Figure 5.21 Simulation and measurement Co-polarized radiation E and H planes radiation pattern: (a),(b) at 9.5 GHz; (c),(d) at 21.1 GHz; (e),(f) at 26.6 GHz

5.4 MIMO with DGS Antenna Diversity Performance Analysis

Various measures, including the ECC, DG, and MEG, are used to evaluate the effectiveness of the said MIMO antenna.

5.4.1 Envelope Correlation Coefficient (ECC)

ECC assessment is essential to assessing antenna system component isolation. Based on antenna specifications, ECC can be calculated by two methods. The main method uses antenna component far field emission patterns. The user provided a numerical reference [98]. The simpler, less resource-intensive second method uses S parameters [99]. The second way is often used in high-efficiency MIMO antennas, making the s-parameter approach the best. ECC values should be below 0.05. The equation (5.1) uses s-parameter approaches for two-element MIMO systems. This study's MIMO antenna system simulations and measurable curves are shown in Figure 5.22.

$$ECC = \frac{|S_{11}^{*}\, S_{12} + S_{21}^{*}\, S_{22}|^2}{(1-|S_{11}|^2-|S_{21}|^2)(1-|S_{12}|^2-|S_{22}|^2)} \quad (5.1)$$

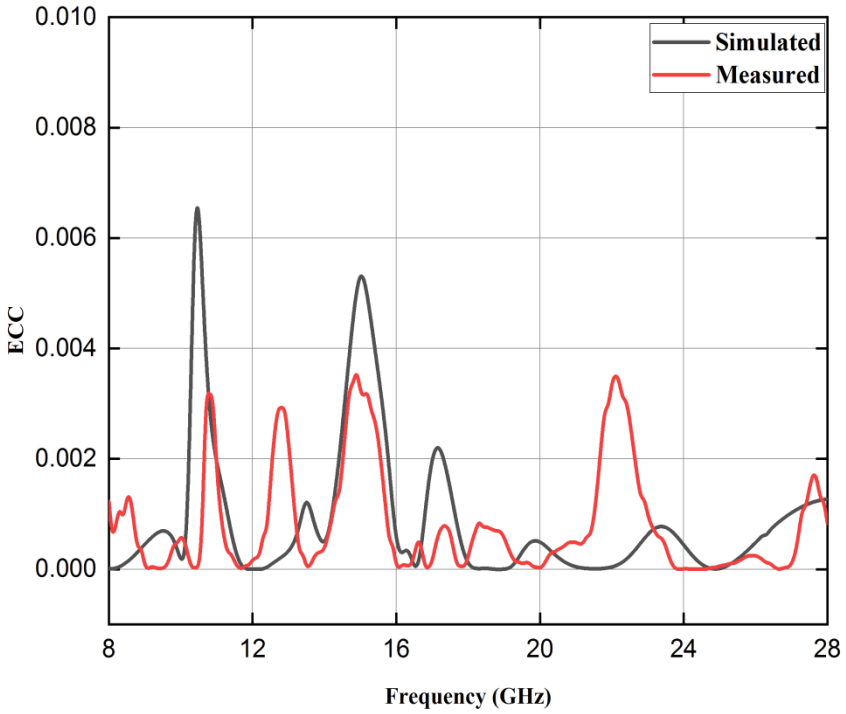

Figure 5.22 ECC of MIMO with DGS

5.4.2 Diversity Gain (DG)

Equation (5.2) calculates diversity gain, which measures diversity's effectiveness [100]. At a significance level of 1% and utilizing maximal ratio combining, achieving a diversity gain of 10 signifies the highest possible level. To ensure practical

application, it is advisable to set the parameter DG at a value greater than 9.99 dB. The diversity gain (DG) of this antenna remains below the permissible limit throughout all working frequencies, as depicted in Figure 5.23.

$$DG = 10\sqrt{1 - ECC^2} \quad (5.2)$$

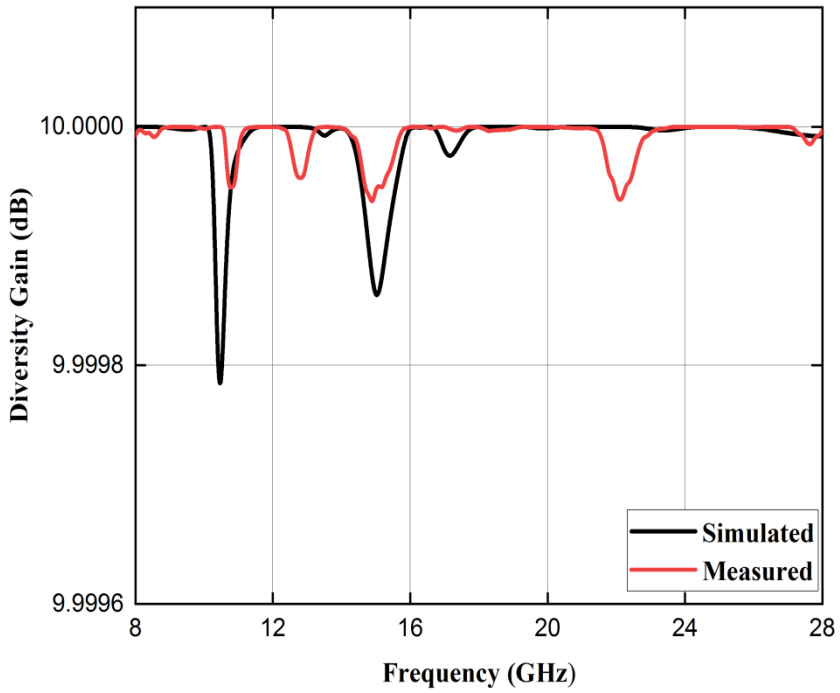

Figure 5.23 DG of MIMO with DGS

5.4.3 Mean Effective Gain (MEG)

Maximum Effective Gain compares diversity antenna power to isotropic antenna power in fading conditions [101]. The computation is performed using Equation (5.3), and the graphical representation is depicted in Figure 5.24.

$$MEG_i = 0.5\,\{1 - \sum_{j=1}^{k} |S_{ij}|^2\} \quad (5.3)$$

In this context, the variable "i" is used to denote a specific antenna being discussed, whereas the variable "k" represents the total count of antennas. In the given context, the variable k is representative of the number 2 in relation to the two-port antenna. Consequently, we have

$$MEG_1 = 0.5\,\{1 - |S_{11}|^2 - |S_{12}|^2\} \quad (5.4)$$

$$MEG_2 = 0.5\,\{1 - |S_{21}|^2 - |S_{22}|^2\} \quad (5.5)$$

As shown by the citation [102], For best diversity performance, the suggested two-port element antenna's MEG1/MEG2 ratio should not exceed 3 dB. MEG values below 1.2 dB can be verified using Figure 5.24. The suggested antenna's performance is shown in Table 5.7. The results suggest that the antenna demonstrates advantageous diversity characteristics, rendering it well-suited for millimeter wave applications.

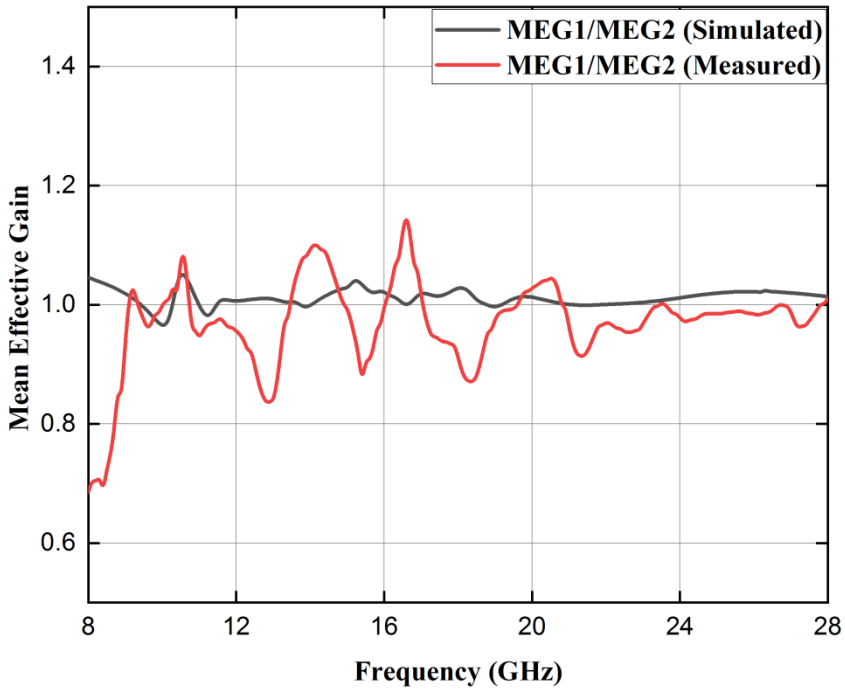

Figure 5.24 MEG of MIMO with DGS

Table 5.7 Diversity performance parameters of MIMO DGS

Criterion	Value
ECC	Less than 0.004
DG (dB)	Greater than 9.99
MEG (dB)	Less than 1.2

5.5 Proposed Antenna with Other Reported Antenna Performance Comparison

In Table 5.8, the MIMO antenna proposed in this study is compared to previous research and the percentage enhancement and losses of various parameters are shown in Figure 5.25. The comparison uses bandwidth, bands, isolation, ECC, and diversity gain. Table 5.8 shows that the proposed antenna may operate across many frequency bands and increase BW with excellent ECC and DG. Results in [74], demonstrate comparable properties with somewhat higher isolation. The proposed MIMO antenna

in this research has higher bandwidth and better value in terms of its capacity to function across many frequency bands than the antenna construction in the literature [74].

Table 5.8 Comparison of present work with previous studies

5Ref	**Bandwidth (MHz)**	**No. of Port**	**No. of Band**	**Element Spacing (mm)**	**Isolation dB)**	**ECC**	**Diversity Gain**
[71]	1069, 1430	2	2	10.13	-29	< 0.0020	----
[74]	6400	2	1	-	-35.8	< 0.005	> 9.99
[75]	1900, 6000	2	1	-	-18	< 0.01	> 9.96
[76]	4700, 4200	2	2	4.3	-30,- 22	< 0.0001, < 0.0002	> 9.99
[77]	8700	2	1	-	-30	< 0.05	> 9.99
[78]	500,1800,800,1000	4	4	10	-25	< 0.06	> 9.99
[79]	1000	2	1	6	-25	< 0.002	----
[80]	821, 1630	2	2	8.8	-16	0.0002, 0.005	>9.98
[81]	6000	2	1	-	24	0.0013	-
Propose	**1000, 1000, 600, 800, 10300**	2	5	4	--32.15, -11.95, -13.3, -17.0, -33.2,	< 0.004	> 9.99

Figure 5.25 (a) shows that the suggested antenna bandwidth is used as a baseline for calculating bandwidth increase in percentages, and when the base value is compared to other references, it appears that other antenna studies yield less bandwidth. For

example, reference no. 79 is just 10% of the base value, indicating that the proposed antenna generates 90% more bandwidth. Figure 4.25 (b) depicts the antenna's multiband behavior. The graph clearly shows that the proposed antenna produces penta (Five) band as compared to other studies.

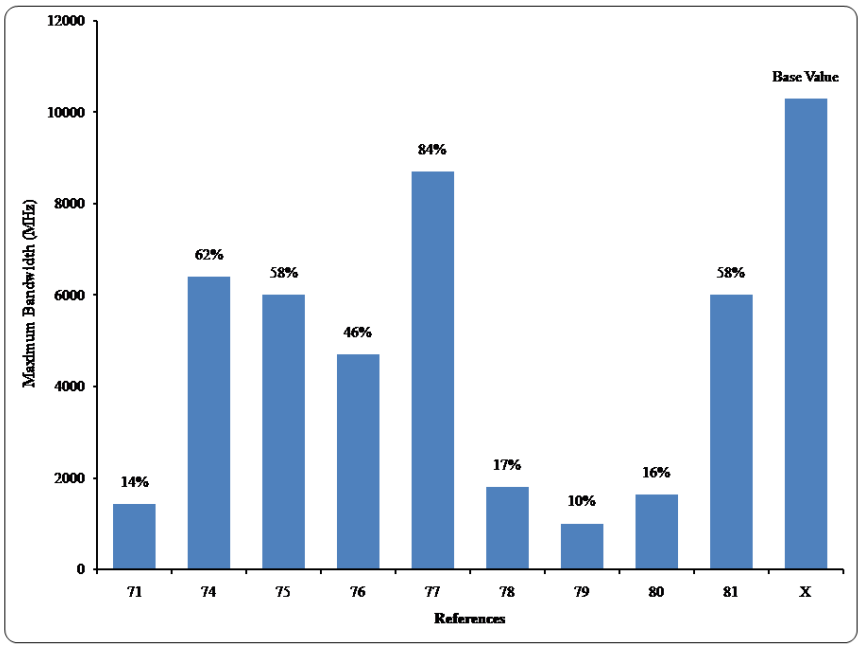

(a)

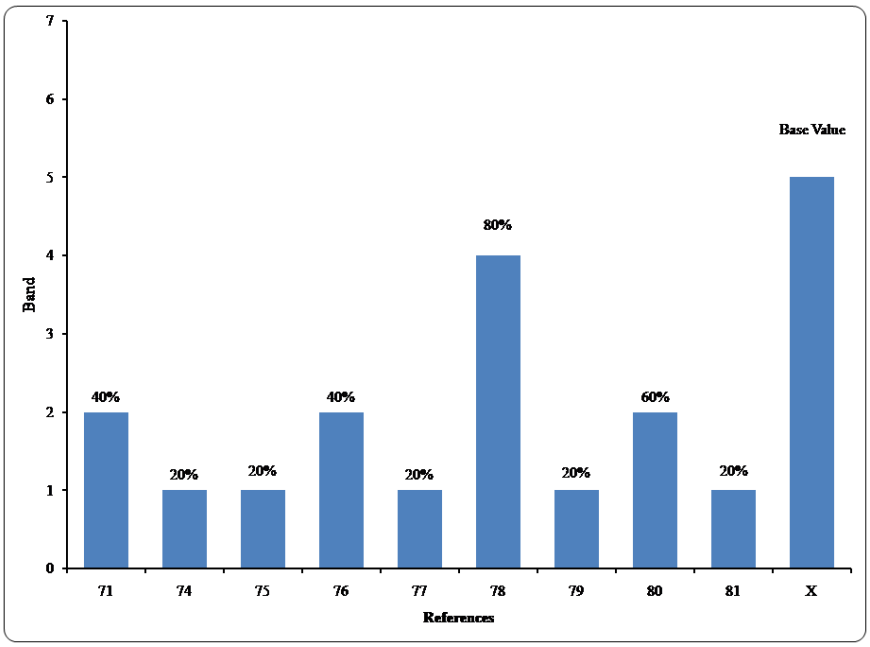

(b)

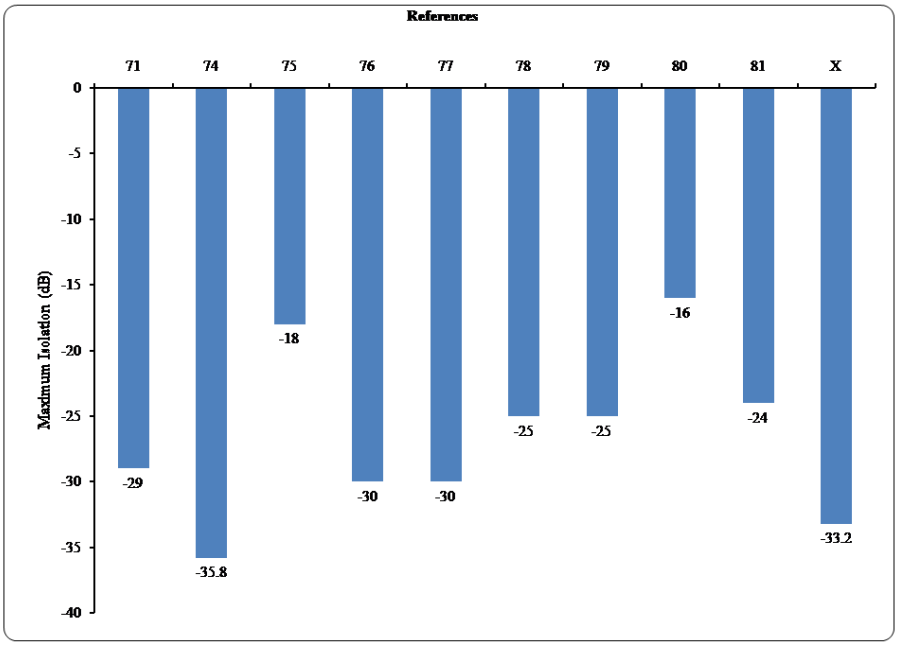

(c)

Figure 5.25 Performance comparison of proposed antenna with other studies in % enhancement and loss (a) Bandwidth, (b) Bands, (c) Isolation

Figure 4.25 (c) illustrates the maximum isolations between the antennas. The value of reference paper 74 is used as a baseline (maximum) when computing isolation enhancement and losses in percentage. The graph reveals that the proposed antenna is producing -33. 2 dB isolation between the two antennas, indicating that its value is smaller than that of reference paper 74, but it is in the acceptable range. However, when compared to the other parameters of this reference, the suggested antenna has a wider bandwidth and shows multiband behavior.

Summary

A DGS-based low-profile, two-port MIMO antenna is reported in this paper. The antenna presented in this paper has one element initially. When a single antenna is integrated into a two-port MIMO system and thoroughly examined, its performance improves. It also has a rectangular ground plane defect to boost antenna performance. This improves antenna element isolation by 8.37 dB. Due to its wide BW, strong isolation, low ECC, compact design, and cost, the MIMO DGS antenna under review

distinguishes apart from similar studies. Thus, this antenna design has promising properties for 5G millimeter-wave n258 band, Ku band and X band application.

CHAPTER 6

CONCLUSION & FUTURE SCOPE

6.1 Conclusion

Recently, wireless communication applications have increased in production. The fifth generation of wireless networks, commonly referred to as 5G, distinguishes itself from previous iterations of wireless networks due to its disruptive potential in reconfiguring the digital world. The efficiency of any given 5G system is contingent upon the design and optimal functioning of its antennas. Today, the majority of 5G applications demand MIMO technology, which was created utilizing a combination of microstrip antennas. Therefore, two prototype antennas are constructed in this thesis while taking into account all the aforementioned 5G system requirements. The initial prototype involves the design and development of a small circular multiband patch antenna with improved BW. Antenna parameters were investigated extensively. Experimental testing verified antenna performance. Results show significant agreement between measured and simulated values. The system has resonance frequencies of 3.35, 6.68, 8.84, 12.62, and 15.68 GHz with reflection coefficients of -17.01, -21.93, -14.68, -35.49, and -20.63 dB. These frequencies cover 3.26-3.36 GHz, 6.32-6.95 GHz, 8.66-9.20 GHz, 11.99-12.98 GHz, and 13.61-20 GHz. The -10 dB operational bandwidths for five frequency bands are 100 MHz, 630 MHz, 540 MHz, 990 MHz, and 6390 MHz. The antenna's design and implementation are feasible. This study compares the proposed antenna to existing multiband antennas published previously. The results indicate that our proposed antenna exhibits superior performance. The suggested antenna structure has a unique feature of functioning in five frequency bands, while also providing improved bandwidths inside a compact and visually appealing design. Furthermore, it maintains consistent radiation patterns and satisfactory gains throughout all the frequency bands it operates in. The antenna is compatible with Ku, X, and Mid-band 5G mobile applications. The second antenna presents a detailed account of a two-port MIMO antenna with a low-profile design, which has been created utilizing Defected Ground Structure (DGS) techniques. This section initially,

describes a single-element antenna. To improve performance, a single antenna is integrated into a two-port MIMO system and analyzed. An integrated rectangular defect in the ground plane improves antenna performance. The isolation between the antenna sections improves by 8.37 dB. The analyzed MIMO DGS antenna has a broad bandwidth, good isolation, low error correction coding, compactness, and cost-efficiency compared to similar studies. Consequently, the aforementioned antenna design exhibits favorable attributes that render it a viable choice for deployment inside the X band, Ku band and n258 band of the millimeter-wave 5G spectrum.

6.2 Contribution of Work

5G antennas are essential for improved connectivity and speed in today's world of wireless communication. This thesis builds two prototype antennas based on this consideration. For the 5G mid band application, the first prototype entails designing and developing a small circular multiband patch antenna with better gain and better BW through iteration. With a broader bandwidth and isolation between the antennas, the second antenna provides a full description of a low-profile, two-port MIMO antenna designed with Defected Ground Structure (DGS) techniques. This research will benefit the real world by enabling high-speed data connectivity in the mid- and mm-band frequency ranges through the integration of small antennas into smartphones and other mobile devices. These antennas are used by network operators and the telecommunications sector in their 5G infrastructure to offer capacity and coverage in the mid-band and mm-band frequency range. Additionally, in order to support 5G connectivity, manufacturers of consumer electronics, such as smartphones, tablets, and other gadgets, include this antenna into their products. This research has also benefited the academic community, including researchers, engineers, and students who use the study for projects and tutorials pertaining to the advancement of the design, optimization, and performance assessment of the aforementioned antennas.

6.3 Future Scope

In the context of 5G antennas, the primary considerations revolve on improving isolation, increasing bandwidth, enhancing gain, and achieving a compact size. This

thesis focuses on the design of two compact antennas for 5G applications, aiming to achieve wider bandwidth, increased gain, and improved isolation. These objectives are pursued through the utilization of fractal geometry and faulty ground structure concepts. Based on the investigations conducted in this thesis about MIMO technology and microstrip patch antenna, certain issues have been identified that require further research:

1. The potential of this study can be further enhanced by using more antenna elements to augment the channel capacity in high data rate scenarios.

2. A reconfigurable antenna in conjunction with a flexible substrate can be used to improve the diversity performance parameters.

3. Neutralisation lines, tapered feedlines, shorting vias, and other methods can be employed to improve an antenna's performance parameters.

6.4 Limitation of Work

1. The proposed antennas require complex design which can complicate manufacturing and integration.
2. Multiple antennas require more physical space which increases space requirement.
3. Advance technologies used can increased the production cost.
4. Achieving wideband performance can compromise gain and efficiency.

LIST OF PUBLICATIONS

Conferences and Journals

1. Nitasha Bisht and Praveen Kumar Malik, "Circular Patch Microstrip Antenna with Slots for Lower 5G Band Applications," TEQIP-III Sponsored International Conference on Technological Transformation and Preparedness in the Post COVID World, March 22-23, 2021, Deenbandhu Chhotu Ram University of Science & Technology, Murthal, India.
2. Nitasha Bisht and Praveen Kumar Malik, "Adoption of Microstrip Antenna to Multiple Input Multiple Output Microstrip Antenna For Wireless Applications: A Review," International Conference on Recent Innovations in Computing (ICRIC 2021), 8 - 9 June, 2021. **(Scopus Indexed)**.
3. Nitasha Bisht, Praveen Kumar Malik and Sudipta Das, "A Modified Circular Disk Shaped Miniaturized Multiband Printed Antenna with Enhance Bandwidth for 5G Mobile Application," International Journal of Microwave and Optical Technology, Vol. 17, No. 5, pp: 487- 495, September 2022. **(Scopus Indexed)**.
4. Nitasha Bisht, Praveen Kumar Malik and Sudipta Das, "Feeding Methods for a Circular Shaped Multiband Patch Antenna at 5G, X And Ku Band to Quantify Their Effects on Antenna Characteristics" Journal of Nano and Electronic Physics, Vol. 15, No. 3, pp:03007 (1-5), June 2023. **(Scopus Indexed)**.
5. Nitasha Bisht, Praveen Kumar Malik and Sudipta Das," Design of a Modified MIMO Antenna Based on Tweaked Spherical Fractal Geometry For 5G New Radio (NR) Band N258(24.25–27.25GHz) Applications," Fractal and Fractional. **2023**, 7,718. https://doi.org/10.3390/fractalfract7100718, **(SCI Indexed)**.

Patent Published

1. Circular Patch Microstrip Antenna for Mid Band 5G Applications" vide Application No. 202211008391.

REFERENCES

[1] S. Haykin, *Digital Communication*. New York, U.K: John Wiley & Sons., 1988.

[2] A. K. Vallappil, B. A. Khawaja, M. K. A. Rahim, M. Uzair, M. Jamil, and Q. Awais, "Minkowski–Sierpinski Fractal Structure-Inspired 2 × 2 Antenna Array for Use in Next-Generation Wireless Systems," *Fractal Fract.*, vol. 7, no. 2, pp. 1–18, 2023, doi: 10.3390/fractalfract7020158.

[3] A. Zhao and Z. Ren, "Wideband MIMO antenna systems based on coupled-loop antenna for 5G N77/N78/N79 applications in mobile terminals," *IEEE Access*, vol. 7, pp. 93761–93771, 2019, doi: 10.1109/ACCESS.2019.2913466.

[4] S. Kumar, A. S. Dixit, R. R. Malekar, H. D. Raut, and L. K. Shevada, "Fifth generation antennas: A comprehensive review of design and performance enhancement techniques," *IEEE Access*, vol. 8, pp. 163568–163593, 2020, doi: 10.1109/ACCESS.2020.3020952.

[5] ITU-R, "Requirements, Evaluation Criteria and Submission Templates for the Development of IMT-2020," *Rep. ITU-R M.2411-0*, pp. 1–32, 2017.

[6] Huawei, "5G Spectrum," *Public Policy Position*, no. November, pp. 1–18, 2020.

[7] ITU-R, "Guidelines for Evaluation of Radio Interface Technologies for IMT-2020," *Rep. ITU-R M.2412-0*, pp. 1–144, 2017.

[8] ITU-R, "M.2376-0 Technical feasibility of IMT in bands above 6 GHz," *Rep. ITU-R M.2376-0*, vol. 0, pp. 1–134, 2015, [Online]. Available: http://www.itu.int/ITU-R/go/patents/en.

[9] N. Shoaib, S. Shoaib, R. Y. Khattak, I. Shoaib, X. Chen, and A. Perwaiz, "MIMO antennas for smart 5g devices," *IEEE Access*, vol. 6, no. c, pp. 77014–77021, 2018, doi: 10.1109/ACCESS.2018.2876763.

[10] X. Chen, S. Zhang, and Q. Li, "A Review of Mutual Coupling in MIMO Systems," *IEEE Access*, vol. 6, no. c, pp. 24706–24719, 2018, doi: 10.1109/ACCESS.2018.2830653.

[11] L. Malviya, R. K. Panigrahi, and M. V. Kartikeyan, "MIMO antennas with diversity and mutual coupling reduction techniques: A review," *Int. J. Microw.*

Wirel. Technol., vol. 9, no. 8, pp. 1763–1780, 2017, doi: 10.1017/S1759078717000538.

[12] A. V. Alejos, M. Garcia Sanchez, and I. Cuiñas, "Performance analysis of polarization diversity for indoor scenarios at 41.4GHz and 61.5GHz," *Int. J. Antennas Propag.*, vol. 2012, 2012, doi: 10.1155/2012/681820.

[13] T. W. C. Brown, S. R. Saunders, S. Stavrou, and M. Fiacco, "Characterization of polarization diversity at the mobile," *IEEE Trans. Veh. Technol.*, vol. 56, no. 5 I, pp. 2440–2447, 2007, doi: 10.1109/TVT.2007.898371.

[14] U. Ahmad *et al.*, "MIMO Antenna System with Pattern Diversity for Sub-6 GHz Mobile Phone Applications," *IEEE Access*, vol. 9, pp. 149240–149249, 2021, doi: 10.1109/ACCESS.2021.3125097.

[15] Z. Niu, H. Zhang, Q. Chen, and T. Zhong, "Isolation Enhancement in Closely Coupled Dual-Band MIMO Patch Antennas," *IEEE Antennas Wirel. Propag. Lett.*, vol. 18, no. 8, pp. 1686–1690, 2019, doi: 10.1109/LAWP.2019.2928230.

[16] L. Xi, H. Zhai, and L. Li, "A low-profile antenna system with compact new structure for reducing mutual coupling," *J. Electromagn. Waves Appl.*, vol. 33, no. 1, pp. 71–83, 2019, doi: 10.1080/09205071.2018.1524796.

[17] C. Du and Z. Zhao, "A CPW-Fed dual-band MIMO antenna with enhanced isolation for 5G application," *Prog. Electromagn. Res. M*, vol. 98, no. August, pp. 11–20, 2020, doi: 10.2528/PIERM20081203.

[18] C. Du, Z. Zhao, X. Wang, and F. Yang, "A compact cpw-fed triple-band mimo antenna with neutralization line decoupling for wlan/wimax/5g applications," *Prog. Electromagn. Res. M*, vol. 103, no. June, pp. 129–140, 2021, doi: 10.2528/PIERM21042301.

[19] H. Ullah and F. A. Tahir, "Broadband planar antenna array for future 5G communication standards," *IET Microwaves, Antennas Propag.*, vol. 13, no. 15, pp. 2661–2668, 2019, doi: 10.1049/iet-map.2018.5603.

[20] L. Zhao, Z. M. Chen, and J. Wang, "A Wideband Dual-Polarized Omnidirectional Antenna for 5G/WLAN," *IEEE Access*, vol. 7, pp. 14266–14272, 2019, doi: 10.1109/ACCESS.2019.2893941.

[21] B. A. F. Esmail *et al.*, "Reconfigurable metamaterial structure for 5G beam tilting antenna applications," *Waves in Random and Complex Media*, vol. 31,

no. 6, pp. 2089–2102, Nov. 2021, doi: 10.1080/17455030.2020.1720933.

[22] S. Hussain, S. W. Qu, W. L. Zhou, P. Zhang, and S. Yang, “Design and Fabrication of Wideband Dual-Polarized Dipole Array for 5G Wireless Systems,” *IEEE Access*, vol. 8, pp. 65155–65163, 2020, doi: 10.1109/ACCESS.2020.2984613.

[23] Z. Li, Y. Sun, M. Yang, Z. Wu, and P. Tang, “A broadband dual-polarized magneto-electric dipole antenna for 2G/3G/LTE/WiMAX applications,” *Prog. Electromagn. Res. C*, vol. 73, no. April, pp. 127–136, 2017, doi: 10.2528/PIERC17022005.

[24] A. Li and K. M. Luk, “Millimeter-Wave End-Fire Magneto-Electric Dipole Antenna and Arrays with Asymmetrical Substrate Integrated Coaxial Line Feed,” *IEEE Open J. Antennas Propag.*, vol. 2, no. November 2020, pp. 62–71, 2021, doi: 10.1109/OJAP.2020.3044437.

[25] R. Arya and D. K. Raghuvanshi, “Design of asymmetrical multiple open slot loaded microstrip antenna for WiBro/WiMAX/WLAN band application,” *Mod. Phys. Lett. B*, vol. 34, no. 18, pp. 1–13, 2020, doi: 10.1142/S0217984920501985.

[26] and W. W. Huaxiao Lu*, Yuan’an Liu, Fang Liu, “Single-Feed Single-Patch Triple-Band Single-Beam/Dual-Beam U-Slotted Patch Antenna,” *Prog. Electromagn. Res. M*, vol. 77, pp. 17–28, 2019.

[27] C. Mbinack, B. Bodo, J. S. A. Eyébé Fouda, and E. Tonye, “Inset-fed rectangular MICROSTRIP patch antenna bandwidth enhancement,” *Microw. Opt. Technol. Lett.*, vol. 61, no. 2, pp. 562–567, 2019, doi: 10.1002/mop.31565.

[28] S. D. Hossain, Rita, K. M. A. Sobahan, R. Mallick, and F. Hossain, “Design of a wide bandwidth and high efficiency circularly polarized microstrip patch antenna using coaxial feeding technique,” *Microw. Opt. Technol. Lett.*, vol. 60, no. 4, pp. 993–996, 2018, doi: 10.1002/mop.31083.

[29] M. Biswas and M. Sen, “Fast and accurate model for a coax-fed rectangular patch antenna with varying aspect ratio, feed location and substrate electrical parameters,” *J. Electromagn. Waves Appl.*, vol. 33, no. 4, pp. 428–453, 2019, doi: 10.1080/09205071.2018.1554512.

[30] M. M. Rabia Shafique, Kelash Kanwar, Fida Hussain, Ruben Morales-

Menendez, Mohammad Khubeb Siddiqui, Haris Jawad Arain, “Comparison of different feeding techniques for a patch antenna at an X frequency band to evaluate its quantitative impact on the antenna’s parameters,” *J. Appl. Res. Technol.*, vol. 18, pp. 341–361, 2020.

[31] R. Mark, N. Mishra, K. Mandal, P. P. Sarkar, and S. Das, “Hexagonal ring fractal antenna with dumb bell shaped defected ground structure for multiband wireless applications,” *AEU - Int. J. Electron. Commun.*, vol. 94, pp. 42–50, 2018, doi: 10.1016/j.aeue.2018.06.039.

[32] M. G. Siddiqui, A. K. Saroj, Devesh, and J. A. Ansari, “Multi-band fractaled triangular microstrip antenna for wireless applications,” *Prog. Electromagn. Res. M*, vol. 65, no. February, pp. 51–60, 2018, doi: 10.2528/pierm18011027.

[33] A. Aoad and M. S. Ufuk Türeli, “Design, simulation, and fabrication of a small size of a new spiral shaped of circular microstrip patch antenna,” *Microw. Opt. Technol. Lett.*, vol. 60, no. 12, pp. 2912–2918, 2018, doi: 10.1002/mop.31444.

[34] F. Antenna, Y. K. Choukiker, and S. K. Behera, “Wideband Frequency Reconfigurable Koch Snowflake,” pp. 1–19.

[35] O. Benkhadda *et al.*, “A Miniaturized Tri-Wideband Sierpinski Hexagonal-Shaped Fractal Antenna for Wireless Communication Applications,” *Fractal Fract.*, vol. 7, no. 2, pp. 1–18, 2023, doi: 10.3390/fractalfract7020115.

[36] Y. F. Cao, S. W. Cheung, and T. I. Yuk, “A multiband slot antenna for GPS/WiMAX/WLAN systems,” *IEEE Trans. Antennas Propag.*, vol. 63, no. 3, pp. 952–958, 2015, doi: 10.1109/TAP.2015.2389219.

[37] J. Liu, Q. Xue, H. Wong, H. W. Lai, and Y. Long, “Design and analysis of a low-profile and broadband microstrip monopolar patch antenna,” *IEEE Trans. Antennas Propag.*, vol. 61, no. 1, pp. 11–18, 2013, doi: 10.1109/TAP.2012.2214996.

[38] P. Chaurasia, B. K. Kanaujia, S. Dwari, and M. K. Khandelwal, “Antenna with hexa-band capabilities for multiple wireless applications,” *Prog. Electromagn. Res. C*, vol. 82, no. December 2017, pp. 109–122, 2018, doi: 10.2528/pierc17120602.

[39] A. Kaur and P. K. Malik, “Multiband Elliptical Patch Fractal and Defected Ground Structures Microstrip Patch Antenna for Wireless Applications,” *Prog.*

Electromagn. Res. B, vol. 91, no. March, pp. 157–173, 2021, doi: 10.2528/PIERB20102704.

[40] D. Tiwari, J. A. Ansari, A. K. Saroj, and M. Kumar, "Analysis of a Miniaturized Hexagonal Sierpinski Gasket fractal microstrip antenna for modern wireless communications," *AEU - Int. J. Electron. Commun.*, vol. 123, p. 153288, 2020, doi: 10.1016/j.aeue.2020.153288.

[41] Devesh, J. A. Ansari, M. G. Siddiqui, and A. K. Saroj, "Analysis of Modified Square Sierpinski Gasket fractal microstrip antenna for Wireless communications," *AEU - Int. J. Electron. Commun.*, vol. 94, pp. 377–385, 2018, doi: 10.1016/j.aeue.2018.07.027.

[42] S. E. El-Khamy, A. Zaki, S. Hamdy, and A. El-Khouly, "A new fractal-like tree structure of circular patch antennas for UWB and 5G multi-band applications," *Microw. Opt. Technol. Lett.*, vol. 59, no. 9, pp. 2168–2174, 2017, doi: 10.1002/mop.30707.

[43] M. Gupta and V. Mathur, "Wheel shaped modified fractal antenna realization for wireless communications," *AEU - Int. J. Electron. Commun.*, vol. 79, pp. 257–266, 2017, doi: 10.1016/j.aeue.2017.06.017.

[44] S. J. Singh, G. Singh, and G. Bharti, "Circular Microstrip Antenna with Fractal Slots for Multiband Applications," *J. Inst. Eng. Ser. B*, vol. 98, no. 5, pp. 441–447, 2017, doi: 10.1007/s40031-017-0278-4.

[45] R. Anand and P. Chawla, "A novel dual-wideband inscribed hexagonal fractal slotted microstrip antenna for C- and X-band applications," *Int. J. RF Microw. Comput. Eng.*, vol. 30, no. 9, pp. 1–16, 2020, doi: 10.1002/mmce.22277.

[46] N. Sharma and V. Sharma, "A design of Microstrip Patch Antenna using hybrid fractal slot for wideband applications," *Ain Shams Eng. J.*, vol. 9, no. 4, pp. 2491–2497, 2018, doi: 10.1016/j.asej.2017.05.008.

[47] R. K. Verma and D. K. Srivastava, "Design and Analysis of Triple-Band Rectangular Microstrip Antenna Loaded with Notches and Slots for Wireless Applications," *Wirel. Pers. Commun.*, vol. 114, no. 2, pp. 1847–1864, 2020, doi: 10.1007/s11277-020-07452-6.

[48] V. Singh, B. Mishra, A. K. Dwivedi, and R. Singh, "Inverted L-notch loaded hexa band circular patch antenna for X, ku/K band applications," *Microw. Opt.*

Technol. Lett., vol. 60, no. 8, pp. 2081–2088, 2018, doi: 10.1002/mop.31296.

[49] M. Meloui and M. Essaaidi, "A dual ultra wide band slotted antenna for C and X bands application," *Prog. Electromagn. Res. Lett.*, vol. 47, no. January 2014, pp. 91–96, 2014, doi: 10.2528/PIERL14052103.

[50] B. K. Ang and B. K. Chung, "A wideband E-shaped microstrip patch antenna for 5-6 GHZ wireless communications," *Prog. Electromagn. Res.*, vol. 75, pp. 397–407, 2007, doi: 10.2528/PIER07061909.

[51] R. A. Panda and D. Mishra, "Efficient Design of Bi-circular Patch Antenna for 5G Communication with Mathematical Calculations for Resonant Frequencies," *Wirel. Pers. Commun.*, vol. 112, no. 2, pp. 717–727, 2020, doi: 10.1007/s11277-020-07069-9.

[52] M. H. Sharaf, A. I. Zaki, R. K. Hamad, and M. M. M. Oma, "A novel dual-band (38/60 ghz) patch antenna for 5g mobile handsets," *Sensors (Switzerland)*, vol. 20, no. 9, 2020, doi: 10.3390/s20092541.

[53] A. Liu, L. Huang, and Y. Lu, "Wideband circular patch antenna with Ishaped structure for horizontal omnidirectional gain enhancement," *IET Microwaves, Antennas Propag.*, vol. 13, no. 5, pp. 608–614, 2019, doi: 10.1049/iet-map.2018.5503.

[54] G. V. Raviteja, "Design and analysis of a novel dual trapezoidal slot-based rectangular microstrip antenna for wide area network using WiMax application," *Microw. Opt. Technol. Lett.*, vol. 60, no. 4, pp. 1057–1060, 2018, doi: 10.1002/mop.31100.

[55] T. N. Suresh Babu and D. Sivakumar, "Stepped slot patch antenna with copper ground plane and solar cell ground plane for future mobile communications," *Prog. Electromagn. Res. C*, vol. 98, no. January, pp. 187–198, 2020, doi: 10.2528/pierc19101603.

[56] W. A. Godaymi Al-Tumah, R. M. Shaaban, and A. Tahir, "Design, simulation and measurement of triple band annular ring microstrip antenna based on shape of crescent moon," *AEU - Int. J. Electron. Commun.*, vol. 117, p. 153133, 2020, doi: 10.1016/j.aeue.2020.153133.

[57] S. P. Gangwar, K. Gangwar, and A. Kumar, "Dual band modified circular ring shaped slot antenna for GSM and WiMAX applications," *Microw. Opt.*

Technol. Lett., vol. 61, no. 12, pp. 2752–2759, 2019, doi: 10.1002/mop.31967.

[58] A. Kumar, A. A. Althuwayb, and M. J. Al-Hasan, "Wideband triple resonance patch antenna for 5G wi-fi spectrum," *Prog. Electromagn. Res. Lett.*, vol. 93, no. July, pp. 89–97, 2020, doi: 10.2528/pierl20071605.

[59] B. Bag, P. Biswas, S. Biswas, P. P. Sarkar, and D. Ghoshal, "Novel Monopole Microstrip Antennas for GPS, WiMAX and WLAN Applications," *J. Circuits, Syst. Comput.*, vol. 29, no. 3, pp. 1–15, 2020, doi: 10.1142/S0218126620500504.

[60] M. Farahani and S. Mohammad-Ali-Nezhad, "A novel wideband microstrip patch antenna with nonuniform feed based on model predictive," *Prog. Electromagn. Res. M*, vol. 89, no. January, pp. 101–109, 2020, doi: 10.2528/pierm19112706.

[61] J. H. Abril-García *et al.*, "Design of a tapered CPW-fed wideband antenna and its application to multi-channel transmission using a hybrid wireless communication system," *AEU - Int. J. Electron. Commun.*, vol. 112, 2019, doi: 10.1016/j.aeue.2019.152966.

[62] R. K. Maurya, B. K. Kanaujia, A. K. Gautam, S. Chatterji, and A. K. Singh, "Circularly polarized hexagonal ring microstrip patch antenna with asymmetrical feed and DGS," *Microw. Opt. Technol. Lett.*, vol. 62, no. 4, pp. 1702–1708, 2020, doi: 10.1002/mop.32220.

[63] B. Chen, X. Yang, and D. Hu, "Fish-shaped ultra-wideband patch antenna with tilt-folded patch feed," *IET Microwaves, Antennas Propag.*, vol. 13, no. 9, pp. 1312–1317, 2019, doi: 10.1049/iet-map.2018.5556.

[64] B. R. Swain and A. K. Sharma, "An investigation of dual-band dual-square ring (DSR) based microstrip antenna for WiFi/WLAN and 5G-NR wireless applications," *Prog. Electromagn. Res. M*, vol. 86, no. October, pp. 17–26, 2019, doi: 10.2528/pierm19060501.

[65] Z. Bendahmane, S. Ferouani, and C. Sayah, "High permittivity substrate and dgs technique for dual-band star-shape slotted microstrip patch antenna miniaturization," *Prog. Electromagn. Res. C*, vol. 102, no. February, pp. 163–174, 2020, doi: 10.2528/PIERC20021501.

[66] and V. S. T. Nand Kishore, Arun Prakash, "A MULTIBAND MICROSTRIP

PATCH ANTENNA WITH DEFECTED GROUND STRUCTURE FOR ITS APPLICATIONS," *Microw. Opt. Technol. Lett.*, vol. 58, no. 12, 2016.

[67] B. S. Hari Prasad and M. V. S. Prasad, "Design and analysis of compact periodic slot multiband antenna with defected ground structure for wireless applications," *Prog. Electromagn. Res. M*, vol. 93, no. June, pp. 77–87, 2020, doi: 10.2528/pierm20032605.

[68] R. Gurjar, D. K. Upadhyay, B. K. Kanaujia, and A. Kumar, "A compact modified sierpinski carpet fractal UWB MIMO antenna with square-shaped funnel-like ground stub," *AEU - Int. J. Electron. Commun.*, vol. 117, p. 153126, 2020, doi: 10.1016/j.aeue.2020.153126.

[69] H. Ullah, S. U. Rahman, Q. Cao, I. Khan, and H. Ullah, "Design of SWB MIMO Antenna with Extremely Wideband Isolation," *Electronics*, vol. 9, no. 1, p. 194, 2020, doi: 10.3390/electronics9010194.

[70] A. Kumar, A. Q. Ansari, B. K. Kanaujia, J. Kishor, and S. Kumar, "An ultra-compact two-port UWB-MIMO antenna with dual band-notched characteristics," *AEU - Int. J. Electron. Commun.*, vol. 114, p. 152997, 2020, doi: 10.1016/j.aeue.2019.152997.

[71] H. M. Marzouk, M. I. Ahmed, and A. A. Shaalan, "Novel dual-band 28/38 GHz MIMO antennas for 5g mobile applications," *Prog. Electromagn. Res. C*, vol. 93, no. May, pp. 103–117, 2019, doi: 10.2528/PIERC19032303.

[72] N. Kumar and R. Khanna, "A two element MIMO antenna for sub-6 GHz and mmWave 5G systems using characteristics mode analysis," *Microw. Opt. Technol. Lett.*, vol. 63, no. 2, pp. 587–595, 2021, doi: 10.1002/mop.32626.

[73] N. Kumar and R. Khanna, "A compact multi-band multi-input multi-output antenna for 4G/5G and IoT devices using theory of characteristic modes," *Int. J. RF Microw. Comput. Eng.*, vol. 30, no. 1, pp. 1–19, 2020, doi: 10.1002/mmce.22012.

[74] N. Hussain, W. A. Awan, W. Ali, S. I. Naqvi, A. Zaidi, and T. T. Le, "Compact wideband patch antenna and its MIMO configuration for 28 GHz applications," *AEU - Int. J. Electron. Commun.*, vol. 132, no. January, p. 153612, 2021, doi: 10.1016/j.aeue.2021.153612.

[75] M. K. Khan, Q. Feng, and Z. Zheng, "Experimental investigation and design of

uwb mimo antenna with enhanced isolation," *Prog. Electromagn. Res. C*, vol. 107, no. October 2020, pp. 287–297, 2021, doi: 10.2528/PIERC20103002.

[76] A. R. Sabek, W. A. E. Ali, and A. A. Ibrahim, "Minimally Coupled Two-Element MIMO Antenna with Dual Band (28/38 GHz) for 5G Wireless Communications," *J. Infrared, Millimeter, Terahertz Waves*, vol. 43, no. 3–4, pp. 335–348, 2022, doi: 10.1007/s10762-022-00857-3.

[77] D. A. Sehrai *et al.*, "A High-Gain and Wideband MIMO Antenna for 5G mm-Wave-Based IoT Communication Networks," *Appl. Sci.*, vol. 12, no. 19, 2022, doi: 10.3390/app12199530.

[78] M. A. El-Hassan, A. E. Farahat, and K. F. A. Hussein, "Quad-Band MIMO Antenna System for 5G Mobile Handsets," *Appl. Comput. Electromagn. Soc. J.*, vol. 36, no. 11, pp. 1418–1428, 2021, doi: 10.13052/2021.ACES.J.361105.

[79] M. S. Sharawi, S. K. Podilchak, M. T. Hussain, and Y. M. M. Antar, "Dielectric resonator based MIMO antenna system enabling millimetre-wave mobile devices," *IET Microwaves, Antennas Propag.*, vol. 11, no. 2, pp. 287–293, 2017, doi: 10.1049/iet-map.2016.0457.

[80] R. Sharma, R. Khanna, and Geetanjali, "Compact Sub-6 GHz and mmWave 5G Wideband 2 × 1 MIMO Antenna with High Isolation Using Parasitically Placed Double Negative (DNG) Isolator," *Wirel. Pers. Commun.*, vol. 122, no. 3, pp. 2839–2857, 2022, doi: 10.1007/s11277-021-09032-8.

[81] S. S. Al-Bawri, M. T. Islam, T. Shabbir, G. Muhammad, M. D. Shabiul Islam, and H. Y. Wong, "Hexagonal shaped near zero index (NZI) metamaterial based MIMO antenna for millimeter-wave application," *IEEE Access*, vol. 8, pp. 181003–181013, 2020, doi: 10.1109/ACCESS.2020.3028377.

[82] A. Ali *et al.*, "A Compact MIMO Multiband Antenna for 5G/WLAN/WIFI-6 Devices," *Micromachines*, vol. 14, no. 6, 2023, doi: 10.3390/mi14061153.

[83] S. Hassan Ghadeer *et al.*, "An innovative fractal monopole MIMO antenna for modern 5G applications," *AEU - Int. J. Electron. Commun.*, vol. 159, p. 154480, 2023, doi: 10.1016/j.aeue.2022.154480.

[84] A. Dkiouak, A. Zakriti, and M. El Ouahabi, "Design of a compact dual-band MIMO antenna with high isolation for WLAN and X-band satellite by using orthogonal polarization," *J. Electromagn. Waves Appl.*, vol. 34, no. 9, pp.

1254–1267, 2020, doi: 10.1080/09205071.2019.1657504.

[85] A. Abdelaziz and E. K. I. Hamad, “Isolation enhancement of 5G multiple-input multiple-output microstrip patch antenna using metamaterials and the theory of characteristic modes,” *Int. J. RF Microw. Comput. Eng.*, vol. 30, no. 11, pp. 1–13, 2020, doi: 10.1002/mmce.22416.

[86] A. A. Ghannad, M. Khalily, P. Xiao, R. Tafazolli, and A. A. Kishk, “Enhanced Matching and Vialess Decoupling of Nearby Patch Antennas for MIMO System,” *IEEE Antennas Wirel. Propag. Lett.*, vol. 18, no. 6, pp. 1066–1070, 2019, doi: 10.1109/LAWP.2019.2906308.

[87] K. V. Babu and B. Anuradha, “Design of multi-band minkowski MIMO antenna to reduce the mutual coupling,” *J. King Saud Univ. - Eng. Sci.*, vol. 32, no. 1, pp. 51–57, 2020, doi: 10.1016/j.jksues.2018.06.003.

[88] M. Abdullah, Q. Li, W. Xue, G. Peng, Y. He, and X. Chen, “Isolation enhancement of MIMO antennas using shorting pins,” *J. Electromagn. Waves Appl.*, vol. 33, no. 10, pp. 1249–1263, 2019, doi: 10.1080/09205071.2019.1606738.

[89] S. F. Jilani and A. Alomainy, “Millimetre-wave T-shaped MIMO antenna with defected ground structures for 5G cellular networks,” *IET Microwaves, Antennas Propag.*, vol. 12, no. 5, pp. 672–677, 2018, doi: 10.1049/iet-map.2017.0467.

[90] H. Al-Saif, M. Usman, M. T. Chughtai, and J. Nasir, “Compact Ultra-Wide Band MIMO Antenna System for Lower 5G Bands,” *Wirel. Commun. Mob. Comput.*, vol. 2018, 2018, doi: 10.1155/2018/2396873.

[91] S. Y. A. Fatah, E. K. I. Hamad, W. Swelam, A. M. M. A. Allam, and H. A. Mohamed, “Design of compact 4-port mimo antenna based on minkowski fractal shape dgs for 5g applications,” *Prog. Electromagn. Res. C*, vol. 113, no. June, pp. 123–136, 2021, doi: 10.2528/PIERC21042703.

[92] M. Khalid *et al.*, “4-port MIMO antenna with defected ground structure for 5G millimeter wave applications,” *Electron.*, vol. 9, no. 1, 2020, doi: 10.3390/electronics9010071.

[93] M. Bilal, S. I. Naqvi, N. Hussain, Y. Amin, and N. Kim, “High-Isolation MIMO Antenna for 5G Millimeter-Wave Communication Systems,” *Electron.*,

vol. 11, no. 6, 2022, doi: 10.3390/electronics11060962.

[94] A. K. Singh, A. K. Dwivedi, C. Jha, S. Singh, V. Singh, and R. S. Yadav, "A Compact MIMO Antenna for 5G NR Frequency Bands n257/n258/n261 Under Millimeter-Wave Communication," *IETE J. Res.*, 2022, doi: 10.1080/03772063.2022.2091044.

[95] T. Firmansyah *et al.*, "Bandwidth enhancement and miniaturization of circular-shaped microstrip antenna based on beleved half-cut structure for MIMO 2×2 application," *Int. J. Electr. Comput. Eng.*, vol. 9, no. 2, pp. 1110–1121, 2019, doi: 10.11591/ijece.v9i2.pp.1110-1121.

[96] E. Thakur, N. Jaglan, and S. D. Gupta, "Design of compact uwb mimo antenna with enhanced bandwidth," *Prog. Electromagn. Res. C*, vol. 97, no. August, pp. 83–94, 2019, doi: 10.2528/pierc19083004.

[97] D. Dileepan, S. Natarajan, and R. Rajkumar, "A high isolation multiband mimo antenna without decoupling structure for wlan/wimax/5g applications," *Prog. Electromagn. Res. C*, vol. 112, no. March, pp. 207–219, 2021, doi: 10.2528/PIERC21032605.

[98] A. K. Singh, S. K. Mahto, and R. Sinha, "A Miniaturized MIMO Antenna for C, X, and Ku Band Applications," *Prog. Electromagn. Res. C*, vol. 117, no. October, pp. 31–40, 2021, doi: 10.2528/PIERC21100202.

[99] S. Jabeen and Q. U. Khan, "An integrated MIMO antenna design for Sub-6 GHz & millimeter-wave applications with high isolation," *AEU - Int. J. Electron. Commun.*, vol. 153, p. 154247, Aug. 2022, doi: 10.1016/j.aeue.2022.154247.

[100] G. Naga Jyothi Sree and S. Nelaturi, "Design and experimental verification of fractal based MIMO antenna for lower sub 6-GHz 5G applications," *AEU - Int. J. Electron. Commun.*, vol. 137, no. February, p. 153797, 2021, doi: 10.1016/j.aeue.2021.153797.

[101] M. N. Naik and H. G. Virani, "A compact four port MIMO antenna for millimeterwave applications," *Bull. Electr. Eng. Informatics*, vol. 11, no. 2, pp. 878–885, 2022, doi: 10.11591/eei.v11i2.3689.

[102] T. Kumari, G. Das, A. Sharma, and R. K. Gangwar, "Design approach for dual element hybrid MIMO antenna arrangement for wideband applications," *Int. J.*

RF Microw. Comput. Eng., vol. 29, no. 1, pp. 1–10, 2019, doi: 10.1002/mmce.21486.

APPENDIX-A

TESTING CERTIFICATE AND REPORT OF CIRCULAR SHAPED ANTENNA

ANTENNA FIDELITY SOLUTIONS

An ISO 9001:2015 Certified Company
GSTIN #:29ABOFA2470P1ZR
ISO Certificate No: 20IQEI11
MSME registered
#47 1st Floor Bikasipura Main road
J.C Industrial area, Yelachenahalli
Bangalore-560062
Mob: +91 80880 75146

Reference No. AFS_C0621/038

Date: 05/04/2021

Antenna Test Certificate

To whomsoever may it concern

This is to certify that the below mentioned antenna with serial number details listed in table is tested as AUT (Antenna Under Test) tests are performed to industry standards, the results provided are true and accurate. The certificate applies only to the particular sample unit(s) tested and to the specific tests carried out as detailed in the report file (Annexure 1) held at Antenna Fidelity Solutions.

This test certificate does not cover Electromagnetic compatibility. It should be noted that the tests have been carried out for research applications field only.

Certificate No.	AFS_C0621/038
Model/Serial No.	JN3559
Test Report	Annexure 1
Client	Asst. Prof. Nitasha Bisht

For Antenna Fidelity Solutions

Antenna Fidelity Solutions
47, 1st Floor, Bikasipura Main Road
J.C Industrial Area Yelachenahalli
Bangalore-560062
www.antennafidelitysolutions.com

Antenna Fidelity Solutions ★ Bangalore-560062 ★

Authorized Signature

Manjula.K

IAS ACCREDITED IAF

#47 1st Floor Bikasipura Main road, J C Industrial area, Yelachenahalli, Bangalore-560062

www.antennafidelitysolutions.com

info@antennafidelitysolutions.com
sales@antennafidelitysolutions.com

Antenna Fidelity solutions
#47 1st floor Bikasipura main road, Opp to Siddi Vinayak temple. J.C industrial area, Yelachenahalli
Bangalore 560062. Email: info@antennafidelitysolutions.com

ELECTRICAL PARAMETERS OF ANTENNA & TEST REPORT

Product Description: 2-20GHz UWB Single MPA Antenna

Model #: JN3559 **Date of Test Conducted: 05/04/2021**

Test Location: AFS Anechoic chamber measurement Set up

1) Test Setup Details

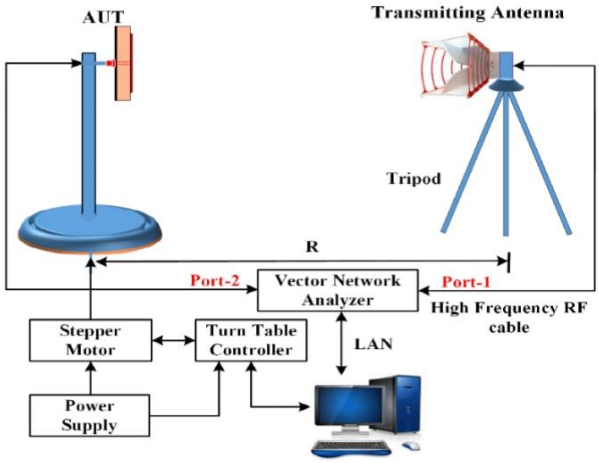

Figure1: Test setup for radiation pattern measurement

a. Distance 'R' between TX (Reference/Transmitting Antenna) and Rx (Antenna under test/receiving antenna)

2) Instruments used for testing:

1. Network Analyzer
2. Spectrum Analyzer
3. Signal Generator

3) Customer: Asst. Prof. Nitasha Bisht

4) Test Procedures for Measuring Various Parameters The following electrical parameters of the antenna under test are checked.

a) Radiation Pattern

A) Radiation Pattern: Test procedure

a) Arrange the test setup as shown in block diagram of Fig-1
b) Set both antennas on the same polarization (either vertical or horizontal).
c) Set the frequency and power level of the generator
d) Connect one of the ports to the receiver and terminate the other with a matching load.
e) Align the transmitting and receiving antenna so that maximum power is received.
f) If applicable, adjust the position of the feed so that the phase centre of the feed horn coincides with the point of the parabola.
g) After the system has set up and optimized, the radiation pattern should be taken in each polarization plane of frequencies in the band, patterns will be recorder on a shared polar/rectangular recorder of 40GHz R&S make and Model ZNB-40. While taking patterns care is to be exercised in assuring the linearity of the system. Also care must be taken to observe and record on the chart any source of reflections that show up on the pattern data.
h) Run through several antenna patterns so that the test equipment may be adjusted and optimized. Correctly measure the frequency of the received signal with a frequency meter.
i) After taking measurements in one plane of polarization, connect the matching load to the other port and receive through the remaining port after reorienting the transmit back ratio levels.
j) Having taken the available information, the pattern may be analysed and radiation levels recorded on the pattern charts including beam width, side lobe and front to back ratio levels. k) After all data is taken and recordings are made on pattern charts, a table should be constructed for each tested antenna tabulating all the results of measurement and submitted with the test report.

Test procedure for Antenna measurements & equipment test setup:

The Antenna is tested by measuring the radiation parameter & Gain as they describe the performance of the antenna. The parameter of interest whose measurement carried out are:

a) S11/VSWR
b) Insertion Loss
c) Gain measurement

a) Test Procedure for VSWR Measurement:

1. Connect the test equipment as shown in the fig below.
2. Switch on the Vector Network Analyzer and set the desired band of frequency and sweep it over the required frequency band.

3. Select S11 parameter for VSWR. Calibrate the Network Analyzer by connecting calibration module. Set the network analyzer for S11 VSWR.

4. Connect the other end of the feeder cable to the antenna under test.
5. Read the response in NA over the band which is the VSWR of the antenna
6. Note the Value of VSWR.

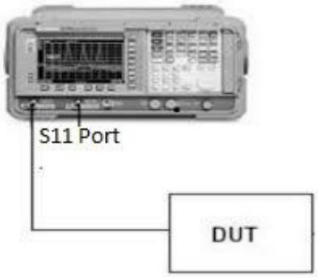

Figure 2: Test setup for VSWR measurement

b) Test Procedure for Insertion Loss Measurement:

1. Connect the test equipment as shown in fig below.
2. Switch on VNA and set the desired band of frequency
3. Select the S21 parameters for Insertion Loss (dB). Calibrate the network analyzer by connecting to Calibration module.
4. Connect both the end of connector as shown in figure
5. Read the response in network analyzer over the band which is Insertion Loss
   Note the Value of Insertion Loss

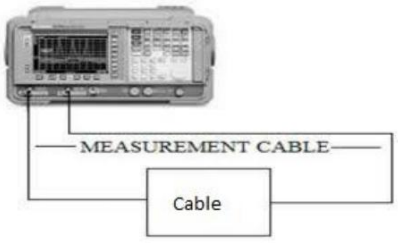

Figure 3: Test setup for Insertion Loss measurement

c) Gain Measurement using Spectrum Analyzer: - Test Setup by description:

a) Connect the test setup & equipment as shown in Fig. 4.
b) Record the maximum signal received by the antenna.
c) Orient the standard gain beam and connect the power meter with the mount. Record the maximum signal level in dB.
d) Find out of the difference in the signal level in dB.
e) Add the value obtained in step "d" to the standard gain reading to get the gain of the antenna.

1) Measure the cable loss and calculate the FSPL (free space path loss) and Total Loss by using formulas.
2) Measure the RSL level from input Port and note the values.

Calculate the Gain using RSL (received Signal Level)

Test Setup for Gain:

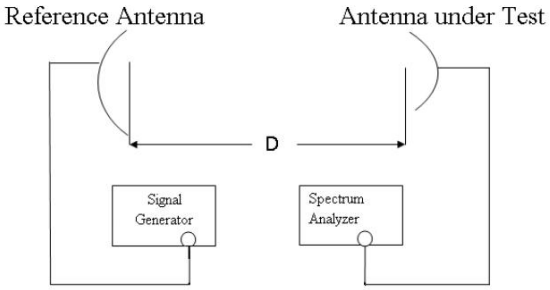

Figure 4: Test setup for Gain measurement

i. Distance 'D' between TX (Reference/Transmitting Antenna) and Rx (Antenna under test/receiving antenna) is 1m.
ii. Cable used is LMR-400/ RG316 (Loss less cable) of length 10 meters.

Test Instruments Used

No.	Instrument Description	Make	Model No	Spec.
1	Network Analyzer	R&S	ZNB-40	100KHz-40GHz
2	Signal Generator	Wiltron	68147B	10MHz-20GHz
3	Spectrum Analyzer	HP	8593E	9KHz-26.5GHz

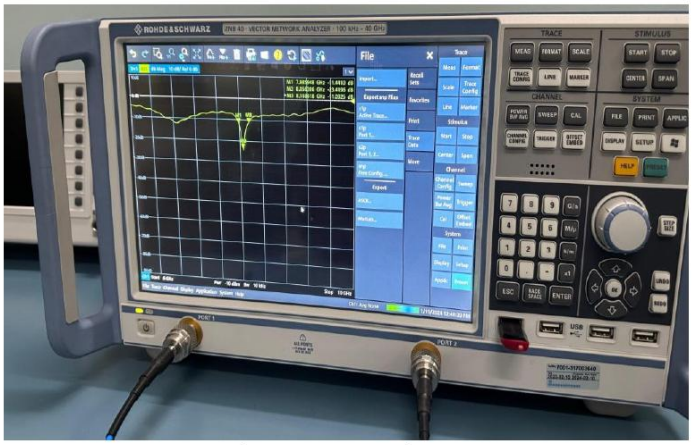

Figure 5: VNA Equipment

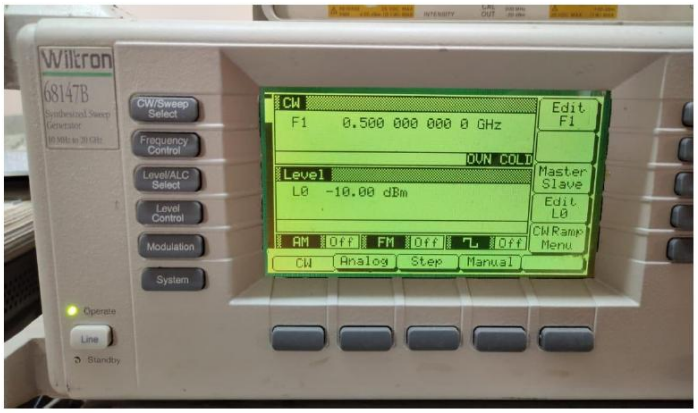

Figure 6: Signal Generator Equipment

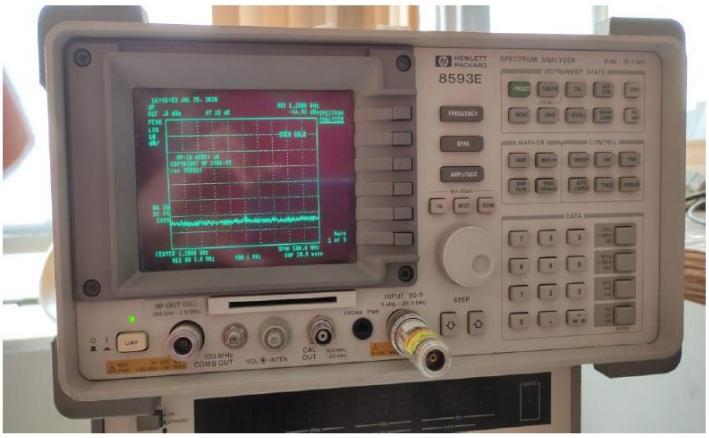

Figure 7: Spectrum Analyzer Equipment

Model 2: Serial no. JN3559

Figure 8: Sample-1 Antenna Serial no. JN3559

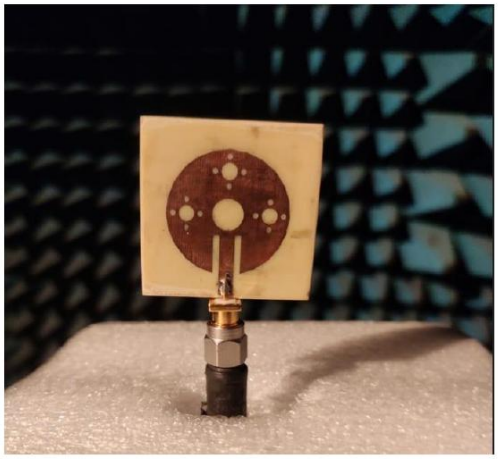

Figure 9: AUT (Antenna under Test) mounted in Anechoic chamber

Test results AUT: JN3559

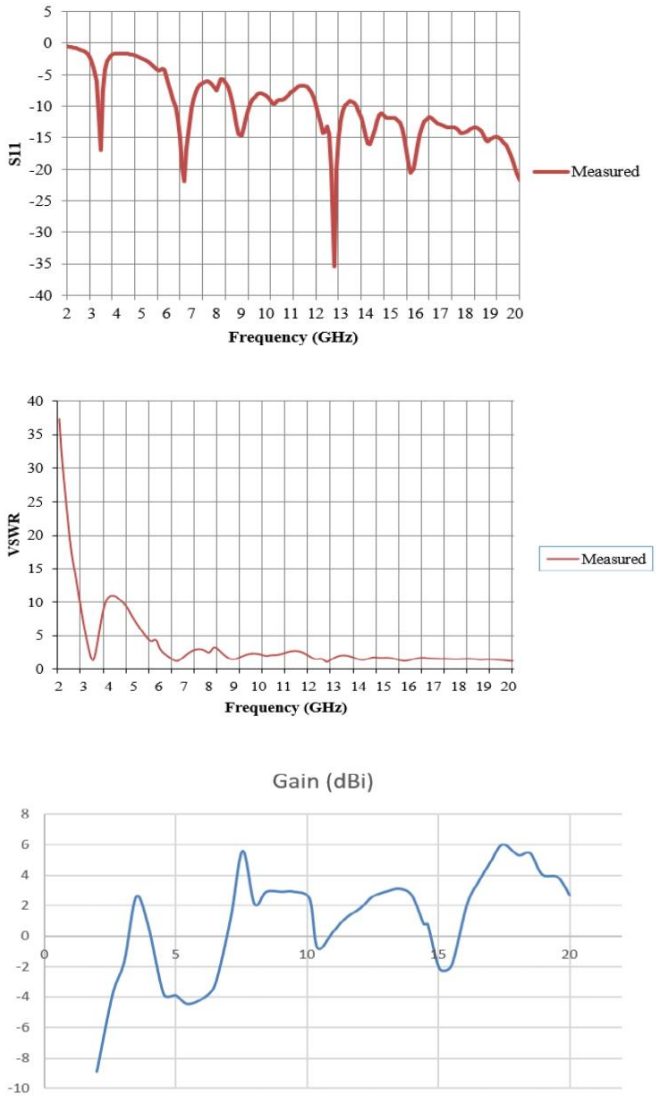

Figure 10: S parameters plot (S11, VSWR, S21 Gain)

Antenna Fidelity solutions
#47 1st floor Bikasipura main road, Opp to Siddi Vinayak temple. J.C industrial area, Yelachenahalli
Bangalore 560062. Email: info@antennafidelitysolutions.com

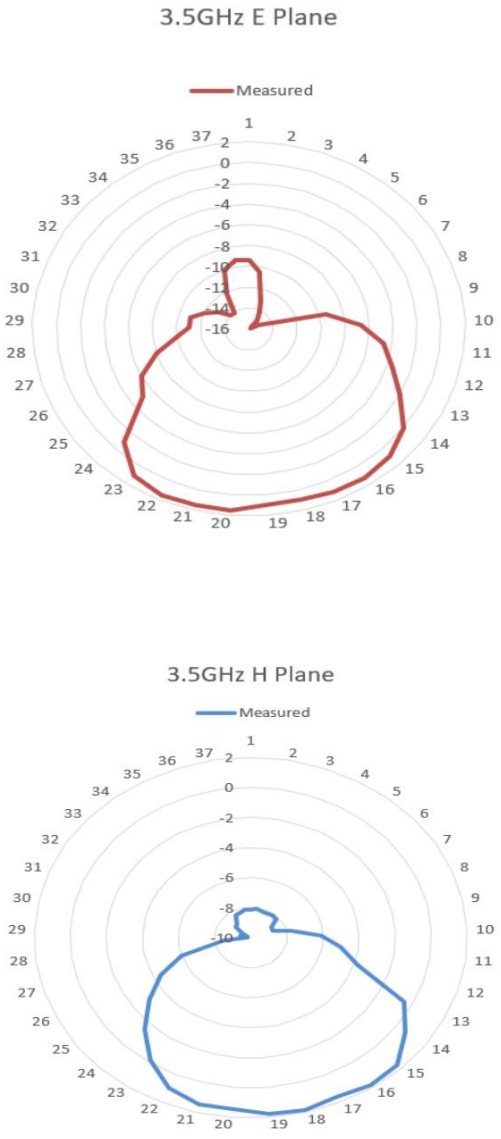

Figure 11: Radiation Pattern E & H Plane 3.5GHz

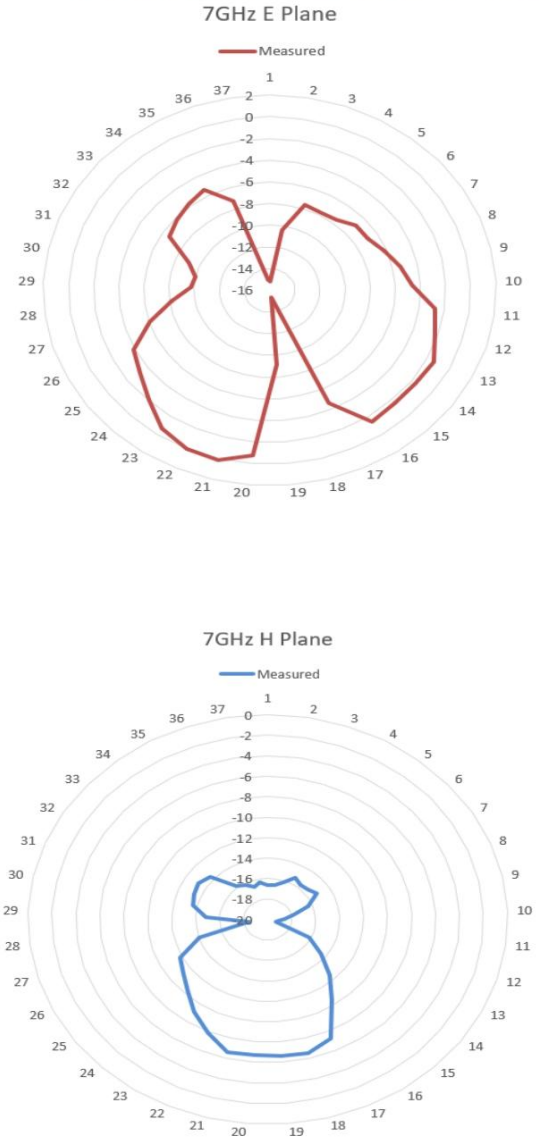

Figure 12: Radiation Pattern E & H Plane 7GHz

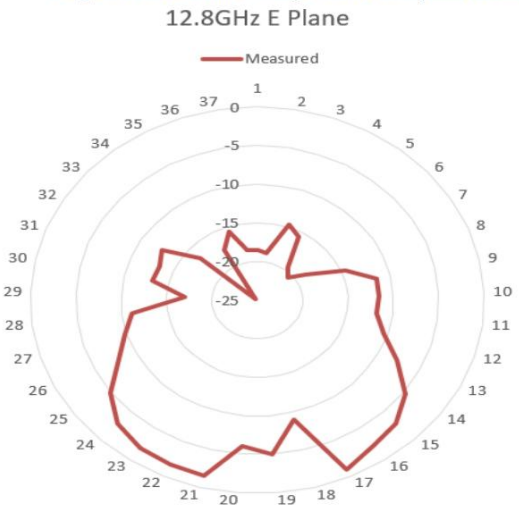

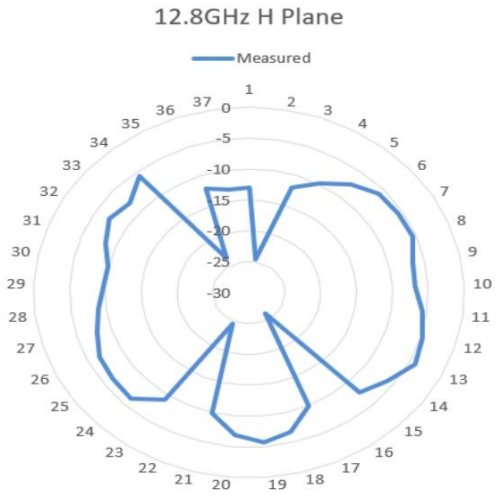

Figure 13: Radiation Pattern E & H Plane 12.8GHz

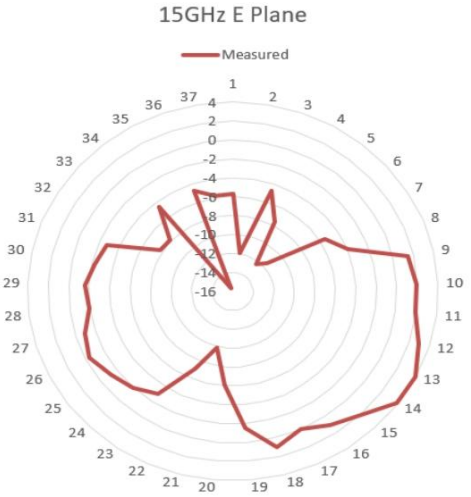

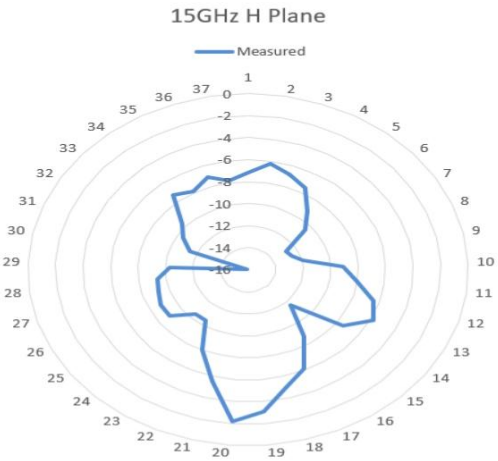

Figure 14: Radiation Pattern E & H Plane 15GHz

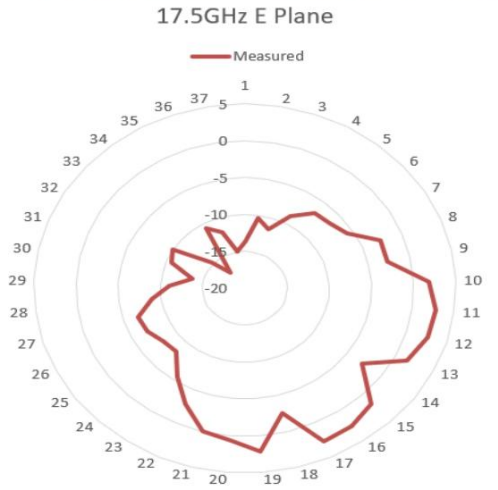

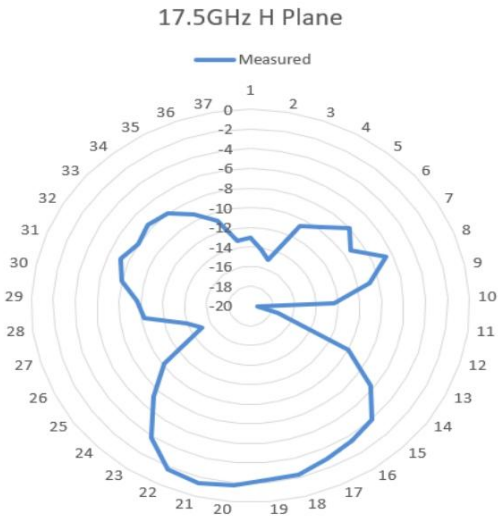

Figure 15: Radiation Pattern E & H Plane 17.5GHz

APPENDIX-B

TESTING CERTIFICATE AND REPORT OF CIRCULAR SHAPED TWO-PORT MIMO ANTENNA

ANTENNA FIDELITY SOLUTIONS

An ISO 9001:2015 Certified Company
GSTIN #:29ABOFA2470P1ZR
ISO Certificate No: 20IQEI11
MSME registered
#47 1st Floor Bikasipura Main road
J.C Industrial area, Yelachenahalli
Bangalore-560062
Mob: +91 80880 75146

Reference No. AFS_C0923/017

Date: 13/03/2023

Antenna Test Certificate

To whomsoever may it concern

This is to certify that the below mentioned antenna with serial number details listed in table is tested as AUT (Antenna Under Test) tests are performed to industry standards, the results provided are true and accurate. The certificate applies only to the particular sample unit(s) tested and to the specific tests carried out as detailed in the report file (Annexure 1) held at Antenna Fidelity Solutions.

This test certificate does not cover Electromagnetic compatibility. It should be noted that the tests have been carried out for research applications field only.

Certificate No.	AFS_C0923/017
Model/Serial No.	JN2648
Test Report	Annexure 1
Client	Asst. Prof. Nitasha Bisht

For Antenna Fidelity Solutions
Antenna Fidelity Solutions
47, 1st Floor, Bikasipura Main Road
J.C Industrial Area Yelachenahalli
Bangalore-560062
www.antennafidelitysolutions.com

Antenna Fidelity Solutions Bangalore-560062

Authorized Signature

Manjula.K

Antenna Fidelity solutions
#47 1st floor Bikasipura main road, Opp to Siddi Vinayak temple. J.C industrial area, Yelachenahalli
Bangalore 560062. Email: info@antennafidelitysolutions.com

ELECTRICAL PARAMETERS OF ANTENNA & TEST REPORT

Product Description: 8-28GHz UWB Antenna

Model #: JN2648 **Date of Test Conducted: 13/03/2023**

Test Location: AFS Anechoic chamber measurement Set up

1) Test Setup Details

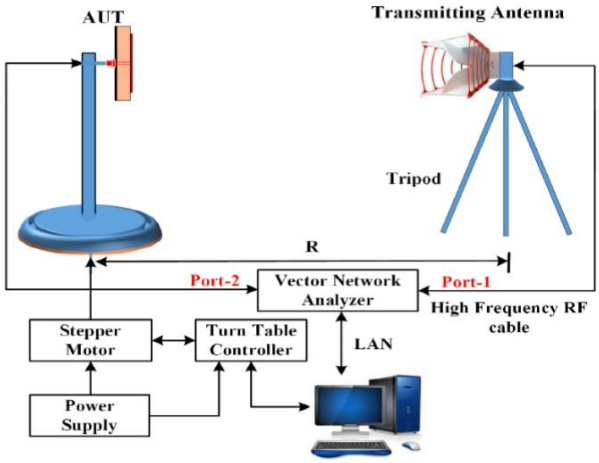

Figure1: Test setup for radiation pattern measurement

a. Distance 'R' between TX (Reference/Transmitting Antenna) and Rx (Antenna under test/receiving antenna)

2) Instruments used for testing:

1. Network Analyzer
2. Spectrum Analyzer
3. Signal Generator

3) Customer: Asst. Prof. Nitasha Bisht

4) Test Procedures for Measuring Various Parameters

The following electrical parameters of the antenna under test are checked.

a) Radiation Pattern

A) Radiation Pattern: Test procedure

a) Arrange the test setup as shown in block diagram of Fig-1
b) Set both antennas on the same polarization (either vertical or horizontal).
c) Set the frequency and power level of the generator
d) Connect one of the ports to the receiver and terminate the other with a matching load.
e) Align the transmitting and receiving antenna so that maximum power is received.
f) If applicable, adjust the position of the feed so that the phase centre of the feed horn coincides with the point of the parabola.
g) After the system has set up and optimized, the radiation pattern should be taken in each polarization plane of frequencies in the band, patterns will be recorder on a shared polar/rectangular recorder of 40GHz R&S make and Model ZNB-40. While taking patterns care is to be exercised in assuring the linearity of the system. Also care must be taken to observe and record on the chart any source of reflections that show up on the pattern data.
h) Run through several antenna patterns so that the test equipment may be adjusted and optimized. Correctly measure the frequency of the received signal with a frequency meter.
i) After taking measurements in one plane of polarization, connect the matching load to the other port and receive through the remaining port after reorienting the transmit back ratio levels.
j) Having taken the available information, the pattern may be analysed and radiation levels recorded on the pattern charts including beam width, side lobe and front to back ratio levels. k) After all data is taken and recordings are made on pattern charts, a table should be constructed for each tested antenna tabulating all the results of measurement and submitted with the test report.

Test procedure for Antenna measurements & equipment test setup:

The Antenna is tested by measuring the radiation parameter & Gain as they describe the performance of the antenna. The parameter of interest whose measurement carried out are:

a) S11/VSWR
b) Insertion Loss

a) Test Procedure for VSWR Measurement:

1. Connect the test equipment as shown in the fig below.
2. Switch on the Vector Network Analyzer and set the desired band of frequency and sweep it over the required frequency band
3. Select S11 parameter for VSWR. Calibrate the Network Analyzer by connecting calibration module. Set the network analyzer for S11 VSWR.

4. Connect the other end of the feeder cable to the antenna under test.
5. Read the response in NA over the band which is the VSWR of the antenna
6. Note the Value of VSWR.

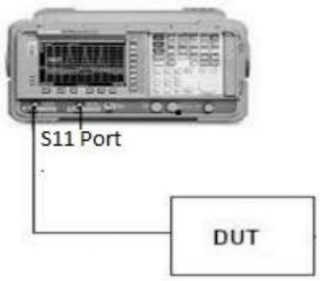

Figure 2: Test setup for VSWR measurement

b) Test Procedure for Insertion Loss Measurement:

1. Connect the test equipment as shown in fig below.
2. Switch on VNA and set the desired band of frequency
3. Select the S21 parameters for Insertion Loss (dB). Calibrate the network analyzer by connecting to Calibration module.
4. Connect both the end of connector as shown in figure
5. Read the response in network analyzer over the band which is Insertion Loss
   Note the Value of Insertion Loss

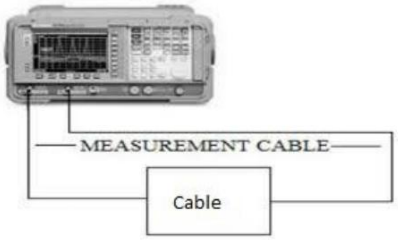

Figure 3: Test setup for Insertion Loss measurement

Test Instruments Used

No.	Instrument Description	Make	Model No	Spec.
1	Network Analyzer	R&S	ZNB-40	100KHz-40GHz
2	Signal Generator	Wiltron	68147B	10MHz-20GHz
3	Spectrum Analyzer	HP	8593E	9KHz-26.5GHz

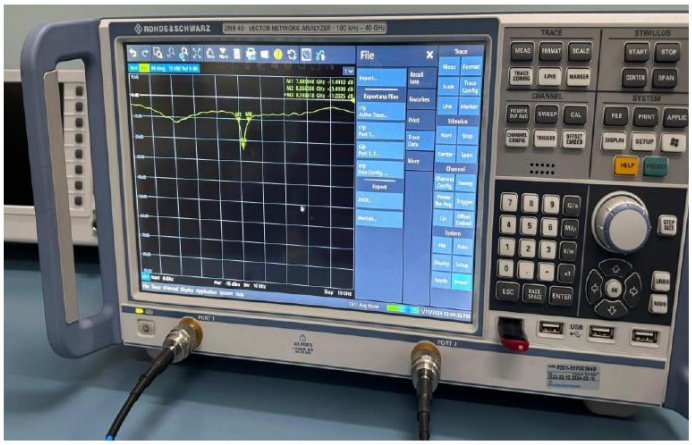

Figure 4: VNA Equipment

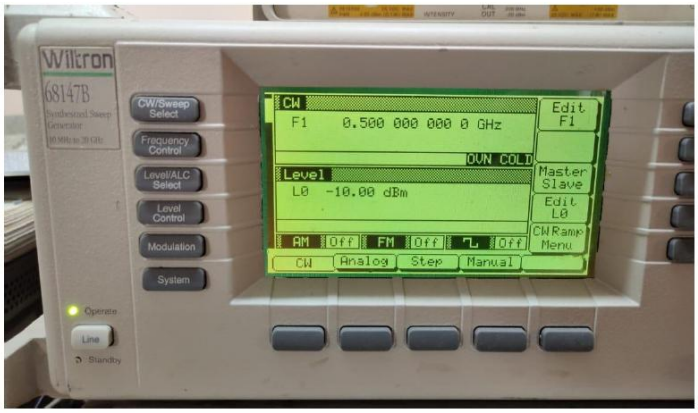

Figure 5: Signal Generator Equipment

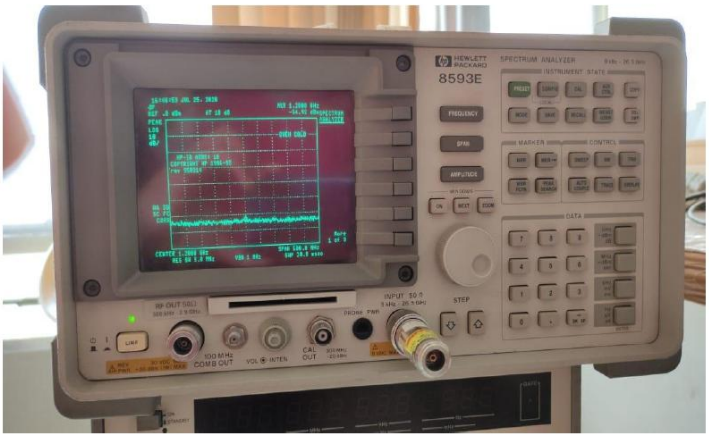

Figure 6: Spectrum Analyzer Equipment

Model 1: Serial no. JN2648

Figure 7: Sample-1 Antenna Serial no. JN2648

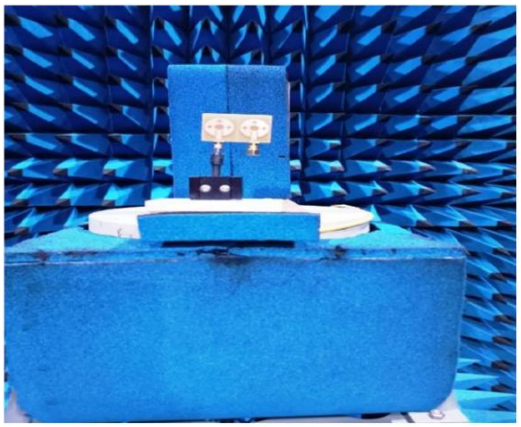

Figure 8: AUT (Antenna under Test mounted in Anechoic chamber)

Antenna Fidelity solutions
#47 1st floor Bikasipura main road, Opp to Siddi Vinayak temple. J.C industrial area, Yelachenahalli
Bangalore 560062. Email: info@antennafidelitysolutions.com

Test results AUT: JN2648

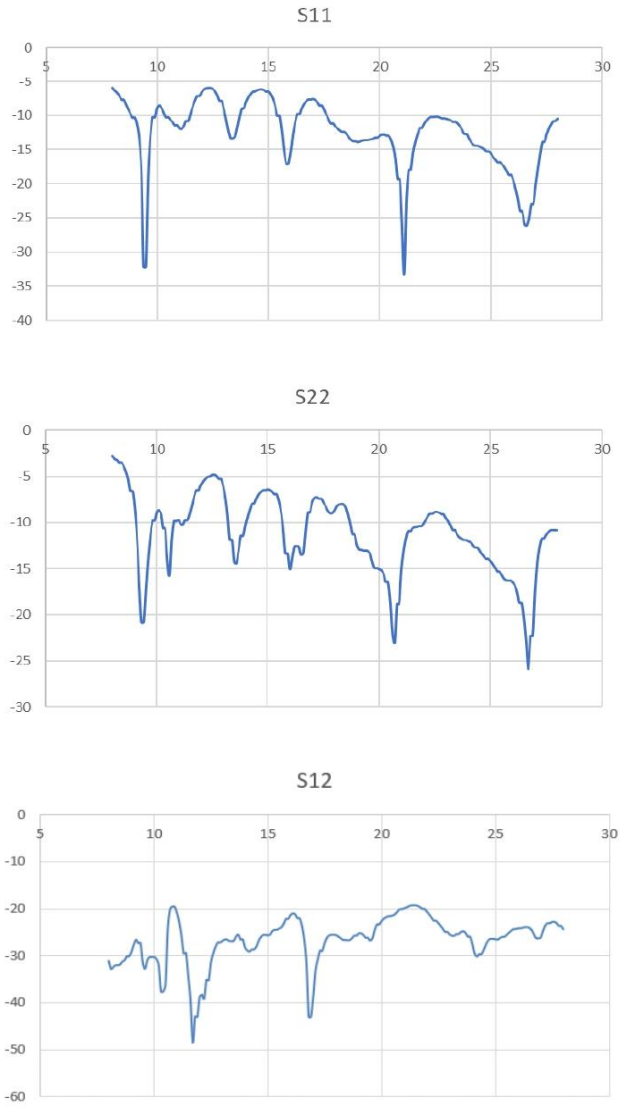

Figure 9: S parameters plot (S11, S22, S12)

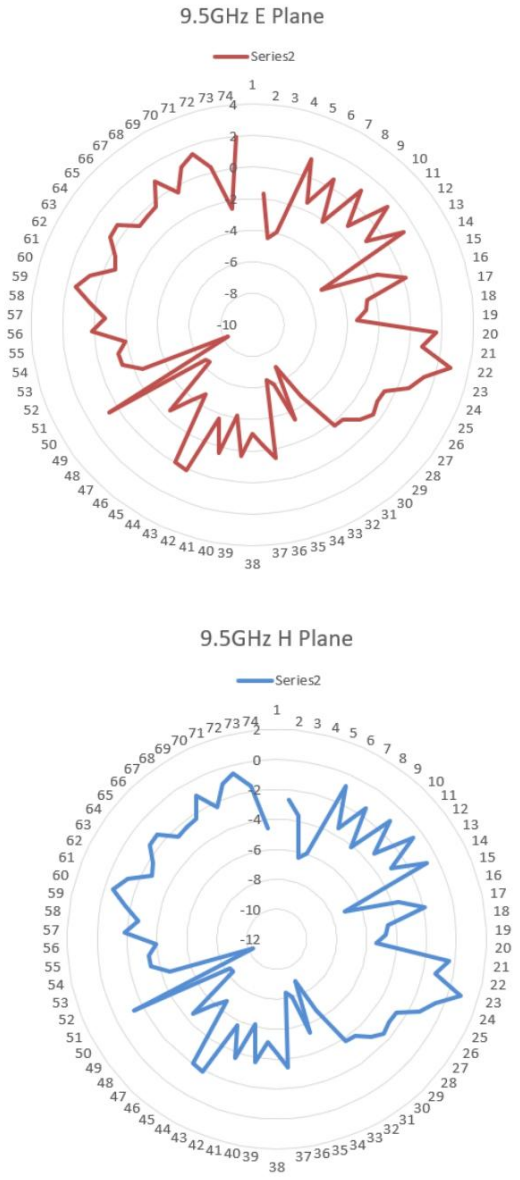

Figure 10: Radiation Pattern E & H Plane 9.5GHz

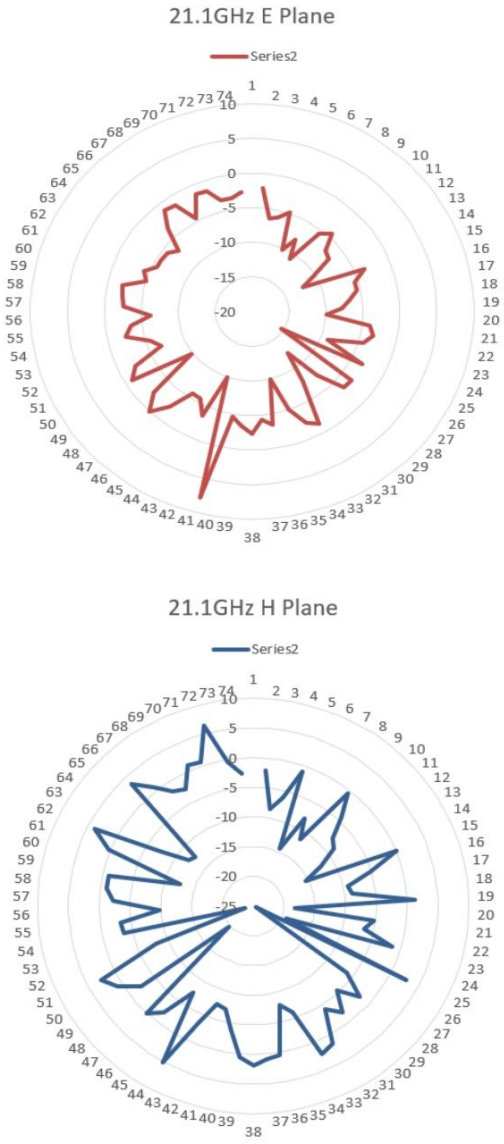

Figure 11: Radiation Pattern E & H Plane 21.1GHz

Antenna Fidelity solutions
#47 1st floor Bikasipura main road, Opp to Siddi Vinayak temple. J.C industrial area, Yelachenahalli
Bangalore 560062. Email: info@antennafidelitysolutions.com

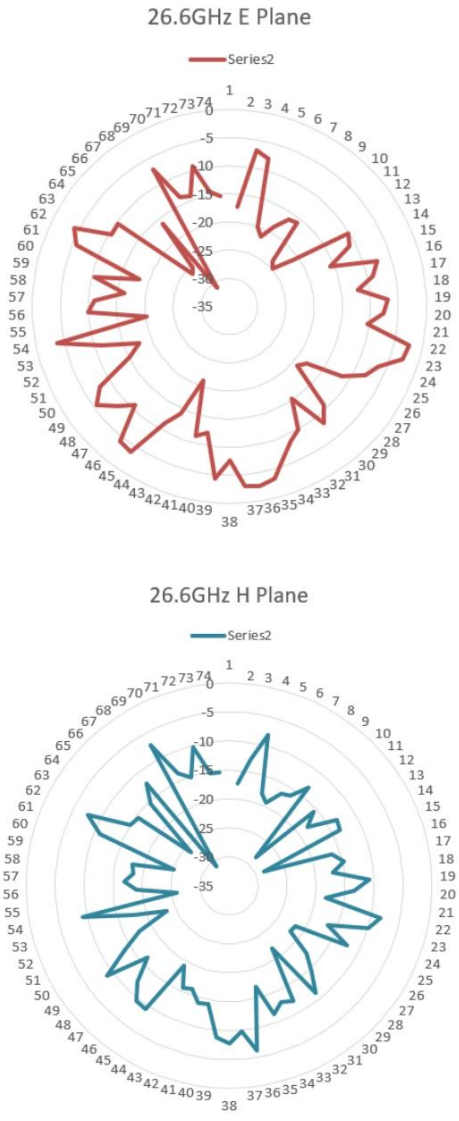

Figure 12: Radiation Pattern E & H Plane 26.6GHz

ABOUT THE AUTHOR

NITASHA BISHT
Assistant Professor (ECE)
Email: bisht19876@yahoo.co.in
Jawaharlal Nehru Govt. Engg. College
District Mandi (HP), Pin-175018
Mobile: +919418005567

Objective

To utilize my teaching skills towards a challenging career in growth oriented and leading edge that will provide mutual benefits and where from I can utilize my capabilities to the fullest benefits of the organization and society.

Educational Qualification

- Pursuing Ph.D (Part Time) in Wireless Communication Systems from Lovely Professional University, Jalandhar, Punjab.
- Master of Technology in Electronics & Communication Engineering from Jaypee University of Information & Technology Waknaghat (HP) with CGPA 8.9 (2009-2011).
- Bachelor of Electronics & Communication Engineering from IITT College of Engineering, Kala Amb, Affiliated to HP University with 71% (2005-2009).

Work Experience: 13+ Years

- Assistant Professor, Department of Electronics & Communication Engineering (Aug 2011 to Till Date) at Jawaharlal Nehru Government Engineering College, Sundernagar District Mandi (HP).

International Journal Publications

1. A Triple Band Fractal Circular Microstrip Antenna for C-Band Application, International Journal of Research in IT, Management and Engineering, Volume 5, Issue 1, January 2015 (ISSN 2249-1619).
2. Nitasha Bisht, Praveen Kumar Malik and Sudipta Das, "A Modified Circular Disk Shaped Miniaturized Multiband Printed Antenna with Enhance Bandwidth for 5G Mobile Application," International Journal of Microwave and Optical Technology, Vol. 17, No. 5, pp: 487- 495, September 2022. **(Scopus Indexed).**

3. Nitasha Bisht, Praveen Kumar Malik and Sudipta Das, "Feeding Methods for a Circular Shaped Multiband Patch Antenna at 5G, X And Ku Band to Quantify Their Effects on Antenna Characteristics" Journal of Nano and Electronic Physics, Vol. 15, No. 3, pp:03007 (1-5), June 2023. **(Scopus Indexed).**
4. Nitasha Bisht, Praveen Kumar Malik and Sudipta Das," Design of a Modified MIMO Antenna Based on Tweaked Spherical Fractal Geometry For 5G New Radio (NR) Band N258(24.25–27.25GHz) Applications," Fractal and Fractional. **2023**, 7,718. https://doi.org/10.3390/fractalfract7100718, **(SCI Indexed).**

International Conference Papers Published

1. Full Subtractor Circuit Design with Independent Double Gate Transistors, IEEE International Conference on Recent Trends in Information Telecommunication and Computing (ITC-2010), March 12-13, 2010, Kochi, India.
2. A Dual Band Fractal Circular Micro Strip Patch Antenna for C-Band Applications, Progress in Electromagnetic Research (PIER), 2011, Suzhou, China.
3. Stacked Couple Circular Patch Micro Strip for Dual Band Application, Progress in Electromagnetic Research (PIERS), 2011, Suzhou, China.
4. Rectangular Micro Strip Patch Antenna with Photonic Band Gap Crystal for 60 GHz Communications, Progress in Electromagnetic Research (PIERS) 2011, Suzhou, China.
5. Nitasha Bisht and Praveen Kumar Malik, "Circular Patch Microstrip Antenna with Slots for Lower 5G Band Applications," TEQIP-III Sponsored International Conference on Technological Transformation and Preparedness in the Post COVID World, March 22-23, 2021, Deenbandhu Chhotu Ram University of Science & Technology, Murthal, India.
6. Nitasha Bisht and Praveen Kumar Malik, "Adoption of Microstrip Antenna to Multiple Input Multiple Output Microstrip Antenna For Wireless Applications: A Review," International Conference on Recent Innovations in Computing (ICRIC 2021), 8 - 9 June, 2021. **(Scopus Indexed).**
7. HS Bedi, PK Malik, R Singh, R Singh, N Bisht," Traffic Surveillance Using Computer Vision and Deep Learning Methods," IOP Conference Series: Earth and Environmental Science 1285 (1), 012018, 2024.
8. AS Duggal, A Gehlot, PK Malik, N Bisht, R Singh,"A Signal Generation System for Galvanic Taste Modulation using ATmega328p Microcontroller," 2023 4th International Conference on Electronics and Sustainable Communication Systems (ICESC).
9. PK Malik, Manoj Kumar Shukla, Kanegonda Ravi Chythanya, Nitasha Bisht, Rashmi Roges, Anita Gehlot, "Intervention of Internet of Things in Home

Automation Applications" 3rd International Conference on Advancement in Electronics & Communication Engineering (Technically Sponsored by IEEE) held on 23rd -24th November, 2023 organized by Department of ECE and Department of CSE at Raj Kumar Goel Institute of Technology, Ghaziabad (U.P.), India.

International Exposure

1. Two Weeks TEQIP-II Sponsored Networking and Study Tour to Singapore and Australia from 16-04-2016 to 28-04-2016.

STC/Workshop/Symposium Organized

1. Course Coordinator of One Week TEQIP-II Sponsored Short Term Course on "Fundamental & Simulink for System & Algorithm Modelling & Optimization Techniques in MATLAB" Organized at Jawaharlal Nehru Government Engineering College Sundernagar District Mandi (HP) from 06-01-2014 to 10-01-2014.
2. Coordinator of TEQIP-II Sponsored National Workshop on "Impact of Information Communication Technology on Technical Education" (IICTTE-2014) Organized at Jawaharlal Nehru Government Engineering College Sundernagar District Mandi (HP) on 04-04-2014.
3. Co-Coordinator of TEQIP-II Sponsored International Symposium on Communication and Distributed System "COMSYS 2014" Organized at Jawaharlal Nehru Government Engineering College Sundernagar District Mandi (HP) on 15-12-2014.
4. Coordinator of TEQIP-II Sponsored National Symposium on "Research Innovation in Wireless Technology" (RIWT-2016) Organized at Jawaharlal Nehru Government Engineering College Sundernagar District Mandi (HP) on 03-09-2016.

STC/ FDP/Workshop/Seminar Attended

1. One Week AICTE Recognized Short Term Course on "PCB Layout, Fabrication and Testing" Conducted by Electronics Service Center of National Institute of Technical Teachers Training and Research Chandigarh from 14-01-2013 to 18-01-2013.
2. One Week TEQIP-II Sponsored "Induction Training Programme" Conducted by Jawaharlal Nehru Government Engineering College Sundernagar District Mandi (HP) in Collaboration with NIT Hamirpur (HP) from 02-08-2014 to 06-08-2014.

3. Indian Society for Technical Education Section Annual Convention on "Challenges of Technical Education in Nation Building" Conducted by NIT Hamirpur (HP) from 30-09-2015 to 01-10-2015.
4. One Day 2nd National Workshop on "Renewable Energy" Conducted by Jawaharlal Nehru Government Engineering College Sundernagar District Mandi (HP) on 22-11-2014.
5. One Week AICTE Recognized Short Term Course on "NBA Accreditation and Quality Management" Conducted by Media and Continuing Education Centre of National Institute of Technical Teachers Training and Research Chandigarh from 24-08-2015 to 28-08-2015.
6. One Week TEQIP-II Sponsored Faculty Development Programme on "Outcome Based Education" Conducted by Jawaharlal Nehru Government Engineering College Sundernagar District Mandi (HP) from 19-10-2015 to 23-10-2015.
7. Two Days Workshop on "Financial, Disciplinary and CCS Rules" Conducted by Jawaharlal Nehru Government Engineering College Sundernagar District Mandi (HP) from 27-02-2016 to 28-02-2016.
8. One Day Workshop on "Office Procedure, Conduct & CCA Rules" Conducted by Jawaharlal Nehru Government Engineering College Sundernagar District Mandi (HP) on 01-07-2016.
9. One Week Short Term Course on "Statistical Methods in Research Methodology" Conducted by Punjab Engineering College Chandigarh from 04-06-2018 to 08-06-2018.
10. One Week Summer Training Program on "Active Learning for Senior Faculty" Conducted by IIT Indore from 25-06-2018 to 29-06-2018.
11. Two Week AICTE Recognized Short Term Course on "Research Methodology" Conducted by Education and Educational Management Department of National Institute of Technical Teachers Training and Research Chandigarh from 16-07-2018 to 27-07-2018.
12. One Day Online Training Program on "Geometry Modelling in HFSS" Conducted by Entuple Technologies on 04-05-2020.
13. Two Day Online Training Program on "Waveguide Component Design Using HFSS" Conducted by Entuple Technologies on 05-05-2020 and 06-05-2020.
14. Two Day Online Training Program on "Optimization of Microstrip Antenna Using HFSS" Conducted by Entuple Technologies on 08-05-2020 and 09-05-2020.
15. Two Day Online Training Program on "Array Antenna Design Using HFSS" Conducted by Entuple Technologies on 12-05-2020 and 13-05-2020.
16. One Day Online Training Program on "Omni Directional Antenna Uisng HFSS" Conducted by Entuple Technologies on 15-05-2020.

17. Two Day Online Training Program on “Microstrip Antennas with Different Types of Feeding Techniques” Conducted by Entuple Technologies on 20-05-2020 and 21-05-2020.
18. Two Day Online FDP on “Microstrip Antennas for Advanced Wireless Communication” Organized by Department of Electronics & Communication Engineering, in association with IETE, Vijaywada division from 15-05-2020 and 16-05-2020.
19. One Week TEQIP-III Sponsored Short Term Course on “Effective Tools and Techniques in Qualitative Research” Conducted by Department of Electronics & Communication Engineering, Dr. B R Ambedkar National Institute of Technology, Jalandhar from 10-08-2020 to 14-08-2020.
20. One Week Training Programme on "Embedded IOT" Conducted by Department of Technical Education, Government College of Engineering , Kannur, Kerala, from 14/02/2022 to 19/02/2022.
21. One Week AICTE Recognized Faculty Development Programme on “Communication Technology: Connectivity Evaluations” Conducted by Electronics & Communication Department of National Institute of Technical Teachers Training and Research Chandigarh from 27-05-2024 to 31-05-2024.

Professional Activities

1. Head/Officer In-Charge, Department of Electronics & Communication Engineering, Jawaharlal Nehru Government Engineering College Sundernagar District Mandi (HP) from (January 20th, 2014 to August 16th, 2014), (February 18th, 2015 - August 29th, 2017), (March 4th, 2023 - Till date).
2. Faculty Coordinator of Jawaharlal Nehru Government Engineering College Annual Techno Cultural Fest “TWASK 2014”.
3. Chairman of Institutional College Magazine “Reflexia” from 06-02-2016 to Till Date.
4. Member Secretary of Institute level (Jawaharlal Nehru Government Engineering College) "Internal Complaints Committee".
5. Member of Institutional Library Committee (Jawaharlal Nehru Government Engineering College) from 10-06-2014 to Till Date.
6. Officer In-Charge of “National Institute Ranking Framework” for the year 2015 at Jawaharlal Nehru Government Engineering College Sundernagar District Mandi (HP).
7. Four Times “Interview Panel Member (Institute Level) Constituted for Recruitment of Various Posts” for Department of Electronics & Communication Engineering, Jawaharlal Nehru Government Engineering College Sundernagar District Mandi (HP).

Subjects Taught

- Basic Electronics Engineering,

- Analog Electronics,
- Microprocessor & its Applications,
- Microcontroller & Embedded Systems,
- Biomedical Electronics,
- Computer Networks & Data Communication,
- Electronic Measuring & Measurement of Instruments,
- Wireless Communication,
- Digital Communication.

(Nitasha Bisht)